Novel Mechanisms of Axonal Growth Inhibition Following Central Nervous System Injury

by

Travis L. Dickendesher

A dissertation submitted in partial fulfillment
of the requirements for the degree of
Doctor of Philosophy
(Neuroscience)
in the University of Michigan
2013

Doctoral Committee:

Associate Professor Roman J. Giger, Chair
Professor Lori L. Isom
Associate Professor Andrew P. Lieberman
Assistant Professor Brian A. Pierchala
Assistant Professor Hisashi Umemori
Assistant Professor Bing Ye

On the brain:

“The brain is the organ of destiny. It holds within its humming mechanism secrets that will determine the future of the human race.”

- Wilder Penfield

On regeneration:

"Once the development was ended, the founts of growth and regeneration of the axons and dendrites dried up irrevocably. In the adult centers, the nerve paths are something fixed, ended, and immutable. Everything may die, nothing may be regenerated. It is for the science of the future to change, if possible, this harsh decree."

- Santiago Ramón y Cajal

On graduate school:

"It's supposed to be hard. If it wasn't hard, everyone would do it. The hard...is what makes it great."

- Jimmy Dugan, played by Tom Hanks (“A League of Their Own”)

DEDICATION

To my parents:

For their unwavering support, unconditional love, and unselfish sacrifice.

ACKNOWLEDGMENTS

This work would not have been possible without the help and support from so many people in my personal and professional life. At every step of my career, I have been lucky to have incredible role models and true friends for guidance and encouragement. It is not possible to put into words how grateful I am to all of you.

I first want to thank the members of my dissertation committee: Lori Isom, Andrew Lieberman, Brian Pierchala, Hisashi Umemori, and Bing Ye. I have always been able to count on all of you for anything that I need, and I cannot imagine having a better group of professors to support me throughout my graduate career. Your attention, advice, constructive criticism, and patience have been invaluable.

To my mentors: Brian Derowski - your unparalleled enthusiasm for science still inspires me to this day; Mary O'Riordan - you took a chance on a clueless undergraduate and brought me into your lab. If you hadn't given me so many second, third, and fourth chances, I would not be in graduate school today; Lori Isom - you are the perfect example of how a mentor can set the tone for a wonderful lab environment that is also intellectually stimulating. From teaching me lessons in time management and independence to discussing with me the expectations of being a scientist (as well as anything else I had on my mind), you are the reason I was prepared for the challenges of a Ph.D; Chunling Chen - the lessons I learned from you at the bench saved me so much frustration during the past five years; Ben Segal - you pushed me to be a better thinker, a better speaker, and a better researcher. I sincerely thank you for that; Irah King - you were a role

model for how a graduate student should be and I hope I have made you proud; Santhadevi Jeyabalan - you have a remarkable gift when it comes to teaching and I have incorporated your methods into every class I have taught; Cathy Collins - thank you for taking the time out of your insanely busy schedule to mentor me as I earned my Graduate Teacher Certificate. The excitement you bring out in undergraduates as they participate in your classes is without equal.

I am very proud to be a member of the neuroscience community at the University of Michigan, an incredibly collaborative group of people that can always be counted on for reagents, input on experiments, and thoughtful discussions. I especially want to thank the other members of the "axon meetings" (laboratories of Asim Beg, Cathy Collins, and Brian Pierchala) and my previous rotation advisors (Cathy Krull and Hisashi Umemori). Additionally, I would not be here without the continued support of the Program in Biomedical Sciences and the Neuroscience Graduate Program, and I thank Lori Isom, Steve Maren, Jill Becker, Lique Coolen, and Ed Stuenkel for having the courage and determination to lead these programs and make them even better environments for training and preparation. I also want to thank Rachel Flaten and Valerie Smith for always taking care of anything the students need (especially paychecks!) - you are the driving force behind the NGP and all of us are indebted to you. My greatest thanks also go out to all of my collaborators, here at the University of Michigan and at other institutions, who I have acknowledged throughout this dissertation. In particular, I would like to thank Travis Stiles for his true collaborative spirit, which was evident from the moment we met at SFN 2011.

I am sincerely grateful to the professors, students, and staff of the Cell and Developmental Biology Department. CDB is my second home and thanks to all of you, it is always a wonderful place to be. From the antics of Ben Allen's lab and the mysteries of the Killer Whale to Shiv's epic adventures at the 2011 CDB Retreat and NCAA March Madness, I

cannot think of a better place to work. In particular, I want to thank Melissa Karby for somehow finding a way to keep our lab running on a daily basis, Kristen Hug and Lori Longeway for always handling my administrative "crises", Billy Tsai and Lois Weisman for being fantastic coordinators when I was a GSI for CDB530, and Christina, Niki, Andrea, David, Irene, Brandon, Alex, Justine, Lynn, Jay, Carmen, and Mary (and many more!) for being downright fabulous.

I do not believe a person can successfully navigate through a doctoral program (or life) without the constant support of friends. David, Liz, Chrissy, Paul, Michelle, Vicki, and Emily - you have been my greatest friends since high school and college, and I thank you for always sticking by my side through all of the "ups" and "downs". Karthik, Annie, and Erin - as former graduate students, your advice has been priceless and I am incredibly grateful that I have been able to count on all of you. To all of the students (past and present) of the NGP - thank you for being a wonderful support system. I have no doubt that all of you will be successful in whatever you choose to do. To the members of the NGP incoming class of 2008 (the "Anteaters"): Ali, Graham, Megan, Shanna, Trace, Stephanie, Shawn, Blair, Ashley, Seth, and Gustavo (honorary member) - it has been quite a journey and I am glad that I was able to experience it with all of you. I have enjoyed every moment and I will miss you all terribly. Ason - although it has only been a short time, life with you in it has been better than I could have possibly imagined. Thank you for your support (and incredible cooking) during my dissertation writing, and I look forward to the future.

To the past and present members of the "Roman Legion": Katie, Yevgeniya, Jing-Ping, Yuntao, Choya, Dava, Sophia, Steve, Jesse, Seung-hee, Derek, Sandy, Oliver, and Nikhil - I can honestly say there is no other lab and no other group of people I would have rather spent my time with during the past five years. All of you have contributed to making the lab a welcoming and

inclusive environment - a place where we can be productive but also have a good time. Additionally, I love the stimulating conversations that I have with all of you, and the fact that everyone is more than willing to help each other out, whether it be with an experiment, a grant or presentation, or even something personal. Jing-Ping - your perseverance and determination is inspirational and I have no doubt that great things lie ahead for you. I am proud to call you my friend. Katie - your incredible intellectual capability, attention to detail, strong independence, sense of humor, and willingness to stick up for others are just some of the many qualities I admire about you. I also consider you a close friend - someone that I greatly respect. Yevgeniya - from the moment we met, it was clear to me that there is no one else quite like you. On a scientific level, you have a remarkable ability to quickly identify the gaps in the literature and propose brilliant experiments to advance the field. You also have a work ethic that rivals anyone I have ever met, and I look forward to seeing you start up your own lab in the not-so-distant future. On a personal level, I consider you my best friend in the world. You know me better than anyone else and I think of you as the sister I never had.

Every time I hear someone describe the qualities that a rotation student should look for in an advisor, I realize that Roman embodies all of these qualities. I want to thank you Roman for being a true mentor in every sense of the word. You have never hesitated to give your students everything they need to put them on the path to success, no matter the cost. Your track record with students is not a coincidence. Any student that comes out of your lab is a better bench worker, writer, speaker, networker, and critical thinker. You do not tell students the experiments they need to do to graduate - you take the time and effort to provide them with the training that allows them to think for themselves. Not only are you respected here at the University of Michigan, but also across the entire field of neuroscience - something I found out firsthand as I

traveled to international conferences. You inspire a fierce loyalty from your students, a sign of just how much respect we all have for you. I will forever be grateful for the time I spent under your mentorship and I look forward to it continuing in the future.

I want to thank my family for their incredible support during my academic career. I thank all of you for the laughter and the tears, the good moments and the bad. I will even overlook the Buckeye allegiance that some of you have (everyone makes mistakes in life) because you have been nothing but encouraging of my career path. I will truly miss every one of you when I move to Boston. To Bastian - bringing you home with me four years ago was one of the single greatest decisions I have ever made. Knowing that I will always find you waiting for me at the door when I come home brings me enough happiness to override even the worst of days. I love you with all of my heart.

Lastly, and most importantly, to my parents - I will never be able to express how much I appreciate the constant love and support you have given me throughout every stage of my life. You continually make sacrifices on my behalf, always helping me out at your own expense. There is no one that I admire and respect more than the both of you, and I consider it the highest honor to be called your son. Thank you from the bottom of my heart.

TABLE OF CONTENTS

LIST OF FIGURES

LIST OF TABLES

LIST OF APPENDICES

ABSTRACT

Depending on location and severity, injury to the adult mammalian central nervous system (CNS) typically results in neurological deficits ranging from mild motor impairment to complete paralysis. As the regenerative capacity of severed axons is extremely limited, there is a great unmet need for strategies that promote neural tissue growth and repair. There are two major extrinsic barriers to axon regeneration in the injured CNS: myelin-associated inhibitors (MAIs) and chondroitin sulfate proteoglycans (CSPGs). MAIs and CSPGs bind to axonal receptors and initiate signaling cascades to prevent significant regenerative growth; thus, these receptors represent potential targets for therapeutic intervention.

The Nogo receptors (NgR1, NgR2, and NgR3) form a small subfamily of proteins, of which NgR1 and NgR2 have been shown to act as receptors for MAIs. Here we report on a novel interaction between select members of the Nogo receptor family and CSPGs. NgR1 and NgR3 bind with high affinity and selectivity to the sugar moiety of CSPGs. *In vitro*, primary neurons isolated from mice lacking both NgR1 and NgR3 (*NgR13*$^{-/-}$) grow longer neurites on substrate-adsorbed CSPGs than neurons isolated from controls. *NgR13*$^{-/-}$ double mutants, but not single mutants, show enhanced axonal regeneration of retinal ganglion cell (RGC) fibers following optic nerve crush injury *in vivo*. When combined with activation of RGC intrinsic growth programs, genetic manipulations result in a further increase in optic nerve regeneration. These results thus identify NgR1 and NgR3 as novel CSPG receptors and provide unexpected evidence for shared mechanisms of MAI and CSPG inhibition. Ongoing experiments are aimed

at examining whether the regenerating fibers of *NgR13*$^{-/-}$ mice are electrically active and able to reach their pre-injury synaptic targets.

We have also identified the low-density lipoprotein receptor-related protein 1 (LRP1) as a novel receptor for one of the MAIs, the myelin-associated glycoprotein (MAG). In addition to its established role in neuronal growth inhibition, MAG has recently been shown to protect neurons from axonal degeneration and excitotoxicity. Here we performed a comprehensive dissection of the growth-inhibitory and protective functions of MAG and identified distinct receptor-signaling systems that mediate these two functions. On the receptor level, we show that paired immunoglobulin (Ig)-like receptor B (PirB) and LRP1 mediate MAG-induced neurite outgrowth inhibition in a cell type-specific manner, whereas NgR1 mediates MAG-induced neuroprotection. Loss of NgR1 results in increased vulnerability to acrylamide toxicity, as determined by rotarod performance and compound action potential recordings of the sciatic nerve. *NgR1*$^{-/-}$ mice also show increased susceptibility to kainic acid-induced epileptic seizures. Additionally, we find that MAG growth inhibition requires negative regulation of the PI3K-AKT-mTOR pathway, whereas MAG protection involves blockade of calpain-induced cleavage of the neuronal cytoskeleton. Finally, structural analysis shows that the neuroprotective activity resides within the N-terminal portion of the MAG ectodomain, whereas the growth-inhibitory activity resides near the C-terminus. Collectively, we provide novel insights into the molecular mechanisms that regulate neuronal growth and protection in CNS neurons.

CHAPTER I:

Introduction

Can development be recapitulated in the adult?
Current strategies and future challenges for mammalian axon regeneration

1.1 Abstract

A devastating form of central nervous system (CNS) injury is traumatic injury to the spinal cord. The National Spinal Cord Injury Statistical Center at the University of Alabama estimates the number of Americans living with spinal cord injury (SCI) to be around 250,000 (with ~11,000 new injuries every year). In higher vertebrates, including humans, the regenerative capacity of severed axons in the adult CNS is extremely limited. Therapeutic interventions are sparse, and the prognosis for significant or complete recovery following moderate to severe SCI is poor. Many neurons located above and below the injury site in the spinal cord survive for several years after SCI; their axons, however, are severed or damaged and fail to propagate information in the form of electrical impulses past the site of injury. A decrease or complete loss of axon potential propagation results in partial or complete paralysis of the body distal to the location of injury. Thus, a major goal of SCI research is to reestablish neuronal connectivity lost as a consequence of injury. There are several strategies for how this can be achieved. Reinnervation can be accomplished by (1) long-distance regeneration of severed axons followed by synapse formation on pre-injury targets, (2) short-distance axonal growth and synapse formation on neural elements that form relays to neuronal targets distal to the injury site;

or (3) compensatory sprouting of spared axons that maintain connectivity beyond the injury site. Mounting evidence suggests that the limited degree of spontaneous recovery observed following CNS injury is a result of compensatory sprouting from spared neuronal systems. While substantial progress has been made in promoting axonal sprouting and regenerative growth in CNS-injured rodents, challenges ahead include translation of the most promising advances to human subjects with SCI.

1.2 Introduction

Accounts of SCI and attempts to treat it date back to ancient times. The Greek physician Hippocrates (460-377 BC) wrote: "there are no treatment options for SCI that resulted in paralysis and unfortunately, those patients suffering from such injuries were destined to die." Although survival after injury and surgical options for SCI patients have dramatically improved in recent years, moderate to severe SCI that causes substantial functional deficits remains a major medical challenge, with limited treatment options and a poor prognosis for complete recovery. Advances in emergency and acute care improve survival rates following SCI and increase the number of individuals who have to cope with severe disabilities. New treatment options to promote repair following SCI are urgently needed.

Although the spinal cord is well protected by hard bones of segmentally aligned vertebrae bodies, the vertebrae column can be fractured or dislocated during a car accident or a severe sports injury. In most cases, SCI is caused by fracture or compression of the vertebral column at a specific location, resulting in contusion or transection of neural tissue. An injury to the spinal cord can damage a few, many, or almost all spinally projecting fiber tracts. Some injuries will allow almost complete recovery. Others will result in complete paralysis. Depending on the

level at which the SCI is inflicted and the severity of neural tissue damage, it may cause partial or full para- or tetraplegia.

On a cellular level, compression or disruption of neural tissue leads to transection of ascending and descending fiber tracts. Axons of spinally projecting neurons are bundled into specific fiber tracts that propagate electrical impulses that carry sensory information or participate in motor coordination. Axons in fiber tracts are insulated by myelin sheaths to ensure rapid propagation of these electrical impulses. If the axon of a projection neuron is severed, this leads to "self-destruction" and total disintegration of the axonal segment located distal (relative to the neuronal cell body) to the transection site. Less severe trauma causes focal demyelination with preservation of axonal continuity. Transection or demyelinating lesions produce a reduction or complete block of electrical impulse propagation past the injury site. The ability of partially demyelinated fibers to faithfully carry long trains of complex electrical impulses is greatly impaired and leads to various degrees of functional impairments. Thus, relatively small lesions to the adult spinal cord can lead to substantial functional loss.

The focus of this chapter is to discuss recent advances in our understanding of the biochemical signaling cascades and molecular mechanisms that limit spontaneous regeneration of neuronal networks following CNS injury. Cell surface receptor complexes and intracellular signaling pathways implicated in neuronal growth inhibition, as well as new treatment strategies for SCI, are summarized.

1.2.1 Spinal Cord Injury Repair: A Complex Problem

A SCI is a complex biological and medical problem. Initial damage caused by the impact (primary damage) not only destroys vital neuronal connections but also triggers a number of

complex cellular and biochemical cascades that cause cell death and degeneration of neural tissue over days and weeks following injury - processes generally referred to as secondary damage. Secondary damage caused by glutamate excitotoxicity and hypoxia happens within minutes following SCI and for logistical reasons is difficult to block. Subsequent waves of cell death, inflammatory immune responses, and oxidative damage may be more realistic targets to limit secondary damage.

Because the molecular and cellular environment of the spinal cord is constantly changing from the moment of injury until several weeks to months later, combination therapies need to be designed and applied to target specific mechanisms of damage at different time points after injury. Strategies for the repair of injured neural tissue may target neuronal growth, formation of new synapses (synaptogenesis), plasticity of newly formed and existing synapses, and axon myelination. Understanding the cellular and molecular mechanisms involved in both the healthy and injured spinal cord will hopefully point the way to therapies that prevent secondary damage, encourage axons to grow and reconnect past injured areas within the spinal cord, and promote adaptive neuronal plasticity. A more detailed understanding of these processes at the molecular level is of great interest biologically and believed to be key to the development of therapeutic interventions for SCI.

1.2.2 Severed Axons in the Injured Adult Mammalian CNS Show Poor Regenerative Growth

Long-distance axon regeneration often occurs following peripheral nervous system (PNS) injury but does not occur spontaneously in the injured adult mammalian CNS (**Table 1.1**). Thus, in mammals, injured neurons of the PNS and CNS exhibit quite distinct adaptive strategies to injury. Compared with the PNS, injury-induced responses in CNS neurons are less robust and

morphologically more diverse (Gaudet et al., 2011). Research on many fronts has revealed that encouraging axons to grow after injury is a complicated and challenging task.

Most CNS neurons have the capacity to extend processes following injury; however, the environment in the injured adult brain or spinal cord does not encourage growth (Aguayo et al., 1978; Aguayo et al., 1981). This environment not only lacks the growth-promoting molecules that are present in the developing CNS, but it also contains substances that actively block axon extension (Schwab et al., 1993). Moreover, intrinsic cell growth programs of mature CNS neurons are "more quiescent" compared with developing neurons. Even when placed in an environment that supports neuronal sprouting and process outgrowth, growth rates of mature neurons are substantially lower compared with developing neurons (Goldberg et al., 2002). As discussed later, different approaches have been used successfully to promote axonal growth and improve behavioral outcomes in the injured adult mammalian CNS. Treatment strategies fall into three general categories: (1) functional depletion of growth-inhibitory environmental cues; (2) application of growth-promoting substrates or growth factors; and (3) activation of neuron intrinsic growth programs.

1.3 Inhibitors of CNS Axon Regeneration

Myelin sheaths produced by oligodendrocytes are wrapped around axons of many CNS neurons and facilitate rapid propagation of electrical impulses. Protein components associated with CNS myelin are profoundly inhibitory for neurite outgrowth when presented to cultured neurons. *In vivo*, myelin-associated inhibitors of growth are thought to contribute to the growth-inhibitory nature of injured adult mammalian CNS tissue (Hu and Strittmatter, 2004; Schwab et al., 1993). Several myelin-associated inhibitors of growth have been identified and characterized

at the molecular level, including myelin-associated glycoprotein (MAG), the reticulon family member Nogo-A, and oligodendrocyte myelin glycoprotein (OMgp) (Filbin, 2003; Xie and Zheng, 2008). Although most attention has focused on the mechanisms of action of these three inhibitors during CNS axon regeneration, it is important to point out that additional growth inhibitors are present in adult CNS tissue, many of which are upregulated by injury (**Figure 1.1**). Repulsive or growth-inhibitory molecules belonging to the semaphorin, ephrin, and netrin families of axon guidance molecules are present in CNS myelin and contribute to the regenerative failure of different types of injured CNS axons (Bolsover et al., 2008; Low et al., 2008). Chondroitin sulfate proteoglycans (CSPGs) comprise an important class of growth inhibitors (Davies et al., 1999; Snow et al., 1990b). Different types of CSPGs are broadly expressed in the CNS and are important components of the extracellular matrix (Zimmermann and Dours-Zimmermann, 2008). Some CSPG family members, including aggrecan, neurocan, and versican, show regional upregulation following injury to the brain or spinal cord (McKeon et al., 1995). Near the injury site, a glial scar starts to form that is composed of reactive astrocytes, migrating meningeal cells, and microglia. Reactive astrocytes express high levels of inhibitory CSPGs that block regenerative axonal growth following SCI in rodents (Bradbury et al., 2002; Shen et al., 2010). Additional molecules that may contribute to the growth-inhibitory nature of adult mammalian CNS tissue include members of the slit family of inhibitory axon guidance cues (Lau and Margolis, 2010), wnt family members (Liu et al., 2008), the lipid sulfatide (Winzeler et al., 2011), and blood-derived factors such as fibrinogen (Schachtrup et al., 2007). Expression levels and distribution of these growth-inhibitory molecules are regulated by injury. Collectively, the growing list and molecular diversity of known CNS inhibitors suggest that

functional depletion of any individual inhibitor alone is likely not sufficient to significantly enhance regenerative growth of injured CNS neurons.

1.3.1 Myelin-Associated Inhibitors

While the growth-inhibitory nature of CNS myelin is well established, an important question concerns the identification and characterization of specific myelin inhibitors at the molecular level. Of equal interest is the identification of the neuronal cell surface receptors employed by myelin inhibitors and the characterization of the intracellular signaling cascades that are activated upon ligand binding and lead to growth inhibition or axon retraction. In this section, we give an overview of the prototypic myelin inhibitors MAG, Nogo, and OMgp, and additional inhibitors of growth found in CNS myelin.

Myelin-associated glycoprotein

As discussed above, CNS myelin contains a number of growth-inhibitory factors. Biochemical purification of one growth-inhibitory activity identified MAG, a previously known myelin component of largely unknown function (McKerracher et al., 1994; Mukhopadhyay et al., 1994). MAG (also known as Siglec4a) is a type 1 transmembrane protein and is a member of the sialic acid-binding immunoglobulin (Ig) lectins, composed of an extracellular region with five Ig-like domains, a transmembrane domain, and a cytoplasmic tail (Filbin, 2003). A short (S-MAG) and large (L-MAG) splice form of MAG exist, differing only in the length of the cytoplasmic regions (Lai et al., 1987; Salzer et al., 1987). The lectin activity of MAG complexes with terminal sialic acids on gangliosides and sialo-glycoproteins, with preferential binding of α2,3-linked terminal sialic acids (Collins et al., 1997; Kelm et al., 1994; Vyas and Schnaar,

2001). The MAG lectin activity critically depends on the presence of a conserved arginine residue (Arg118) located in the first Ig-like domain (Tang et al., 1997). The importance of the MAG lectin activity for neuronal growth inhibition has been examined extensively and was found to augment the inhibitory action when MAG is presented at limiting concentrations. At high concentrations of MAG, however, the lectin activity is not required for neurite outgrowth inhibition *in vitro* (Tang et al., 1997; Vinson et al., 2001; Vyas et al., 2002). Of interest, terminal sialic acid moieties appear to limit spinal axon growth into implanted peripheral nerve grafts in a rat model of brachial plexus avulsion *in vivo* (Yang et al., 2006). Moreover, intrathecal infusion of sialidase in rats following spinal cord contusion injury enhances axonal sprouting and leads to improved behavioral outcomes (Mountney et al., 2010).

Of interest for axonal growth and regeneration is the observation that MAG is a bifunctional molecule that influences axonal extension in an age-dependent manner. Initially, MAG was shown to mildly promote the neurite outgrowth of postnatal day 1 (P1) dorsal root ganglion (DRG) neurons and embryonic day 17 (E17) spinal neurons plated on fibroblast monolayers stably expressing recombinant L-MAG (Johnson et al., 1989; Turnley and Bartlett, 1998). At more mature stages, these neuronal cell types, as well as several other types of primary neurons, are all strongly inhibited by MAG (DeBellard et al., 1996; McKerracher et al., 1994; Mukhopadhyay et al., 1994). Despite the well-established growth-inhibitory action of MAG *in vitro*, nervous system regeneration studies in $MAG^{-/-}$ mice showed little or no enhanced axonal regeneration following CNS injury (Bartsch et al., 1995; Li et al., 1996). Following optic nerve crush injury in adult $MAG^{-/-}$ mice, no improvement in regeneration of retinal ganglion cell (RGC) axons is seen. Following bilateral transection of the dorsal spinal cord, longitudinal growth of severed axons is not enhanced in $MAG^{-/-}$ mice compared to wild-type control mice

(Bartsch et al., 1995). A subsequent study showed minimal enhancement of corticospinal tract (CST) fiber regeneration following dorsal hemisection lesions at the thoracic level in adult *MAG*$^{-/-}$ mice (Li et al., 1996). Based on these studies, it can be concluded that germline ablation of MAG alone is not sufficient to significantly promote regenerative axonal growth following CNS injury.

Nogo

Myelin-associated inhibitory activities with molecular masses of 35- and 250-kDa were first described by Caroni and Schwab (Caroni and Schwab, 1988a). A function-blocking monoclonal antibody (called IN-1) was raised against a partially purified inhibitory activity and shown to reduce the myelin inhibitory effects toward sensory and sympathetic neurons *in vitro* (Caroni and Schwab, 1988b). *In vivo*, IN-1 was found to promote some degree of axonal sprouting and regeneration of severed CST axons (Schnell and Schwab, 1990). Regenerating raphespinal and coeruleospinal projections were also increased following IN-1 treatment. Importantly, anatomical growth and sprouting in IN-1-treated animals correlated with improved recovery of locomotor function (Bregman et al., 1995).

Despite the promising results with IN-1 in spinal cord-injured rodents, the antigen(s) recognized and neutralized by the IN-1 antibody remained elusive for some time. Based on partial sequence information of the IN-1 antigen, three groups independently identified the reticulon family member Nogo-A (also known as RTN4a) as a growth-inhibitory protein (Chen et al., 2000; GrandPre et al., 2000; Prinjha et al., 2000). Recombinant Nogo-A is sufficient to inhibit neurite outgrowth *in vitro*, and the growth-inhibitory activity of Nogo-A is largely blocked in the presence of IN-1 (Chen et al., 2000). The identification of a reticulon family

member as an inhibitor of axonal growth was unexpected, given that other reticulon proteins are largely confined to the endoplasmic reticulum (Voeltz et al., 2006). Nogo appears to be an exception as the protein is found on the cell surface of oligodendrocytes and neurons (Yang and Strittmatter, 2007). Alternative splicing of the Nogo gene results in three isoforms, Nogo-A, -B, and -C, all of which are membrane-associated proteins that contain a common carboxy-terminal region but differ in their amino-terminal portions (Dodd et al., 2005). Included within the common carboxy-terminal region is an inhibitory 66 amino acid hydrophilic loop, Nogo-66, which is extracellular and located between two hydrophobic transmembrane-spanning regions (GrandPre et al., 2000). Another inhibitory activity, NogoΔ20, is located in the amino-terminal region and specific for the Nogo-A isoform. Both Nogo-66 and NogoΔ20 have been shown to inhibit neurite outgrowth and induce growth cone collapse *in vitro* (Oertle et al., 2003). NogoΔ20-induced growth cone collapse is mediated through Nogo-A signaling endosomes, which result from Pincher-dependent endocytosis. These signalosomes can act within growth cones and can also be transported from neurites to cell bodies of DRG neurons (Joset et al., 2010).

While all Nogo isoforms are expressed in the developing and adult mammalian nervous system, the expression pattern of Nogo-A is of particular interest. Nogo-A is expressed by several types of neurons, as well as oligodendrocytes and their processes. Consistent with a role of Nogo-A as a myelin-associated inhibitor of axon regeneration, its expression is detected at areas of oligodendrocyte-axon contact, as well as in the inner and outer loops of the myelin sheath (Huber et al., 2002; Wang et al., 2002c). Following spinal cord transection, an increase of Nogo-A is seen around the injury site, which does not return to baseline levels until 1 month post-injury (Wang et al., 2002c). Nogo-A is not expressed by Schwann cells, the myelinating

glia of the PNS. Consistent with the idea that Nogo-A contributes to the regenerative failure of adult CNS neurons in higher vertebrates, inhibitory domains of mammalian Nogo-A are either missing or mutated in lower vertebrates. The Nogo-66 loop is present in zebrafish but does not inhibit neurite outgrowth *in vitro* (Abdesselem et al., 2009; Schweigreiter, 2008).

Regeneration studies in spinal cord-injured Nogo mutants have been inconclusive and remain a matter of debate. Following dorsal column lesion of adult mice that lack all three Nogo gene splice forms (*Nogo-A/-B/-C*$^{-/-}$ mice), no detectable enhancement of CST axon regeneration is seen beyond the lesion site (Lee et al., 2009b; Zheng et al., 2003). In an independent study, extensive sprouting of corticospinal axons rostral to the spinal cord transection site and recovery of motor function in young adult *Nogo-A/-B*$^{-/-}$ mice was reported (Kim et al., 2003). A mild anatomical regeneration phenotype was reported for *Nogo-A*$^{-/-}$ mice by the group of Martin Schwab. A confounding effect of *Nogo-A*$^{-/-}$ mice is the strong upregulation of Nogo-B in the CNS (Simonen et al., 2003). Due to differences in the gene targeting strategy to functionally ablate Nogo, mouse genetic backgrounds, lesion models, and axon tracing techniques employed, a direct comparison of these apparently conflicting results cannot be made (Cafferty et al., 2007; Dimou et al., 2006; Steward et al., 2007).

Oligodendrocyte myelin glycoprotein

A third inhibitor of growth associated with CNS myelin is OMgp, a member of the leucine-rich repeat (LRR) family of proteins (Kottis et al., 2002; Wang et al., 2002b). The ectodomain of OMgp is composed of eight canonical LRRs followed by a serine/threonine-rich region and a glycosylphosphatidylinositol (GPI) anchor for membrane attachment (Mikol and Stefansson, 1988; Mikol et al., 1990). As its name implies, OMgp is present on

oligodendrocytes; however, it is also expressed in a wide range of neuronal populations, including hippocampal pyramidal cells, Purkinje cells of the cerebellum, and brainstem motoneurons (Habib et al., 1998; Huang et al., 2005; Lee et al., 2009a; Mikol and Stefansson, 1988). As a myelin inhibitor, OMgp is able to induce growth cone collapse and restrict neurite outgrowth in a number of primary neuronal cell types *in vitro* (Kottis et al., 2002; Wang et al., 2002b). *In vivo*, regeneration studies of spinal cord-injured *OMgp*$^{-/-}$ mice show minimal anatomical growth or functional improvements (Ji et al., 2008).

Collectively, individual germline ablation of Nogo, MAG, or OMgp has failed to demonstrate long-distance regeneration of severed CST axons, the most important spinal tract for motor function. As discussed above, the presence of multiple growth-inhibitory proteins in the injured adult CNS indicates that some degree of functional redundancy exists. To test this idea, mice were generated that are deficient in Nogo, OMgp, and MAG combined. Two independent studies with spinal cord-injured *Nogo/OMgp/MAG*$^{-/-}$ mice were recently carried out. In one study, it was reported that the combined loss of OMgp and MAG does not lead to enhanced sprouting of CST axons following dorsal hemisection. *Nogo-A/-B*$^{-/-}$ mice show enhanced sprouting of CST axons across the midline, and sprouting is further enhanced in *Nogo-A/-B/OMgp/MAG*$^{-/-}$ mice. Based on these observations it was suggested that Nogo-A/-B is a major inhibitor of axonal growth and that loss of OMgp and MAG has a synergistic effect on axonal sprouting when simultaneously ablated with Nogo-A/-B (Cafferty et al., 2010). In addition to the enhanced collateral sprouting from uninjured CST fibers, Cafferty et al. observed regenerative CST and raphespinal fiber growth past the injury site in *Nogo-A/-B*$^{-/-}$ mice, which was further enhanced in *Nogo-A/-B/OMgp/MAG*$^{-/-}$ mice. Improved locomotor recovery was also noted in triple mutants (Cafferty et al., 2010).

In an independent study by Lee et al., *Nogo-A/-B/-C/OMgp/MAG*$^{-/-}$ mice failed to show enhanced CST sprouting or longitudinal axon growth of CST and raphespinal fibers past the injury site (Lee et al., 2010a). Interestingly, raphespinal axon sprouting was enhanced with *OMgp*$^{-/-}$ or *MAG*$^{-/-}$ mice but not with *Nogo-A/-B/-C*$^{-/-}$ mice. There was no further enhancement of axonal sprouting with *Nogo-A/-B/-C/OMgp/MAG*$^{-/-}$ mice, and behavioral outcomes were not improved (Lee et al., 2010a). Possible explanations for the discrepancies between the two studies include differences in how the mutant mice were generated and the injury models employed to assess CNS axon regeneration and sprouting. However, both studies indicate that the combined ablation of three major inhibitors of growth may not be sufficient to achieve substantial regenerative growth. There are several reasons that may account for the limited regeneration observed in *Nogo/OMgp/MAG*$^{-/-}$ mice: (1) canonical axon guidance molecules are still present in these mice and may be sufficient to block CNS axon regeneration; (2) inhibitors associated with the glial scar may be sufficient to prevent long-distance axonal growth; (3) trophic factors are absent; and (4) intrinsic growth programs need to be activated. Finally, it is important to point out that germline ablation of Nogo, MAG, and OMgp may lead to activation of compensatory mechanisms in the nervous system of mutant mice, masking potential positive effects on axonal growth or behavioral outcomes following SCI.

Other myelin-associated inhibitors

In addition to the prototypic myelin-associated inhibitors Nogo, MAG and OMgp, axon guidance molecules expressed in the mature CNS or upregulated following CNS injury have been implicated in axon growth inhibition. For example, the semaphorin family of both secreted and membrane-associated proteins is traditionally recognized for their chemorepulsive and

chemoattractant roles in developmental axon pathfinding, fasciculation, and branching (Dent et al., 2004; Luo et al., 1993; Taniguchi et al., 1997; Tran et al., 2007). However, several semaphorin proteins are present in the mature CNS and have roles in limiting neuronal growth (Cohen et al., 2003; Pasterkamp and Verhaagen, 2006). The transmembrane semaphorin Sema4D is selectively expressed by oligodendrocytes and CNS myelin in the postnatal mouse brain. Furthermore, a strong upregulation of Sema4D expression is seen 1 week following spinal cord lesion in adult mice, specifically in oligodendrocytes at the periphery of the lesion (Moreau-Fauvarque et al., 2003). In addition, the GPI-anchored semaphorin Sema7A is expressed by oligodendrocytes in the spinal cord white matter of the postnatal rat (Pasterkamp et al., 2007). Recent evidence has also implicated Sema6A and one of its receptors, PlexinA2, in limiting axonal growth following a unilateral pyramidotomy injury model (Shim et al., 2012).

Another guidance cue that has been shown to function as a myelin-associated inhibitor of axon regeneration is netrin-1 (Low et al., 2008). During nervous system development, netrin-1 functions as a long-range chemotropic guidance molecule that either attracts or repels axons depending on surface expression of the netrin receptors DCC, UNC5, or DSCAM (Kennedy et al., 1994; Moore et al., 2007; Serafini et al., 1994). As with members of the semaphorin family, netrin-1 is expressed in the adult CNS, particularly by neurons and oligodendrocytes in the spinal cord (Manitt et al., 2001). Furthermore, netrin-1 is enriched in periaxonal myelin and associates with the extracellular matrix. Following adult rat SCI, netrin-1 is expressed by neurons and oligodendrocytes immediately adjacent to the lesion (Manitt et al., 2006). *In vitro*, neutralization of netrin-1 with soluble UNC5 receptor leads to enhanced neurite outgrowth of embryonic spinal motor neurons. Following a cervical spinal cord lesion *in vivo*, axonal growth into a graft

containing netrin-1-secreting fibroblasts is significantly reduced compared to axonal growth into control grafts (Low et al., 2008).

A third family of axon guidance molecules implicated in limiting CNS axon regeneration is the ephrins. Ephrins are membrane-bound proteins that participate in both forward and reverse signaling through Eph receptor tyrosine kinases to influence developmental axon guidance, fasciculation, and cell migration (O'Leary and Wilkinson, 1999; Wilkinson, 2001). Expression of several ephrins and Eph receptors continues beyond development in rats and humans (Liebl et al., 2003; Sobel, 2005), many of which are upregulated following SCI, optic nerve injury, brain injury, or CNS disease (Bundesen et al., 2003; Goldshmit et al., 2004; Knoll et al., 2001; Moreno-Flores and Wandosell, 1999; Sobel, 2005; Wang et al., 2003; Willson et al., 2002). In particular, ephrinB3, which is expressed in postnatal myelinating oligodendrocytes, inhibits growth of EphA4-expressing cortical neurons *in vitro*. In addition, EphA4 activation is eliminated and outgrowth inhibition is significantly reduced when cortical neurons are plated on myelin from *ephrinB3*$^{-/-}$ mice compared to control myelin (Benson et al., 2005). In spinal cord-injured rats, infusion of an EphA4 peptide antagonist enhances CST sprouting and promotes functional recovery; however, axon regeneration across the lesion site is not seen (Fabes et al., 2007). More recent studies have demonstrated substantial axon regeneration and behavioral improvements in a hemisection model of SCI using prolonged administration of EphA4 blockers (Goldshmit et al., 2011), as well as significant axon regeneration following optic nerve crush injury in *ephrinB3*$^{-/-}$ mice (Duffy et al., 2012). Collectively, these studies suggest that canonical axon guidance molecules contribute to the growth-inhibitory nature of adult mammalian CNS tissue.

More recently, the lipid sulfatide was shown to be a novel myelin-associated inhibitor of growth (Winzeler et al., 2011). Purified sulfatide from brain is sufficient to inhibit outgrowth of primary neurons, an effect that requires both the sulfate group and fatty acid moiety. Loss of sulfatide function significantly reduces the inhibitory effects of crude CNS myelin *in vitro*; however, mice lacking sulfatide do not show enhanced RGC axon regeneration following optic nerve crush injury *in vivo*. This is not altogether unexpected, given the presence of several other inhibitory molecules at the CNS injury site. Interestingly, an *in vivo* role for sulfatides in RGC axon regeneration is uncovered when RGC intrinsic growth programs are activated by intravitreal injection of the yeast cell wall extract Zymosan. Either injection of Zymosan or lens injury has been shown to stimulate an inflammatory response (Yin et al., 2003), with the subsequent release of RGC growth-promoting factors, including oncomodulin (Yin et al., 2009), ciliary neurotrophic factor (CNTF), and leukemia inhibitory factor (LIF) (Leibinger et al., 2009). This response alone is sufficient to enhance regeneration of RGC axons following crush injury to the optic nerve. Intravitreal injection of Zymosan in the absence of sulfatides results in significantly more axon regeneration than Zymosan alone, suggesting that there are additive effects when extrinsic inhibitory and intrinsic growth-promoting pathways are manipulated (Winzeler et al., 2011).

1.3.2 Receptor Complexes for the Prototypic Myelin-Associated Inhibitors

Nogo-66 receptor 1

While the growth-inhibitory nature of adult mammalian CNS myelin is well established and much progress has been made in defining the molecular players that inhibit axon

regeneration, comparatively little is known about the mechanisms by which myelin inhibitors signal growth inhibition to neurons. To monitor growth inhibition by Nogo, MAG, and OMgp *in vitro*, and to test the role of potential receptor candidates, two different experimental paradigms are used: (1) chronic presentation of substrate-bound inhibitor to measure neurite extension and (2) acute application of soluble inhibitor to assay collapse of neuronal growth cones at the leading tip of neuritis. The potent action of Nogo, MAG, and OMgp in neuronal inhibition assays suggests the existence of high-affinity cell surface receptors that recognize and bind these inhibitors to activate intracellular signaling cascades that ultimately destabilize the neuronal cytoskeleton.

Shortly after the identification of Nogo, a high-affinity binding partner for one of its inhibitory domains (Nogo-66) was discovered and named the Nogo-66 receptor 1 (NgR1) (Fournier et al., 2001). To demonstrate the functional significance of the newly identified NgR1/Nogo-66 interaction, a gain-of-function approach was used. E7 DRG neurons do not express NgR1, and their growth cones do not collapse in the presence of acutely applied Nogo-66. Ectopic expression of NgR1 in these neurons was sufficient to induce growth cone collapse in the presence of Nogo-66 (Fournier et al., 2001). These studies identified NgR1 as a functional receptor for Nogo-66-elicited growth cone collapse.

NgR1 is a GPI-anchored protein comprised of 8.5 canonical LRRs flanked by cysteine-rich N- and C-terminal capping domains (LRRNT and LRRCT) (Fournier et al., 2001). The LRRNT-LRR-LRRCT cluster of NgR1 is connected to the cell membrane via a ~100-amino acid stalk region and a GPI anchor. NgR1 can be shed off the cell surface by metalloproteinases (Ferraro et al., 2011; Walmsley et al., 2004) and is abundantly expressed in different types of neurons of the juvenile and adult CNS. The highest levels of NgR1 are found in the

hippocampus, neocortex, and basolateral amygdala (Funahashi et al., 2008; Hunt et al., 2002; Josephson et al., 2002; Lee et al., 2008).

Shortly after the identification of NgR1 as a high affinity receptor for Nogo-66, it was found that NgR1 also binds to the myelin inhibitors MAG and OMgp (Domeniconi et al., 2002; Liu et al., 2002; Wang et al., 2002b). These findings were quite surprising, given the lack of any apparent structural similarities among the three NgR1 ligands. Consistent with the idea that NgR1 functions as a high-affinity receptor for Nogo-66, MAG, and OMgp, DRG neurons isolated from *NgR1*$^{-/-}$ mice are more resistant to inhibitor-induced growth cone collapse than age-matched wild-type control neurons (Kim et al., 2004). Unexpectedly, when assayed for neurite outgrowth inhibition on substrate-coated myelin or Nogo-66, DRG neurons and cerebellar granule neurons (CGNs) isolated from *NgR1*$^{-/-}$ mice are strongly inhibited and do not extend processes that are longer than those from wild-type littermate controls (Zheng et al., 2005). Thus, loss of NgR1 is not sufficient to overcome myelin or Nogo-66 inhibition when presented in substrate-bound form. These seemingly disparate results (Kim et al., 2004; Zheng et al., 2005) were later reconciled by a study showing that NgR1 is dispensable for MAG- and OMgp-mediated inhibition of neurite extension but is necessary for MAG- and OMgp-induced growth cone collapse (Chivatakarn et al., 2007). These results provide evidence that the growth cone collapsing activities and substrate growth-inhibitory activities of inhibitory ligands can be dissociated. Furthermore, based on these observations it was concluded that additional and NgR1-independent mechanisms must exist for Nogo-,MAG-, and OMgp-mediated inhibition of neurite outgrowth.

NgR1 is the founding member of a small gene family that also includes NgR2 and NgR3 (Barton et al., 2003; He et al., 2003). The three family members show identical domain

organization and are expressed in overlapping, yet distinct patterns in the juvenile and adult CNS. NgR2 strongly associates with MAG but unlike NgR1, it does not support binding of Nogo-66 or OMgp. Ectopic expression of NgR2 in neonatal DRG neurons is sufficient to confer inhibitory responses to MAG (Venkatesh et al., 2005). Loss of NgR2 alone is not sufficient to attenuate MAG-elicited neurite outgrowth inhibition. The combined loss of NgR1 and NgR2 results in a significant yet incomplete attenuation of MAG inhibition *in vitro* (Worter et al., 2009).

In vivo, transection injury to the dorsal spinal cord of *NgR1*$^{-/-}$ mice failed to demonstrate improved longitudinal growth of CST axons beyond the lesion site (Kim et al., 2004; Zheng et al., 2005). However, in a separate injury model involving unilateral pyramidotomy, collateral sprouting of uninjured CST axons into the denervated cervical gray matter was enhanced and associated with improved recovery of fine motor skills in the forelimb compared to wild-type controls (Cafferty and Strittmatter, 2006). Furthermore, some degree of regeneration of raphespinal and rubrospinal axons following dorsal hemisection of the spinal cord was seen in *NgR1*$^{-/-}$ mice. In particular, a significant increase in weightbearing postures was reported, most likely mediated in part by raphespinal tract recovery (Kim et al., 2004). In an optic nerve injury model, however, transduction of RGCs with a viral vector that mediates expression of a dominant-negative form of NgR1 (NgR^{DN}) had no effect on axon regeneration. However, when combined with lens injury to activate cell intrinsic growth programs in RGCs, NgR^{DN} significantly enhanced axon regeneration following optic nerve crush (Fischer et al., 2004a).

NgR1 co-receptors

As NgR1 is a GPI-anchored protein, it is predicted to interact with one or several membrane-spanning co-receptors to allow signal transduction across the neuronal plasma membrane following inhibitor binding. It has been proposed that neurite outgrowth inhibition by Nogo-66, MAG, and OMgp is mediated by a multi-component receptor complex, which includes NgR1, the transmembrane LRR protein Lingo-1, and a member of the tumor necrosis factor (TNF) receptor superfamily, either $p75^{NTR}$ or TROY (Mi et al., 2004; Park et al., 2005; Shao et al., 2005; Wang et al., 2002a; Yamashita et al., 2002). *In vitro*, Lingo-1 is an essential functional component of the NgR1/$p75^{NTR}$ complex, and Lingo-1 has been shown to associate with both molecules *in vivo* (Llorens et al., 2008; Mi et al., 2004). Furthermore, treatment of rats with a Lingo-1 antagonist (Lingo-1-Fc), which inhibits the binding of Lingo-1 to NgR1, significantly improves functional recovery and promotes axonal sprouting following dorsal or lateral hemisection of the spinal cord (Ji et al., 2006).

Interestingly, neuronal expression of $p75^{NTR}$ and TROY is quite restricted in the mature nervous system and absent from several neuronal cell types strongly inhibited by myelin (Barrette et al., 2007; Park et al., 2005; Roux and Barker, 2002). Furthermore, the importance of $p75^{NTR}$ for neurite outgrowth inhibition is neuronal cell type dependent. In DRG neurons, loss of $p75^{NTR}$ results in longer process outgrowth on substrate-bound CNS myelin or membrane-bound MAG. Myelin or MAG inhibition of CGNs, on the other hand, does not depend on $p75^{NTR}$ (Venkatesh et al., 2007; Zheng et al., 2005). $p75^{NTR}$ specifically interacts with NgR1 and is required for the inhibitory activity of the myelin inhibitors in select neuronal cell types (Park et al., 2005; Wang et al., 2002a; Yamashita et al., 2002). It has been shown that binding of MAG to certain neuronal cell types induces α- and then γ-secretase proteolytic cleavage of $p75^{NTR}$ in a protein kinase C (PKC)-dependent manner. Cleavage by γ-secretase releases the intracellular

domain of $p75^{NTR}$, which is necessary for RhoA activation and, in turn, initiates the downstream steps that inhibit axonal growth (Domeniconi et al., 2005). In *$p75^{NTR-/-}$* mice, however, no significant improvement in the regeneration of corticospinal tract axons was observed following a dorsal column lesion to the spinal cord (Song et al., 2004; Zheng et al., 2005).

Paired immunoglobulin-like receptor B

Paired immunoglobulin-like receptor B (PirB) is a member of the leukocyte immunoglobulin receptor (LIR) subfamily with known regulatory functions in innate and adaptive immune responses. PirB is a negative regulator of immune cell activation and a receptor for major histocompatibility complex (MHC) class I molecules (Takai, 2005). Importantly, PirB is not only expressed by cells of the immune system but is also detected in the CNS. Initial studies revealed expression of PirB in the neocortex, CGNs, and to a lesser extent in pyramidal neurons of the hippocampus (Syken et al., 2006). As discussed below, neural PirB has been implicated in limiting nervous system plasticity in the healthy CNS (Syken et al., 2006).

More recently, PirB was identified as a novel, high-affinity receptor for myelin inhibitors (Atwal et al., 2008). *In vitro*, PirB acts as a growth-inhibitory receptor for Nogo-66, MAG, and OMgp. Primary neurons isolated from *$PirB^{-/-}$* mice, or wild-type neurons cultured in the presence of a PirB function-blocking antibody, extend significantly longer neurites when plated on substrate-bound crude CNS myelin or individual inhibitors compared to wild-type neurons or neurons treated with a control antibody (Atwal et al., 2008). This finding stands in contrast to NgR1 loss of function, which is not sufficient to attenuate longitudinal neurite outgrowth inhibition on substrate-bound CNS myelin or individual myelin inhibitors (Chivatakarn et al., 2007; Zheng et al., 2005). Interestingly, *$NgR1^{-/-}$* neurons treated with a PirB function-blocking

antibody grow longer neurites on CNS myelin substrate than wild-type neurons treated with a PirB function-blocking antibody. This suggests that NgR1 and PirB collaborate in signaling myelin inhibition of neurite outgrowth (Atwal et al., 2008). As is the case for NgR1, loss of PirB renders growth cones of DRG neurons resistant to Nogo-66-elicited growth cone collapse. Collectively, these *in vitro* studies show that PirB and NgR1 are both mediators of the acute growth cone collapsing activity of myelin inhibitors, while PirB (but not NgR1) is also required for neurite outgrowth inhibition on substrate-bound myelin inhibitors.

Recent *in vivo* studies have shown that genetic deletion of PirB does not result in enhanced RGC regeneration following optic nerve crush injury (Fujita et al., 2011). Following traumatic brain injury to the sensorimotor cortex in $PirB^{-/-}$ mice, no axonal sprouting in the corticospinal or corticorubral tracts, or functional recovery in various motor tests, is noted (Omoto et al., 2010). In a dorsal hemisection model of SCI, $PirB^{-/-}$ mice show no enhanced CST regeneration or sprouting, and no improvement in hindlimb motor function (Nakamura et al., 2011).

Gangliosides and β1-integrin in MAG-mediated inhibition

In addition to its interactions with NgR1, NgR2, and PirB, MAG associates in a sialic acid-dependent manner with complex brain gangliosides, including GD1a and GT1b (Collins et al., 1997; Yang et al., 1996). The functional significance of the MAG/ganglioside interaction for neurite outgrowth inhibition was originally assayed by comparing neurite length of CGNs deficient for GalNAcT, an enzyme in the biosynthetic pathway for gangliosides, to wild-type CGNs. GalNAcT-deficient CGNs show enhanced neurite outgrowth in the presence of substrate-adsorbed MAG or myelin (Vyas et al., 2002). In other cell types, including DRG

neurons and RGCs, gangliosides are largely dispensable for MAG inhibition (Mehta et al., 2007; Venkatesh et al., 2007). More recently, β1-integrin has also been reported to interact with MAG through a direct association with the MAG RGD motif. β1-integrin mediates MAG-induced growth cone turning responses in both hippocampal and cerebellar neurons, independent of NgRs (Goh et al., 2008).

MAG employs different mechanisms to inhibit neurite outgrowth of various cell types *in vitro*. Loss of complex gangliosides or enzymatic removal of terminal sialic acids is sufficient to antagonize MAG inhibition of CGNs. However, neither removal of terminal sialic acids nor genetic ablation of NgR1 is sufficient to attenuate MAG inhibition of RGCs cultured on cell lines expressing MAG. The combined loss of terminal sialic acids and NgR1 in RGCs, however, leads to a significant decrease in MAG inhibition (Venkatesh et al., 2007). Similarly, combined pharmacological blockade of ganglioside biosynthesis and NgR1 antagonism leads to significantly more neuronal growth of DRG neurons cultured on substrate-adsorbed MAG than either treatment alone (Mehta et al., 2007). Taken together, these studies strongly argue for the existence of cell type-specific mechanisms for MAG inhibition. Furthermore, there appears to be a significant degree of redundancy among different MAG receptor systems (Mehta et al., 2007; Venkatesh et al., 2007). If myelin-associated inhibitors employ cell type-specific mechanisms to block regenerative axonal growth *in vivo*, this observation may have important implications for the development of treatment strategies aimed at overcoming myelin inhibition.

1.3.3 Intracellular Signaling Pathways for Neurite Outgrowth Inhibition

Rho/ROCK and downstream signaling

In order to exert their inhibitory effects, myelin inhibitor/receptor complexes have to trigger specific signaling cascades that regulate neuronal actin and microtubule dynamics. Our understanding of the mechanisms by which this is accomplished, including the molecules and signaling pathways involved, is still incomplete; however, some key components have been identified (**Figure 1.2**). Several studies show that the activation of RhoA, a member of the Rho family of small GTPases, is necessary for the inhibitory activity of several growth-inhibitory cues, including MAG, Nogo-66, and OMgp (McKerracher and Higuchi, 2006; Schmandke and Strittmatter, 2007). RhoA protein can be inactivated by ADP ribosylation via C3 transferase of *Clostridium botulinum*. Inactivation of RhoA with C3 promotes neurite outgrowth on CNS myelin substrate *in vitro* (Dergham et al., 2002; Lehmann et al., 1999). The combination of C3 treatment and lens injury, which activates the intrinsic growth state of RGCs, enhances regeneration of optic nerve axons following crush injury (Fischer et al., 2004b). Blocking of the RhoA downstream effector Rho-kinase (ROCK) with Y-27632, a pharmacological inhibitor of ROCK1 and ROCK2, prevents myelin-induced growth cone collapse and neurite outgrowth inhibition (Borisoff et al., 2003; Fournier et al., 2003). Furthermore, SCI in *ROCK2*$^{-/-}$ mice leads to enhanced growth of raphespinal and corticospinal axons into the lesion site (Duffy et al., 2009).

If RhoA and ROCK are critical signaling intermediates for myelin-mediated inhibition, what downstream effectors do they regulate? Recently, it has been shown that the phosphorylation status of cofilin, which controls actin dynamics through the depolymerization of F-actin, is regulated by Nogo-66 (Hsieh et al., 2006). The switch between the active (dephosphorylated) and inactive (phosphorylated) state of cofilin is controlled in part by the LIM kinase (LIM) and the phosphatase Slingshot (SSH). Nogo-66 signals through LIM and SSH in a

ROCK-dependent manner (Hsieh et al., 2006). In addition to regulating actin dynamics, myelin-associated inhibitors also regulate the assembly of microtubules. The collapsin response mediator protein-2 (CRMP-2), which promotes microtubule assembly during axon growth, is inactivated, and microtubule levels are downregulated, in postnatal rat cerebellar neurons upon treatment with MAG. Furthermore, expression of dominant negative CRMP-2 mimics the effect of MAG *in vitro* (Mimura et al., 2006). Myelin inhibitors have also been shown to regulate the cytoskeleton through CRMP-4b, as Nogo-66 increases the association between CRMP-4b and RhoA. Furthermore, siRNA knockdown of CRMP-4, or the use of a competitive peptide inhibitor that interferes with the CRMP4b/RhoA complex, promotes neurite outgrowth on myelin (Alabed et al., 2007). More recently, the mechanism by which Nogo regulates the CRMP4b/RhoA association has been shown to include GSK-3β. Nogo induces the phosphorylation and inactivation of GSK-3β, which leads to the dephosphorylation of CRMP-4b and the subsequent increase in CRMP-4b/RhoA complex formation (Alabed et al., 2010). In support of this relationship, GSK-3β has also been shown to phosphorylate and inactivate the CRMP-4b-related molecule, CRMP-2 (Yoshimura et al., 2005).

Crosstalk between myelin inhibitor and neurotrophin pathways

Members of the neurotrophin family of growth factors and their downstream signaling pathways have been shown to attenuate the action of myelin inhibitors *in vitro* and *in vivo*. Local infusion of neurotrophins increases regenerative sprouting of corticospinal and rubrospinal tract fibers following transection to the adult rat spinal cord (Kobayashi et al., 1997; Lu and Tuszynski, 2008; Schnell et al., 1994). In particular, NT-3, and to a lesser extent nerve growth factor (NGF), has a moderate but significant effect on CST axon regeneration, while brain-

derived neurotrophic factor (BDNF) enhances rubrospinal tract axon regeneration (Kobayashi et al., 1997; Schnell et al., 1994). Of particular interest is the "priming effect" of neurotrophins toward neurons. Pretreatment of sensory or cerebellar neurons with neurotrophins renders these cells non-responsive to the inhibitory action of myelin *in vitro* (Cai et al., 1999). BDNF priming for 24 hours overrides MAG inhibition by triggering signaling cascades that lead to elevated levels of intracellular cyclic adenosine monophosphate (cAMP), a signaling intermediate previously shown to profoundly alter neuronal responses to inhibitory guidance cues in developing neurons (Song et al., 1997). It has been proposed that binding of neurotrophins to tropomyosin receptor kinase (Trk) receptors leads to activation of the extracellular signal-regulated kinases (Erk1/2), which inhibit phosphodiesterase 4 (PDE4), an enzyme responsible for cAMP hydrolysis, thereby leading to elevated cAMP-PKA signaling (Gao et al., 2003; Hannila and Filbin, 2008). Consistent with this model, a dominant negative form of Erk blocks the ability of BDNF to overcome MAG inhibition of CGNs (Gao et al., 2003). Collectively, these studies show that pretreatment of primary neurons with neurotrophins leads to a lasting switch in their growth behavior that renders them resistant to myelin inhibitors.

As mentioned above, there is an age-dependent switch from MAG growth promotion to growth inhibition for several neuronal cell types. This switch coincides with a decrease in endogenous cAMP levels (Cai et al., 2001). Studies have shown that elevation of cAMP levels in older retinal ganglion neurons attenuates CNS myelin- and MAG-mediated inhibition of neurite outgrowth and that, *in vivo*, the ability of neonatal spinal axons to regenerate following injury is dependent on the cAMP downstream effector, PKA (Cai et al., 2001). The elevation of cAMP activates the transcription factor, cAMP-response element-binding protein (CREB), which is necessary and sufficient for overcoming MAG-mediated inhibition and encouraging

regeneration *in vivo* (Gao et al., 2004). Activation of CREB leads to increased expression of a variety of genes, including arginase I and interleukin-6 (IL-6), both of which produce proteins that can overcome the inhibitory effects of myelin (Cai et al., 2002; Cao et al., 2006; Gao et al., 2004). These proteins are potential therapeutic targets following CNS injury, as are calcium/calmodulin-dependent kinase IV (CaMKIV) and spermidine, which also feed into this cAMP-dependent pathway (Deng et al., 2009; Spencer et al., 2008). Recently, a transcriptional inducer of arginase I, daidzein, was identified as a small molecular compound that promotes axonal growth *in vitro* and axonal regeneration in the injured optic nerve *in vivo* (Ma et al., 2010).

PI3K-AKT-mTOR pathways

Conditional deletion of the phosphatase and tensin homolog (PTEN) gene in adult mouse RGCs results in robust and long-distance axon regeneration following crush injury to the optic nerve (Park et al., 2008). PTEN is a negative regulator of PI3K, and deletion of PTEN results in enhanced PI3K activation. Of the many pathways downstream of PI3K, the AKT-mTOR cascade is of particular interest, as it was found that long-distance axon regeneration in PTEN-deficient RGCs is largely blocked in the presence of rapamycin, a potent inhibitor of the mammalian target of rapamycin (mTOR) (Park et al., 2008). This suggests that increased activation of the AKT-mTOR pathway is necessary to promote axon regeneration in PTEN-deficient RGCs *in vivo*. Consistent with this idea, overexpression of AKT, an activator of mTOR signaling, in axotomized motoneurons enhances axon regeneration *in vivo* at 2-4 weeks post-nerve transection (Namikawa et al., 2000). As is the case for PTEN deletion, conditional ablation of tuberous sclerosis complex 1 (TSC1), a negative regulator of mTOR, also results in

robust regeneration of RGC axons following optic nerve crush injury (Park et al., 2008). Thus, in adult mice, increased activation of the mTOR complex promotes regeneration of RGC axons. More recently, deletion of PTEN has been shown to promote robust regeneration of adult CST axons, as well as compensatory sprouting of uninjured CST axons, following spinal cord lesion. Furthermore, evidence was provided that regenerating CST axons are able to form new synapses caudal to the lesion site (Liu et al., 2010). The mTOR kinase is a well-known regulator of cell growth and size and has been studied for some time in the CNS because of its regulatory role in synaptic plasticity and local translation of synaptic mRNA (Costa-Mattioli et al., 2009; Guertin and Sabatini, 2007). In the regenerating CNS, PI3K-AKT-mTOR is now emerging as a key regulator of a "dormant" neuron intrinsic growth program. When increased activation of the PI3K pathway is combined with other manipulations, including elevation of cAMP levels and intravitreal Zymosan injection (discussed above), RGC axons show even greater long-distance regeneration through the entire optic nerve and beyond the optic chiasm following crush injury (Kurimoto et al., 2010). These combination approaches are quickly becoming some of the most promising regenerative strategies following CNS injury.

While a growing number of studies have demonstrated that mTOR signaling plays an important role in axonal regeneration, injury-induced growth signals are still needed to initiate axonal regeneration. Many of these injury-induced signals, including IL-6, CNTF, LIF, and cardiotrophin-1, activate the Janus kinase (JAK)/signal transducer and activator of the transcription (STAT) pathway. Recently, it was shown that deletion of the suppressor of cytokine signaling 3 (SOCS3) in RGCs enhances regeneration of injured axons in the optic nerve (Smith et al., 2009). SOCS3 is a known negative regulator of the JAK/STAT pathway. Furthermore, enhancing the local production of SOCS3 in rat dorsal spinal cord glia blocks the

upregulation of inflammatory mediators, including IL-6 (Dominguez et al., 2010). Interestingly, a recent study has suggested that while mTOR is involved in maintaining RGCs in an active regenerative state, it does not seem to be critical for the initial transformation of RGCs into this regenerative state upon release of injury-induced signals (Leibinger et al., 2012). This might explain why the combined deletion of PTEN and SOCS3 results in significantly more regeneration following optic nerve crush injury than deletion of either gene alone (Sun et al., 2011).

In the future, it will be of great interest to determine how mTOR is regulated in injured CNS neurons. What are the upstream ligand-receptor systems that negatively regulate mTOR signaling in neurons and what are the protein products subjected to mTOR-regulated translation? Of interest are recent reports showing that inhibitory guidance cues, including ephrins (Nie et al., 2010) and semaphorins (Oinuma et al., 2010), inhibit neurite outgrowth by negative regulation of the PI3K-AKT-mTOR pathway. Furthermore, Nogo and OMgp negatively regulate neurotrophin-induced mTOR signaling in primary cortical neurons (Raiker et al., 2010). This suggests that several classes of growth-inhibitory molecules impinge on the negative regulation of the mTOR pathway. In further support of this, a recent study has shown that association of myelin inhibitors with PirB causes PirB to interact with Trk receptors and recruit Src homology 2-containing protein tyrosine phosphatase (SHP)-1 and SHP-2 to this complex. SHP-1/2 is then able to inactivate Trk receptors by tyrosine dephosphorylation, leading to neurite outgrowth inhibition (Fujita et al., 2011). As Trk receptors activate proteins such as PI3K and AKT, this provides more evidence that myelin inhibitors negatively regulate the mTOR pathway and, more broadly, that they antagonize multiple signaling cascades activated by growth factors.

1.3.4 The Glial Scar and Its Inhibitory Components

Reactive astrogliosis and inflammatory cell activation

In addition to the myelin-derived CNS inhibitors, a major source of growth-inhibitory cues is the glial scar. Within days following CNS injury, a glial scar is formed at the injury site, composed of reactive astrocytes, infiltrating meningeal cells, macrophages, and microglia. Reactive astrocytes are the major cellular component of the scar. Astrocytes become activated and proliferate as a response to CNS injury, upregulating the expression of numerous proteins, including glial fibrillary acidic protein (GFAP), vimentin, fibronectin, laminin, and inhibitory CSPGs (Busch and Silver, 2007; Nash et al., 2009). The inflammatory response to the damaged tissue also activates microglia and oligodendrocyte precursor cells (OPCs), and recruits macrophages to the lesion site. Like reactive astrocytes, microglia and OPCs continue to proliferate and eventually cover the entire lesion site. Activated as a self-protection mechanism, the formation of the glial scar is meant to facilitate wound healing by sealing the injury site, helping to rebuild the blood-brain barrier (BBB), and preventing secondary degeneration of surrounding healthy tissue from the excitotoxic environment and inflammatory attack induced by the damaged tissue (Rolls et al., 2009). It has been shown that targeted elimination of reactive astrocytes after injury causes failure of BBB repair, profound tissue loss, and more severe deficits of motor function (Faulkner et al., 2004). However, the glial scar is a double-edged sword. While it prevents further damage to the CNS parenchyma, it also forms a chemical barrier that contains multiple inhibitors that limit long-distance axon regeneration across the lesion site.

Chondroitin sulfate proteoglycans

The major inhibitors associated with the glial scar are CSPGs. CSPGs belong to a diverse family of membrane-bound and extracellular matrix glycoproteins composed of a protein core covalently linked to specific types of glycosaminoglycan (GAG) side chains. CSPGs are widely expressed throughout the brain and spinal cord. During early development, CSPGs function as repulsive molecules to guide migrating neural crest cells. CSPGs also assist with axonal pathfinding in the visual system and of sensory neurons at the dorsal root entry zone (Becker and Becker, 2002; Kubota et al., 1999; Pindzola et al., 1993; Snow et al., 1990a). CSPGs are highly expressed in perineuronal nets (PNNs) of various neuronal populations to restrict growth and plasticity in the adult brain (Kwok et al., 2008). Neural CSPGs with known inhibitory activities include members of the lectican family (aggrecan, brevican, neurocan, and versican), phosphacan, and NG2 (Fidler et al., 1999; Pizzorusso et al., 2002). It is well established that CSPGs can induce growth cone collapse and strongly inhibit neurite outgrowth of various types of neurons *in vitro* (Braunewell et al., 1995; Dou and Levine, 1994; McKeon et al., 1991; Ughrin et al., 2003; Yamada et al., 1997).

Following injury, the levels of many CSPGs are dramatically upregulated in the glial scar (Jones et al., 2003; McKeon et al., 1995). Aggrecan, neurocan, and phosphacan are abundantly expressed by reactive astrocytes, whereas NG2 is primarily produced by macrophages and hypertrophic OPCs (Dawson et al., 2000; Jones et al., 2002). However, the inhibitory effect of some CSPGs, such as NG2, largely depends on the cellular context. A recent study has shown that certain cells in the glial scar can actually provide a permissive substrate to stabilize the degenerating sensory axons that are under macrophage attack (Busch et al., 2010). Although this axon-stabilizing effect is mainly due to high levels of the growth-promoting molecules laminin

and fibronectin, these cells also express NG2 (Busch et al., 2010). Thus, NG2 is expressed on both the macrophages that attack axons and the cells that stabilize them. This indicates that the inhibitory effect of NG2 can be balanced by other growth-promoting molecules. In support of this, substrate-bound NG2 has been shown to lose its inhibitory effect on DRG neurons when co-coated with L1, another growth-promoting molecule (Dou and Levine, 1994).

It is well established that the inhibitory activity of CSPGs is primarily mediated by their GAG chains, as this inhibitory action is largely abrogated by treatment with chondroitinase ABC (Ch'aseABC), a bacterial enzyme that selectively digests CS-GAG chains. However, some inhibitory activity is thought to be associated with the protein core. NG2, for example, inhibits neurite outgrowth of cultured cerebellar and DRG neurons in the absence of GAG chains (Ughrin et al., 2003). *In vitro* studies have shown that when treated with Ch'aseABC, several neuronal populations grow longer neurites on either CSPG-coated substrate or injured CNS tissue sections (McKeon et al., 1995; Sango et al., 2003; Zuo et al., 1998). *In vivo*, administration of Ch'aseABC directly into the injury site leads to an enhancement of axon regeneration for severed CST fibers and central fibers of sensory neurons in the spinal cord (Bradbury et al., 2002) (**Figure 1.3b**). Axons from several other neuronal populations, including nigrostriatal (Moon et al., 2001), reticulospinal (Garcia-Alias et al., 2011), and serotonergic (Barritt et al., 2006; Fouad et al., 2005; Garcia-Alias et al., 2009; Tom et al., 2009) respond to Ch'aseABC treatment as well. Based on these observations, Ch'aseABC treatments are now being developed as a therapeutic strategy to promote axon regeneration following SCI.

Although the inhibitory function of CSPGs was established more than 2 decades ago, the underlying mechanisms of how CSPGs exert their growth-inhibitory action toward neurons remained largely unknown until recently. The laboratory of John Flanagan identified the

receptor protein tyrosine phosphatase sigma (RPTPσ), a member of the leukocyte antigen-related (LAR) subfamily, as the first neuronal receptor for the inhibitory action of aggrecan and neurocan (Shen et al., 2010). The extracellular domain of RPTPσ is composed of three Ig-like repeats and eight fibronectin type III (FNIII)-like repeats. RPTPσ binds to CSPGs directly, and the interaction site of RPTPσ with CS-GAG chains has been mapped to the first Ig-like domain of RPTPσ. Furthermore, this interaction is sensitive to Ch'aseABC treatment (Shen et al., 2010). Interestingly, two other LAR family members, LAR and RPTPδ, also share the same GAG-binding motif within the Ig-like repeats, suggesting some degree of functional redundancy among LAR family members in signaling CSPG inhibitory responses (Duan and Giger, 2010). Indeed, a recent study has confirmed LAR as a functional receptor for versican and neurocan, with the first Ig-like domain of LAR being important for binding (Fisher et al., 2011). Similar to Ch'aseABC treatment, functional ablation of *Ptprs*, the gene encoding RPTPσ, promotes neurite outgrowth in the presence of CSPGs *in vitro* and enhances axonal regeneration into CSPG-rich scar tissue following SCI *in vivo* (Fry et al., 2009; Shen et al., 2010) (**Figure 1.3b**). Enhanced axon regeneration following injury has been reported previously in *RPTPσ*$^{-/-}$ mice. In the adult PNS, loss of RPTPσ enhances axonal regrowth in the sciatic and facial nerves following injury (McLean et al., 2002; Thompson et al., 2003), whereas in the CNS, loss of RPTPσ promotes axon regeneration in the injured optic nerve (Sapieha et al., 2005). In addition, the use of LAR-targeting peptides in mice with spinal cord transection injuries promotes significant growth of descending serotonergic fibers, as well as locomotor functional recovery (Fisher et al., 2011).

The identification of RPTPσ as a receptor for inhibitory CSPGs provides a mechanistic basis for these previously reported regeneration phenotypes in *RPTPσ*$^{-/-}$ mice (McLean et al., 2002; Sapieha et al., 2005; Thompson et al., 2003). However, what remains unclear are the

downstream signaling pathways of LAR family members that are triggered upon binding of CSPGs. Considerable progress has been made in defining the downstream signaling mechanisms of LAR family members. Some of the known pathways link LAR proteins to the neuronal cytoskeleton and thus are poised to mediate CSPG inhibitory responses. The cytoplasmic portion of LAR family members contains a conserved tandem pair of phosphatase domains. Only the membrane proximal phosphatase domain (D1) is catalytically active, whereas the membrane distal domain (D2) associates with guanine nucleotide exchange factors, as well as the tyrosine kinase Abl and its substrates Ena, β-catenin, and liprin-σ (Stryker and Johnson, 2007). Future studies will need to address how LAR family signaling is linked to molecules already implicated in CSPG inhibition, such as RhoA (Monnier et al., 2003) and PKC isoforms (Sivasankaran et al., 2004). The CSPG/LAR interaction has already been suggested to inactivate AKT and activate the RhoA pathway (Fisher et al., 2011).

Associated inhibitors in the glial scar

In addition to CSPGs, several axon guidance molecules with known inhibitory function are upregulated in the glial scar. These include members of canonical axon guidance molecules belonging to the ephrin and semaphorin gene families (Bolsover et al., 2008). Following CNS injury, increased expression of secreted semaphorins and their receptors has been reported (De Winter et al., 2002; Pasterkamp et al., 1999). The role of secreted semaphorins in limiting axonal regeneration following SCI remains a matter of debate. While pharmacological inhibition of Sema3A was found to enhance regenerative growth of serotonergic fibers (Kaneko et al., 2006), genetic ablation of PlexinA3 and PlexinA4, two major receptors for secreted

semaphorins, does not lead to enhanced regeneration of serotonergic neurons following spinal cord transection injury (Lee et al., 2010b).

1.4 The Physiological Function of CNS Regeneration Inhibitors and Their Receptors

1.4.1 The Prototypic Myelin Inhibitors in Nervous System Development and Maintenance

While most attention has focused on the role of Nogo, MAG, and OMgp during CNS regeneration, comparatively little is known about the physiological function of these proteins in the healthy CNS. Nogo-A, for example, is expressed in developing and mature oligodendrocytes (Huber et al., 2002; Wang et al., 2002c). Functional ablation of the Nogo-A gene results in a transient delay of oligodendrocyte differentiation and myelin sheath formation in the developing optic nerve and cerebellum (Pernet et al., 2008). Additionally, Nogo-A has a role in controlling myelinogenic potential in the developing CNS, as genetic deletion of Nogo-A results in a spatial expansion of myelin *in vivo*. Consistent with this result, remyelination following lysolecithin injection into the adult mouse spinal cord is accelerated in *Nogo-A*$^{-/-}$ mice (Chong et al., 2012). In the CNS, Nogo-A expression is not restricted to oligodendrocytes - Nogo-A is abundantly expressed by different types of developing and mature neurons. Somewhat paradoxically, Nogo-A expression is highest in neurons known best for their high degree of structural plasticity, including principal neurons in the hippocampus and neocortex (Huber et al., 2002). In the developing cortex, loss of Nogo-A/-B/-C accelerates radial cortical migration and leads to delayed tangential migration of GABAergic cortical interneurons from the ganglionic eminence *in vivo*. *In vitro*, Nogo-A/-B/-C-deficient cortical neurons have increased neurite branching and faster polarization compared to control cells (Mathis et al., 2010; Mingorance-Le Meur et al.,

2007). Furthermore, in the PNS, genetic deletion of Nogo-A leads to increased fasciculation and reduced branching of peripheral nerves as they innervate fore- and hindlimbs at embryonic stages (Petrinovic et al., 2010).

The physiological role for MAG in the uninjured mammalian nervous system has been studied in some detail. While MAG has been shown to mediate axon-oligodendrocyte adhesion *in vitro*, analysis of *MAG*$^{-/-}$ mice revealed that MAG is not necessary for CNS or PNS axon myelination *in vivo* (Li et al., 1994; Montag et al., 1994; Quarles, 2007). However, as *MAG*$^{-/-}$ mice age, they exhibit a peripheral neuropathy characterized by degeneration of myelinated axons, decreased axonal caliber, reduced phosphorylation of the neurofilament proteins NFH and NFM, and reduction of neurofilament spacing (Yin et al., 1998). It is known that phosphorylation of neurofilaments increases axonal caliber, and it has been shown that MAG increases phosphorylation of neurofilaments as well as their associated kinases, ERK1/2 and cdk5 (Dashiell et al., 2002). In the CNS, focal swellings and spheroids, as well as decreases in axonal diameter and neurofilament spacing, have been noted in older *MAG*$^{-/-}$ mice. The genetic background of these mice seems to influence the severity of the phenotype (Loers et al., 2004; Pan et al., 2005). Other abnormalities in the absence of MAG have been reported, including an irregular distribution of sodium channels at the nodes of Ranvier, dystrophic oligodendrocytes, the formation of redundant myelin, and doubly myelinated axons (Bartsch, 1996; Marcus et al., 2002; Weiss et al., 2000). These subtle phenotypes suggest that MAG influences axonal maintenance, which is further supported by the fact that MAG promotes axon stability and resistance to degeneration and excitotoxicity in the presence of stresses such as vincristine, acrylamide, kainic acid, and inflammatory insults (Lopez et al., 2011; Nguyen et al., 2009).

1.4.2 CNS Regeneration Inhibitors and Receptors in Synaptic Plasticity

As discussed above, acute perturbation of myelin inhibition has been shown to promote a limited degree of sprouting and axonal regeneration past the injury site following SCI. It is believed that the observed anatomical fiber growth is the cellular basis for improved behavioral outcomes in experimentally-treated animals. Lowering the growth-inhibitory barrier of myelin most likely leads to enhanced neuronal plasticity at multiple spinal and supraspinal levels, including growth of severed axons, compensatory sprouting of uninjured fibers, and more subtle structural rearrangements of neuronal networks directly or indirectly affected by the injury. Because adaptive responses to CNS injury occur at multiple levels, it is difficult to pinpoint the cellular basis of improved behavioral outcomes in spinal cord-injured animals. In the healthy mature CNS, myelin inhibitors and their receptors have been shown to limit structural neuronal plasticity (McGee et al., 2005; Syken et al., 2006). In the developing visual system, experience-dependent refinement of neuronal connectivity is most robust during the "critical period" (CP), a limited time window during which changes in visual input lead to robust adaptive plasticity in the binocular zone of the visual cortex. After the critical period, adaptive responses to changes in visual input are more restricted. In *Nogo-A/-B*$^{-/-}$ mice and mice deficient in NgR1 and PirB, the CP is prolonged into adulthood (McGee et al., 2005; Syken et al., 2006). Remarkably, another class of well-known inhibitors of axonal regeneration, the CSPGs, also limits experience-dependent plasticity in the visual cortex. CSPGs accumulate in PNNs at the end of the CP, and enzymatic degradation of CS-GAG chains is sufficient to reopen the CP in the adult visual cortex (Pizzorusso et al., 2002) (**Figure 1.3a**). Together, these findings strongly suggest that the physiological role of myelin inhibitors and CSPGs in the mature CNS is to restrict neuronal plasticity.

In addition to extracellular growth-inhibitory cues, cessation of experience-dependent plasticity is regulated by the maturation of inhibitory GABAergic circuits (Hensch et al., 1998). Recent evidence suggests that NgR1 not only participates in the regulation of structural neuronal plasticity but also plays an important role in activity-dependent synaptic plasticity (Lee et al., 2008; Raiker et al., 2010). In *NgR1*$^{-/-}$ mice, long-term potentiation (LTP) of synaptic transmission is enhanced in the presence of the neurotrophic factor FGF2 (Lee et al., 2008), and conversely, Nogo-66 and OMgp suppress LTP in an NgR1-dependent manner (Raiker et al., 2010). In acute hippocampal slices, loss of NgR1 impairs long-term depression (LTD) of synaptic transmission (Lee et al., 2008). Because NgR1 expression itself is regulated by activity (Josephson et al., 2003) and has been shown to regulate the shape of dendritic spines (Lee et al., 2008), NgR1 is well suited to link electrical activity to structural changes in mature CNS neurons. In addition, NogoA was recently shown to regulate activity-dependent synaptic strength (Delekate et al., 2011). Based on these observations, it appears likely that antagonism of growth inhibitors in the injured CNS not only facilitates structural neuronal plasticity but also simultaneously lowers the inhibitory tonus in neuronal networks. This is further supported by the growing evidence that myelin-associated inhibitors/CSPGs and their receptors have a critical role in negatively regulating synapse formation in the developing CNS (Horn et al., 2012; Pyka et al., 2011; Wills et al., 2012). Taken together, this suggests that the mechanisms that limit neuronal growth following CNS injury are similar to the mechanisms that negatively regulate synapse formation and plasticity during development.

1.5 Therapeutic Implications and Future Directions

Basic science discoveries continue to identify targets that may lead to the development of new treatment strategies for SCI repair. Because some key mechanisms that block spontaneous repair of severed CNS axons have already been discovered and characterized in some detail, a number of new compounds and treatment strategies are currently being developed for or have already entered clinical trials. Treatment strategies for SCI aimed at reestablishing neuronal connectivity fall broadly into three categories: (1) neutralization of extracellular growth-inhibitory cues by blocking one or several inhibitors of growth; (2) local production or infusion of growth-promoting molecules, cells, or substrates that favor neuronal growth and survival; or (3) activation of "dormant" cell intrinsic growth programs in adult CNS neurons to promote axonal growth and sprouting. Evidence from experiments in spinal cord-injured rodents suggests that some of these strategies may need to be combined in order to maximize anatomical and behavioral outcomes (Bunge 2008; Kadoya et al., 2009; Karimi-Abdolrezaee et al., 2010).

Due to the growth-inhibitory nature of injured adult mammalian CNS tissue, approaches to lower the inhibitory barrier for regenerating axons remain an area of great interest (**Tables 1.2, 1.3, 1.4**). These include a monoclonal antibody directed against the N-terminal portion of Nogo-A (Zorner and Schwab, 2010) and a soluble form of NgR1 (NgR(310)-Fc) (Harvey et al., 2009; MacDermid et al., 2004; Peng et al., 2009; Wang et al., 2006). As anti-Nogo-A and NgR(310)-Fc target different inhibitory epitopes present in CNS myelin, they may have additive effects *in vivo*. A phase I clinical trial involving anti-Nogo-A treatment of subjects with acute SCI has been conducted successfully and is expected to enter phase II (Zorner and Schwab, 2010).

Targeting of glycoproteins, including CSPGs and sialoglycans, has been met with some success in CNS regeneration studies. Local infusion of Ch'aseABC promotes growth of severed

CST axons past the lesion site and also leads to improved functional outcomes (Bradbury et al., 2002). Furthermore, delivery of Taxol, a clinically approved anti-cancer drug that stabilizes microtubules, promotes serotonergic axonal regeneration and functional locomotor recovery following a dorsal hemisection SCI (Hellal et al., 2011). Taxol-mediated microtubule stabilization hinders the nuclear translocation of Smad2/3, a key signaling component for CSPG release following injury. Taxol treatment of the optic nerve also reduces CSPG expression and promotes regeneration of injured RGC axons (Sengottuvel et al., 2011). Recently, it was found that local infusion of *Vibrio cholerae* neuramindase promotes repair following contusion injury to the spinal cord in rats (Mountney et al., 2010). Furthermore, increasing extracellular signals that promote neuronal growth and sprouting has been successful. Local infusion of neurotrophic factors (Blesch and Tuszynski, 2009) or implantation of specific cell types (Bunge and Pearse, 2003; Davies et al., 2008; Radtke et al., 2008) into the injured rodent spinal cord promotes axonal growth of different types of spinal projection neurons. A recent study showed impressive long-distance axonal outgrowth, synapse formation, and behavioral/electrophysiological recovery following grafting of neural stem cells (along with a growth factor cocktail) into transected spinal cords in rodents. Of clinical relevance is the fact that the grafting was performed one or two weeks post-injury and that human neural stem cell grafts were also effective in injured rodent spinal cords (Lu et al., 2012).

In addition to extracellular molecules, intracellular signaling molecules implicated in neuronal growth inhibition are potential targets for therapeutic intervention. The RhoA-ROCK cascade has been extensively studied and shown to be a convergence point for multiple inhibitory signaling pathways. Pharmacological inhibition of both RhoA and ROCK with specific inhibitors has proven to be beneficial for repair following CNS injury. For example,

inhibition of RhoA by C3 transferase promotes axon regeneration in both the crushed optic nerve and hemisected CST (Dergham et al., 2002; Fournier et al., 2003; Lehmann et al., 1999). Moreover, Rho activation was found to mediate apoptotic cell death induced by SCI in a $p75^{NTR}$-dependent manner (Dubreuil et al., 2003). Therefore, C3 may not only promote regeneration of severed axons but also prevent further neuronal cell death following injury. A modified version of C3 with improved membrane permeability, BA-210, has been commercialized under the name Cethrin and is currently being tested in clinical trials (Fehlings et al., 2011). The recent identification of the PI3K-AKT-mTOR signaling pathway as a key regulatory mechanism of neuronal growth in mature neurons (Namikawa et al., 2000; Park et al., 2008; Smith et al., 2009) suggests that additional small molecular compounds can be developed to promote robust axonal growth.

Collectively, there is considerable optimism in the field of nervous system regeneration that robust fiber growth following CNS injury can be accomplished. It remains, however, somewhat less clear to what extent regenerating CNS axons are able to reach pre-injury targets and form functionally meaningful synaptic connections. Direct evidence that long-distance axon regeneration in spinal cord-injured animals contributes to the observed functional improvements is sparse. In one study it was shown that newly grown sensory axons are capable of reaching pre-injury targets and forming new synapses but fail to propagate electrical impulses (Alto et al., 2009). One possible explanation for this lack of efficient propagation of action potentials may be incomplete myelination. If new axons can be grown and connectivity can be reestablished, these axons will need to be myelinated in order to rapidly and faithfully conduct complex electrical impulses. As many human spinal cord injuries are anatomically incomplete and maintain tissue with spared fibers that bypass the injury site (Tuszynski et al., 1999), “reactivation” of these

already existing fibers may be easier to accomplish than regrowing new axons. For patients with complete (or nearly complete) transection of ascending and descending spinal axons, long-distance axon regeneration will be necessary to improve behavioral outcomes following SCI.

1.6 Acknowledgments

Portions of this chapter have been published (see citation below) and permission was received from the editors to use this work as part of a dissertation:

Dickendesher TL, Duan Y, Giger RJ (2013) Chapter 8: axon regeneration. J.L.R. Rubenstein & P. Rakic (editors) Comprehensive Developmental Neuroscience: Cellular Migration and Formation of Neuronal Connections, Amsterdam: Academic Press, pp.151-175.

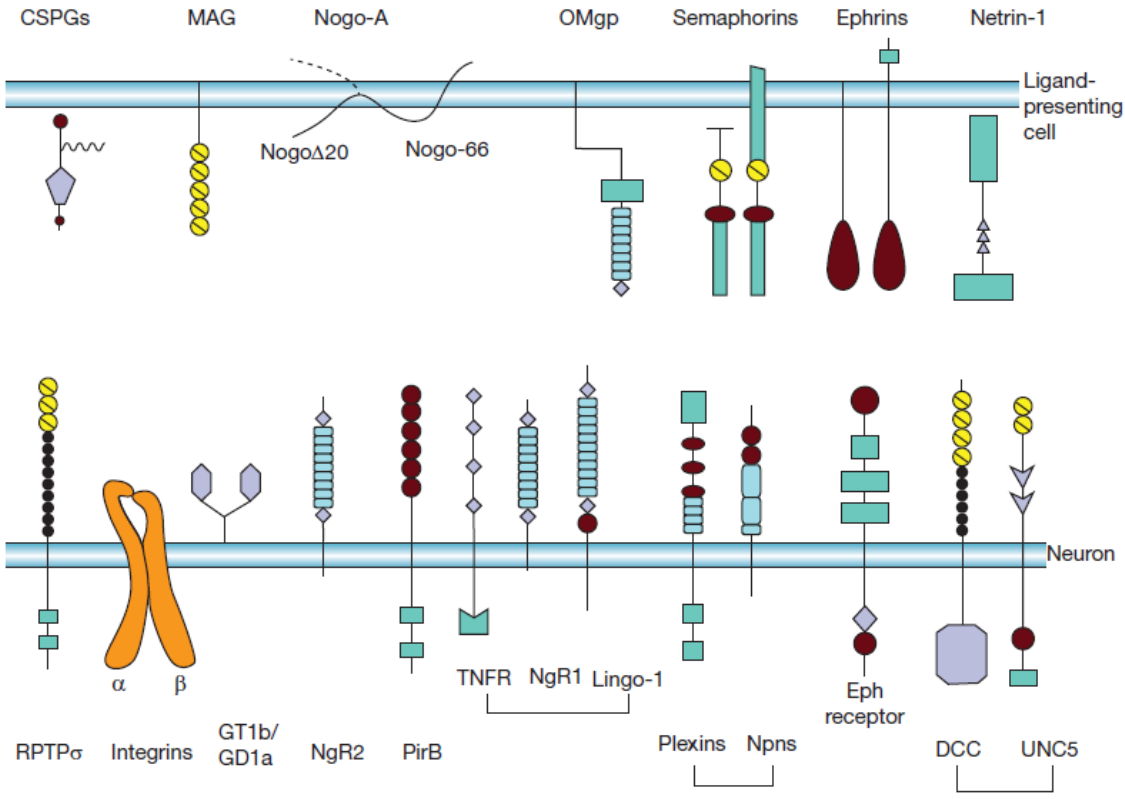

Figure 1.1: The major ligands and receptor complexes involved in CNS neurite outgrowth inhibition. The best characterized outgrowth inhibitors include the prototypic myelin-associated inhibitors (MAG, Nogo-A, and OMgp), CSPGs, and members of the semaphorin, ephrin, and netrin families of axon guidance molecules. MAG (Siglec4a) is a sialic acid-binding lectin containing five Ig-like domains, a transmembrane domain, and a cytoplasmic portion. Nogo-A (RTN4a) is comprised of two distinct inhibitory domains: Nogo-66 and NogoΔ20. NogoΔ20 can be detected extracellularly but is also thought to have a cytoplasmic orientation (dotted line). OMgp is a member of the LRR protein family and is linked via a GPI anchor to the cell surface. MAG, Nogo-A, and OMgp have little structural similarity but share two common axonal receptors: NgR1 and PirB. In some neuronal cell types, NgR1 is thought to form a receptor complex with Lingo-1 and a TNF receptor superfamily member (either $p75^{NTR}$ or TROY). In addition, NgR2 acts as a receptor for MAG but not Nogo-A or OMgp. MAG also forms a complex with the gangliosides GT1b and GD1a, and participates in a functional interaction with integrins. CSPGs, a group of glycoproteins composed of a core protein linked to GAG side chains, interact with RPTPσ and LAR (not shown) to signal neuronal growth inhibition. Both secreted semaphorins and membrane-bound semaphorins, which are glycoproteins containing an amino-terminal semaphorin (sema) domain and a plexin-semaphorin-integrin (PSI) domain, have been implicated in growth inhibition. Plexins are the most prominent semaphorin receptors, while most class 3 semaphorins require neuropilins as obligatory co-receptors. GPI-anchored ephrinAs and transmembrane ephrinBs also act as inhibitors through bidirectional signaling with their Eph receptor tyrosine kinase counterparts. Secreted netrin-1 acts as a myelin-associated inhibitor through the DCC and UNC5 receptors, either alone or in combination.

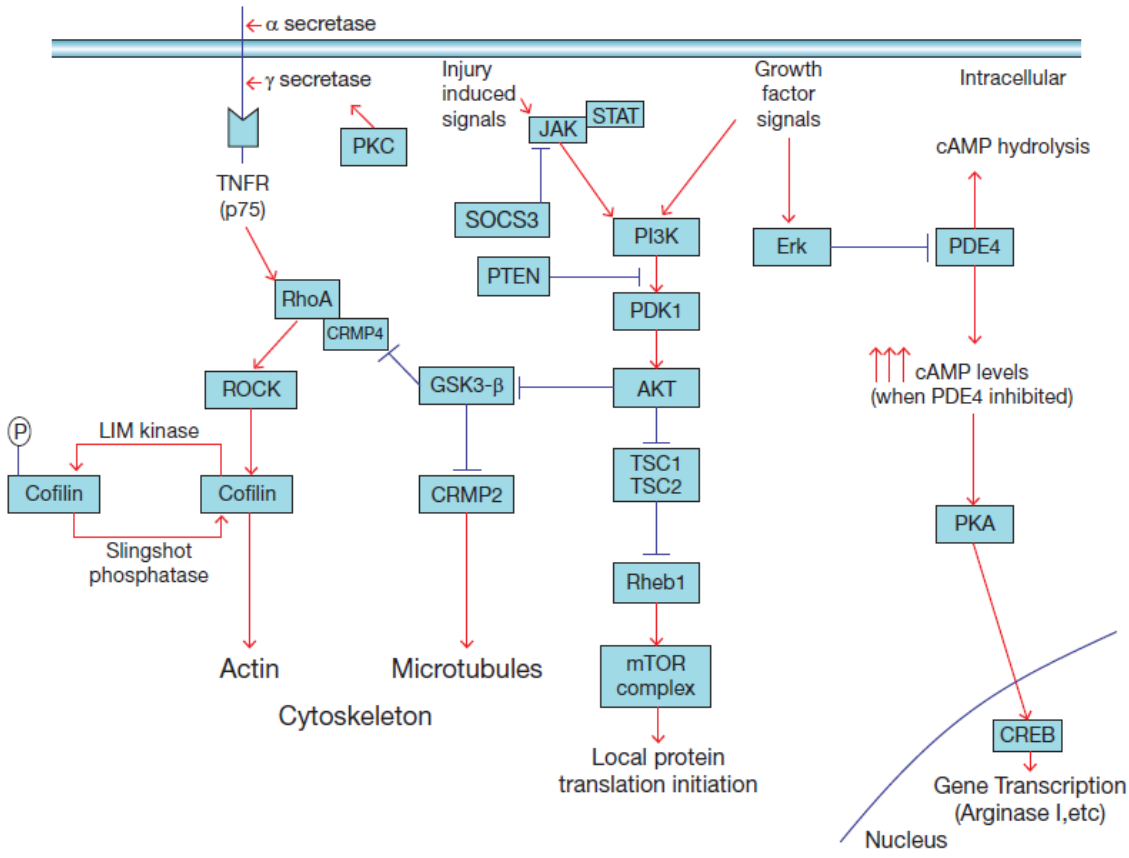

Figure 1.2: The major intracellular signaling pathways involved in CNS neurite outgrowth inhibition. While our understanding of the signaling pathways that mediate neurite outgrowth inhibition is limited, a few major pathways have thus far been implicated. Activation of the Rho/ROCK pathway is necessary for the inhibitory activity of MAG, Nogo-A, and OMgp, and provides a link to the actin cytoskeleton through the control of cofilin phosphorylation. Currently, the only direct link between myelin inhibitor-receptor complexes and RhoA involves the release of RhoA and its subsequent activation following binding of prototypic myelin inhibitors to $p75^{NTR}$. The sequential cleavage of $p75^{NTR}$ by α- and γ-secretases is necessary for RhoA activation. Myelin inhibitors can also regulate the cytoskeleton through the inactivation of CRMP-2 to influence microtubule dynamics or the inactivation of GSK-3β (and dephosphorylation of CRMP-4b) to influence actin dynamics. Additionally, there is crosstalk between myelin inhibitor and neurotrophin pathways, as priming with neurotrophins can block outgrowth inhibition through the activation of Erk and subsequent inhibition of PDE4. This leads to elevated levels of intracellular cAMP, activation of PKA, and initiation of CREB-induced transcription in the nucleus, all of which have been shown to be necessary for release from inhibition. More recently, the PI3K-AKT-mTOR pathway has been implicated in outgrowth inhibition. mTOR complex activation promotes axon regeneration, supported by studies that show enhanced regeneration when proteins that negatively influence mTOR activity (PTEN, TSC1, SOCS3) are deleted.

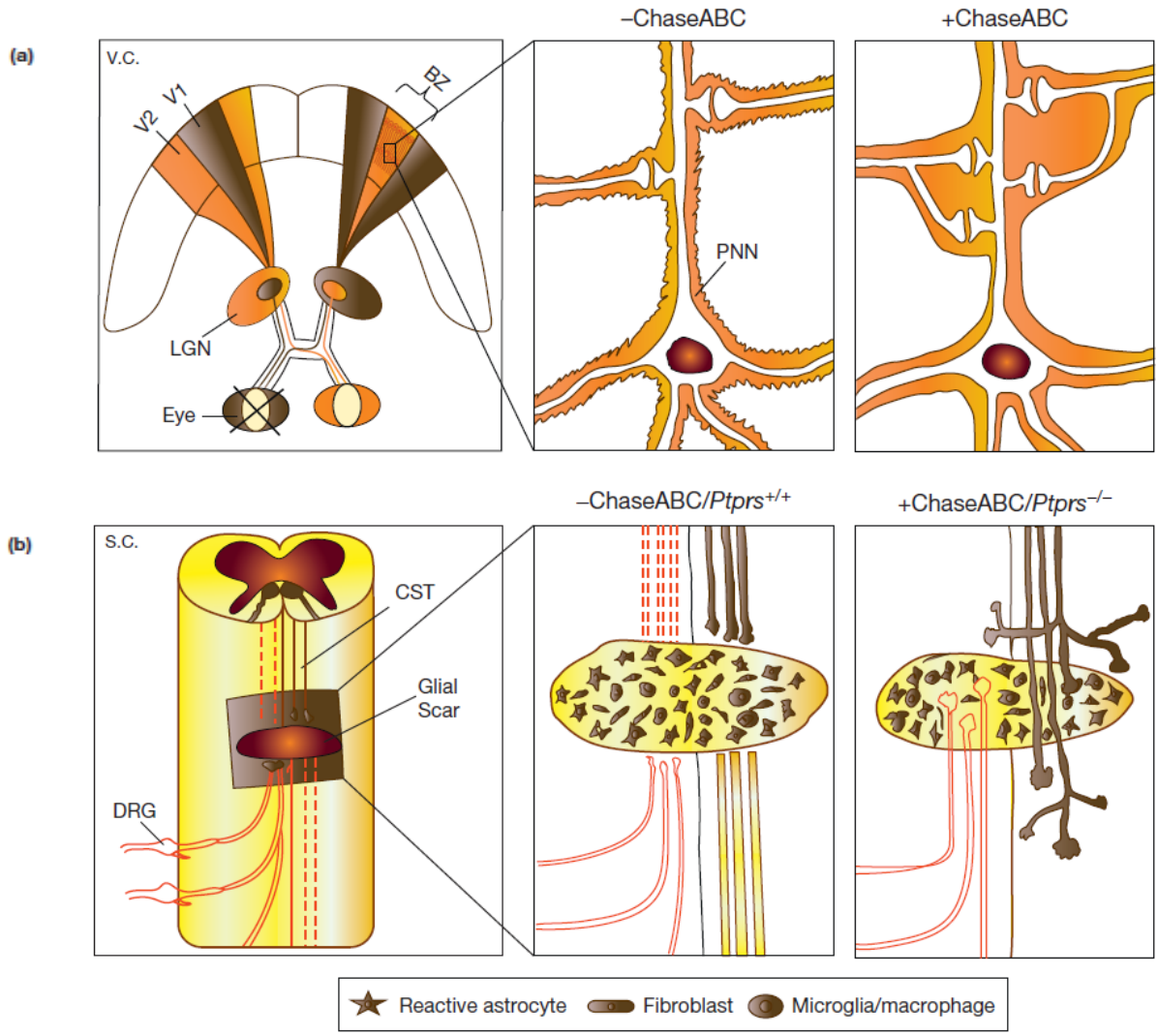

Figure 1.3: The physiological role of CSPGs in ocular dominance (OD) plasticity and their pathological role in axon regeneration inhibition following spinal cord injury (SCI). (**a**) Schematic of the mammalian visual system, showing the visual pathway of the left eye in brown and of the right eye in orange through the lateral geniculate nuclei (LGN) to the primary visual cortex (V1 and V2). The binocular zone (BZ) receives input from both eyes. Monocular deprivation (MD)-induced OD plasticity is extremely limited after the critical period (-ChaseABC). Local infusion of ChaseABC near the BZ of the rat visual cortex is sufficient to reactivate OD plasticity after the closure of the critical period (+ChaseABC). This indicates that CSPGs in perineuronal nets (PNNs) restrict experience-dependent neuronal plasticity in adulthood. Enzymatic degradation of CS-GAG chains removes non-permissive substrates surrounding synapses and presumably facilitates rearrangement and formation of new synapses in favor of the nondeprived eye. v.c = visual cortex. (**b**) Injury to the spinal cord results in axonal damage and formation of a glial scar at the injury site. Injury to the dorsal column severs both descending axons of the corticospinal tract (CST) and ascending axons of dorsal root

ganglion (DRG) neurons. The glial scar is composed of reactive astrocytes, microglia, macrophages, and meningeal fibroblasts, and forms a boundary for regenerating axons. CSPGs are highly upregulated in the glial scar and exert the major inhibitory effect. In wild-type mice with no treatment, regenerating axons stall at the border of scar tissue and show dystrophic end bulbs at their leading tips (-ChaseABC/*Ptprs*$^{+/+}$). Treatment with ChaseABC after SCI leads to various improvements of CST axon regeneration, including enhanced regeneration across the lesion site and increased axonal sprouting before and after the lesion site (+ChaseABC). Similarly, genetic deletion of the CSPG receptor, RPTPσ, allows severed axons to grow deeper into the glial scar tissue (*Ptprs*$^{-/-}$). s.c = spinal cord.

	Peripheral Nervous System (substantial axonal regeneration)	Central Nervous System (limited axonal regeneration)
(1) Environmental Factors		
- Wallerian Degeneration	Myelin debris is cleared rapidly by glial/immune cells	Incomplete and protracted clearance of myelin debris
- Role of Glial Cells	Positive - Schwann cells promote debris clearance, release growth factors, guide axons back to their targets, and remyelinate	Negative - Oligodendrocytes express inhibitory factors and do not aid in the clearance of debris
- Myelin-Associated Inhibitors	Not present or less abundant than in the CNS	Multiple inhibitors are present
- Glial Scar	Not formed	Forms rapidly and contains multiple inhibitory factors
- Growth Factors	Upregulated	Not highly expressed
(2) Intrinsic Growth Programs	Activated	Deficient or downregulated
(3) Secondary Damage	Minimal	Extensive parenchymal destruction

Table 1.1: The key factors that influence axonal regeneration following injury to the adult mammalian peripheral and central nervous system.

Regeneration or Sprouting			
	Method	**Neural Pathway**	**Reference**
Nogo	IN-1 antibody	CST	Schnell, 1990
	IN-1 antibody	CRST, CST, 5HT	Bregman, 1995
	Nogo-A/-B mutant	CST	Kim, 2003
	Nogo-A mutant	CST	Simonen, 2003
	Nogo-A mutant	CST	Dimou, 2006
	Nogo-A/-B mutant; Nogo-A/-B/OMgp/MAG mutant	CST, 5HT	Cafferty, 2010
	Nogo-A/-B/-C/OMgp/MAG mutant	5HT	Lee, 2010a
OMgp	OMgp mutant	5HT	Lee, 2010a
MAG	MAG mutant	5HT	Lee, 2010a
CSPGs	Chondroitinase ABC	NST	Moon, 2001
	Chondroitinase ABC	CST, DC	Bradbury, 2002
	Chondroitinase ABC	5HT	Fouad, 2005
	Chondroitinase ABC	5HT	Barritt, 2006
	Chondroitinase ABC	5HT	Garcia-Alias, 2009
	Chondroitinase ABC	5HT	Tom, 2009
	Chondroitinase ABC	RTST	Garcia-Alias, 2011

Table 1.2: Summary of key studies that demonstrate axon regeneration or sprouting upon targeting of major inhibitory ligands in the injured mammalian CNS. Abbreviations: CRST (coeruleospinal tract axons), CST (corticospinal tract axons), DC (ascending dorsal column axons), NST (nigrostriatal tract axons), RTST (reticulospinal tract axons), 5HT (serotonergic axons).

Regeneration or Sprouting			
	Method	**Neural Pathway**	**Reference**
NgR1	NgR1 mutant	RBST, 5HT	Kim, 2004
	NgR1 ectodomain	5HT	MacDermid, 2004
	NgR1 mutant	CST	Cafferty, 2006
	NgR1 ectodomain	CST, 5HT	Wang, 2006
Lingo-1	Lingo-1 antagonist	CST, RBST	Ji, 2006
RPTPσ	RPTPσ mutant	ON	Sapieha, 2005
	RPTPσ mutant	CST	Fry, 2009
	RPTPσ mutant	CST	Shen, 2010
LAR	LAR-targeting peptides	5HT	Fisher, 2011

Table 1.3: Summary of key studies that demonstrate axon regeneration or sprouting upon targeting of major inhibitory receptors in the injured mammalian CNS. Abbreviations: CST (corticospinal tract axons), ON (optic nerve axons), RBST (rubrospinal tract axons), 5HT (serotonergic axons).

Little or No Regeneration			
	Method	**Neural Pathway**	**Reference**
Nogo	Nogo-A/-B/-C mutant	CST	Zheng, 2003
	Nogo-A/-B/-C mutant	CST	Lee, 2009b
	Nogo-A/-B/-C mutant	CST, 5HT	Lee, 2010a
	Nogo-A/-B/-C/OMgp/MAG mutant	CST	Lee, 2010a
OMgp	OMgp mutant	CST	Ji, 2008
	OMgp/MAG mutant	CST, 5HT	Cafferty, 2010
MAG	MAG mutant	CST, ON	Bartsch, 1995
	MAG mutant	CST	Li, 1996
NgR1	NgR1 dominant negative	ON	Fischer, 2004a
	NgR1 mutant	CST	Kim, 2004
	NgR1 mutant	CST	Zheng, 2005
$p75^{NTR}$	$p75^{NTR}$ mutant	CST	Song, 2004
	$p75^{NTR}$ mutant	CST	Zheng, 2005
PirB	PirB mutant	CRT, CST	Omoto, 2010
	PirB mutant	ON	Fujita, 2011
	PirB mutant	CST	Nakamura, 2011

Table 1.4: Summary of key studies that demonstrate a lack of substantial axon regeneration upon targeting of major inhibitory ligands or receptors in the injured mammalian CNS. Abbreviations: CRT (corticorubral tract axons), CST (corticospinal tract axons), ON (optic nerve axons), 5HT (serotonergic axons).

1.7 Bibliography

Abdesselem H, Shypitsyna A, Solis GP, Bodrikov V, Stuermer CA (2009) No Nogo66- and NgR-mediated inhibition of regenerating axons in the zebrafish optic nerve. J Neurosci 29:15489-15498.

Aguayo AJ, Dickson R, Trecarten J, Attiwell M, Bray GM, Richardson P (1978) Ensheathment and myelination of regenerating PNS fibres by transplanted optic nerve glia. Neurosci Lett 9:97-104.

Aguayo AJ, David S, Bray GM (1981) Influences of the glial environment on the elongation of axons after injury: transplantation studies in adult rodents. J Exp Biol 95:231-240.

Alabed YZ, Pool M, Ong Tone S, Fournier AE (2007) Identification of CRMP4 as a convergent regulator of axon outgrowth inhibition. J Neurosci 27:1702-1711.

Alabed YZ, Pool M, Ong Tone S, Sutherland C, Fournier AE (2010) GSK3β regulates myelin-dependent axon outgrowth inhibition through CRMP4. J Neurosci 30:5635-5643.

Alto LT, Havton LA, Conner JM, Hollis Ii ER, Blesch A, Tuszynski MH (2009) Chemotropic guidance facilitates axonal regeneration and synapse formation after spinal cord injury. Nat Neurosci 12:1106-1113.

Atwal JK, Pinkston-Gosse J, Syken J, Stawicki S, Wu Y, Shatz C, Tessier-Lavigne M (2008) PirB is a functional receptor for myelin inhibitors of axonal regeneration. Science 322:967-970.

Barrette B, Vallieres N, Dube M, Lacroix S (2007) Expression profile of receptors for myelin-associated inhibitors of axonal regeneration in the intact and injured mouse central nervous system. Mol Cell Neurosci 34:519-538.

Barritt AW, Davies M, Marchand F, Hartley R, Grist J, Yip P, McMahon SB, Bradbury EJ (2006) Chondroitinase ABC promotes sprouting of intact and injured spinal systems after spinal cord injury. J Neurosci 26:10856-10867.

Barton WA, Liu BP, Tzvetkova D, Jeffrey PD, Fournier AE, Sah D, Cate R, Strittmatter SM, Nikolov DB (2003) Structure and axon outgrowth inhibitor binding of the Nogo-66 receptor and related proteins. EMBO J 22:3291-3302.

Bartsch U, Bandtlow CE, Schnell L, Bartsch S, Spillmann AA, Rubin BP, Hillenbrand R, Montag D, Schwab ME, Schachner M (1995) Lack of evidence that myelin-associated glycoprotein is a major inhibitor of axonal regeneration in the CNS. Neuron 15:1375-1381.

Bartsch U (1996) Myelination and axonal regeneration in the central nervous system of mice deficient in the myelin-associated glycoprotein. J Neurocytol 25:303-313.

Becker CG, Becker T (2002) Repellent guidance of regenerating optic axons by chondroitin sulfate glycosaminoglycans in zebrafish. J Neurosci 22:842-853.

Benson MD, Romero MI, Lush ME, Lu QR, Henkemeyer M, Parada LF (2005) Ephrin-B3 is a myelin-based inhibitor of neurite outgrowth. Proc Natl Acad Sci 102:10694-10699.

Blesch A, Tuszynski MH (2009) Spinal cord injury: plasticity, regeneration and the challenge of translational drug development. Trends Neurosci 32:41-47.

Bolsover S, Fabes J, Anderson PN (2008) Axonal guidance molecules and the failure of axonal regeneration in the adult mammalian spinal cord. Restor Neurol Neurosci 26:117-130.

Borisoff JF, Chan CC, Hiebert GW, Oschipok L, Robertson GS, Zamboni R, Steeves JD, Tetzlaff W (2003) Suppression of Rho-kinase activity promotes axonal growth on inhibitory CNS substrates. Mol Cell Neurosci 22:405-416.

Bradbury EJ, Moon LD, Popat RJ, King VR, Bennett GS, Patel PN, Fawcett JW, McMahon SB (2002) Chondroitinase ABC promotes functional recovery after spinal cord injury. Nature 416:636-640.

Braunewell KH, Martini R, LeBaron R, Kresse H, Faissner A, Schmitz B, Schachner M (1995) Up-regulation of a chondroitin sulphate epitope during regeneration of mouse sciatic nerve: evidence that the immunoreactive molecules are related to the chondroitin sulphate proteoglycans decorin and versican. Eur J Neurosci 7:792-804.

Bregman BS, Kunkel-Bagden E, Schnell L, Dai HN, Gao D, Schwab ME (1995) Recovery from spinal cord injury mediated by antibodies to neurite growth inhibitors. Nature 378:498-501.

Bundesen LQ, Scheel TA, Bregman BS, Kromer LF (2003) Ephrin-B2 and EphB2 regulation of astrocyte-meningeal fibroblast interactions in response to spinal cord lesions in adult rats. J Neurosci 23:7789-7800.

Bunge MB, Pearse DD (2003) Transplantation strategies to promote repair of the injured spinal cord. J Rehabil Res Dev 40:55-62.

Bunge MB (2008) Novel combination strategies to repair the injured mammalian spinal cord. J Spinal Cord Med 31:262-269.

Busch SA, Silver J (2007) The role of extracellular matrix in CNS regeneration. Curr Opin Neurobiol 17:120-127.

Busch SA, Horn KP, Cuascut FX, Hawthorne AL, Bai L, Miller RH, Silver J (2010) Adult NG2+ cells are permissive to neurite outgrowth and stabilize sensory axons during macrophage-induced axonal dieback after spinal cord injury. J Neurosci 30:255-265.

Cafferty WB, Strittmatter SM (2006) The Nogo-Nogo receptor pathway limits a spectrum of adult CNS axonal growth. J Neurosci 26:12242-12250.

Cafferty WB, Kim JE, Lee JK, Strittmatter SM (2007) Response to correspondence: Kim et al., "axon regeneration in young adult mice lacking Nogo-A/B." Neuron 38, 187-199. Neuron 54:195-199.

Cafferty WB, Duffy P, Huebner E, Strittmatter SM (2010) MAG and OMgp synergize with Nogo-A to restrict axonal growth and neurological recovery after spinal cord trauma. J Neurosci 30:6825-6837.

Cai D, Shen Y, De Bellard M, Tang S, Filbin MT (1999) Prior exposure to neurotrophins blocks inhibition of axonal regeneration by MAG and myelin via a cAMP-dependent mechanism. Neuron 22:89-101.

Cai D, Qiu J, Cao Z, McAtee M, Bregman BS, Filbin MT (2001) Neuronal cyclic AMP controls the developmental loss in ability of axons to regenerate. J Neurosci 21:4731-4739.

Cai D, Deng K, Mellado W, Lee J, Ratan RR, Filbin MT (2002) Arginase I and polyamines act downstream from cyclic AMP in overcoming inhibition of axonal growth MAG and myelin in vitro. Neuron 35:711-719.

Cao Z, Gao Y, Bryson JB, Hou J, Chaudhry N, Siddiq M, Martinez J, Spencer T, Carmel J, Hart RB, Filbin MT (2006) The cytokine interleukin-6 is sufficient but not necessary to mimic the peripheral conditioning lesion effect on axonal growth. J Neurosci 26:5565-5573.

Caroni P, Schwab ME (1988a) Two membrane protein fractions from rat central myelin with inhibitory properties for neurite growth and fibroblast spreading. J Cell Biol 106:1281-1288.

Caroni P, Schwab ME (1988b) Antibody against myelin-associated inhibitor of neurite growth neutralizes nonpermissive substrate properties of CNS white matter. Neuron 1:85-96.

Chen MS, Huber AB, van der Haar ME, Frank M, Schnell L, Spillmann AA, Christ F, Schwab ME (2000) Nogo-A is a myelin-associated neurite outgrowth inhibitor and an antigen for monoclonal antibody IN-1. Nature 403:434-439.

Chivatakarn O, Kaneko S, He Z, Tessier-Lavigne M, Giger RJ (2007) The Nogo-66 receptor NgR1 is required only for the acute growth cone-collapsing but not the chronic growth-inhibitory actions of myelin inhibitors. J Neurosci 27:7117-7124.

Chong SY, Rosenberg SS, Fancy SP, Zhao C, Shen YA, Hahn AT, McGee AW, Xu X, Zheng B, Zhang LI, Rowitch DH, Franklin RJ, Lu QR, Chan JR (2012) Neurite outgrowth inhibitor Nogo-A establishes spatial segregation and extent of oligodendrocyte myelination. Proc Natl Acad Sci U S A 109:1299-1304.

Cohen RI, Rottkamp DM, Maric D, Barker JL, Hudson LD (2003) A role for semaphorins and neuropilins in oligodendrocyte guidance. J Neurochem 85:1262-1278.

Collins BE, Yang LJ, Mukhopadhyay G, Filbin MT, Kiso M, Hasegawa A, Schnaar RL (1997) Sialic acid specificity of myelin-associated glycoprotein binding. J Biol Chem 272:1248-1255.

Costa-Mattioli M, Sossin WS, Klann E, Sonenberg N (2009) Translational control of long-lasting synaptic plasticity and memory. Neuron 61:10-26.

Dashiell SM, Tanner SL, Pant HC, Quarles RH (2002) Myelin-associated glycoprotein modulates expression and phosphorylation of neuronal cytoskeletal elements and their associated kinases. J Neurochem 81:1263-1272.

Davies JE, Proschel C, Zhang N, Noble M, Mayer-Proschel M, Davies SJ (2008) Transplanted astrocytes derived from BMP- or CNTF-treated glial-restricted precursors have opposite effects on recovery and allodynia after spinal cord injury. J Biol 7:24.

Davies SJ, Goucher DR, Doller C, Silver J (1999) Robust regeneration of adult sensory axons in degenerating white matter of the adult rat spinal cord. J Neurosci 19:5810-5822.

Dawson MR, Levine JM, Reynolds R (2000) NG2-expressing cells in the central nervous system: are they oligodendroglial progenitors? J Neurosci Res 61:471-479.

De Winter F, Oudega M, Lankhorst AJ, Hamers FP, Blits B, Ruitenberg MJ, Pasterkamp RJ, Gispen WH, Verhaagen J (2002) Injury-induced class 3 semaphorin expression in the rat spinal cord. Exp Neurol 175:61-75.

DeBellard ME, Tang S, Mukhopadhyay G, Shen YJ, Filbin MT (1996) Myelin-associated glycoprotein inhibits axonal regeneration from a variety of neurons via interaction with a sialoglycoprotein. Mol Cell Neurosci 7:89-101.

Delekate A, Zagrebelsky M, Kramer S, Schwab ME, Korte M (2011) NogoA restricts synaptic plasticity in the adult hippocampus on a fast time scale. Proc Natl Acad Sci U S A 108:2569-2574.

Deng K, He H, Qiu J, Lorber B, Bryson JB, Filbin MT (2009) Increased synthesis of spermidine as a result of upregulation of arginase I promotes axonal regeneration in culture and in vivo. J Neurosci 29:9545-9552.

Dent EW, Barnes AM, Tang F, Kalil K (2004) Netrin-1 and semaphorin 3A promote or inhibit cortical axon branching, respectively, by reorganization of the cytoskeleton. J. Neurosci 24:3002-3012.

Dergham P, Ellezam B, Essagian C, Avedissian H, Lubell WD, McKerracher L (2002) Rho signaling pathway targeted to promote spinal cord repair. J Neurosci 22:6570-6577.

Dimou L, Schnell L, Montani L, Duncan C, Simonen M, Schneider R, Liebscher T, Gullo M, Schwab ME (2006) Nogo-A-deficient mice reveal strain-dependent differences in axonal regeneration. J Neurosci 26:5591-5603.

Dodd DA, Niederoest B, Bloechlinger S, Dupuis L, Loeffler JP, Schwab ME (2005) Nogo-A, -B, and -C are found on the cell surface and interact together in many different cell types. J Biol Chem 280:12494-12502.

Domeniconi M, Cao Z, Spencer T, Sivasankaran R, Wang K, Nikulina E, Kimura N, Cai H, Deng K, Gao Y, He Z, Filbin M (2002) Myelin-associated glycoprotein interacts with the Nogo66 receptor to inhibit neurite outgrowth. Neuron 35:283-290.

Domeniconi M, Zampieri N, Spencer T, Hilaire M, Mellado W, Chao MV, Filbin MT (2005) MAG induces regulated intramembrane proteolysis of the p75 neurotrophin receptor to inhibit neurite outgrowth. Neuron 46:849-855.

Dominguez E, Mauborgne A, Mallet J, Desclaux M, Pohl M (2010) SOCS3-mediated blockade of JAK/STAT3 signaling pathway reveals its major contribution to spinal cord neuroinflammation and mechanical allodynia after peripheral nerve injury. J Neurosci 30:5754-5766.

Dou CL, Levine JM (1994) Inhibition of neurite growth by the NG2 chondroitin sulfate proteoglycan. J Neurosci 14:7616-7628.

Duan Y, Giger RJ (2010) A new role for RPTPsigma in spinal cord injury: signaling chondroitin sulfate proteoglycan inhibition. Sci Signal 3:pe6.

Dubreuil CI, Winton MJ, McKerracher L (2003) Rho activation patterns after spinal cord injury and the role of activated Rho in apoptosis in the central nervous system. J Cell Biol 162:233-243.

Duffy P, Schmandke A, Sigworth J, Narumiya S, Cafferty WB, Strittmatter SM (2009) Rho-associated kinase II (ROCKII) limits axonal growth after trauma within the adult mouse spinal cord. J Neurosci 29:15266-15276.

Duffy P, Wang X, Siegel CS, Tu N, Henkemeyer M, Cafferty WB, Strittmatter SM (2012) Myelin-derived ephrinB3 restricts axonal regeneration and recovery after adult CNS injury. Proc Natl Acad Sci U S A 109:5063-5068.

Fabes J, Anderson P, Brennan C, Bolsover S (2007) Regeneration-enhancing effects of EphA4 blocking peptide following corticospinal tract injury in adult rat spinal cord. Eur J Neurosci 26:2496-2505.

Faulkner JR, Herrmann JE, Woo MJ, Tansey KE, Doan NB, Sofroniew MV (2004) Reactive astrocytes protect tissue and preserve function after spinal cord injury. J Neurosci 24:2143-2155.

Fehlings MG, Theodore N, Harrop J, Maurais G, Kuntz C, Shaffrey CI, Kwon BK, Chapman J, Yee A, Tighe A, McKerracher L (2011) A phase I/IIa clinical trial of a recombinant Rho protein antagonist in acute spinal cord injury. J Neurotrauma 28:787-796.

Ferraro G B, Morrison CJ, Overall CM, Strittmatter SM, Fournier AE (2011) Membrane-type matrix metalloproteinase-3 regulates neuronal responsiveness to myelin through Nogo-66 receptor 1 cleavage. J Biol Chem 286:31418-31424.

Fidler PS, Schuette K, Asher RA, Dobbertin A, Thornton SR, Calle-Patino Y, Muir E, Levine JM, Geller HM, Rogers JH, Faissner A, Fawcett JW (1999) Comparing astrocytic cell lines that are inhibitory or permissive for axon growth: the major axon-inhibitory proteoglycan is NG2. J Neurosci 19:8778-8788.

Filbin MT (2003) Myelin-associated inhibitors of axonal regeneration in the adult mammalian CNS. Nat Rev Neurosci 4:703-713.

Fischer D, He Z, Benowitz LI (2004a) Counteracting the Nogo receptor enhances optic nerve regeneration if retinal ganglion cells are in an active growth state. J Neurosci 24:1646-1651.

Fischer D, Petkova V, Thanos S, Benowitz LI (2004b) Switching mature retinal ganglion cells to a robust growth state in vivo: gene expression and synergy with RhoA inactivation. J Neurosci 24:8726-8740.

Fisher D, Xing B, Dill J, Li H, Hoang HH, Zhao Z, Yang XL, Bachoo R, Cannon S, Longo FM, Sheng M, Silver J, Li S (2011) Leukocyte common antigen-related phosphatase is a functional receptor for chondroitin sulfate proteoglycan axon growth inhibitors. J Neurosci 31:14051-14066.

Fouad K, Schnell L, Bunge MB, Schwab ME, Liebscher T, Pearse DD (2005) Combining Schwann cell bridges and olfactory-ensheathing glia grafts with chondroitinase promotes locomotor recovery after complete transection of the spinal cord. J Neurosci 25:1169-1178.

Fournier AE, GrandPre T, Strittmatter SM (2001) Identification of a receptor mediating Nogo-66 inhibition of axonal regeneration. Nature 409:341-346.

Fournier AE, Takizawa BT, Strittmatter SM (2003) Rho kinase inhibition enhances axonal regeneration in the injured CNS. J Neurosci 23:1416-1423.

Fry EJ, Chagnon MJ, Lopez-Vales R, Tremblay ML, David S (2009) Corticospinal tract regeneration after spinal cord injury in receptor protein tyrosine phosphatase sigma deficient mice. Glia 58:423-433.

Fujita Y, Endo S, Takai T, Yamashita T (2011) Myelin suppresses axon regeneration by PIR-B/SHP-mediated inhibition of Trk activity. EMBO J 30:1389-1401.

Funahashi S, Hasegawa T, Nagano A, Sato K (2008) Differential expression patterns of messenger RNAs encoding Nogo receptors and their ligands in the rat central nervous system. J Comp Neurol 506:141-160.

Gao Y, Nikulina E, Mellado W, Filbin MT (2003) Neurotrophins elevate cAMP to reach a threshold required to overcome inhibition by MAG through extracellular signal-regulated kinase-dependent inhibition of phosphodiesterase. J Neurosci 23:11770-11777.

Gao Y, Deng K, Hou J, Bryson JB, Barco A, Nikulina E, Spencer T, Mellado W, Kandel ER, Filbin MT (2004) Activated CREB is sufficient to overcome inhibitors in myelin and promote spinal axon regeneration in vivo. Neuron 44:609-621.

Garcia-Alias G, Barkhuysen S, Buckle M, Fawcett JW (2009) Chondroitinase ABC treatment opens a window of opportunity for task-specific rehabilitation. Nat Neurosci 12:1145-1151.

Garcia-Alias G, Petrosyan HA, Schnell L, Horner PJ, Bowers WJ, Mendell LM, Fawcett JW, Arvanian VL (2011) Chondroitinase ABC combined with NT3 secretion and NR2D expression promotes axonal plasticity and functional recovery in rats with lateral hemisection of the spinal cord. J Neurosci 31:17788-17799.

Gaudet AD, Popovich PG, Ramer MS (2011) Wallerian degeneration: gaining perspective on inflammatory events after peripheral nerve injury. J Neuroinflammation 8:110.
Goh EL, Young JK, Kuwako K, Tessier-Lavigne M, He Z, Griffin JW, Ming GL (2008) Beta1-integrin mediates myelin-associated glycoprotein signaling in neuronal growth cones. Mol Brain 1:10.
Goldberg JL, Klassen MP, Hua Y, Barres BA (2002) Amacrine-signaled loss of intrinsic axon growth ability by retinal ganglion cells. Science 296:1860- 1864.
Goldshmit Y, Galea MP, Wise G, Bartlett PF, Turnley AM (2004) Axonal regeneration and lack of astrocytic gliosis in EphA4-deficient mice. J Neurosci 24:10064-10073.
Goldshmit Y, Spanevello MD, Tajouri S, Li L, Rogers F, Pearse M, Galea M, Bartlett PF, Boyd AW, Turnley AM (2011) EphA4 blockers promote axonal regeneration and functional recovery following spinal cord injury in mice. PLoS One 6:e24636.
GrandPre T, Nakamura F, Vartanian T, Strittmatter SM (2000) Identification of the Nogo inhibitor of axon regeneration as a Reticulon protein. Nature 403:439-444.
Guertin DA, Sabatini DM (2007) Defining the role of mTOR in cancer. Cancer Cell 12:9-22.
Habib AA, Marton LS, Allwardt B, Gulcher JR, Mikol DD, Hognason T, Chattopadhyay N, Stefansson K (1998) Expression of the oligodendrocyte-myelin glycoprotein by neurons in the mouse central nervous system. J Neurochem 70:1704-1711.
Hannila SS, Filbin MT (2008) The role of cyclic AMP signaling in promoting axonal regeneration after spinal cord injury. Exp Neurol 209:321-332.
Harvey PA, Lee DH, Qian F, Weinreb PH, Frank E (2009) Blockade of Nogo receptor ligands promotes functional regeneration of sensory axons after dorsal root crush. J Neurosci 29:6285-6295.
He XL, Bazan JF, McDermott G, Park JB, Wang K, Tessier-Lavigne M, He Z, Garcia KC (2003) Structure of the Nogo receptor ectodomain: a recognition module implicated in myelin inhibition. Neuron 38:177-185.
Hellal F, Hurtado A, Ruschel J, Flynn KC, Laskowski CJ, Umlauf M, Kapitein LC, Strikis D, Lemmon V, Bixby J, Hoogenraad CC, Bradke F (2011) Microtubule stabilization reduces scarring and causes axon regeneration after spinal cord injury. Science 331:928-931.
Hensch TK, Fagiolini M, Mataga N, Stryker MP, Baekkeskov S, Kash SF (1998) Local GABA circuit control of experience-dependent plasticity in developing visual cortex. Science 282:1504-1508.
Hines JH, Abu-Rub M, Henley JR (2010) Asymmetric endocytosis and remodeling of β1-integrin adhesions during growth cone chemorepulsion by MAG. Nat Neurosci 13:829-837.
Horn KE, Xu B, Gobert D, Hamam BN, Thompson KM, Wu CL, Bouchard JF, Uetani N, Racine RJ, Tremblay ML, Ruthazer ES, Chapman CA, Kennedy TE (2012) Receptor protein tyrosine phosphatase sigma regulates synapse structure, function and plasticity. J Neurochem 122:147-161.
Hsieh SH, Ferraro GB, Fournier AE (2006) Myelin-associated inhibitors regulate cofilin phosphorylation and neuronal inhibition through LIM kinase and Slingshot phosphatase. J Neurosci 26:1006-1015.
Hu F, Strittmatter SM (2004) Regulating axon growth within the postnatal central nervous system. Semin Perinatol 28:371-378.

Huang JK, Phillips GR, Roth AD, Pedraza L, Shan W, Belkaid W, Mi S, Fex-Svenningsen A, Florens L, Yates JR 3rd, Colman DR (2005) Glial membranes at the node of Ranvier prevent neurite outgrowth. Science 310:1813-1817.

Huber AB, Weinmann O, Brosamle C, Oertle T, Schwab ME (2002) Patterns of Nogo mRNA and protein expression in the developing and adult rat and after CNS lesions. J Neurosci 22:3553-3567.

Hunt D, Mason MR, Campbell G, Coffin R, Anderson PN (2002) Nogo receptor mRNA expression in intact and regenerating CNS neurons. Mol Cell Neurosci 20:537-552.

Ji B, Li M, Wu WT, Yick LW, Lee X, Shao Z, Wang J, So KF, McCoy JM, Pepinsky RB, Mi S, Relton JK (2006) LINGO-1 antagonist promotes functional recovery and axonal sprouting after spinal cord injury. Mol Cell Neurosci 33:311-320.

Ji B, Case LC, Liu K, Shao Z, Lee X, Yang Z, Wang J, Tian T, Shulga-Morskaya S, Scott M, He Z, Relton JK, Mi S (2008) Assessment of functional recovery and axonal sprouting in oligodendrocyte-myelin glycoprotein (OMgp) null mice after spinal cord injury. Mol Cell Neurosci 39:258-267.

Johnson PW, Abramow-Newerly W, Seilheimer B, Sadoul R, Tropak MB, Arquint M, Dunn RJ, Schachner M, Roder JC (1989) Recombinant myelin-associated glycoprotein confers neural adhesion and neurite outgrowth function. Neuron 3:377-385.

Jones LL, Yamaguchi Y, Stallcup WB, Tuszynski MH (2002) NG2 is a major chondroitin sulfate proteoglycan produced after spinal cord injury and is expressed by macrophages and oligodendrocyte progenitors. J Neurosci 22:2792-2803.

Jones LL, Margolis RU, Tuszynski MH (2003) The chondroitin sulfate proteoglycans neurocan, brevican, phosphacan, and versican are differentially regulated following spinal cord injury. Exp Neurol 182:399-411.

Josephson A, Trifunovski A, Widmer HR, Widenfalk J, Olson L, Spenger C (2002) Nogo-receptor gene activity: cellular localization and developmental regulation of mRNA in mice and humans. J Comp Neurol 453:292-304.

Josephson A, Trifunovski A, Scheele C, Widenfalk J, Wahlestedt C, Brene S, Olson L, Spenger C (2003) Activity-induced and developmental downregulation of the Nogo receptor. Cell Tissue Res 311:333-342.

Joset A, Dodd DA, Halegoua S, Schwab ME (2010) Pincher-generated Nogo-A endosomes mediate growth cone collapse and retrograde signaling. J Cell Biol 188:271-285.

Kadoya K, Tsukada S, Lu P, Coppola G, Geschwind D, Filbin MT, Blesch A, Tuszynski MH (2009) Combined intrinsic and extrinsic neuronal mechanisms facilitate bridging axonal regeneration one year after spinal cord injury. Neuron 64:165-172.

Kaneko S, Iwanami A, Nakamura M, Kishino A, Kikuchi K, Shibata S, Okano HJ, Ikegami T, Moriya A, Konishi O, Nakayama C, Kumagai K, Kimura T, Sato Y, Goshima Y, Taniguchi M, Ito M, He Z, Toyama Y, Okano H (2006) A selective Sema3A inhibitor enhances regenerative responses and functional recovery of the injured spinal cord. Nat Med 12:1380-1389.

Karimi-Abdolrezaee S, Eftekharpour E, Wang J, Schut D, Fehlings MG (2010) Synergistic effects of transplanted adult neural stem/progenitor cells, chondroitinase, and growth factors promote functional repair and plasticity of the chronically injured spinal cord. J Neurosci 30:1657-1676.

Kelm S, Pelz A, Schauer R, Filbin MT, Tang S, de Bellard ME, Schnaar RL, Mahoney JA, Hartnell A, Bradfield P, Crocker PR (1994) Sialoadhesin, myelin-associated glycoprotein

and CD22 define a new family of sialic acid-dependent adhesion molecules of the immunoglobulin superfamily. Curr Biol 4:965-972.
Kennedy TE, Serafini T, de la Torre JR, Tessier-Lavigne M (1994) Netrins are diffusible chemotropic factors for commissural axons in the embryonic spinal cord. Cell 78:425-435.
Kim JE, Li S, GrandPre T, Qiu D, Strittmatter SM (2003) Axon regeneration in young adult mice lacking Nogo-A/B. Neuron 38:187-199.
Kim JE, Liu BP, Park JH, Strittmatter SM (2004) Nogo-66 receptor prevents raphespinal and rubrospinal axon regeneration and limits functional recovery from spinal cord injury. Neuron 44:439-451.
Knoll B, Isenmann S, Kilic E, Walkenhorst J, Engel S, Wehinger J, Bahr M, Drescher U (2001) Graded expression patterns of ephrin-As in the superior colliculus after lesion of the adult mouse optic nerve. Mech Dev 106:119-127.
Kobayashi NR, Fan DP, Giehl KM, Bedard AM, Wiegand SJ, Tetzlaff W (1997) BDNF and NT-4/5 prevent atrophy of rat rubrospinal neurons after cervical axotomy, stimulate GAP-43 and Talpha1-tubulin mRNA expression, and promote axonal regeneration. J Neurosci 17:9583-9595.
Kottis V, Thibault P, Mikol D, Xiao ZC, Zhang R, Dergham P, Braun PE (2002) Oligodendrocyte-myelin glycoprotein (OMgp) is an inhibitor of neurite outgrowth. J Neurochem 82:1566-1569.
Kubota Y, Morita T, Kusakabe M, Sakakura T, Ito K (1999) Spatial and temporal changes in chondroitin sulfate distribution in the sclerotome play an essential role in the formation of migration patterns of mouse neural crest cells. Dev Dyn 214:55-65.
Kurimoto T, Yin Y, Omura K, Gilbert HY, Kim D, Cen LP, Moko L, Kügler S, Benowitz LI (2010) Long-distance axon regeneration in the mature optic nerve: contributions of oncomodulin, cAMP, and pten gene deletion. J Neurosci 30:15654-15663.
Kwok JC, Afshari F, Garcia-Alias G, Fawcett JW (2008) Proteoglycans in the central nervous system: plasticity, regeneration and their stimulation with chondroitinase ABC. Restor Neurol Neurosci 26:131-145.
Lai C, Brow MA, Nave KA, Noronha AB, Quarles RH, Bloom FE, Milner RJ, Sutcliffe JG (1987) Two forms of 1B236/myelin-associated glycoprotein, a cell adhesion molecule for postnatal neural development, are produced by alternative splicing. Proc Natl Acad Sci U S A 84:4337-4341.
Lau E, Margolis RU (2010) Inhibitors of slit protein interactions with the heparan sulphate proteoglycan glypican-1: potential agents for the treatment of spinal cord injury. Clin Exp Pharmacol Physiol 37:417-421.
Lee H, Raiker SJ, Venkatesh K, Geary R, Robak LA, Zhang Y, Yeh HH, Shrager P, Giger RJ (2008) Synaptic function for the Nogo-66 receptor NgR1: regulation of dendritic spine morphology and activity-dependent synaptic strength. J Neurosci 28:2753-2765.
Lee JK, Case LC, Chan AF, Zhu Y, Tessier-Lavigne M, Zheng B (2009a) Generation of an OMgp allelic series in mice. Genesis 47:751-756.
Lee JK, Chan AF, Luu SM, Zhu Y, Ho C, Tessier-Lavigne M, Zheng B (2009b) Reassessment of corticospinal tract regeneration in Nogo-deficient mice. J Neurosci 29:8649-8654.
Lee JK, Geoffroy CG, Chan AF, Tolentino KE, Crawford MJ, Leal MA, Kang B, Zheng B (2010a) Assessing spinal axon regeneration and sprouting in Nogo-, MAG-, and OMgp-deficient mice. Neuron 66:663-670.

Lee JK, Chow R, Xie F, Chow SY, Tolentino KE, Zheng B (2010b) Combined genetic attenuation of myelin and semaphorin-mediated growth inhibition is insufficient to promote serotonergic axon regeneration. J Neurosci 30:10899-10904.

Lehmann M, Fournier A, Selles-Navarro I, Dergham P, Sebok A, Leclerc N, Tigyi G, McKerracher L (1999) Inactivation of Rho signaling pathway promotes CNS axon regeneration. J Neurosci 19:7537-7547.

Leibinger M, Muller A, Andreadaki A, Hauk TG, Kirsch M, Fischer D (2009) Neuroprotective and axon growth-promoting effects following inflammatory stimulation on mature retinal ganglion cells in mice depend on ciliary neurotrophic factor and leukemia inhibitory factor. J Neurosci 29:14334-14341.

Leibinger M, Andreadaki A, Fischer D (2012) Role of mTOR in neuroprotection and axon regeneration after inflammatory stimulation. Neurobiol Dis 46:314-324.

Li C, Tropak MB, Gerlai R, Clapoff S, Abramow-Newerly W, Trapp B, Peterson A, Roder J (1994) Myelination in the absence of myelin-associated glycoprotein. Nature 369:747-750.

Li M, Shibata A, Li C, Braun PE, McKerracher L, Roder J, Kater SB, David S (1996) Myelin-associated glycoprotein inhibits neurite/axon growth and causes growth cone collapse. J Neurosci Res 46:404-414.

Liebl DJ, Morris CJ, Henkemeyer M, Parada LF (2003) mRNA expression of ephrins and Eph receptor tyrosine kinases in the neonatal and adult mouse central nervous system. J Neurosci Res 71:7-22.

Liu BP, Fournier A, GrandPre T, Strittmatter SM (2002) Myelin-associated glycoprotein as a functional ligand for the Nogo-66 receptor. Science 297:1190-1193.

Liu K, Lu Y, Lee JK, Samara R, Willenberg R, Sears-Kraxberger I, Tedeschi A, Park KK, Jin D, Cai B, Xu B, Connolly L, Steward O, Zheng B, He Z (2010) PTEN deletion enhances the regenerative ability of adult corticospinal neurons. Nat Neurosci. 13:1075-1081.

Liu Y, Wang X, Lu CC, Kerman R, Steward O, Xu XM, Zou Y (2008) Repulsive Wnt signaling inhibits axon regeneration after CNS injury. J Neurosci 28:8376-8382.

Llorens F, Gil V, Iraola S, Carim-Todd L, Marti E, Estivill X, Soriano E, del Rio JA, Sumoy L (2008) Developmental analysis of Lingo-1/Lern1 protein expression in the mouse brain: interaction of its intracellular domain with Myt1l. Dev Neurobiol 68:521-541.

Loers G, Aboul-Enein F, Bartsch U, Lassmann H, Schachner M (2004) Comparison of myelin, axon, lipid, and immunopathology in the central nervous system of differentially myelin-compromised mutant mice: a morphological and biochemical study. Mol Cell Neurosci 27:175-189.

Lopez PH, Ahmad AS, Mehta NR, Toner M, Rowland EA, Zhang J, Dore S, Schnaar RL (2011) Myelin-associated glycoprotein protects neurons from excitotoxicity. J Neurochem 116:900-908.

Low K, Culbertson M, Bradke F, Tessier-Lavigne M, Tuszynski MH (2008) Netrin-1 is a novel myelin-associated inhibitor to axon growth. J Neurosci 28:1099-1108.

Lu P, Tuszynski MH (2008) Growth factors and combinatorial therapies for CNS regeneration. Exp Neurol 209:313-320.

Lu P, Wang Y, Graham L, McHale K, Gao M, Wu D, Brock J, Blesch A, Rosenzweig ES, Havton LA, Zheng B, Conner JM, Marsala M, Tuszynski MH (2012) Long-distance

growth and connectivity of neural stem cells after severe spinal cord injury. Cell 150:1264-1273.
Luo Y, Raible D, Raper J (1993) Collapsin: a protein in brain that induces the collapse and paralysis of neuronal growth cones. Cell 75:217-227.
Ma TC, Campana A, Lange PS, Lee HH, Banerjee K, Bryson JB, Mahishi L, Alam S, Giger RJ, Barnes S, Morris SM Jr, Willis DE, Twiss JL, Filbin MT, Ratan RR (2010) A large-scale chemical screen for regulators of the arginase 1 promoter identifies the soy isoflavone daidzeinas a clinically approved small molecule that can promote neuronal protection or regeneration via a cAMP-independent pathway. J Neurosci 30:739-748.
MacDermid VE, McPhail LT, Tsang B, Rosenthal A, Davies A, Ramer MS (2004) A soluble Nogo receptor differentially affects plasticity of spinally projecting axons. Eur J Neurosci 20:2567-2579.
Manitt C, Colicos MA, Thompson KM, Rousselle E, Peterson AC, Kennedy TE (2001) Widespread expression of netrin-1 by neurons and oligodendrocytes in the adult mammalian spinal cord. J Neurosci 21:3911-3922.
Manitt C, Wang D, Kennedy TE, Howland DR (2006) Positioned to inhibit: netrin-1 and netrin receptor expression after spinal cord injury. J Neurosci Res 84:1808-1820.
Marcus J, Dupree JL, Popko B (2002) Myelin-associated glycoprotein and myelin galactolipids stabilize developing axo-glial interactions. J Cell Biol 156:567-577.
Mathis C, Schroter A, Thallmair M, Schwab ME (2010) Nogo-A regulates neural precursor migration in the embryonic mouse cortex. Cereb Cortex.
McGee AW, Yang Y, Fischer QS, Daw NW, Strittmatter SM (2005) Experience-driven plasticity of visual cortex limited by myelin and Nogo receptor. Science 309:2222-2226.
McKeon RJ, Schreiber RC, Rudge JS, Silver J (1991) Reduction of neurite outgrowth in a model of glial scarring following CNS injury is correlated with the expression of inhibitory molecules on reactive astrocytes. J Neurosci 11:3398-3411.
McKeon RJ, Hoke A, Silver J (1995) Injury-induced proteoglycans inhibit the potential for laminin-mediated axon growth on astrocytic scars. Exp Neurol 136:32-43.
McKerracher L, David S, Jackson DL, Kottis V, Dunn RJ, Braun PE (1994) Identification of myelin-associated glycoprotein as a major myelin-derived inhibitor of neurite growth. Neuron 13:805-811.
McKerracher L, Higuchi H (2006) Targeting Rho to stimulate repair after spinal cord injury. J Neurotrauma 23:309-317.
McLean J, Batt J, Doering LC, Rotin D, Bain JR (2002) Enhanced rate of nerve regeneration and directional errors after sciatic nerve injury in receptor protein tyrosine phosphatase sigma knock-out mice. J Neurosci 22:5481-5491.
Mehta NR, Lopez PH, Vyas AA, Schnaar RL (2007) Gangliosides and Nogo receptors independently mediate myelin-associated glycoprotein inhibition of neurite outgrowth in different nerve cells. J Biol Chem 282:27875-27886.
Mi S, Lee X, Shao Z, Thill G, Ji B, Relton J, Levesque M, Allaire N, Perrin S, Sands B, Crowell T, Cate RL, McCoy JM, Pepinsky RB (2004) LINGO-1 is a component of the Nogo-66 receptor/p75 signaling complex. Nat Neurosci 7:221-228.
Mikol DD, Stefansson K (1988) A phosphatidylinositol-linked peanut agglutinin-binding glycoprotein in central nervous system myelin and on oligodendrocytes. J Cell Biol 106:1273-1279.

Mikol DD, Gulcher JR, Stefansson K (1990) The oligodendrocyte-myelin glycoprotein belongs to a distinct family of proteins and contains the HNK-1 carbohydrate. J Cell Biol 110:471-479.

Mimura F, Yamagishi S, Arimura N, Fujitani M, Kubo T, Kaibuchi K, Yamashita T (2006) Myelin-associated glycoprotein inhibits microtubule assembly by a Rho-kinase-dependent mechanism. J Biol Chem 281:15970-15979.

Mingorance-Le Meur A, Zheng B, Soriano E, del Rio JA (2007) Involvement of the myelin-associated inhibitor Nogo-A in early cortical development and neuronal maturation. Cereb Cortex 17:2375-2386.

Monnier PP, Sierra A, Schwab JM, Henke-Fahle S, Mueller BK (2003) The Rho/ROCK pathway mediates neurite growth-inhibitory activity associated with the chondroitin sulfate proteoglycans of the CNS glial scar. Mol Cell Neurosci 22:319-330.

Montag D, Giese KP, Bartsch U, Martini R, Lang Y, Bluthmann H, Karthigasan J, Kirschner DA, Wintergerst ES, Nave KA, Zielasek J, Toyka KV, Lipp H, Schachner M (1994) Mice deficient for the myelin-associated glycoprotein show subtle abnormalities in myelin. Neuron 13:229-246.

Moon LD, Asher RA, Rhodes KE, Fawcett JW (2001) Regeneration of CNS axons back to their target following treatment of adult rat brain with chondroitinase ABC. Nat Neurosci 4:465-466.

Moore SW, Tessier-Lavigne M, Kennedy TE (2007) Netrins and their receptors. Adv Exp Med Biol 621:17-31.

Mountney A, Zahner MR, Lorenzini I, Oudega M, Schramm LP, Schnaar RL (2010) Sialidase enhances recovery from spinal cord contusion injury. Proc Natl Acad Sci U S A 107:11561-11566.

Moreau-Fauvarque C, Kumanogoh A, Camand E, Jaillard C, Barbin G, Boquet I, Love C, Jones EY, Kikutani H, Lubetzki C, Dusart I, Chedotal A (2003) The transmembrane semaphorin Sema4D/CD100, an inhibitor of axonal growth, is expressed on oligodendrocytes and upregulated after CNS lesion. J Neurosci 23:9229-9239.

Moreno-Flores MT, Wandosell F (1999) Up-regulation of Eph tyrosine kinase receptors after excitotoxic injury in adult hippocampus. Neuroscience 91:193-201.

Mukhopadhyay G, Doherty P, Walsh FS, Crocker PR, Filbin MT (1994) A novel role for myelin-associated glycoprotein as an inhibitor of axonal regeneration. Neuron 13:757-767.

Nakamura Y, Fujita Y, Ueno M, Takai T, Yamashita T (2011) Paired immunoglobulin-like receptor B knockout does not enhance axonal regeneration or locomotor recovery after spinal cord injury. J Biol Chem 286:1876-1883.

Namikawa K, Honma M, Abe K, Takeda M, Mansur K, Obata T, Miwa A, Okado H, Kiyama H (2000) Akt/protein kinase B prevents injury-induced motoneuron death and accelerates axonal regeneration. J Neurosci 20:2875-2886.

Nash M, Pribiag H, Fournier AE, Jacobson C (2009) Central nervous system regeneration inhibitors and their intracellular substrates. Mol Neurobiol 40:224-235.

Nguyen T, Mehta NR, Conant K, Kim KJ, Jones M, Calabresi PA, Melli G, Hoke A, Schnaar RL, Ming GL, Song H, Keswani SC, Griffin JW (2009) Axonal protective effects of the myelin-associated glycoprotein. J Neurosci 29:630-637.

Nie D, Di Nardo A, Han JM, Baharanyi H, Kramvis I, Huynh T, Dabora S, Codeluppi S, Pandolfi PP, Pasquale EB, Sahin M (2010) Tsc2-Rheb signaling regulates EphA-mediated axon guidance. Nat Neurosci 13:163-172.

Oertle T, van der Haar ME, Bandtlow CE, Robeva A, Burfeind P, Buss A, Huber AB, Simonen M, Schnell L, Brosamle C, Kaupmann K, Vallon R, Schwab ME (2003) Nogo-A inhibits neurite outgrowth and cell spreading with three discrete regions. J Neurosci 23:5393-5406.

Oinuma I, Ito Y, Katoh H, Negishi M (2010) Semaphorin 4D/plexin-B1 stimulates PTEN activity through R-Ras GAP activity, inducing growth cone collapse in hippocampal neurons. J Biol Chem 285:28200-28209.

O'Leary DD, Wilkinson DG (1999) Eph receptors and ephrins in neural development. Curr Opin Neurobiol 9:65-73.

Omoto S, Ueno M, Mochio S, Takai T, Yamashita T (2011) Genetic deletion of paired immunoglobulin-like receptor B does not promote axonal plasticity or functional recovery after traumatic brain injury. J Neurosci 30:13045-13052.

Pan B, Fromholt SE, Hess EJ, Crawford TO, Griffin JW, Sheikh KA, Schnaar RL (2005) Myelin-associated glycoprotein and complementary axonal ligands, gangliosides, mediate axon stability in the CNS and PNS: neuropathology and behavioral deficits in single- and double-null mice. Exp Neurol 195:208-217.

Park JB, Yiu G, Kaneko S, Wang J, Chang J, He XL, Garcia KC, He Z (2005) A TNF receptor family member, TROY, is a coreceptor with Nogo receptor in mediating the inhibitory activity of myelin inhibitors. Neuron 45:345-351.

Park KK, Liu K, Hu Y, Smith PD, Wang C, Cai B, Xu B, Connolly L, Kramvis I, Sahin M, He Z (2008) Promoting axon regeneration in the adult CNS by modulation of the PTEN/mTOR pathway. Science 322:963-966.

Pasterkamp RJ, Giger RJ, Ruitenberg MJ, Holtmaat AJ, De Wit J, De Winter F, Verhaagen J (1999) Expression of the gene encoding the chemorepellent semaphorin III is induced in the fibroblast component of neural scar tissue formed following injuries of adult but not neonatal CNS. Mol Cell Neurosci 13:143-166.

Pasterkamp RJ, Verhaagen J (2006) Semaphorins in axon regeneration: developmental guidance molecules gone wrong? Philos Trans R Soc Lond B Biol Sci 361:1499-1511.

Pasterkamp RJ, Kolk SM, Hellemons AJ, Kolodkin AL (2007) Expression patterns of semaphorin7A and plexinC1 during rat neural development suggest roles in axon guidance and neuronal migration. BMC Dev Biol 7:98.

Peng X, Zhou Z, Hu J, Fink DJ, Mata M (2009) Soluble nogo receptor down-regulates expression of neuronal Nogo-A to enhance axonal regeneration. J Biol Chem 285:2783-2795.

Pernet V, Joly S, Christ F, Dimou L, Schwab ME (2008) Nogo-A and myelin-associated glycoprotein differently regulate oligodendrocyte maturation and myelin formation. J Neurosci 28:7435-7444.

Petrinovic MM, Duncan CS, Bourikas D, Weinman O, Montani L, Schroeter A, Maerki D, Sommer L, Stoeckli ET, Schwab ME (2010) Neuronal Nogo-A regulates neurite fasciculation, branching and extension in the developing nervous system. Development 137:2539-2550.

Pindzola RR, Doller C, Silver J (1993) Putative inhibitory extracellular matrix molecules at the dorsal root entry zone of the spinal cord during development and after root and sciatic nerve lesions. Dev Biol 156:34-48.

Pizzorusso T, Medini P, Berardi N, Chierzi S, Fawcett JW, Maffei L (2002) Reactivation of ocular dominance plasticity in the adult visual cortex. Science 298:1248-1251.

Prinjha R, Moore SE, Vinson M, Blake S, Morrow R, Christie G, Michalovich D, Simmons DL, Walsh FS (2000) Inhibitor of neurite outgrowth in humans. Nature 403:383-384.

Pyka M, Wetzel C, Aguado A, Geissler M, Hatt H, Faissner A (2011) Chondroitin sulfate proteoglycans regulate astrocyte-dependent synaptogenesis and modulate synaptic activity in primary embryonic hippocampal neurons. EurJ Neurosci 33:2187-2202.

Quarles RH (2007) Myelin-associated glycoprotein: past, present and beyond. J Neurochem 100:1431-1448.

Radtke C, Sasaki M, Lankford KL, Vogt PM, Kocsis JD (2008) Potential of olfactory ensheathing cells for cell-based therapy in spinal cord injury. J Rehabil Res Dev 45:141-151.

Raiker SJ, Lee H, Baldwin KT, Duan Y, Shrager P, Giger RJ (2010) Oligodendrocyte-myelin glycoprotein and Nogo negatively regulate activity-dependent synaptic plasticity. J Neurosci 30:12432-12445.

Rolls A, Shechter R, Schwartz M (2009) The bright side of the glial scar in CNS repair. Nat Rev Neurosci 10:235-241.

Roux PP, Barker PA (2002) Neurotrophin signaling through the p75 neurotrophin receptor. Prog Neurobiol 67:203-233.

Salzer JL, Holmes WP, Colman DR (1987) The amino acid sequences of the myelin-associated glycoproteins: homology to the immunoglobulin gene superfamily. J Cell Biol 104:957-965.

Sango K, Oohira A, Ajiki K, Tokashiki A, Horie M, Kawano H (2003) Phosphacan and neurocan are repulsive substrata for adhesion and neurite extension of adult rat dorsal root ganglion neurons in vitro. Exp Neurol 182:1-11.

Sapieha PS, Duplan L, Uetani N, Joly S, Tremblay ML, Kennedy TE, Di Polo A (2005) Receptor protein tyrosine phosphatase sigma inhibits axon regrowth in the adult injured CNS. Mol Cell Neurosci 28:625-635.

Schachtrup C, Lu P, Jones LL, Lee JK, Lu J, Sachs BD, Zheng B, Akassoglou K (2007) Fibrinogen inhibits neurite outgrowth via beta 3 integrin-mediated phosphorylation of the EGF receptor. Proc Natl Acad Sci U S A 104:11814-11819.

Schmandke A, Strittmatter SM (2007) ROCK and Rho: biochemistry and neuronal functions of Rho-associated protein kinases. Neuroscientist 13:454-469.

Schnell L, Schwab ME (1990) Axonal regeneration in the rat spinal cord produced by an antibody against myelin-associated neurite growth inhibitors. Nature 343:269-272.

Schnell L, Schneider R, Kolbeck R, Barde YA, Schwab ME (1994) Neurotrophin-3 enhances sprouting of corticospinal tract during development and after adult spinal cord lesion. Nature 367:170-173.

Schwab ME, Kapfhammer JP, Bandtlow CE (1993) Inhibitors of neurite growth. Annu Rev Neurosci 16:565-595.

Schweigreiter R (2008) The natural history of the myelin-derived nerve growth inhibitor Nogo-A. Neuron Glia Biol 4:83-89.

Sengottuvel V, Leibinger M, Pfreimer M, Andreadaki A, Fischer D (2011) Taxol facilitates axon regeneration in the mature CNS. J Neurosci 31:2688-2699.

Serafini T, Kennedy TE, Galko MJ, Mirzayan C, Jessell TM, Tessier-Lavigne M (1994) The netrins define a family of axon outgrowth-promoting proteins homologous to C. elegans UNC-6. Cell 78:409-424.

Shao Z, Browning JL, Lee X, Scott ML, Shulga-Morskaya S, Allaire N, Thill G, Levesque M, Sah D, McCoy JM, Murray B, Jung V, Pepinsky RB, Mi S (2005) TAJ/TROY, an orphan TNF receptor family member, binds Nogo-66 receptor 1 and regulates axonal regeneration. Neuron 45:353-359.

Shen Y, Tenney AP, Busch SA, Horn KP, Cuascut FX, Liu K, He Z, Silver J, Flanagan JG (2009) PTPsigma is a receptor for chondroitin sulfate proteoglycan, an inhibitor of neural regeneration. Science 326:592-596.

Shim SO, Cafferty WB, Schmidt EC, Kim BG, Fujisawa H, Strittmatter SM (2012) PlexinA2 limits recovery from corticospinal axotomy by mediating oligodendrocyte-derived Sema6A growth inhibition. Mol Cell Neurosci 50:193-200.

Simonen M, Pedersen V, Weinmann O, Schnell L, Buss A, Ledermann B, Christ F, Sansig G, van der Putten H, Schwab ME (2003) Systemic deletion of the myelin-associated outgrowth inhibitor Nogo-A improves regenerative and plastic responses after spinal cord injury. Neuron 38:201-211.

Sivasankaran R, Pei J, Wang KC, Zhang YP, Shields CB, Xu XM, He Z (2004) PKC mediates inhibitory effects of myelin and chondroitin sulfate proteoglycans on axonal regeneration. Nat Neurosci 7:261-268.

Smith PD, Sun F, Park KK, Cai B, Wang C, Kuwako K, Martinez-Carrasco I, Connolly L, He Z (2009) SOCS3 deletion promotes optic nerve regeneration in vivo. Neuron 64:617-623.

Snow DM, Steindler DA, Silver J (1990a) Molecular and cellular characterization of the glial roof plate of the spinal cord and optic tectum: a possible role for a proteoglycan in the development of an axon barrier. Dev Biol 138:359-376.

Snow DM, Lemmon V, Carrino DA, Caplan AI, Silver J (1990b) Sulfated proteoglycans in astroglial barriers inhibit neurite outgrowth in vitro. Exp Neurol 109:111-130.

Sobel RA (2005) Ephrin A receptors and ligands in lesions and normal-appearing white matter in multiple sclerosis. Brain Pathol 15:35-45.

Song HJ, Ming GL, Poo MM (1997) cAMP-induced switching in turning direction of nerve growth cones. Nature 388:275-279.

Song XY, Zhong JH, Wang X, Zhou XF (2004) Suppression of p75NTR does not promote regeneration of injured spinal cord in mice. J Neurosci 24:542-546.

Spencer TK, Mellado W, Filbin MT (2008) BDNF activates CaMKIV and PKA in parallel to block MAG-mediated inhibition of neurite outgrowth. Mol Cell Neurosci 38:110-116.

Steward O, Zheng B, Banos K, Yee KM (2007) Response to: Kim et al., "axon regeneration in young adult mice lacking Nogo-A/B." Neuron 38, 187-199. Neuron 54:191-195.

Stryker E, Johnson KG (2007) LAR, liprin alpha and the regulation of active zone morphogenesis. J Cell Sci 120:3723-3728.

Sun F, Park KK, Belin S, Wang D, Lu T, Chen G, Zhang K, Yeung C, Feng G, Yankner BA, He Z (2011) Sustained axon regeneration induced by co-deletion of PTEN and SOCS3. Nature 480:372-375.

Syken J, Grandpre T, Kanold PO, Shatz CJ (2006) PirB restricts ocular-dominance plasticity in visual cortex. Science 313:1795-1800.

Takai T (2005) Paired immunoglobulin-like receptors and their MHC class I recognition. Immunology 115:433-440.
Tang S, Shen YJ, DeBellard ME, Mukhopadhyay G, Salzer JL, Crocker PR, Filbin MT (1997) Myelin-associated glycoprotein interacts with neurons via a sialic acid binding site at ARG118 and a distinct neurite inhibition site. J Cell Biol 138:1355-1366.
Taniguchi M, Yuasa S, Fujisawa H, Naruse I, Saga S, Mishina M, Yagi T (1997) Disruption of semaphorin III/D gene causes severe abnormality in peripheral nerve projection. Neuron 19:519-530.
Thompson KM, Uetani N, Manitt C, Elchebly M, Tremblay ML, Kennedy TE (2003) Receptor protein tyrosine phosphatase sigma inhibits axonal regeneration and the rate of axon extension. Mol Cell Neurosci 23:681-692.
Tom VJ, Kadakia R, Santi L, Houle JD (2009) Administration of chondroitinase ABC rostral or caudal to a spinal cord injury site promotes anatomical but not functional plasticity. J Neurotrauma 26:2323-2333.
Tran TS, Kolodkin AL, Bharadwaj R (2007) Semaphorin regulation of cellular morphology. Annu Rev Cell Dev Biol 23:263-292.
Turnley AM, Bartlett PF (1998) MAG and MOG enhance neurite outgrowth of embryonic mouse spinal cord neurons. Neuroreport 9:1987-1990.
Tuszynski MH, Gabriel K, Gerhardt K, Szollar S (1999) Human spinal cord retains substantial structural mass in chronic stages after injury. J Neurotrauma 16:523-531.
Ughrin YM, Chen ZJ, Levine JM (2003) Multiple regions of the NG2 proteoglycan inhibit neurite growth and induce growth cone collapse. J Neurosci 23:175-186.
Venkatesh K, Chivatakarn O, Lee H, Joshi PS, Kantor DB, Newman BA, Mage R, Rader C, Giger RJ (2005) The Nogo-66 receptor homolog NgR2 is a sialic acid-dependent receptor selective for myelin-associated glycoprotein. J Neurosci 25:808-822.
Venkatesh K, Chivatakarn O, Sheu SS, Giger RJ (2007) Molecular dissection of the myelin-associated glycoprotein receptor complex reveals cell type-specific mechanisms for neurite outgrowth inhibition. J Cell Biol 177:393-399.
Vinson M, Strijbos PJ, Rowles A, Facci L, Moore SE, Simmons DL, Walsh FS (2001) Myelin-associated glycoprotein interacts with ganglioside GT1b. A mechanism for neurite outgrowth inhibition. J Biol Chem 276:20280-20285.
Voeltz GK, Prinz WA, Shibata Y, Rist JM, Rapoport TA (2006) A class of membrane proteins shaping the tubular endoplasmic reticulum. Cell 124:573-586.
Vyas AA, Schnaar RL (2001) Brain gangliosides: functional ligands for myelin stability and the control of nerve regeneration. Biochimie 83:677-682.
Vyas AA, Patel HV, Fromholt SE, Heffer-Lauc M, Vyas KA, Dang J, Schachner M, Schnaar RL (2002) Gangliosides are functional nerve cell ligands for myelin-associated glycoprotein (MAG), an inhibitor of nerve regeneration. Proc Natl Acad Sci U S A 99:8412-8417.
Walmsley AR, McCombie G, Neumann U, Marcellin D, Hillenbrand R, Mir AK, Frentzel S (2004) Zinc metalloproteinase-mediated cleavage of the human Nogo-66 receptor. J Cell Sci 117:4591-4602.
Wang KC, Kim JA, Sivasankaran R, Segal R, He Z (2002a) P75 interacts with the Nogo receptor as a co-receptor for Nogo, MAG and OMgp. Nature 420:74-78.
Wang KC, Koprivica V, Kim JA, Sivasankaran R, Guo Y, Neve RL, He Z (2002b) Oligodendrocyte-myelin glycoprotein is a Nogo receptor ligand that inhibits neurite outgrowth. Nature 417:941-944.

Wang X, Chun SJ, Treloar H, Vartanian T, Greer CA, Strittmatter SM (2002) Localization of Nogo-A and Nogo-66 receptor proteins at sites of axon-myelin and synaptic contact. J Neurosci 22:5505-5515.

Wang X, Baughman KW, Basso DM, Strittmatter SM (2006) Delayed Nogo receptor therapy improves recovery from spinal cord contusion. Ann Neurol 60:540-549.

Wang Y, Ying G, Liu X, Zhou C (2003) Semi-quantitative expression analysis of ephrin mRNAs in the deafferented hippocampus. Mol Brain Res 120:79-83.

Weiss MD, Hammer J, Quarles RH (2000) Oligodendrocytes in aging mice lacking myelin-associated glycoprotein are dystrophic but not apoptotic. J Neurosci Res 62:772-780.

Wilkinson DG (2001) Multiple roles of EPH receptors and ephrins in neural development. Nat Rev Neurosci 2:155-164.

Wills ZP, Mandel-Brehm C, Mardinly AR, McCord AE, Giger RJ, Greenberg ME (2012) The nogo receptor family restricts synapse number in the developing hippocampus. Neuron 73:466-481.

Willson CA, Irizarry-Ramirez M, Gaskins HE, Cruz-Orengo L, Figueroa JD, Whittemore SR, Miranda JD (2002) Upregulation of EphA receptor expression in the injured adult rat spinal cord. Cell Transplant 11:229-239.

Winzeler AM, Mandemakers WJ, Sun MZ, Stafford M, Phillips CT, Barres BA (2011) The lipid sulfatide is a novel myelin-associated inhibitor of CNS axon outgrowth. J Neurosci 31:6481-6492.

Worter V, Schweigreiter R, Kinzel B, Mueller M, Barske C, Bock G, Frentzel S, Bandtlow CE (2009) Inhibitory activity of myelin-associated glycoprotein on sensory neurons is largely independent of NgR1 and NgR2 and resides within Ig-Like domains 4 and 5. PLoS One 4:e5218.

Xie F, Zheng B (2008) White matter inhibitors in CNS axon regeneration failure. Exp Neurol 209:302-312.

Yamada H, Fredette B, Shitara K, Hagihara K, Miura R, Ranscht B, Stallcup WB, Yamaguchi Y (1997) The brain chondroitin sulfate proteoglycan brevican associates with astrocytes ensheathing cerebellar glomeruli and inhibits neurite outgrowth from granule neurons. J Neurosci 17:7784-7795.

Yamashita T, Higuchi H, Tohyama M (2002) The p75 receptor transduces the signal from myelin-associated glycoprotein to Rho. J Cell Biol 157:565-570.

Yang LJ, Zeller CB, Shaper NL, Kiso M, Hasegawa A, Shapiro RE, Schnaar RL (1996) Gangliosides are neuronal ligands for myelin-associated glycoprotein. Proc Natl Acad Sci U S A 93:814-818.

Yang LJ, Lorenzini I, Vajn K, Mountney A, Schramm LP, Schnaar RL (2006) Sialidase enhances spinal axon outgrowth in vivo. Proc Natl Acad Sci U S A 103:11057-11062.

Yang YS, Strittmatter SM (2007) The reticulons: a family of proteins with diverse functions. Genome Biol 8:234.

Yin X, Crawford TO, Griffin JW, Tu P, Lee VM, Li C, Roder J, Trapp BD (1998) Myelin-associated glycoprotein is a myelin signal that modulates the caliber of myelinated axons. J Neurosci 18:1953-1962.

Yin Y, Cui Q, Li Y, Irwin N, Fischer D, Harvey AR, Benowitz LI (2003) Macrophage-derived factors stimulate optic nerve regeneration. J Neurosci 23:2284-2293.

Yin Y, Cui Q, Gilbert HY, Yang Y, Yang Z, Berlinicke C, Li Z, Zaverucha-do-Valle C, He H, Petkova V, Zack DJ, Benowitz LI (2009) Oncomodulin links inflammation to optic nerve regeneration. Proc Natl Acad Sci U S A 106:19587-19592.

Yoshimura T, Kawano Y, Arimura N, Kawabata S, Kikuchi A, Kaibuchi K (2005) GSK-3beta regulates phosphorylation of CRMP-2 and neuronal polarity. Cell 120:137-149.

Zheng B, Ho C, Li S, Keirstead H, Steward O, Tessier-Lavigne M (2003) Lack of enhanced spinal regeneration in Nogo-deficient mice. Neuron 38:213-224.

Zheng B, Atwal J, Ho C, Case L, He XL, Garcia KC, Steward O, Tessier-Lavigne M (2005) Genetic deletion of the Nogo receptor does not reduce neurite inhibition in vitro or promote corticospinal tract regeneration in vivo. Proc Natl Acad Sci U S A 102:1205-1210.

Zimmermann DR, Dours-Zimmermann MT (2008) Extracellular matrix of the central nervous system: from neglect to challenge. Histochem Cell Biol 130:635-653.

Zorner B, Schwab ME (2010) Anti-Nogo on the go: from animal models to a clinical trial. Ann N Y Acad Sci 1198:E22-34.

Zuo J, Neubauer D, Dyess K, Ferguson TA, Muir D (1998) Degradation of chondroitin sulfate proteoglycan enhances the neurite-promoting potential of spinal cord tissue. Exp Neurol 154:654-662.

CHAPTER II:

NgR1 and NgR3 are Receptors for Chondroitin Sulfate Proteoglycans

2.1 Abstract

In the adult mammalian central nervous system (CNS), chondroitin sulfate proteoglycans (CSPGs) and myelin-associated inhibitors (MAIs) stabilize neuronal structure and restrict compensatory sprouting following injury. The Nogo receptor family members NgR1 and NgR2 bind to MAIs and have been implicated in neuronal inhibition. Here we show that NgR1 and NgR3 bind with high affinity to the sugar moiety of CSPGs and participate in CSPG inhibition in cultured neurons. Nogo receptor triple mutants (*NgR123*$^{-/-}$), but not single mutants, show enhanced axonal regeneration following retro-orbital optic nerve crush injury. The combined loss of NgR1 and NgR3 (*NgR13*$^{-/-}$), but not NgR1 and NgR2 (*NgR12*$^{-/-}$), is sufficient to mimic the *NgR123*$^{-/-}$ regeneration phenotype. Regeneration in *NgR13*$^{-/-}$ mice is further enhanced by simultaneous ablation of RPTPσ, a known CSPG receptor. Collectively, these results identify NgR1 and NgR3 as novel CSPG receptors, demonstrate functional redundancy among CSPG receptors, and provide unexpected evidence for shared mechanisms of MAI and CSPG inhibition.

2.2 Introduction

In the adult mammalian CNS, structural neuronal plasticity is restricted by a number of extrinsic (environmental) and cell-intrinsic growth-inhibitory mechanisms (Liu et al., 2006; Park et al., 2008). While such mechanisms are believed to be important for stabilization of intricate networks of neuronal connectivity in CNS health, they also limit adaptive neuronal growth and sprouting following brain or spinal cord injury (SCI). Spontaneous repair following severe CNS injury is incomplete and commonly associated with permanent neurological deficits. Thus, a detailed understanding of the mechanisms that block neuronal growth and repair is of great interest, both biologically and clinically.

A large number of CNS inhibitory cues have been identified (Liu et al., 2006; Silver and Miller, 2004; Winzeler et al., 2011). In experimental animal models of SCI, acute blockage of MAIs (Bregman et al., 1995; Li et al., 2004) or enzymatic degradation of CSPGs with chondroitinase ABC (Ch'aseABC) (Bradbury et al., 2002; Garcia-Alias et al., 2009; Massey et al., 2006) promotes neuronal sprouting and correlates with improved behavioral outcomes. The best characterized MAIs are the reticulon family member Nogo, myelin-associated glycoprotein (MAG), and oligodendrocyte myelin glycoprotein (OMgp) (Liu et al., 2006). Three isoforms of Nogo have been identified, all of which contain a 66 amino acid loop (Nogo66) that signals neuronal inhibition. Mechanistic studies identified the Nogo66 receptor-1 (NgR1) and paired immunoglobulin (Ig)-like receptor B (PirB) as functional receptors for MAIs (Atwal et al., 2008; Fournier et al., 2001). NgR1 is comprised of 8.5 leucine-rich repeats (LRRs), flanked by N-terminal (NT-) and C-terminal (CT-) LRR capping domains. The NT-LRR-CT cluster of NgR1 is fused to a ~ 100 amino acid residue stalk region and connected to the plasma membrane by a glycosylphosphatidylinositol (GPI) anchor (Fournier et al., 2001). NgR1 and its close relative NgR2 show overlapping, yet distinct binding preferences toward MAIs. Nogo66 and OMgp

bind selectively to NgR1 (Liu et al., 2006), while MAG associates with NgR1 and NgR2 (Venkatesh et al., 2005). The related molecule NgR3 is poorly characterized, and thus far no functional NgR3 ligand(s) have been identified. *In vitro*, loss of NgR1 renders neurons more resistant to Nogo66-, MAG-, and OMgp-induced growth cone collapse but not to longitudinal neurite outgrowth inhibition on substrate-bound inhibitors (Chivatakarn et al., 2007; Kim et al., 2004; Zheng et al., 2005). MAIs activate RhoA, RockII, and conventional isoforms of protein kinase C (PKC) to destabilize the neuronal cytoskeleton (Schweigreiter et al., 2004; Sivasankaran et al., 2004). Similar to NgR1, PirB supports binding of Nogo66, MAG, and OMgp. In culture, functional ablation of PirB promotes neurite outgrowth on substrate-bound MAIs and crude CNS myelin. Interestingly, the combined perturbation of PirB and NgR1 signaling leads to a further release of neurite outgrowth inhibition on crude CNS myelin but not on recombinant Nogo66 or MAG (Atwal et al., 2008).

CSPGs are a diverse class of extracellular matrix molecules that influence axonal growth and guidance of developing neurons (Kantor et al., 2004). Following injury to the adult CNS, CSPG expression is upregulated and abundant in reactive astrocytes associated with glial scar tissue (McKeon et al., 1995; Rhodes and Fawcett, 2004; Silver and Miller, 2004). CSPGs are comprised of a protein core with covalently attached glycosaminoglycan (GAG) side chains. GAG chains are large, unbranched polymers composed of ~20-200 repeating disaccharide units. Chondroitin sulfate (CS)-GAGs contain alternating units of N-acetyl-galactosamine and glucuronic acid. Most commonly, the hydroxyl groups at position 4 (CS-A) or position 6 (CS-C) of N-acetyl-galactosamine are sulfated. In CS-B, iduronic acid replaces glucuronic acid in the CS disaccharide unit. In CS-D and CS-E, two sulfate groups per disaccharide unit are present. CSPG inhibition is largely abrogated by bacterial Ch'aseABC, indicating that CS-GAGs are

important for neuronal growth inhibition (Bradbury et al., 2002; Garcia-Alias et al., 2009; Houle et al., 2006; Pizzorusso et al., 2002).

Similar to MAIs, CSPG-mediated inhibition depends on activation of RhoA and conventional PKCs (Powell et al., 2001; Schweigreiter et al., 2004; Sivasankaran et al., 2004). Mechanistic studies recently identified the receptor protein tyrosine phosphatase sigma (RPTPσ) as a high-affinity receptor for CSPGs (Shen et al., 2009). RPTPσ is a member of the leukocyte common antigen-related protein (LAR) family that also includes LAR and RPTPδ. RPTPσ binds to CS-GAG chains and the structurally related heparan sulfate (HS)-GAG chains via its first Ig-like domain (Aricescu et al., 2002; Shen et al., 2009). The association of RPTPσ with CS- and HS-GAGs critically depends on the presence of an evolutionarily conserved cluster of basic amino acid residues. Functional ablation of RPTPσ enhances neurite outgrowth in the presence of CSPGs *in vitro,* and, following CNS injury, promotes growth of sensory afferents (Shen et al., 2009), corticospinal tract axons (Fry et al., 2010), and retinal ganglion cell axons (Sapieha et al., 2005). The incomplete release of CSPG inhibition in RPTPσ-deficient neurons suggests the existence of additional mechanisms of CSPG inhibition. Here we report on the identification of the Nogo receptor family members NgR1 and NgR3 as novel CSPG receptors.

2.3 Results

Nogo receptors participate in Nogo-, MAG-, and OMgp-independent inhibition

To determine the role of Nogo receptor (NgR) family members in CNS myelin inhibition, we generated *NgR1*$^{-/-}$; *NgR2*$^{-/-}$; *NgR3*$^{-/-}$ triple null mice (*NgR123*$^{-/-}$) (**Figure 2.1**). *NgR123*$^{-/-}$ mice are born at Mendelian ratios, viable into adulthood, fertile, and indistinguishable from wild-type (WT) littermate controls at the gross anatomical level. When plated on crude CNS myelin,

postnatal day 7 (P7) cerebellar granule neurons (CGNs), but not dorsal root ganglion (DRG) neurons, of *NgR123*$^{-/-}$ mice show a significant ($P< 0.001$, one-way ANOVA, Tukey's *post hoc*), yet incomplete release of growth inhibition (**Figures 2.2, 2.3**). Compared to CGNs isolated from WT, *NgR1*$^{-/-}$, *NgR12*$^{-/-}$, or *NgR3*$^{-/-}$ mice, CGNs from *NgR123*$^{-/-}$ mutants grow significantly longer neurites on myelin. Remarkably, in two different types of neurons, CGNs and DRG neurons, the combined loss of NgR1 and NgR2 does not result in enhanced neurite growth on crude CNS myelin (**Figures 2.2, 2.3**). Because only NgR1 and NgR3, but not NgR2, are expressed in P7 CGNs (Venkatesh et al., 2005; Zheng et al., 2005), this suggests that NgR3 participates in myelin inhibition. This is somewhat surprising, as NgR3 does not associate with recombinant Nogo, MAG or OMgp (Venkatesh et al., 2005).

To directly test whether NgR3 participates in neurite outgrowth inhibition of endogenously expressed Nogo, MAG, or OMgp, experiments were repeated with CNS myelin isolated from *NogoABC*$^{-/-}$; *MAG*$^{-/-}$; *OMgp*$^{-/-}$ triple mutant mice (*NMO*$^{-/-}$) (Lee et al., 2010). Consistent with previous reports (Cafferty et al., 2010; Lee et al., 2010), *NMO*$^{-/-}$ myelin is less inhibitory than WT myelin (**Figures 2.2, 2.3**). Importantly, on *NMO*$^{-/-}$ myelin, CGNs from *NgR123*$^{-/-}$ mice continue to extend longer neurites ($P< 0.001$, one-way ANOVA, Tukey's *post hoc*) than CGNs from WT, *NgR1*$^{-/-}$, *NgR12*$^{-/-}$, or *NgR3*$^{-/-}$ mice (**Figure 2.2)**. This observation indicates that NgR3 participates in Nogo-, MAG- and OMgp-independent growth inhibition. Because loss of NgR1 or NgR3 alone is not sufficient to promote growth on myelin, this suggests some degree of functional redundancy among these two receptors.

NgR1 and NgR3, but not NgR2, associate with neural GAGs

To identify candidate NgR3 ligand(s), we generated alkaline phosphatase (AP)-tagged receptor fusion proteins and assayed binding to rat brain tissue sections. Prior to the onset of CNS myelination, NgR1 and NgR3, but not NgR2, bind strongly to numerous fiber tracts in the brain and spinal cord (**Figures 2.4a, 2.5**). After myelination, a more uniform binding pattern is observed with a much less pronounced labeling of fiber tracts (data not shown). Importantly, brain sections of *NMO*$^{-/-}$ and *NgR123*$^{-/-}$ triple mutants, *p75*$^{NTR-/-}$ single mutants, and mice lacking select gangliosides show no substantial reduction in soluble receptor binding (**Figure 2.6**). In COS-7 cells, components of the NgR1 holoreceptor complex, including p75^{NTR}, TROY, and Lingo-1 (Yamashita et al., 2005), fail to support NgR3 binding (**Figure 2.7**). This suggests that binding of NgR3 to brain is not mediated by previously identified components of the NgR1 complex. Receptor deletion studies further revealed that the LRRs are not required for binding, and identified two discontinuous and evolutionarily conserved sequence motifs, in both NgR1 and NgR3, that are necessary for binding to brain (**Figures 2.4b-e, 2.8**). Motif 1 is located in the CT capping domain and overlaps with the FRG motif, which was previously shown to participate in sialic acid-dependent binding of the ganglioside GT1b to NgR1 (Williams et al., 2008). Motif 2, separated from motif 1 by approximately 130 amino acid residues, is located near the juxtamembrane region of the NgR1 and NgR3 stalk domain. Motif 2 in NgR1 and NgR3 is comprised of a highly conserved cluster of basic amino acid residues, deletion of which completely abolishes binding to brain (**Figures 2.4b-e, 2.8**). Furthermore, a soluble form of NgR1 in which the basic residues of motif 2 are replaced by seven alanines [NgR1(7ala)-Fc] no longer binds to brain tissue (**Figure 2.4d**).

To assess whether the association of NgR1 and NgR3 with neural tissue is the result of a protein-protein interaction, brain sections were subjected to heat or protease treatment.

Remarkably, binding was largely resistant to either treatment (**Figure 2.6**), suggesting a possible interaction with neural glycan(s). Pretreatment of brain tissue sections with various glycosidases revealed sensitivity to heparinase and Ch'aseABC. Moreover, in the presence of heparin, binding was completely abolished (**Figures 2.6, 2.9a**). Together, these studies suggest that NgR1 and NgR3 associate with neural glycosaminoglycans.

NgR1 and NgR3 complex with select CS-GAGs

To examine the specificity of the GAG association, AP-NgR1 and AP-NgR3 fusion proteins were preincubated with various types of CS-GAGs. Strikingly, CS-B, CS-D and CS-E, but not CS-A or CS-C, effectively compete with brain sections for binding to soluble NgR1 and NgR3 (**Figure 2.9b**). To test whether NgR1 and NgR3 bind to purified GAGs directly, we developed a sandwich ELISA, in which biotinylated GAGs were adsorbed to streptavidin-coated microtiter plates and then incubated with soluble AP-tagged NgRs (**Figure 2.10a**). Consistent with binding experiments to rat brain tissue, NgR1 and NgR3 bind robustly to heparin and purified CS-GAGs, indicating that these receptors bind GAGs directly (**Figures 2.9c, 2.10b**). NgR1 and NgR3 bind with high specificity and selectivity to different types of monosulfated and disulfated GAGs. Strong binding was observed to monosulfated CS-B, and disulfated CS-D and CS-E. The dissociation constants for these interactions are in the low nanomolar range (**Figures 2.9c, 2.10b**). No interactions with CS-A or CS-C were detected. This argues against a nonspecific interaction with negatively-charged compounds and underscores the selectivity of the NgR1- and NgR3-GAG associations.

Notably, the first three Ig-like domains of RPTPσ [RPTPσ(1-3)] show very similar GAG-binding profiles (**Figure 2.9c**). At increasing doses, RPTPσ(1-3)-Fc effectively competes with

NgR1 for binding to CS-E, indicating that these two receptors complex with, at least in part, overlapping CS-GAG epitopes (**Figure 2.10c**). Functional studies with primary neurons show that soluble RPTPσ(1-3)-Fc and NgR1-Fc block the growth-inhibitory activity of CSPGs toward P7 CGNs *in vitro*. The neutralizing effects of NgR1-Fc critically depend on the presence of the GAG-binding motif 2, as soluble NgR1(7ala)-Fc fails to block CSPG inhibition (**Figure 2.9d**).

The CSPG and MAI binding sites on NgR1 are distinct and dissociable

To further characterize the relation of CSPG and MAI binding sites on NgR1, we generated a chimeric receptor construct in which the GAG-binding portion of NgR1 (amino acid residues 278-445) was replaced by the corresponding, non-GAG-binding sequence of NgR2 (amino acid residues 281-420). Nogo66, MAG, and OMgp bind strongly to this chimeric NgR1/NgR2 receptor, indicating that the GAG-binding sequences of NgR1 are not necessary for MAI binding (**Figure 2.11a**). A soluble form of this same chimeric receptor fails to bind to rat brain tissue sections or to GAGs directly (**Figure 2.10d-e**). This suggests that MAIs and CSPGs bind to distinct and dissociable sites on NgR1 (**Figure 2.11b**). Moreover, the presence of CS-B, CS-D, or CS-E does not substantially influence binding of AP-Nogo66 to NgR1 (**Figure 2.11c**).

Neuronal Nogo receptors participate in CSPG inhibition

To determine whether loss of NgRs leads to disinhibition of neurite growth on substrate-bound CSPGs, CGNs from NgR single and compound mutants were analyzed (**Figure 2.12**). Loss of NgR1 or NgR3 alone, or the combined loss of NgR1 and NgR2 (*NgR12*$^{-/-}$), is not sufficient to attenuate CSPG inhibition. Loss of all three NgRs (*NgR123*$^{-/-}$), however, results in significant ($P< 0.001$, one-way ANOVA, Tukey's *post hoc*), yet incomplete release of CSPG

inhibition. Furthermore, release of inhibition for CGNs isolated from *NgR123*$^{-/-}$ and *RPTPσ*$^{-/-}$ pups is comparable (**Figure 2.12**).

Dose-response experiments show that when challenged with high concentrations of CSPGs, *NgR123*$^{-/-}$ and *RPTPσ*$^{-/-}$ neurons are strongly inhibited and lose their growth advantage over WT neurons (**Figure 2.13a**). This suggests that these receptor systems share some degree of functional redundancy. At high doses of CSPGs, loss of NgRs may be compensated by RPTPσ and vice versa. NgRs are not abundantly expressed in P7 DRG neurons (Zheng et al., 2005) and *NgR123*$^{-/-}$ DRG neurons are not disinhibited on CSPG substrate. In a parallel experiment with DRG neurons from *RPTPσ*$^{-/-}$ mice, neurite length is increased on CSPGs (**Figure 2.13b**). Collectively, these studies show that NgR1 and NgR3 bind CS-GAGs directly and participate in CSPG-mediated neurite outgrowth inhibition in a neuronal cell type-specific manner.

NgR1 and NgR3 associate in a ligand-dependent manner

NgRs are GPI-anchored proteins and therefore depend on interactions with transmembrane receptor components to signal growth inhibition across the neuronal plasma membrane. To assess whether NgR1 and NgR3 employ shared signaling mechanisms, we assayed binding of NgR3-Fc to the previously identified NgR1 receptor components p75^{NTR}, TROY, and Lingo-1 in COS-7 cells. We observed no binding of soluble NgR3 to p75^{NTR}, TROY, Lingo-1, or NgR1 (**Figure 2.7**). There are conflicting results on whether NgR1 and NgR3 interact (Barton et al., 2003; Zhang et al., 2011). We therefore revisited this issue and found that NgR1 and NgR3 are part of the same immune complex when co-expressed in HEK293T cells. The NgR1-NgR3 association is ligand-dependent and is only observed in the

presence of exogenously-applied CSPGs (**Figure 2.7**), suggesting that the two receptors may be part of the same receptor complex. In this same assay, no association of NgR1 with NgR2 is observed, neither in the presence nor the absence of CSPGs**.** Next we examined whether NgR1, NgR3, and $p75^{NTR}$ may be part of the same receptor complex. In HEK293T cells co-transfected with NgR1, NgR3, and $p75^{NTR}$, anti-NgR1 pull-down experiments revealed that the three receptors are present in the same immune complex if cells are treated with CSPGs (**Figure 2.7**).

To directly test whether $p75^{NTR}$ is important for CSPG-mediated neurite outgrowth inhibition, P7 CGNs from *$p75^{NTR-/-}$* mice were plated on substrate-bound CSPGs. Loss of $p75^{NTR}$ does not result in a substantial release of CSPG inhibition (**Figure 2.7**). Together these data indicate that $p75^{NTR}$, NgR1, and NgR3 do interact in the presence of CSPGs; however, $p75^{NTR}$ is not necessary for CSPG-mediated outgrowth inhibition. Our studies confirm and expand on previous work showing that the versican isoform V2 mediates neurite outgrowth inhibition in CGNs and DRG neurons in a $p75^{NTR}$-independent manner (Schweigreiter et al., 2004).

CSPGs in the injured CNS support binding of NgR1 and NgR3

Similar to other CNS fiber tracts, severed retinal ganglion cell (RGC) axons in the rodent optic nerve fail to show spontaneous long-distance axonal regeneration. Retro-orbital crush injury to the optic nerve results in a global upregulation of CSPGs along the nerve (Ohlsson et al., 2004). Importantly, injured but not control optic nerve sections support enhanced binding of soluble NgR1-Fc and NgR3-Fc, and the GAG-binding motif 2 of NgR1 and NgR3 is necessary for this binding (**Figure 2.14**). Moreover, binding of soluble receptors is largely abrogated by pretreatment of injured optic nerve sections with Ch'aseABC. Residual binding of NgR1-Fc is

likely due to association with endogenous MAIs (**Figure 2.14**). Together, these studies suggest that CSPGs are endogenous ligands for neuronal NgR1 and NgR3.

Regeneration is enhanced in *NgR123*$^{-/-}$ and *NgR13*$^{-/-}$ mice

In the adult mouse retina, NgR1, NgR2, and NgR3 are all strongly expressed in RGCs (**Figure 2.15a**). Retinal stratification (**Figure 2.15b**) and optic nerve myelination (**Figure 2.15c**) in *NgR123*$^{-/-}$ mice appear normal. To assess RGC axon targeting to the superior colliculus, the suprachiasmatic nucleus, and the lateral geniculate nucleus, the right eye of adult WT and *NgR123*$^{-/-}$ mice was injected with Alexa 594-conjugated Cholera Toxin β (CTB-red) tracer, and the left eye with Alexa 488-conjugated Cholera Toxin β (CTB-green) tracer. No defects in RGC axon central projections or target innervation were observed (**Figure 2.15d-f**). Thus, germline ablation of all three NgRs does not appear to compromise retinal stratification, optic nerve myelination, or RGC axonal pathfinding.

To assess whether NgRs contribute to the regenerative failure of injured CNS axons, we performed retro-orbital optic nerve crush injury in Nogo receptor single and compound mutant mice. Compared to injured wild-type controls, *NgR123*$^{-/-}$ mice show a modest but significant ($P< 0.001$, one-way ANOVA, Tukey's *post hoc*) increase in RGC axon regeneration (**Figure 2.16**). At two weeks post-injury, more GAP-43-positive fibers are observed at 0.2-1.0mm distal to the injury site in *NgR123*$^{-/-}$ mice compared to WT mice. Because NgR1 and NgR2 are known to associate with MAIs, the *NgR123*$^{-/-}$ regeneration phenotype may be a reflection of (i) decreased Nogo, MAG and OMgp inhibition, (ii) decreased CSPG inhibition, or (iii) a combination thereof. To address this issue, we directly compared regeneration of *NgR1*$^{-/-}$, *NgR2*$^{-/-}$, and *NgR3*$^{-/-}$ single mutants, as well as *NgR12*$^{-/-}$ and *NgR13*$^{-/-}$ double mutants, to

NgR123$^{-/-}$ triple mutants. Loss of NgR1, NgR2, or NgR3 alone, or the combined loss of NgR1 and NgR2 (*NgR12*$^{-/-}$), does not result in substantially enhanced RGC axon regeneration compared to WT mice (**Figures 2.16, 2.17; Table 2.1**). However, *NgR13*$^{-/-}$ mice show a similar degree of axon regeneration as *NgR123*$^{-/-}$ mice. This suggests a novel role for NgR3 in signaling neuronal growth inhibition. When coupled with our neurite outgrowth studies *in vitro*, showing that NgR1 and NgR3 operate as functionally redundant CSPG receptors, this suggests that the optic nerve regeneration in *NgR13*$^{-/-}$ and *NgR123*$^{-/-}$ mice is at least in part a reflection of decreased CSPG inhibition.

As RPTPσ is expressed in adult RGCs (Sapieha et al., 2005), we examined whether the combined loss of NgR1 and NgR3 on an *RPTPσ*$^{-/-}$ background (*NgR13/RPTPσ*$^{-/-}$) results in a further increase of regenerating axons. Few regenerating axons were observed in *RPTPσ*$^{-/-}$ single mutants, with no significant difference compared to WT controls ($P > 0.05$)**.** Compared to *NgR13*$^{-/-}$ double mutants, *NgR13/RPTPσ*$^{-/-}$ triple mutants show a further increase in the number of regenerating axons ($P < 0.001$, one-way ANOVA, Tukey's *post hoc*), suggesting a genetic interaction among these receptors (**Figures 2.16, 2.17; Table 2.1**).

In growth-enabled RGCs, loss of all NgRs greatly enhances optic nerve axon regeneration

An advantage of optic nerve regeneration studies is that the growth potential of RGCs can be sensitized by intraocular (i.o.) injection of the yeast cell wall extract Zymosan, resulting in the release of RGC survival and growth-promoting factors, including oncomodulin (Yin et al., 2009), ciliary neurotrophic factor (CNTF), and leukemia inhibitory factor (LIF) (Leibinger et al., 2009). WT mice that receive i.o. Zymosan show greatly enhanced regeneration of RGC axons, exceeding the regeneration observed in non-Zymosan-treated *NgR123*$^{-/-}$ and *NgR13/RPTPσ*$^{-/-}$

mice (**Figure 2.16**). Importantly, *NgR123*$^{-/-}$ mice that receive i.o. Zymosan show significantly more ($P< 0.05$, one-way ANOVA, Tukey's *post hoc*) regenerating axons than WT, *NgR1*$^{-/-}$, *NgR2*$^{-/-}$, *NgR3*$^{-/-}$, or *RPTPσ*$^{-/-}$ single mutants, as well as *NgR12*$^{-/-}$ double mutants, subjected to i.o. Zymosan. *NgR13*$^{-/-}$ and *NgR123*$^{-/-}$ mice with i.o. Zymosan show a similar regeneration phenotype. At several distances from the injury site, *NgR13/RPTPσ*$^{-/-}$ triple mutants with i.o. Zymosan show a further increase in the number of regenerating axons compared to *NgR123*$^{-/-}$ mice with i.o. Zymosan ($P< 0.05$, one-way ANOVA, Tukey's *post hoc*) (**Figures 2.16, 2.17; Table 2.1**).

In mice, optic nerve injury leads to the death of ~ 70% of RGCs by two weeks post-injury (**Figure 2.18**). The enhanced regeneration observed in *NgR123*$^{-/-}$ mice is not a result of increased RGC survival, as similar numbers of injury-induced RGC death were observed in WT and *NgR123*$^{-/-}$ triple mutants. Intraocular Zymosan administration partially protects RGCs from axotomy-induced cell death; however, the protective effect of Zymosan is similar in WT and *NgR123*$^{-/-}$ mice (**Figure 2.18**). Consistent with the view that a decrease in RGC death is not sufficient to promote axonal regeneration, p53-deficient RGCs are more resistant to injury-induced cell death but fail to show enhanced regeneration (Park et al., 2008). To assess whether i.o. Zymosan influences expression of NgRs or RPTPσ in RGCs, we performed *in situ* hybridization at 3 and 7 days post-Zymosan injection, but did not observe any obvious changes (**Figure 2.19**).

2.4 Discussion

The main finding of the present study is the identification of two novel CSPG receptors. We show that NgR1 and NgR3 bind directly and with high affinity to select types of CS-GAGs

and operate as functionally redundant CSPG receptors. Loss of NgR family members individually is not sufficient to overcome CSPG inhibition; however, the combined loss of NgR1 and NgR3 leads to a significant release of CSPG inhibition ($P< 0.05$). In *NgR123*$^{-/-}$ triple mutants, severed RGC axons show enhanced regenerative growth. Interestingly, *NgR13*$^{-/-}$, but not *NgR12*$^{-/-}$ mutants, phenocopy the optic nerve regeneration phenotype of *NgR123*$^{-/-}$ mice. A further enhancement of axon regeneration is observed in *NgR13*/*RPTPσ* triple mutants, revealing a genetic interaction among NgR family members and the previously identified CSPG receptor RPTPσ. Collectively, our studies provide unexpected evidence for shared receptor mechanisms for "prototypic myelin inhibitors" and CSPGs, two major classes of growth-inhibitory molecules abundant in the adult mammalian CNS.

NgR1 and NgR3 bind with high selectivity to specific CS-GAGs

CSPG inhibition depends on the presence of CS-GAG chains; we therefore explored the molecular basis of Nogo receptor-GAG interactions. We identified two sequence motifs in each receptor, both of which are necessary for GAG binding. Motif 1 is located in the LRR-CT capping domain and is identical to the GT1b binding motif identified in NgR1 (Williams et al., 2008). Motif 2 is located in the distal stalk region juxtaposed to the GPI anchor.

Remarkably, NgR1 and NgR3 show exquisite specificity toward select types of CS-GAGs. Binding to monosulfated CS-B, but not CS-A or CS-C, is very robust. In addition, the disulfated GAGs CS-D and CS-E bind strongly to NgR1 and NgR3. Identical binding preferences were observed for RPTPσ. Competition of soluble NgR1 and RPTPσ(1-3) ectodomain for CS-E binding suggests that two very different protein modules complex with at least partially overlapping CS-GAG structures. Dose-response experiments show that loss of all

NgRs or RPTPσ is sufficient to attenuate inhibition of neurite outgrowth at low and intermediate, but not at high, doses of CSPGs. A very recent study identified the receptor tyrosine phosphatase LAR as a CSPG receptor (Fisher et al., 2011). Together, these findings reveal a significant degree of functional redundancy among CSPG receptor mechanisms and suggest that antagonism of multiple NgR and LAR family members will be required to fully overcome CSPG inhibition.

Additive effects of manipulating extrinsic and intrinsic pathways

The relatively modest regeneration phenotype observed in *NgR123*$^{-/-}$ and *NgR13/RPTPσ*$^{-/-}$ mice at two weeks post-injury is consistent with previous studies showing that expression of a dominant negative form of NgR1 in RGCs (Fischer et al., 2004a) or blocking of RhoA with C3 transferase (Fischer et al., 2004b) is not sufficient to promote substantial regeneration of severed optic nerve axons. In a similar vein, removal of one or several MAIs results in inconsistent and often poor regeneration in spinal cord-injured mice (Cafferty et al., 2010; Lee et al., 2010). Collectively, mouse genetic studies suggest that germline ablation of multiple growth-inhibitory ligands or receptors is not sufficient to promote robust and long-distance regeneration in different fiber tracts of the injured adult CNS.

A significant impact of environmental inhibitory signals on limiting axon regeneration was revealed, however, when genetic manipulations were combined with activation of RGC intrinsic growth programs. On an *NgR13*$^{-/-}$, *NgR123*$^{-/-}$, or *NgR13/RPTPσ*$^{-/-}$ background, i.o. Zymosan injection results in significantly enhanced axonal growth distal to the injury site compared to WT, *NgR12*$^{-/-}$, or *RPTPσ*$^{-/-}$ mutant mice with i.o. Zymosan. While the additive effects of simultaneous release of growth-inhibitory mechanisms and activation of intrinsic

growth programs have been reported (Fischer et al., 2004a; Fujita et al., 2011; Kadoya et al., 2009), our data show that in growth-enabled RGCs, members of the NgR family and LAR family collaborate to negatively impact the number and length of regenerating axons following CNS injury.

NgR3 participates in neuronal growth inhibition

Enhanced axon regeneration observed in the optic nerve of *NgR123*$^{-/-}$ mice is mimicked by *NgR13*$^{-/-}$, but not *NgR12*$^{-/-}$, mutants. This suggests that on an *NgR1*$^{-/-}$ background, NgR3, but not NgR2, contributes to the regenerative failure of severed RGC axons. As NgR3 does not directly associate with Nogo, MAG, or OMgp, but supports CSPG binding and participates in CSPG inhibition *in vitro*, our findings suggest that NgR3-CSPG-mediated growth inhibition contributes to the regenerative failure of CNS axons *in vivo*.

While CSPGs are the first ligands identified for NgR3, they also bind to NgR1, further underscoring the high promiscuity of NgR1. CSPGs are found in crude CNS myelin preparations (Niederost et al., 1999; Schweigreiter et al., 2004) and present in the CNS myelin used for this study (data not shown). Similar to the enhanced neurite outgrowth of *NgR123*$^{-/-}$ neurons on CNS myelin (**Figure 2.2**), the enhanced growth of neurons functionally depleted of NgR1 and PirB (Atwal et al., 2008) may be, at least in part, a reflection of decreased MAI and CSPG inhibition.

Implications for experience-dependent neural plasticity

While it has been known for some time that MAIs and CSPGs share similar downstream signaling pathways (Schweigreiter et al., 2004; Sivasankaran et al., 2004), the level at which

MAI and CSPG signaling cascades converge to regulate neuronal cytoskeletal dynamics has not yet been determined. Here we identify NgR1 and NgR3 as novel and functionally redundant CSPG receptors. We provide evidence that Nogo, MAG, OMgp, and CSPGs share receptor components and perhaps signal through related receptor complexes to block neuronal plasticity, sprouting, and axonal regeneration. In support of this idea, the myelin inhibitor Nogo-A shares structural and sequential similarities with neurocan, an inhibitory CSPG implicated in blocking neuronal regeneration (Shypitsyna et al., 2010), suggesting a common origin for two seemingly unrelated inhibitors of growth. The newly discovered connection between CSPGs and NgRs is not only relevant for neuronal repair, but may also provide a mechanistic explanation for why two seemingly unrelated manipulations, such as Ch'aseABC infusion into the mature visual cortex and germline ablation of NgR1 or Nogo, result in enhanced ocular dominance plasticity following monocular deprivation (McGee et al., 2005; Pizzorusso et al., 2002). Mounting evidence suggests that mechanisms that limit neuronal growth and plasticity following CNS injury and disease resemble those that negatively regulate neuronal growth and synaptic structure under physiological conditions (Lee et al., 2008; Zagrebelsky et al., 2010).

The identification of NgRs as shared receptors for MAIs and CSPGs provides new insights into how a diverse group of inhibitory cues regulates neuronal structure and function under physiological conditions and following injury. We propose that Nogo receptors are part of a multicomponent receptor system that serves as a signaling platform to initiate pathways that limit neuronal growth and increase structural stability of synapses. When combined with recent findings that NgR1and its ligands Nogo and OMgp influence synaptic transmission (Raiker et al., 2010), experience-dependent network refinement (McGee et al., 2005), and spatial memory (Karlen et al., 2009), the present findings expand the function of these molecules beyond neural

repair, and shed light on a vital part of the neuronal machinery that limits growth and plasticity in CNS health and disease.

2.5 Future Directions

Identification of specific CSPG ligands that bind and signal via NgRs

While we have found that NgR1 and NgR3 bind with high affinity to select types of GAG side chains, the identity of specific CSPG ligands (protein cores) has not yet been determined. Following CNS injury, a number of CSPG ligands are dramatically upregulated by reactive astrocytes, including aggrecan, neurocan, and phosphacan (Jones et al., 2003; McKeon et al., 1995). These astrocytes are made "reactive" by the release of soluble serum factors and microglia-derived molecules at the injury site, including various interleukins and cytokines (Pekny and Nilsson, 2005; Silver and Miller, 2004; Sofroniew, 2009). One of these molecules, TGFβ1, has been shown to make astrocytes "reactive" *in vitro*, based on increased glial fibrillary acidic protein (GFAP) expression and CSPG production (Wang et al., 2008; Yu et al., 2012). Indeed, cultures of mouse cortical astrocytes that have been treated with TGFβ1 for 7 days are "reactive" (**Figure 2.20a**) and show robust binding to NgR1-Fc, NgR2-Fc, and RPTPσ(Ig1-3)-Fc, but not to AP-Fc or NgR2-Fc (**Figure 2.20b**). Importantly, this binding is dependent on the GAG-binding motif 2 of NgR1 and NgR3 and is abolished with Ch'aseABC treatment, suggesting an interaction with astrocyte-derived CSPGs.

To identify the CSPG binding partners of NgR1 and NgR3, reactive astrocyte-conditioned medium (ACM) was concentrated and tumbled with affinity-purified NgR1-Fc, NgR2-Fc, NgR3-Fc, and RPTPσ(Ig1-3)-Fc (bound to Protein G Plus/Protein A-Agarose beads). Any CSPGs bound to the beads were eluted and digested with Ch'aseABC to degrade the CS-

GAG chains, leaving only the CSPG protein cores. Successful enzyme treatment was shown by western blotting with an antibody (anti-chondroitin sulfate, "stub") selectively reacting with the CS-GAG stub epitopes generated following enzymatic digestion. Following Ch'aseABC treatment of the NgR1, NgR3, and RPTPσ(Ig1-3)-Fc (but not NgR2) conditions, several bands are noted in the 100-250 kilodalton range (**Figure 2.20c**). These bands are of similar sizes between all three conditions, suggesting that NgR1, NgR3, and RPTPσ interact with the same CSPG protein cores. As expected, no bands are recognized by the "stub" antibody without Ch'aseABC treatment (**Figure 2.20c**). Importantly, all Fc fusion proteins were immunoprecipitated at comparable levels (data not shown).

To identify specific CSPG protein cores present in the precipitates, samples were subjected to SDS-PAGE, stained with Coomassie Blue to identify protein bands, and proteolytically digested prior to liquid chromatography-tandem mass spectrometry (LC-MS/MS). Coomassie Blue staining revealed distinct bands (in the 100-250 kilodalton range) present in the NgR1, but not NgR2, conditions (**Figure 2.20d**); however, LC-MS/MS analysis revealed no presence of proteoglycans (**Table 2.2**). As expected, NgR, Fc, and Ch'aseABC components were identified by LC-MS/MS (data not shown), as well as proteins known to be expressed by reactive astrocytes (vimentin, 14-3-3) (Satoh et al., 2004; Schiffer et al., 1986). Surprisingly, all identified proteins were present in both the NgR1 and NgR2 conditions (**Table 2.2**). A number of factors likely contributed to the failure of this approach, including the relatively low amount of input material (astrocyte-conditioned medium) and the fact that proteoglycans are among the most difficult proteins to analyze due to their extensive glycosylation and structural complexity (Harvey, 2005).

As an alternative approach to proteomics, precipitates will be subjected to western blotting, using antibodies raised against likely candidate CSPG protein cores (aggrecan, neurocan, phosphacan, etc.). Functional neurite outgrowth inhibition assays will then be used to determine if neurons lacking NgR1 and/or NgR3 show enhanced growth on these protein cores. Preliminary evidence suggests that *NgR123*$^{-/-}$ CGNs do not grow longer neurites on either substrate-bound aggrecan or neurocan, compared to control CGNs ($P > 0.05$) (**Figure 2.20e-f**), despite the fact that RPTPσ interacts with these CSPG ligands and *RPTPσ*$^{-/-}$ neurons are less inhibited on neurocan substrate (Shen et al., 2009). As RPTPσ also interacts with heparan sulfate proteoglycans (HSPGs) to signal neuronal growth promotion (Coles et al., 2011), and NgR1 and NgR3 bind tissue in a heparinase-sensitive manner (**Figures 2.6, 2.9**), future studies will also address the molecular identity of HSPG ligands for NgRs and the functional consequence of these interactions.

Development of blocking peptides that inhibit CSPG-receptor interactions

While CNS regeneration studies in genetically engineered mice are a powerful tool for target validation, genetic approaches cannot be readily translated to more clinically-relevant settings. Thus, future studies will include the design of polypeptides that block interactions of CSPGs with their high-affinity receptors. As we have identified two short peptide motifs in NgR1 (motif 1: residues 278-281, motif 2: residues 414-426) and NgR3 (motif 1: residues 273-276, motif 2: residues 403-415) that are sufficient to mediate binding to neural CSPGs (**Figures 2.4, 2.8**), standard PCR cloning can be used to generate truncated polypeptides of NgR1 (278-426) and NgR3 (273-415), which can be tested by ELISA for their ability to compete with NgR1 and NgR3 (and RPTPσ) for binding to CS-GAGs. The corresponding sequences of NgR2 may

be used as a negative control. In addition, smaller peptides consisting of only motif 1 or motif 2 can be generated and tested for their ability to block CSPG binding to NgRs. It would also be interesting to know whether the spacing between motif 1 and motif 2 can be reduced without compromising CS-GAG binding. If these peptides successfully block CSPG-receptor interactions, future studies can address their ability to override CSPG inhibition of primary neurons *in vitro* and to promote axonal regeneration following crush injury to the optic nerve *in vivo*.

Long-term regeneration studies with an emphasis on functional recovery

While the optic nerve injury model is becoming more widely accepted as an appropriate system for the study of anatomical regeneration in rodents (Fischer et al., 2004a; Fujita et al., 2011; Park et al., 2008), only one research group has demonstrated functional recovery in this model (de Lima et al., 2012). In this study, combined genetic and pharmacological manipulations allowed for RGC fiber regeneration through the optic nerve and into target areas of the brain, with a partial restoration of the optomotor response, depth perception, and circadian photoentrainment (de Lima et al., 2012). As an alternative and more sensitive readout for functional recovery of RGC fibers, we have developed an electrophysiological approach, in which compound action potential (CAP) propagation is measured in acutely isolated optic nerves to determine if regenerating fibers are electrically active. CAP recordings from uninjured, adult optic nerves reveal a large peak with multiple components (**Figure 2.21a**), likely representing the fast and slow myelinated fibers of the optic nerve (average peak amplitude: 5mV, average conduction velocity: 4m/s). This peak almost completely disappears at 2 weeks post-crush injury (data not shown - average peak amplitude: 15μV, average conduction velocity: 0.5m/s),

correlating with the lack of RGC fiber regeneration in the injured mammalian CNS. Despite the significant amount of anatomical regeneration seen in both wild-type animals with Zymosan administration and *NgR123*$^{-/-}$ animals with Zymosan administration (**Figure 2.16**), CAP recordings at several timepoints following injury reveal no substantial improvements in peak amplitude or conduction velocity in either of these conditions (**Figure 2.21b; Table 2.3**). This could represent either technical limitations in the recording strategy or the fact that these regenerating fibers are not electrically active. Thus, future experiments will need to be performed to distinguish between these two possibilities.

As shown in **Figure 2.16** (and discussed above), we have discovered additive effects on RGC fiber regeneration when extrinsic factors are genetically deleted (NgRs) and intrinsic pathways are activated (Zymosan injection). Recent evidence has suggested that manipulation of another intrinsic signaling pathway, the mTOR pathway, can also promote axon regeneration following CNS injury. Genetic deletion of PTEN, which results in enhanced PI3K and mTOR activation, greatly enhances regeneration of both RGC fibers following optic nerve crush injury and corticospinal tract axons following spinal cord injury (Liu et al., 2010; Park et al., 2008). Indeed, intraocular injection of adeno-associated virus 2, which is expressing GFP and PTENshRNA (AAV2-GFP-PTENshRNA), results in substantial transduction of RGCs (**Figure 2.21c**). Furthermore, phospho-S6 (pS6) levels are greatly increased in RGCs upon transduction with AAV2-GFP-PTENshRNA compared to a scrambled shRNA control (AAV2-GFP-scrambled) (**Figure 2.21d**), suggesting that mTOR levels are thus increased. In addition, substantial RGC fiber growth is seen distal to the injury site, two weeks following optic nerve crush injury (and four weeks following AAV2-GFP-PTENshRNA injection) (**Figure 2.21d**). Future studies will address whether there is an additive effect with PTEN knockdown and

genetic deletion of NgRs, as well as how far these regenerating fibers can travel at several weeks and months post-injury. If significant fiber growth is seen into target regions of the brain, the possibility of remyelination, synaptogenesis, and functional recovery will be explored. Improved imaging techniques will also be utilized, including tetrahydrofuran-based chemical clearing of the brain and optic nerve (**Figure 2.21e-f**), which renders fixed and unsectioned tissue transparent for high-resolution ultramicroscopy and 3D reconstruction (Erturk et al., 2011; Luo et al., 2013). With this method, axonal trajectories can be unequivocally traced and regenerating axons can be evaluated as a whole unit, rather than in separate 2D fragments.

2.6 Methods

Transgenic mice: All animal handling and surgical procedures were performed in compliance with local and national animal care guidelines and approved by the University of Michigan Committee on Use and Care of Animals (UCUCA). *NogoABC*$^{-/-}$;*MAG*$^{-/-}$;*OMgp*$^{-/-}$, *RPTPσ*$^{-/-}$, *NgR1*$^{-/-}$, *NgR2*$^{-/-}$, and *p75*$^{NTR-/-}$ mice have been described (Lee et al., 2010; Shen et al., 2009; Zheng et al., 2005). *NgR3*$^{-/-}$ germline mutants were generated by Lexicon Genetics and kindly provided by M. Greenberg (Harvard Medical School). NgR1 and NgR2 conditional mutants have been described elsewhere (Williams et al., 2008). NgR3 conditional knockout mice were generated by flanking exon2 with loxP sites (**Figure 2.1**). To generate germline deletion mutants, conditional knockouts were crossed with protamine-cre transgenic mice and then intercrossed with each other, or onto an *RPTPσ*$^{-/-}$ background, to generate double and triple mutants.

To confirm that *NgR123*$^{-/-}$ mice are null for NgR1, NgR2, and NgR3, brain extracts of adult WT and *NgR123*$^{-/-}$ mice were analyzed by western blotting. To enrich for NgRs, brain

membranes were isolated, lysed in RIPA buffer (Sigma) containing protease inhibitor cocktail (Sigma), and affinity precipitated with agarose-Concanavalin A beads (Vector Laboratories) overnight at 4°C. Bound glycoproteins were subjected to SDS-PAGE, blotted onto nitrocellulose membranes (Thermo Fisher Scientific), and probed with polyclonal anti-NgR1, anti-NgR2, anti-NgR3 or anti-β-actin (Sigma).

Neurite outgrowth assays: To assay myelin inhibition, 96-well plates were coated with poly-D-lysine hydrobromide (50μg/ml; Sigma) overnight, rinsed in water, air dried, and then incubated with a 5μl spot of BSA (40μg/ml) or CNS myelin (40μg/ml) prepared from wild-type or *NogoABC*$^{-/-}$;*MAG*$^{-/-}$;*OMgp*$^{-/-}$ (*NMO*$^{-/-}$) mice (Lee et al., 2010). Proteins were adsorbed to poly-D-lysine for 3 hours at 37°C. Wells were then rinsed and incubated with laminin (10μg/ml; Sigma) for 1 hour at 37°C. P7 mouse cerebellum was dissected, trypsinized, gently triturated, and CGNs were purified in a discontinuous Percoll gradient before resuspension in Neurobasal medium (Invitrogen) with B-27® supplement (Invitrogen), glutamine, glucose, and penicillin/streptomycin, as described previously (Venkatesh et al., 2005). P7 mouse DRG neurons were dissected, incubated in 0.05% trypsin and 0.1% collagenase, and triturated before resuspension in Neurobasal medium with B-27® supplement, glutamine, penicillin/streptomycin, and 15ng/ml nerve growth factor. CGNs and DRG neurons were then plated at 8,000 cells/well, and cultured for 24 hours before fixation with 4% paraformaldehyde, blocking in 1% horse serum and 0.1% Triton X-100 in PBS, and staining with anti-class III β-tubulin (TuJ1; Promega). To visualize the spotted myelin, wells were also stained with anti-myelin basic protein (Sigma). Alexa Fluor-conjugated secondary antibodies (Invitrogen) were used for fluorescent labeling.

Images were taken using an inverted microscope (IX71; Olympus) attached to a digital camera (DP72; Olympus).

To assay CSPG inhibition, 5µl spots (1, 2, 10, 100µg/ml) of either a mixture of large, extracellular chondroitin sulfate proteoglycans isolated from embryonic chicken brain (Millipore), aggrecan (Sigma), neurocan (Millipore) or BSA were adsorbed on 96-well plates for 3 hours at 37°C before coating with poly-D-lysine hydrobromide and laminin. After 24 hours in culture, neurite length of CGNs or DRG neurons was determined as described above. To visualize the spotted CSPGs, wells were also stained with anti-chondroitin sulfate (CS56; Sigma). For some experiments, receptor fusion proteins (10µg/ml) or the ROCK inhibitor Y-27632 (10µM) were added to the wells at the time of CGN plating.

Construction of fusion proteins: AP- and Fc-tagged fusion proteins were constructed by standard PCR cloning using the Tth-DNA polymerase (Applied Biosystems). Constructs for AP-Fc, AP-NgR1(ΔGPI), AP-NgR2(ΔGPI), AP-NgR3(ΔGPI), AP-Nogo66, AP-OMgp, AP-Sema3A, AP-Sema3F, and MAG-Fc have been described previously (Kantor et al., 2004; Venkatesh et al., 2005). Additional constructs included AP-NgR1$^{\text{NT-LRR-CT}}$(Ala^{24}-Val^{311}), AP-NgR2$^{\text{NT-LRR-CT}}$(Ser^{30}-Thr^{314}), AP-NgR3$^{\text{NT-LRR-CT}}$(Ser^{22}-Pro^{307}), AP-NgR1$^{\text{CT+stalk}}$ (Val^{263}-Glu^{445}), AP-NgR2$^{\text{CT+stalk}}$ (Ala^{264}-Ser^{397}), AP-NgR3$^{\text{CT+stalk}}$ (Asp^{258}-Val^{413}), AP-NgR1$^{\text{stalk}}$(Ala^{310}-Glu^{445}), AP-NgR1$^{\text{CT}}$(Phe^{278}-Cys^{336}), AP-NgR1$^{\Delta\text{15CT+stalk}}$(Phe^{278}-Glu^{445}), AP-NgR3 $^{\Delta\text{15CT+stalk}}$(Phe^{273}-Val^{413}), AP-NgR1$^{\Delta\text{17CT+stalk}}$(Gly^{280}-Glu^{445}), and AP-NgR1$^{(\text{CT+stalk})\Delta\text{m2}}$(Phe^{278}-Gly^{412}). Soluble Fc fusion proteins contain a PAM-myc signal sequence and a C-terminal Fc region of human IgG1. Constructs were assembled in the expression vector pcDNA3.0 as described (Venkatesh et al., 2005) and include NgR1-Fc(Cys^{27}-Gly^{448}), NgR1$^{\Delta\text{m2}}$-Fc(Cys^{27}-Gly^{412}), NgR1(7ala)-Fc (residues

414-429 **RRR**PGCS**RK**N**R**T**R**SHC of NgR1 were replaced by **AAA**PGCS**AA**TS**T**A**S**HC - the location of an internal Spe1 restriction site introduced for PCR construction is underlined), NgR2-Fc(Cys^{31}-Gly^{399}), NgR3-Fc(Pro^{25}-Val^{420}), $NgR3^{\Delta m2}$-Fc(Pro^{25}-Met^{397}), NgR1(Cys^{27}-Lys^{277})/NgR2(Val^{281}-Gly^{399})-Fc, and RPTPσ(Ig1-3)-Fc(Glu^{30}-Val^{315}).

Binding assays: COS-7 cells grown in 24-well plates were transiently transfected (Lipofectamine® 2000) with plasmid DNA encoding $p75^{NTR}$, TROY, Lingo-1, L-MAG, NgR1, NgR3, NgR1(7ala), chimeric NgR1(Cys^{27}-Lys^{277})/NgR2(Val^{281}-Leu^{420}), or GFP. Ligand-receptor binding studies were carried out and developed as described previously (Venkatesh et al., 2005). For some COS-7 cell binding assays, CS-GAGs, at a concentration of 1mg/ml, were added to the wells at the time of ligand incubation. Binding studies with astrocytes were performed in a similar fashion, using P1 mouse cortical astrocytes. Briefly, mouse cerebral cortex from 4 pups was dissected (including removal of the meninges and hippocampus), trypsinized, triturated, and plated in a T75 tissue culture flask in DMEM (Invitrogen) with 10% fetal bovine serum and penicillin/streptomycin (Yu et al., 2012). Once confluent, the flasks were placed on a platform shaker (200rpm, 37ºC) for 24 hours to remove neurons, microglia, and oligodendrocyte progenitor cells (Yu et al., 2012). The culture medium was immediately replaced and the astrocytes were harvested onto 24-well plates. Once confluent, astrocytes were switched to DMEM (without serum) for 24 hours, followed by addition of 1μg/ml TGFβ1 (R&D Systems) for 7 days before binding studies were carried out. Some wells were incubated with chondroitinase ABC (Calbiolchem; 1unit/ml in Tris-acetate buffer - pH 8.0 - with 0.02% BSA) for 3 hours at 37°C prior to addition of receptor fusion proteins. Additionally, some wells were

stained with anti-chondroitin sulfate (CS56; Sigma) and anti-GFAP (Millipore) to confirm astrocyte reactivity.

To monitor binding of soluble Nogo receptors to brain tissue sections *in situ*, binding studies with embryonic (E18) and neonatal (P1-P3) rat or mouse brains were carried out as described previously (Kantor et al., 2004; Venkatesh et al., 2005). Additional binding studies included longitudinal optic nerve sections of adult mice. To assess whether the association of AP-NgR1$^{CT+stalk}$ or AP-NgR3$^{CT+stalk}$ to brain tissue sections is mediated by protein-protein interactions, brain sections were preincubated at 75ºC for 3 hours or treated with trypsin (10 units for 30 minutes at 37°C) prior to incubation with AP-fusion proteins. To explore whether glycoconjugates participate in binding of soluble Nogo receptors to brain tissue, sections were enzymatically treated with glycosidases according to manufacturer's instructions prior to adding the AP-fusion proteins. Enzymes included N-acetylglucosaminidase, *Vibrio cholerae* neuraminidase, heparinase III (*Flavobacterium heparinium*), chondroitinase ABC (all from Calbiochem), glycopeptidase F (New England Biolabs), and endoneuraminidase-N (kindly provided by U. Rutishauser, Sloan-Kettering Institute). Some injured optic nerve sections were incubated with chondroitinase ABC (1unit/ml) for 3 hours at 37°C prior to addition of receptor fusion proteins. To assay whether specific types of GAG side chains block binding of soluble NgRs to brain tissue, competition binding experiments were carried out in the presence of heparin or different types of CS-GAG chains (50μg/ml; Seikagaku Glycobiology).

To determine whether NgRs or RPTPσ bind directly to GAG chains, enzyme-linked immunosorbent assays (ELISAs) were performed as described previously (Briani et al., 1998). Briefly, GAG chains were biotinylated with EDC and EZ-Link Sulfo-NHS-LC-LC-Biotin (Thermo Scientific) and adsorbed for 15 minutes to ELISA plates (Immulon4; NUNC) precoated

with streptavidin (5μg/ml; Invitrogen). Plates were blocked (5% BSA), rinsed with HBS, and incubated with various amounts of fusion proteins (diluted with 5% BSA) for 2 hours at 22˚C. Following five washes with HBS, bound AP activity was monitored with a BluePhos Microwell Substrate Kit (KPL). For competitive binding experiments, immobilized GAG chains were preincubated with various amounts of RPTPσ(Ig1-3)-Fc for 16 hours at 4˚C, and then incubated with AP-NgR1 (1nM) for 2 hours at 22˚C. Bound AP activity was measured as described above.

Immunoprecipitation/proteomics analysis: HEK293T cells (in 10cm culture dishes) were transfected with various combinations of $p75^{NTR}$, NgR1, NgR1-myc, NgR2-myc, and NgR3-myc expression constructs. After 48 hours, the cells were incubated in lysis buffer containing the following: 20mM Tris-HCl (pH 7.5), 150mM NaCl, 5mM EDTA, 1% NP-40, and protease inhibitor mixture. For some assays, cells were incubated for 30 minutes with 100μg/ml of CSPG mixture prior to lysis. Cell lysates were tumbled overnight at 4°C in the presence of either anti-$p75^{NTR}$ (Promega) or anti-NgR1, and precipitated with Protein G Plus/Protein A-Agarose (Calbiochem) after incubation at 4°C for 2 hours. Precipitated beads were rinsed three times with lysis buffer, and bound proteins were eluted with 2X SDS sample buffer. Precipitates were analyzed by immunoblotting, using anti-NgR1, anti-$p75^{NTR}$ (Promega), anti-myc (Cell Signaling), or anti-β-actin.

For proteomics analysis, astrocyte-conditioned medium (ACM) from TGFβ1-treated cultures (see above) was collected and concentrated tenfold using centrifugal filter units (Millipore). Concentrated ACM was tumbled overnight at 4°C in the presence of either affinity-purified NgR1-Fc, NgR2-Fc, NgR3-Fc, or RPTPσ(Ig1-3)-Fc, and precipitated with Protein G Plus/Protein A-Agarose after incubation at 4°C for 2 hours. Precipitated beads were rinsed six

times with DMEM, and some samples were then incubated with chondroitinase ABC (1unit/ml) for 3 hours at 37°C. Bound proteins were eluted with 2X SDS sample buffer, and some precipitates were analyzed by immunoblotting, using anti-chondroitin sulfate "stub" (MAB2030, Millipore) or anti-human IgG, Fc (Millipore). The remaining precipitates were submitted to the University of Michigan Proteomics and Peptide Synthesis Core (Henriette Remmer, Director). These samples were subjected to SDS-PAGE, Coomassie Blue staining, and in-gel digestion (reduction with dithiothreitol, alkylation with iodoacetamide, overnight incubation with trypsin at 37°C, peptide extraction). The digests were analyzed using liquid chromatography-tandem mass spectrometry (LC-MS/MS) on a LTQ ion trap mass spectrometer (Thermo Fisher Scientific). Briefly, digests were loaded and gradient elution was performed over a 10cm by 75μm ID C18 column at 400nL/min. A 30 minute gradient was employed. The mass spectrometer was operated in data-dependent mode and the seven most abundant ions were selected for MS/MS. Product ion data were searched against the NCBI and UniProt protein database using the Mascot and X! Tandem search engines. Mascot output files were parsed into the Scaffold program for filtering to assess false discovery rates and allow only correct protein identifications.

Optic nerve surgery: Adult mice (6-8 weeks of age) of either sex were anesthetized with an intraperitoneal injection of Ketamine (100mg/kg; Fort Dodge Animal Health) and Xylazine (10mg/kg; Akorn, Inc.). The optic nerve was exposed through an incision in the conjunctiva and compressed for 10 seconds with angle jeweler's forceps (Dumont #5; Fine Science Tools) at approximately 1mm behind the eyeball. Care was taken not to damage or rupture the ophthalmic artery. For intraocular injection of Zymosan, 5μl of a suspension (12.5μg/μl in sterile PBS;

Sigma) was injected manually using a Hamilton syringe with a 30 gauge removable needle. Following optic nerve surgery, the operated eye was rinsed with sterile PBS and ophthalmic ointment was applied (Butler AHS). All surgeries were performed under aseptic conditions. Fourteen days after optic nerve injury, mice were given a lethal dose of anesthesia and perfused through the heart with PBS followed by ice-cold 4% paraformaldehyde (with the exception of mice used for electrophysiology studies). For studies that included intraocular injection of adeno-associated virus 2 (AAV2), 2µl of AAV2-GFP-scrambled was injected into the left eye, while 2µl of AAV2-GFP-PTENshRNA was injected into the right eye, fourteen days prior to optic nerve injury.

Electrophysiology: Age-matched, background-matched mice (uninjured or 3-11 weeks post-optic nerve crush) were killed by CO_2 inhalation. Optic nerves from each animal were dissected and placed in oxygenated artificial CSF (ACSF). ACSF contains the following: 125mM NaCl, 1.25mM NaH_2PO_4, 25mM glucose, 25mM $NaHCO_3$, 2.5mM $CaCl_2$, 1.3mM $MgCl_2$, and 2.5mM KCl (saturated with 95% O_2/5% CO_2). Nerves were incubated in oxygenated ACSF for 45-60 minutes at room temperature and then transferred to a temperature-controlled recording chamber held at 37 ± 0.4°C. The retinal end of the nerve was drawn into the tip of a suction pipette electrode, and nerve at a distance of 1.7mm distal to the retinal end was drawn into the tip of a second suction pipette electrode. One electrode was connected to a constant-current stimulus isolation unit (WPI) driven by Axon™ pClamp® 10.3 software, and the other to one input of a differential alternating current amplifier (custom-made). The other amplifier input was connected to a pipette that was placed near the recording pipette but not in contact with the nerve. This electrode served to subtract most of the stimulus artifact from the

recordings. Signals were filtered at 10 kHz, sampled at 50-100 kHz, and fed into the Axon™ Digidata 1440A - Axon™ pClamp® 10.3 data acquisition system. For analysis, conduction velocity was taken as the length of the nerve divided by the time-to-peak.

Histochemical studies: *In situ* hybridization of mouse retina with cRNA probes specific for NgR1, NgR2, NgR3, and RPTPσ was carried out as described previously (Sapieha et al., 2005; Venkatesh et al., 2005). For immunohistochemical procedures, cryosections of adult retina were stained with anti-calbindin (Swant; 1:2500 dilution) or anti-calretinin (Swant; 1:2500 dilution), and then counterstained with Hoechst 33342 (1:30000 dilution). For retinal whole-mount immunostaining, eyes were post-fixed in 4% paraformaldehyde overnight at 4°C, and retinal "cups" were dissected out and fixed in 4% paraformaldehyde for 30 minutes at 4°C. Retinas were washed with PBS, blocked in 10% goat serum and 0.2% Triton X-100 for 1 hour, incubated with primary antibodies (anti-GFP, Invitrogen; anti-phospho-S6, Cell Signaling) for 1-2 days at 4°C, and washed with PBS. Following incubation with the appropriate Alexa Fluor-conjugated secondary antibodies (Invitrogen) overnight at 4°C and another round of washing with PBS, retinas were mounted onto slides for imaging. To assess axon density and myelination, optic nerves were embedded in epon and stained with Toluidine Blue. To assess retinal ganglion cell death at various time points following optic nerve injury, retinal sections were stained with anti-class III β-tubulin (TuJ1), and in some instances, with anti-active caspase-3 (Promega).

For intraocular injections of anterograde tracer, 6-week-old mice received bilateral injections (2μl) of 1μg/μl Alexa 488- and Alexa 594-conjugated Cholera Toxin β (Invitrogen) in the left and right eye, respectively. Five days post-injection, mice were perfused transcardially,

and their brains were dissected, post-fixed in 4% paraformaldehyde overnight, and cryoprotected in 30% sucrose overnight. Brain tissue was embedded in OCT Tissue-Tek Medium (Sakura Finetek) and coronal sections (50μm thickness) were imaged.

To visualize regenerating axons in the injured optic nerve, eyes with optic nerves attached were dissected, post-fixed, and cryoprotected. Optic nerves were embedded and longitudinal sections (14μm thickness) were stained with anti-GAP-43 and/or anti-GFP. The appropriate Alexa Fluor-conjugated secondary antibodies (Invitrogen) were then used for fluorescent labeling. Images were acquired using an inverted microscope (IX71; Olympus) attached to a digital camera (DP72; Olympus).

For chemical clearing of CNS tissue (Luo et al., 2013), adult mice were perfused transcardially, five days post-Cholera Toxin β injection. The optic nerve and brain tissue were dissected and post-fixed in 4% paraformaldehyde overnight. Samples underwent dehydration by incubation in increasing concentrations of tetrahydrofuran (THF; Sigma) solutions under constant rocking at room temperature (protected from light). Optic nerves were incubated in 50% THF (diluted in water), 80% THF, and 100% THF for 20 minutes each. Dehydrated optic nerves were rendered clear by incubating in a ratio of 1:2 benzyl alcohol: benzyl benzoate (Sigma) for 30 minutes. Brain tissue was incubated in 50% THF for 12 hours, 80% THF for 12 hours, 100% THF for 2 × 12 hours, and BABB for 12 hours.

Statistical analysis: For quantification of neurite outgrowth, UTHSCSA ImageTool for Windows was used, and processes equal or longer to approximately one cell body diameter were measured. For each condition, at least 150 neurites were quantified, and the mean and SEM of neurite length for each genotype was determined from multiple, independent experiments. For

quantification of retinal ganglion cell death, the density of TuJ1-positive cells in the ganglion cell layer per field of view (at least 10 sections, 3 independent experiments per condition) was counted. For quantification of activated caspase-3-positive retinal ganglion cells, the number of cells labeled for activated caspase-3 was calculated as a percentage of the total number of cells (TuJ1-positive) per field of view (at least 10 sections, 3 independent experiments per condition). Quantification of optic nerve binding assays and *in situ* hybridization (at least 20 sections, 4 independent experiments per condition) was performed as previously described (Robak et al., 2009), using Microsuite Five (Olympus) quantification software. All data were analyzed using one-way analysis of variance followed by Tukey's *post hoc* comparisons. All statistics were performed using SigmaStat 3.0 for Windows (Systat Software).

To assess regenerative axonal growth, the number of GAP-43-positive axons at prespecified distances from the injury site was counted in at least three sections per nerve. These numbers were converted into the number of regenerating axons per nerve at various distances as described previously (Fischer et al., 2004a). All data were analyzed using one-way analysis of variance followed by Tukey's *post hoc* comparisons. All statistics were performed using GraphPad Prism 5.00 (GraphPad Software). Our finding that loss of all three NgRs elicits significant retinal ganglion cell regeneration is based on two independently generated data sets produced by two independent surgeons (K.T.B. and Y. Koriyama). Both data sets were analyzed separately and lead to the same conclusions (**Table 2.1**). In addition, no significant differences ($P > 0.05$) in axon regeneration following injury (with or without intraocular Zymosan injection) were observed between mice on three different genetic backgrounds (129, C57BL/6, BALB/c) (**Figure 2.22**).

2.7 Acknowledgments

Portions of this chapter have been published (see citation below) and permission was received from the editors to use this work as part of a dissertation:

Dickendesher TL, Baldwin KT, Mironova YA, Koriyama Y, Raiker SJ, Askew KL, Wood A, Geoffroy CG, Zheng B, Liepmann CD, Katagiri Y, Benowitz LI, Geller HM, Giger RJ (2012) NgR1 and NgR3 are receptors for chondroitin sulfate proteoglycans. Nat Neurosci 15:703-712.

This work was supported by the Neuroscience Training Grant T32EY017878, the University of Michigan Rackham Merit Fellowship (Travis L. Dickendesher.), the Cellular and Molecular Biology Training Grant T32GM007315 (Katherine T. Baldwin and Yevgeniya A. Mironova), the National Research Service Award Ruth Kirschstein Fellowship F31NS061589 (Stephen J. Raiker.), the New York State Spinal Cord Injury Research Program, the Dr. Miriam and Sheldon G. Adelson Medical Foundation on Neural Repair and Rehabilitation, the US Department of Veterans Affairs Grant 1I01RX000229-01, the National Institute of Neurological Disorders and Stroke R56NS047333 (Roman J. Giger) and the National Eye Institute (Larry I. Benowitz). We thank Michel Tremblay for *RPTPσ*$^{-/-}$ mice; Michael Greenberg for *NgR3*$^{-/-}$ mice; Brian Pierchala for *p75*$^{NTR-/-}$ mice; Brian Bates, David Howland, and Mary L. Mercado for their assistance in the generation and initial analysis of *NgR123*$^{-/-}$ triple mutant mice; Zhigang He for AAV2-GFP-scrambled and AAV2-GFP-PTENshRNA; Urs Rutishauser for Endo-N; the University of Michigan Proteomics and Peptide Synthesis Core (Henriette Remmer, Director) for assistance in proteomics analysis; Peter Shrager for the use of his optic nerve conduction recording data; David Figge and Yuko Yasui for assistance in ELISA binding assays; Yuqin Yin

for training in optic nerve surgery; Yuntao Duan for generation of the RPTPσ(Ig1-3)-Fc construct; Justin Barbieri for technical assistance; and Margaret M. Zaleska for project administration.

2.8 Author Contributions

Travis L. Dickendesher (T.L.D.), Larry I. Benowitz, Herbert M. Geller, and Roman J. Giger (R.J.G.) designed the experiments; T.L.D., Katherine T. Baldwin (K.T.B.), Yevgeniya A. Mironova (Y.A.M.), Yoshiki Koriyama (Y.K.), Stephen J. Raiker, Claire D. Liepmann, Yasuhiro Katagiri, and R.J.G. performed experiments; T.L.D., K.T.B., and Y.K. contributed to data analysis and figure preparation; Kim L. Askew, Andrew Wood, Cedric G. Geoffroy, and Binhai Zheng generated and provided mice or reagents for the study; and T.L.D. and R.J.G. wrote the manuscript.

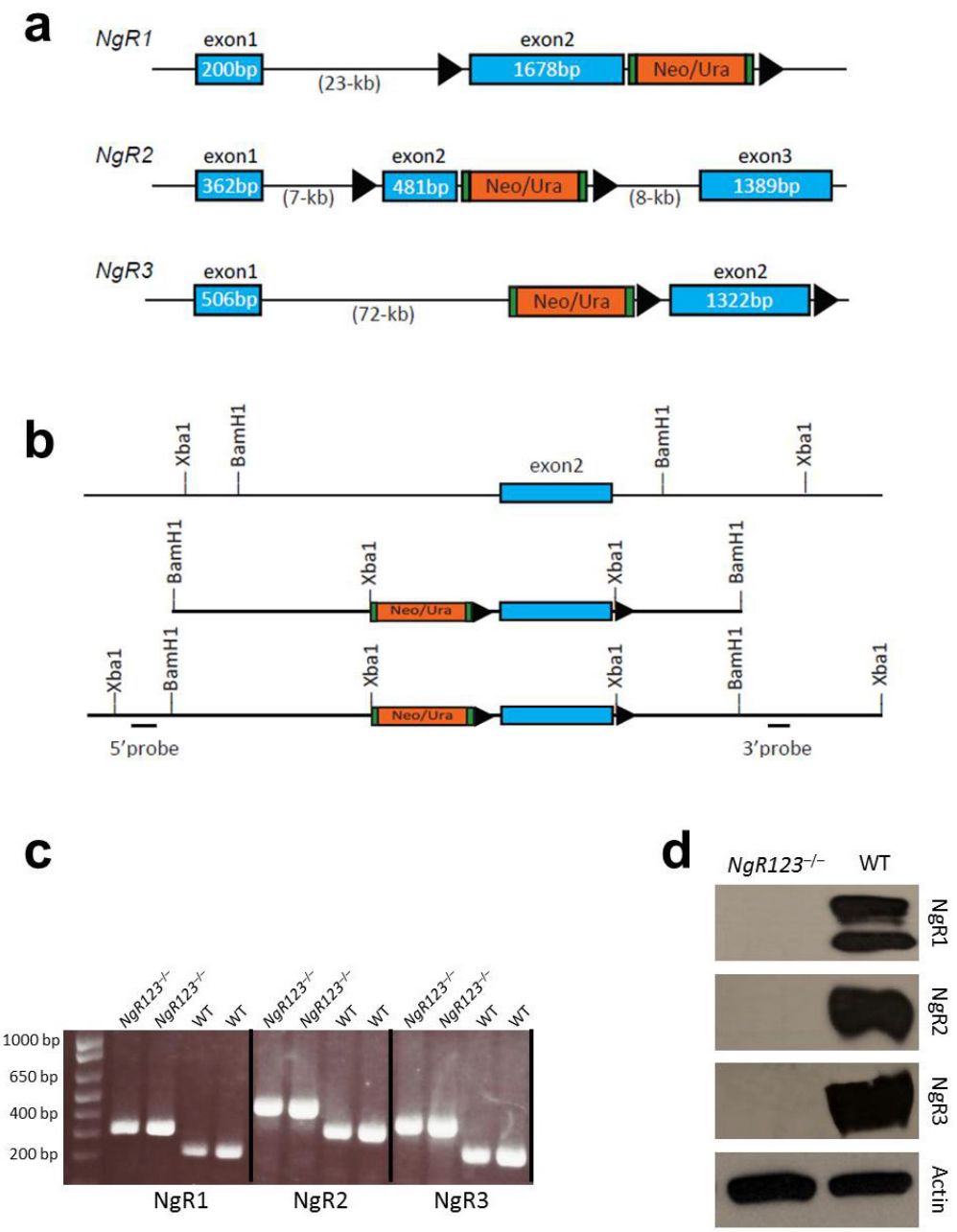

Figure 2.1: Generation of Nogo receptor conditional knockout mice. (**a**) Targeting strategy for the generation of NgR1, NgR2, and NgR3 conditional knockout mice. The mouse NgR1 and NgR3 genes are each comprised of 2 coding exons and the mouse NgR2 gene is comprised of 3 coding exons. For all three genes, exon 2 was flanked by loxP sites (black triangles). Exons are shown in blue. The size of exons in base pairs (bp) and introns in kilobases (kb) is indicated. A neo/ura selection marker (orange) flanked by frt sites (green boxes) was inserted in each of the three gene loci. (**b**) NgR3 gene targeting strategy. (Top) Distribution of BamH1 and Xba1 restriction sites relative to exon2 of the mouse NgR3 gene. (Middle) Targeting vector for

generation of NgR3 conditional knockout mice. (Bottom) Targeted locus in NgR3 conditional mutants. The position of the 5' and 3' outside probes used for Southern blot analysis (XbaI) of double selected embryonic stem cells is indicated. To generate germline deletion mutants, mice carrying conditional alleles were crossed with protamine-cre transgenic mice and then intercrossed to generate double and triple mutants. (**c**) PCR genotyping of DNA isolated from tail biopsies of WT and *NgR123*$^{-/-}$ mice. For all primer sets (NgR1, NgR2, NgR3), the null PCR product is larger than the WT PCR product. PCR primers for NgR1 conditional mice include: 5'-GGTCTAGGGATGCATCTCAG-3', 5'-ACATCTGAAGGCCTTCTGG-3', and 5'-GTGGTCTGTGTGGCTCCTGC-3' (WT allele - 200bp, conditional allele - 300bp, null allele - 320bp); PCR primers for *NgR2* conditional mice include: 5'-CAGTCTTGCAGCTGACTGTAGCTGAG-3', 5'-GACCTGTGGGGAGAGCATAGTGAG-3', and 5'-GTTTAACGGCTAGCCAGCCAACATC-3' (WT allele - 333bp, conditional allele - 425bp, null allele - 458bp); and PCR primers for NgR3 conditional mice include: 5'-AGTGCTCTGAGATTGCTGGTTGC-3', 5'-GGAAGGGTATCACGTCTCACTCGG-3', and 5'-CAGAAAAGCAGGCTGGGAAGC-3' (WT allele - 255bp, conditional allele - 340bp, null allele - 370bp). (**d**) Western blot analysis of Concanavalin A affinity-purified proteins from adult brain lysates of WT and *NgR123*$^{-/-}$ mice, using polyclonal rabbit anti-NgR1, -NgR2, and -NgR3 immune sera (normalized to β-actin), shows that triple mutants are null for NgR1, NgR2, and NgR3 protein.

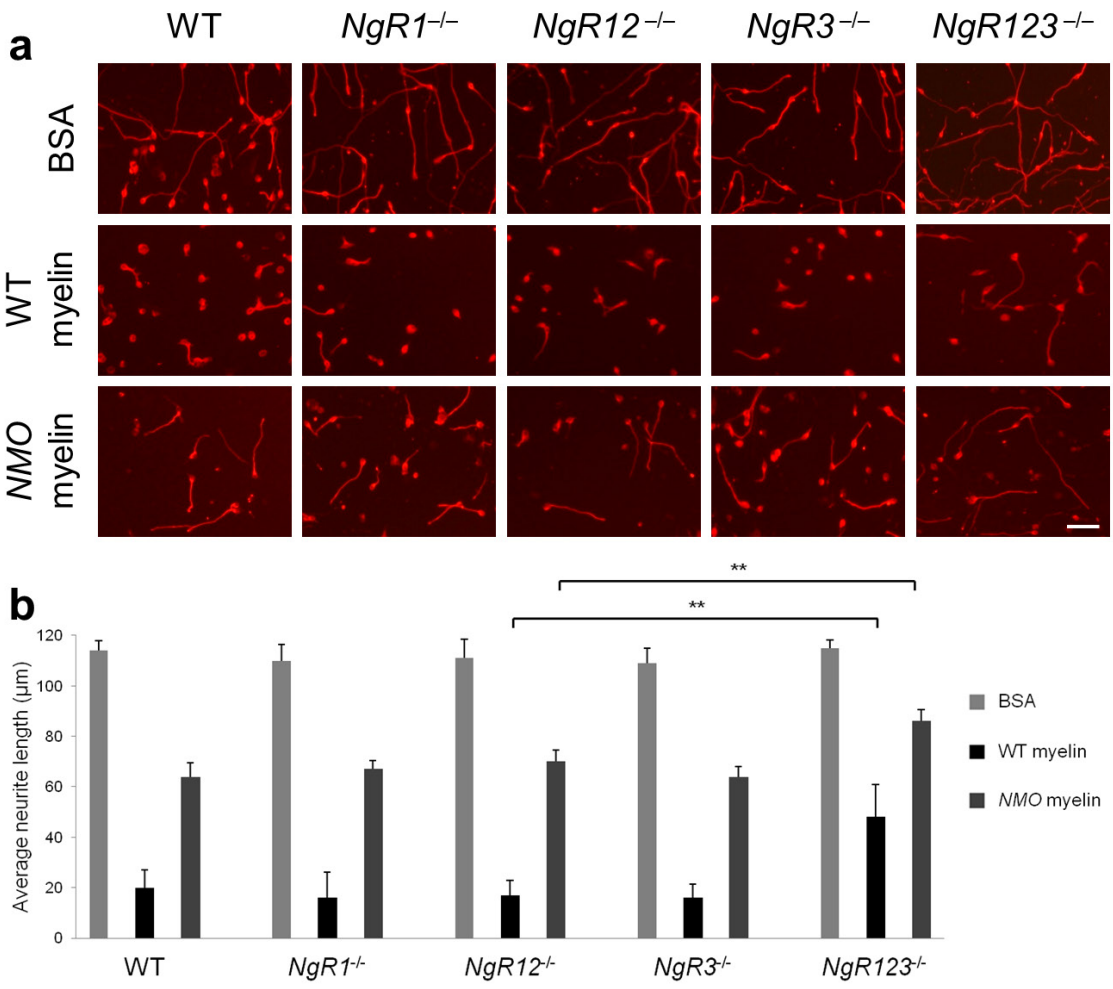

Figure 2.2: Loss of all three Nogo receptors results in enhanced growth on CNS myelin. (**a**) P7 CGNs from WT, *NgR1*$^{-/-}$, *NgR12*$^{-/-}$, and *NgR3*$^{-/-}$ pups are strongly inhibited when plated on crude CNS myelin substrate (40µg/ml). In marked contrast, CGNs from NgR triple mutant (*NgR123*$^{-/-}$) mice grow longer neurites on CNS myelin. On CNS myelin isolated from NogoABC;MAG;OMgp triple null (*NMO*$^{-/-}$) mice (40µg/ml), CGNs from WT, *NgR1*$^{-/-}$, *NgR12*$^{-/-}$, and *NgR3*$^{-/-}$ pups show enhanced neurite outgrowth. A further release of inhibition is observed when *NgR123*$^{-/-}$ neurons are plated on *NMO*$^{-/-}$ CNS myelin. On a BSA control substrate, neurite length of all five genotypes is comparable. (**b**) Quantification of neurite length. At least 300 neurites of TuJ1-labeled cells were counted per condition (n=9 independent experiments). Light gray bars (BSA); black bars (WT myelin); dark gray bars (*NMO* myelin). Results are presented as mean ±SEMs. ** $P < 0.001$ (one-way ANOVA, Tukey's *post hoc*). Scale bar, 50µm.

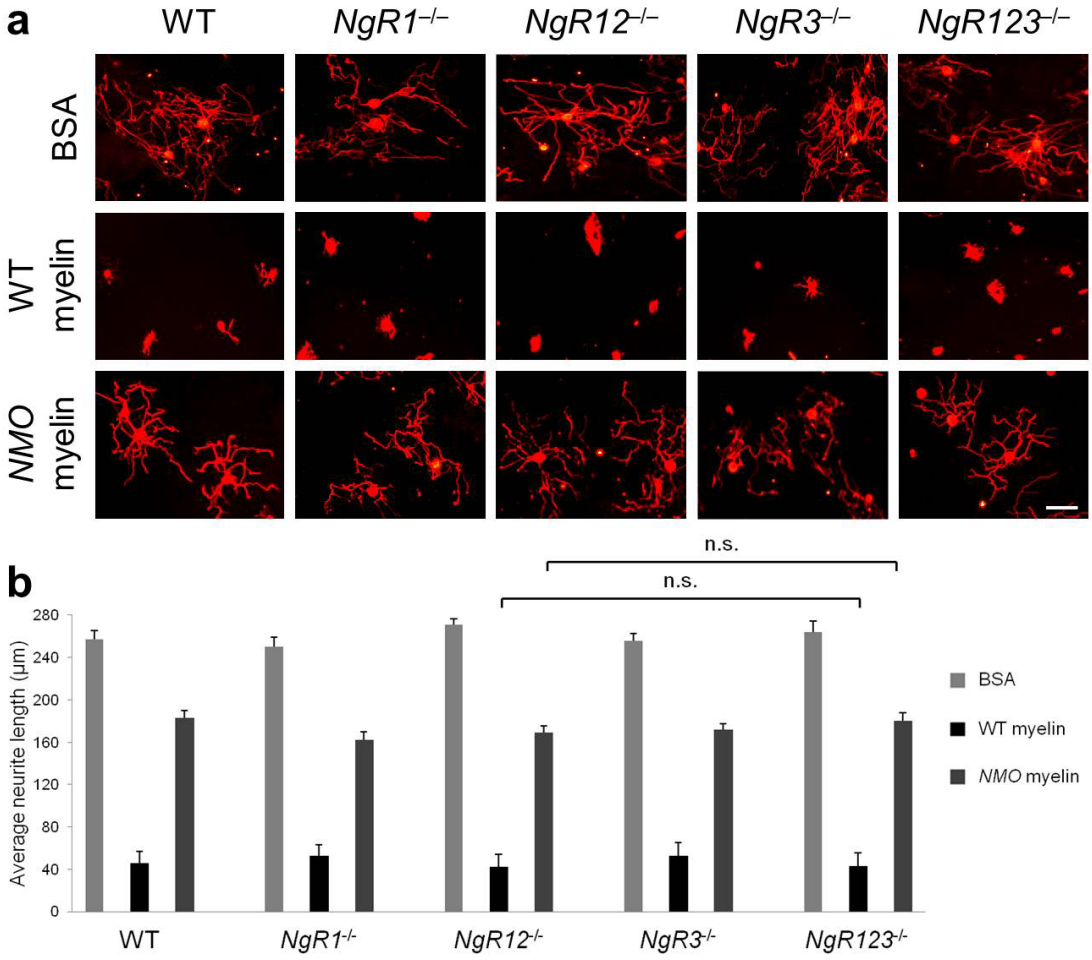

Figure 2.3: Myelin inhibition of DRG neurons is mediated by Nogo receptor-independent mechanisms. (**a**) P7 DRG neurons from WT, *NgR1*$^{-/-}$, *NgR12*$^{-/-}$, *NgR3*$^{-/-}$, and *NgR123*$^{-/-}$ pups are strongly and equally inhibited when plated on crude CNS myelin substrate (40μg/ml). On CNS myelin isolated from NogoABC;MAG;OMgp triple null (*NMO*$^{-/-}$) mice (40μg/ml), DRG neurons from all genotypes show enhanced neurite outgrowth, with no significant difference between WT and NgR single or compound mutant neurons. On a BSA control substrate, neurite length of all five genotypes is comparable. (**b**) Quantification of neurite length. At least 300 neurites of TuJ1-labeled cells were counted per condition (n=7 independent experiments). Light gray bars (BSA); black bars (WT myelin); dark gray bars (*NMO* myelin). Results are presented as mean ±SEMs (one-way ANOVA, Tukey's *post hoc*), n.s.=not significant. Scale bar, 50μm.

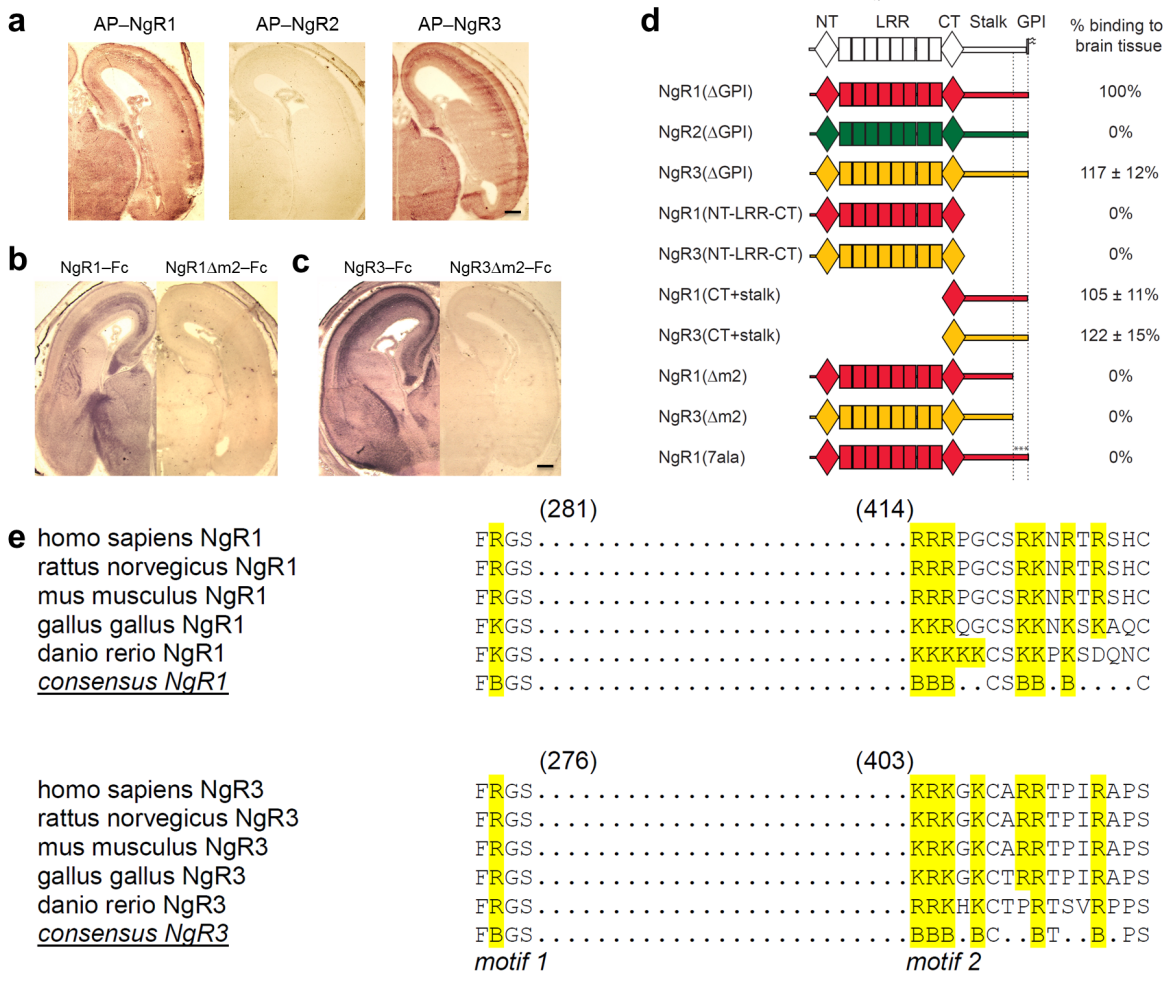

Figure 2.4: NgR1 and NgR3, but not NgR2, contain two discontinuous and evolutionarily conserved sequence motifs necessary for binding to brain tissue. (**a**) Coronal sections of E18 rat brain showing the binding pattern of AP-NgR1 and AP-NgR3. No binding is observed for AP-NgR2. (**b-c**) Binding of (**b**) NgR1-Fc and (**c**) NgR3-Fc to E18 brain sections is abolished upon deletion of a cluster of basic residues (motif 2) in the stalk region. (**d**) Schematic of receptor deletion constructs and their relative binding to E18 rat brain tissue compared to soluble NgR1 [NgR1(ΔGPI)]. Soluble NgR1 (red) and NgR3 (yellow), but not NgR2 (green), bind strongly to brain tissue sections. The LRRs of NgR1, previously shown to participate in myelin inhibitor binding, are dispensable for binding to neural tissue. Deletion of a cluster of basic amino acid residues in the C-terminal region of the NgR1 and NgR3 stalk (motif 2), or replacement of these residues with alanines [NgR1(7ala)], completely abolishes binding. (**e**) Sequence alignment of binding motifs 1 and 2 of NgR1 and NgR3. In the LRR-CT domain, residues F278 and R279 in NgR1 and residues F273 and R274 in NgR3 (motif 1) are important for GAG binding. Motif 2 is comprised of a cluster of basic amino acids, including residues 414-426 in NgR1 and residues 403-415 in NgR3. The basic residues of motif 1 and motif 2 are highlighted. Scale bar, 40μm.

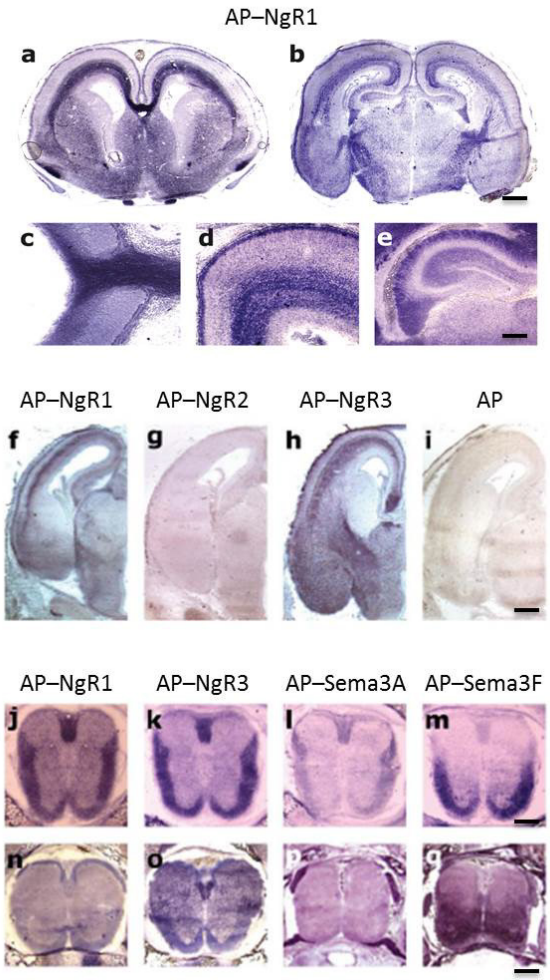

Figure 2.5: Soluble NgR1 and NgR3, but not NgR2, bind strongly and broadly to neural fiber systems. Binding of soluble NgR1 (AP-NgR1), NgR2 (AP-NgR2), and NgR3 (AP-NgR3) to embryonic and neonatal rat brain and spinal cord tissue sections at E18-P1. (**a**-**e**) Binding of AP-NgR1 to brain tissue sections. **a.** and **b.** Coronal brain sections show strong binding of AP-NgR1 to the corpus callosum, internal capsule, lateral olfactory tract, anterior commissure, and fimbria. **c.** The developing fiber layer in the inner retina and the optic nerve strongly support binding of AP-NgR1. **d.** In the cortical mantle, the marginal zone and axons in the intermediate zone are strongly labeled. **e.** Higher magnification view of the hippocampus. Robust labeling is associated with the alveus, fimbria, and the CA1 and CA3 dendritic fields. (**f**-**i**) AP-NgR1 and AP-NgR3, but not AP-NgR2, bind to E18 rat brain tissue sections. AP is shown as a negative control. (**j**-**q**) Binding of soluble fusion proteins to E18 spinal cord (**j**-**m**) and P1 spinal cord (**n**-**q**) cross sections. AP-NgR1 and AP-NgR3 bind strongly and broadly to spinal fiber tracts at E18 and P1. In contrast, AP-Sema3A binds weakly to spinal fibers at E18 and preferentially binds to the dorsal root entry zone and ventral motor roots at P1. AP-Sema3F binds strongly to the ventral spinal cord at E18 and P1. Scale bar: a,b, 50µm; c-e, 15µm; f-m, 40µm; n-q, 20µm.

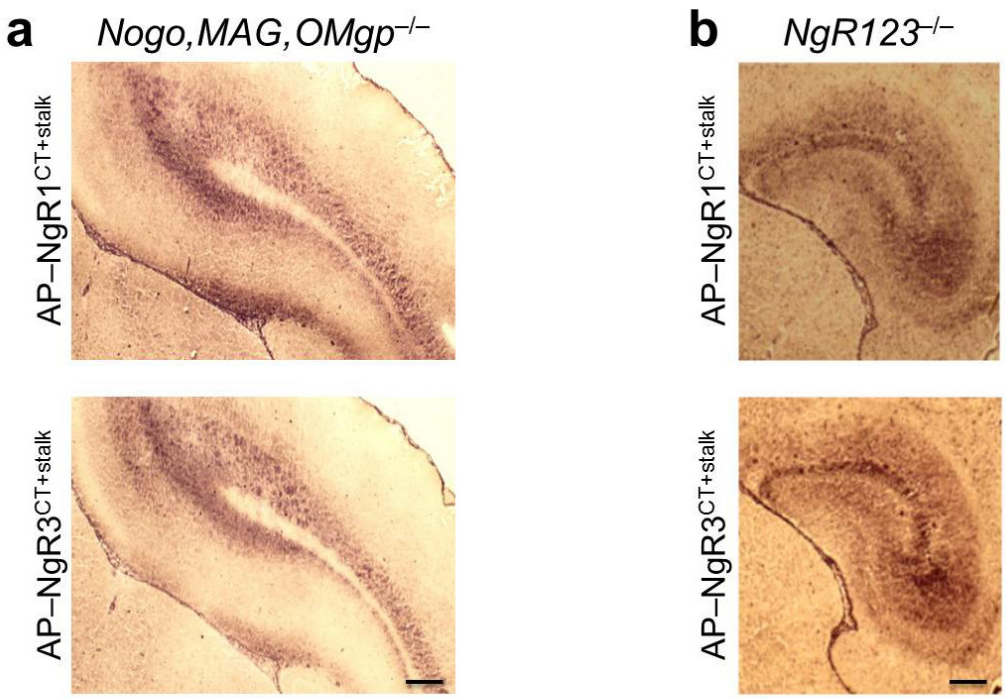

c

	AP–NgR1$^{CT+stalk}$	AP–NgR2$^{CT+stalk}$	AP–NgR3$^{CT+stalk}$
WT E18 mouse brain	+++	-	+++
WT P3 mouse brain	+++	-	+++
p75$^{-/-\ (exon\ III)}$ E18 mouse brain	+++	-	+++
p75$^{-/-\ (exon\ IV)}$ P3 mouse brain	+++	-	+++
NgR1$^{-/-}$ E18 mouse brain	+++	-	+++
GalNAcT$^{-/-}$ P3 mouse brain	+++	-	+++
GD3S$^{-/-}$ P3 mouse brain	+++	-	+++
Binding to brain tissue sections following treatment with:			
– heat	+++	-	+++
– trypsin	+++	-	+++
– glycopeptidase-F	+++	-	+++
– N-acetylglucosaminidase	+++	-	+++
– *Vibrio cholerae* neuraminidase	+++	-	+++
– endoneuraminidase-N	+++	-	+++
– heparinase III	+	-	+
– heparin	-	-	-
– chondroitinase-ABC lysase	+	-	+

Figure 2.6: Proteoglycans participate in binding of soluble NgR1 and NgR3 to brain sections. Binding of soluble AP-NgR1$^{CT+stalk}$ (5nM) or AP-NgR3$^{CT+stalk}$ (5nM) to brain tissue sections of (**a**) *NogoABC*$^{-/-}$;*MAG*$^{-/-}$;*OMgp*$^{-/-}$ triple mutants, (**b**) *NgR123*$^{-/-}$ triple mutants, or

(**c**) *p75*$^{NTR-/-(exonIII)}$, *p75*$^{NTR-/-(exonIV)}$, *NgR1*$^{-/-}$, *GalNAcT*$^{-/-}$ (GM2/GD2 synthase), and *GD3S*$^{-/-}$ (GD3 synthase) mutants is indistinguishable from WT mice. This suggests that binding of AP-NgR1$^{CT+stalk}$ and AP-NgR3$^{CT+stalk}$ to brain is mediated by novel, as of yet unidentified binding partners. To examine whether binding of AP-NgR1$^{CT+stalk}$ or AP-NgR3$^{CT+stalk}$ to brain is mediated by a protein-protein interaction, tissue sections were pretreated with heat or preincubated with trypsin. Neither treatment significantly reduced binding. This suggests that carbohydrate structures participate in Nogo receptor binding. To examine whether Nogo receptors associate with neural glycoconjugates, brain tissue sections were preincubated with glycopeptidase-F, N-acetylglucosaminidase, *Vibrio cholerae* neuraminidase (VCN), endoneuraminidase-N (Endo-N), heparinase III, or chondroitinase ABC. Digestion with heparinase III or chondroitinase ABC leads to a partial, yet substantial reduction in binding of AP-NgR1$^{CT+stalk}$ or AP-NgR3$^{CT+stalk}$. The most pronounced reduction is observed in the presence of heparin (50μg/ml). In marked contrast, glycopeptidase-F, N-acetylglucosaminidase, VCN, or Endo-N incubation does not lead to a substantial reduction in fusion protein binding. Together, these results suggest that neural glycosaminoglycans (GAGs) participate in soluble NgR1 and NgR3 binding to brain tissue. Scale bar, 50μm.

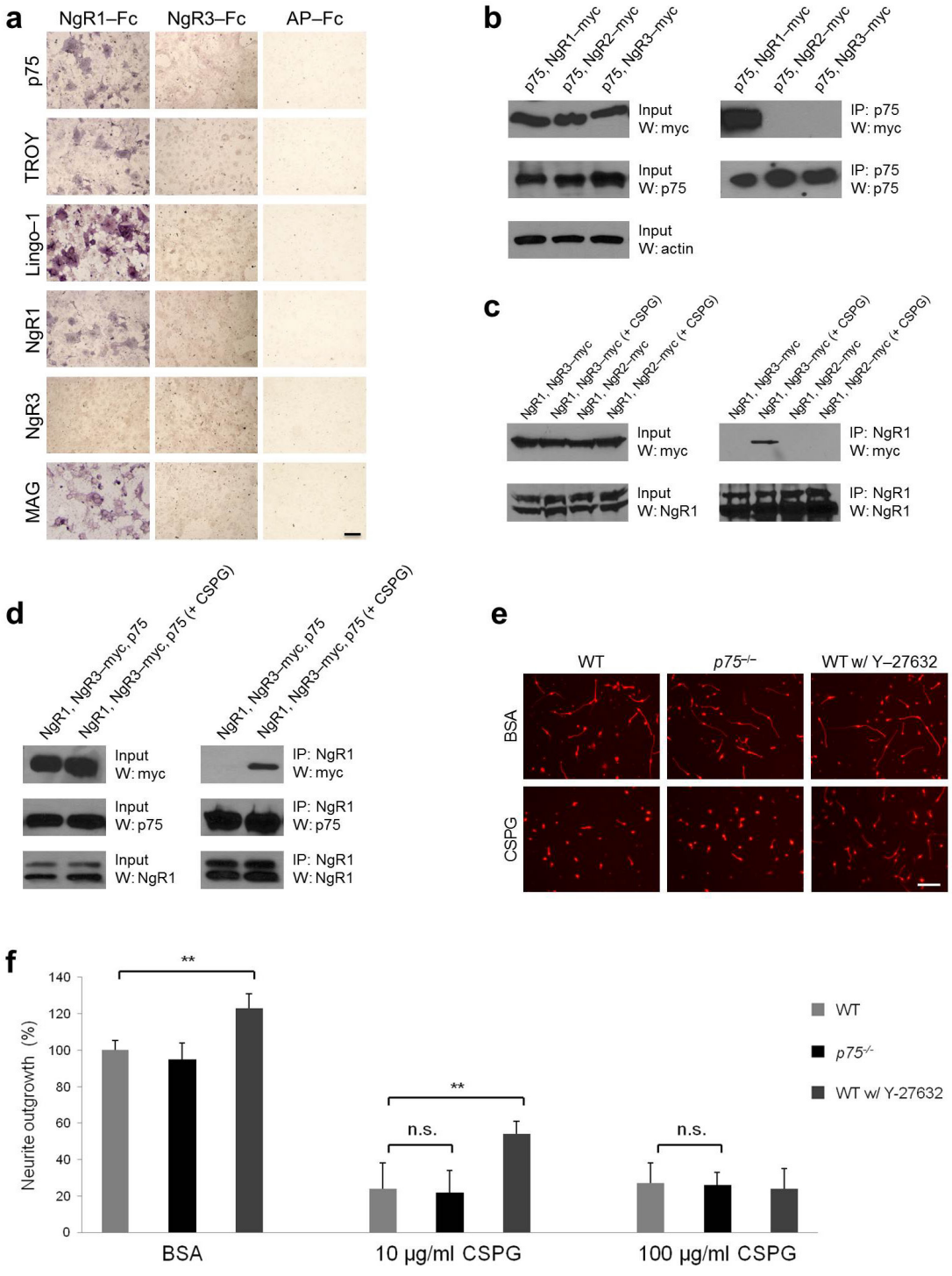

Figure 2.7: Ligand-dependent association of NgR1 and NgR3. (**a**) In transfected COS-7 cells, the NgR1 co-receptors $p75^{NTR}$, TROY, and Lingo-1 show binding to bath-applied, soluble NgR1-Fc, but not to NgR3-Fc. AP-Fc was used as a negative control. (**b**) Co-

immunoprecipitation (IP) experiments in HEK293T cells confirm that $p75^{NTR}$ interacts with NgR1 in *cis*, but not with NgR2 or NgR3. For IP experiments, HEK293T cells were co-transfected with $p75^{NTR}$ and either NgR1-myc, NgR2-myc, or NgR3-myc. Cell lysates were immunoprecipitated with anti-$p75^{NTR}$, and the immune complex was analyzed by anti-myc western blotting. (**c**) HEK293T cells were transfected with NgR1 and either NgR2-myc or NgR3-myc. Prior to lysis and IP with anti-NgR1, cells were incubated for 30 minutes with CSPGs. The precipitated immune complex was analyzed by anti-myc western blotting. A CSPG-dependent association of NgR1 and NgR3, but not NgR1 and NgR2, was observed. (**d**) The ligand-dependent interaction of NgR1and NgR3 is not sensitive to co-expression of $p75^{NTR}$. HEK293T cells were transfected with NgR1, NgR3-myc, and $p75^{NTR}$; cell lysates were immunoprecipitated with anti-NgR1; and the immune complex was analyzed by anti-myc and anti-$p75^{NTR}$ western blotting, revealing the presence of $p75^{NTR}$ and NgR3. (**e**) In CGNs, $p75^{NTR}$ is not necessary for inhibition on substrate-bound CSPGs (10μg/ml). P7 CGNs from WT and $p75^{NTR-/-}$ pups are strongly and equally inhibited when plated on CSPGs. A partial release of inhibition was observed in the presence of the bath-applied ROCK inhibitor Y-27632 (10μM). On a BSA control substrate, neurite lengths of WT and $p75^{NTR-/-}$ CGNs are comparable, and increased in the presence of Y-27632. (**f**) Quantification of neurite length. At least 150 neurites of TuJ1-labeled cells were counted per condition (n=3 independent experiments). Light gray bars (WT); black bars ($p75^{NTR-/-}$) dark gray bars (WT w/ Y-27632). Results are presented as mean ±SEMs. ** $P< 0.001$ (one-way ANOVA, Tukey's *post hoc*), n.s.= not significant. Scale bar: a, 20μm; e, 70μm.

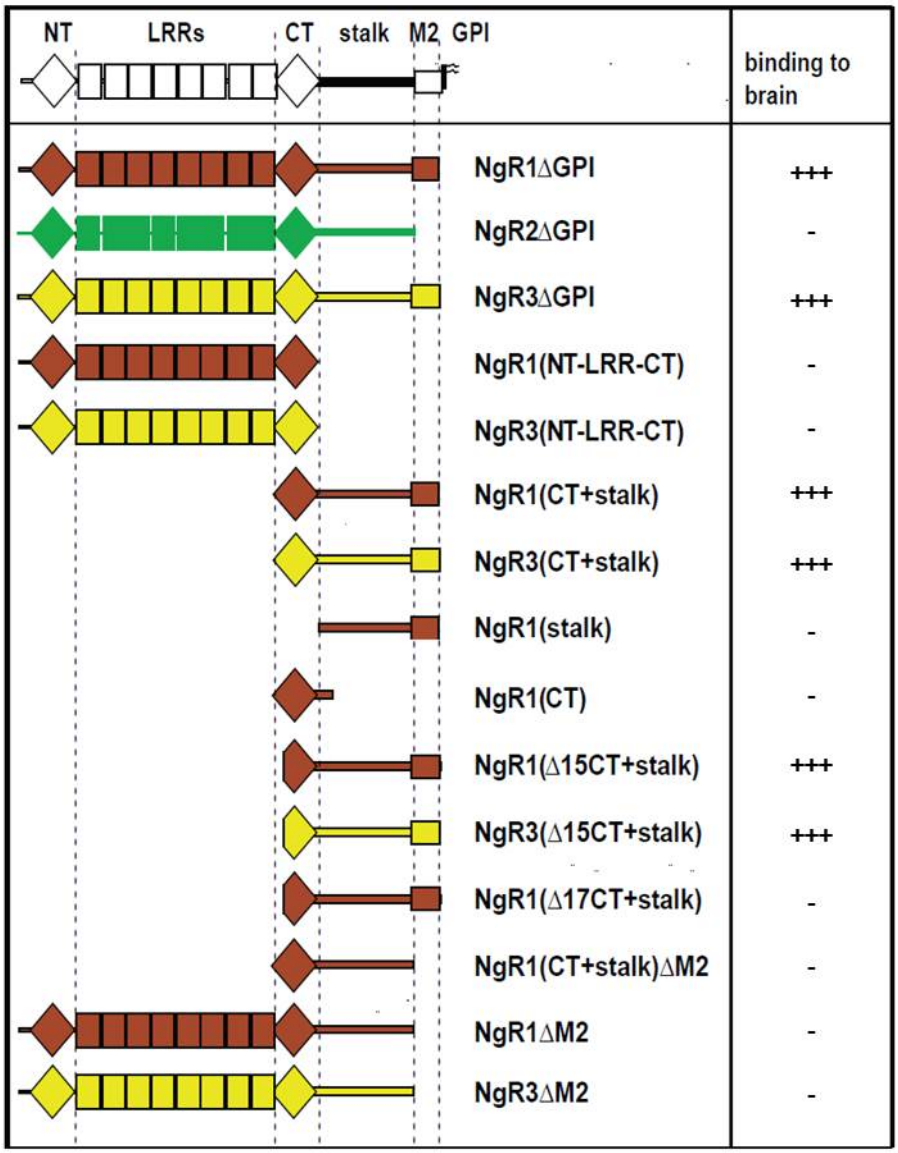

Figure 2.8: Molecular basis of the NgR1 and NgR3 interaction with embryonic brain tissue. To determine the molecular basis of the NgR1 and NgR3 interactions with rat brain tissue sections, AP- and Fc-tagged deletion mutants were generated and assessed for binding to E18 brain. The binding sites for myelin inhibitors (Nogo66, MAG, and OMgp) have previously been mapped to the NgR1 LRR cluster, including amino acid residues 27-310. The LRR cluster is comprised of 8.5 LRRs flanked N- and C-terminally by LRR-NT and LRR-CT capping domains. The LRR clusters of NgR1 (AP-NgR1$^{NT\text{-}LRR\text{-}CT}$) or NgR3 (AP-NgR3$^{NT\text{-}LRR\text{-}CT}$) do not support binding to embryonic brain tissue sections. However, AP fusion proteins comprised of the LRR-CT capping domain and the stalk domain of NgR1 (AP-NgR1$^{CT+stalk}$) or NgR3 (AP-NgR3$^{CT+stalk}$) are sufficient to mediate strong binding to brain tissue sections. The LRR-CT capping domain of all three NgR family members is 46 amino acid residues in length and connected to a GPI anchor

via a proline- and serine/threonine-rich stalk region of approximately 100 amino acids. Neither the LRR-CT domain (AP-NgR1^{CT}) nor the stalk region (AP-NgR1^{stalk}) of NgR1 is sufficient for binding to brain. Deletion of the first 15 amino acid residues of the LRR-CT domains of NgR1 and NgR3, resulting in constructs AP-NgR1$^{\Delta 15CT+stalk}$ and AP-NgR3$^{\Delta 15CT+stalk}$, does not decrease binding to brain tissue. However, deletion of F278 and R279 of NgR1 (AP-NgR1$^{\Delta 17CT+stalk}$) completely abolishes binding. This suggests that residues F278/R279 of NgR1 (motif 1) are necessary but not sufficient for binding. Deletion of sequences from the C-terminal end of the stalk (AP-NgR1$^{CT+stalk\Delta m2}$) identified a sequence motif, located juxtaposed to the GPI anchor of NgR1 [^{410}TSGP**RRR**PGCS**RK**N**R**T**R**SHC^{429}], that is necessary for binding (motif 2). Most notable in this region is a prevalence of basic amino acid residues. A similar cluster of basic amino acids is present near the C-terminus of the NgR3 stalk [^{399}TA**R**P**KRK**G**K**CA**RR**TPI**R**APS^{418}] and is necessary for binding of AP-NgR3 to brain tissue sections. Of interest, no cluster of basic amino acids is found in the juxtamembrane region of NgR2, providing a molecular basis for the lack of binding to brain sections. Taken together, mutagenesis studies identified two discontinuous sequence motifs, one located in the LRR-CT capping domain (motif 1) and a second one located in the juxtamembrane stalk region (motif 2), both of which are necessary for binding to embryonic rat brain tissue sections.

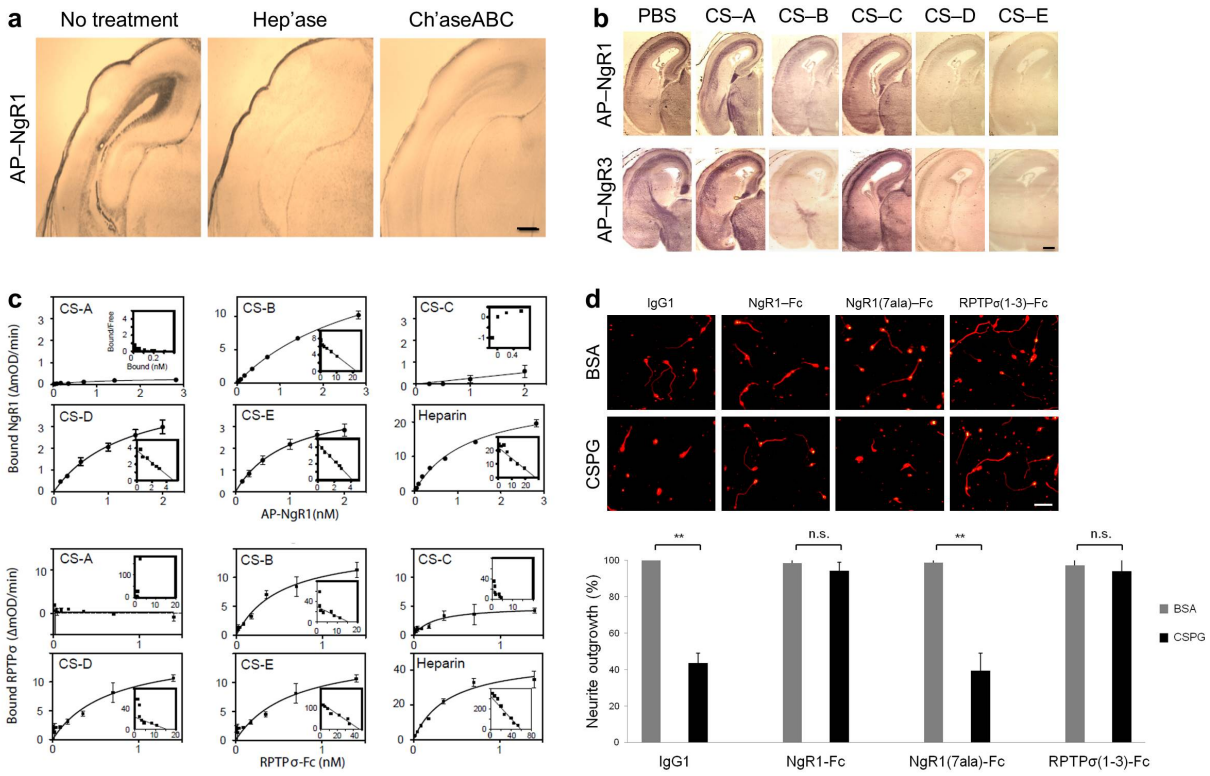

Figure 2.9: NgR1 and NgR3 interact directly with specific GAGs. (**a**) Binding of soluble AP-NgR1 to P1 rat brain tissue sections is sensitive to heparinase (Hep'ase) and chondroitinase ABC (Ch'aseABC) treatment (1unit/ml). (**b**) Binding of soluble AP-NgR1 and AP-NgR3 to E18 rat brain tissue sections in the presence of PBS (vehicle control), 50µg/ml monosulfated CS-GAGs (CS-A, CS-B, or CS-C), or 50µg/ml disulfated CS-GAGs (CS-D or CS-E). Only CS-B, CS-D, and CS-E compete effectively with brain tissue sections for binding to NgR1 and NgR3. (**c**) ELISA binding studies revealed a direct association of soluble NgR1 and RPTPσ(1-3) with specific GAGs (insets show Scatchard plot analysis). The calculated Kds for CS-B, CS-D, CS-E, and heparin are 3.2, 1.3, 1.0, and 1.2nM (NgR1) and 1.4, 3.0, 0.1, and 0.1nM [RPTPσ(1-3)], respectively. (**d**) WT P7 mouse CGNs are strongly inhibited when plated on substrate-bound CSPGs. Long neurites are seen on a BSA control substrate. In the presence of NgR1-Fc or RPTPσ(1-3)-Fc, but not NgR1(7ala)-Fc or IgG1 control, CSPG inhibition is abolished. On a BSA substrate, soluble receptors do not influence neurite outgrowth. Quantification of neurite length is shown as a percentage of the IgG1-BSA control (100%). At least 300 neurites of TuJ1-labeled cells were counted per condition (n=4 independent experiments). Gray bars (BSA); black bars (CSPGs). Results are presented as mean ±SEMs. ** $P < 0.001$ (one-way ANOVA, Tukey's *post hoc*), n.s.= not significant. Scale bar: a, 20µm; b, 40µm; d, 50µm.

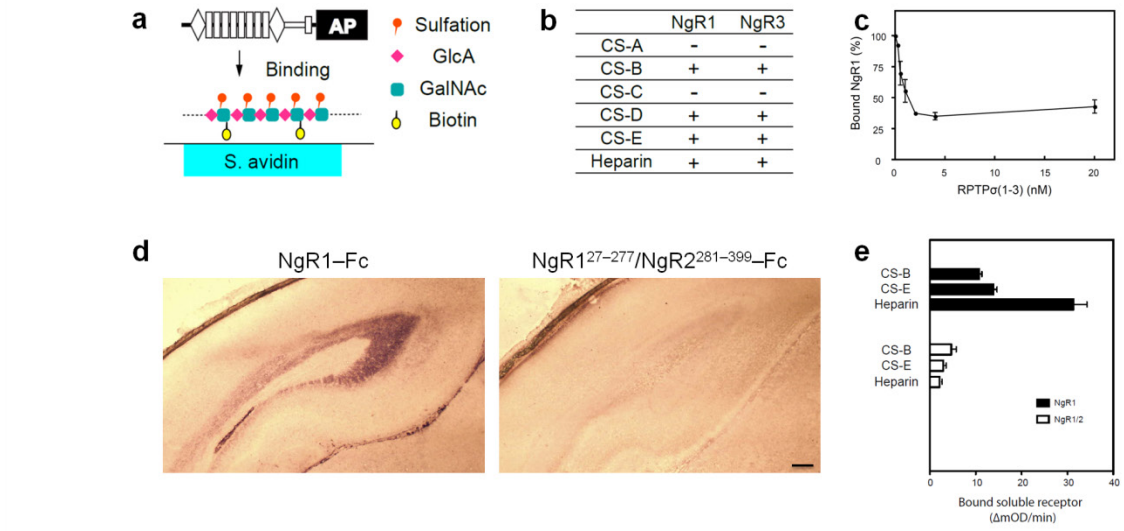

Figure 2.10: NgR1 and NgR3 show very similar GAG binding preferences. (**a**) Schematic of the ELISA strategy used to test whether soluble NgRs and RPTPσ bind directly to immobilized GAGs. ELISA plates were precoated with streptavidin and incubated with biotinylated GAGs. Increasing concentrations of soluble receptor fusion proteins were added to the plates, the plates were rinsed, and bound AP activity was quantified. (**b**) Summary of ELISA data. NgR1 and NgR3 bind directly to CS-B, CS-D, CS-E, and heparin, but not to CS-A or CS-C. (**c**) Soluble RPTPσ(1-3) competes effectively with NgR1 for binding to CS-E. The binding of AP-NgR1 to CS-E decreases in the presence of increasing doses of RPTPσ(1-3)-Fc. (**d**) Replacement of both GAG-binding motifs of NgR1 with the corresponding sequences of NgR2 ($NgR1^{C27-K277}/NgR2^{V281-G399}$-Fc) abolishes binding to P1 rat brain tissue sections. (**e**) Quantification of NgR1-Fc and $NgR1^{C27-K277}/NgR2^{V281-G399}$-Fc binding to CS-B, CS-E, and heparin by ELISA. Scale bar, 50μm.

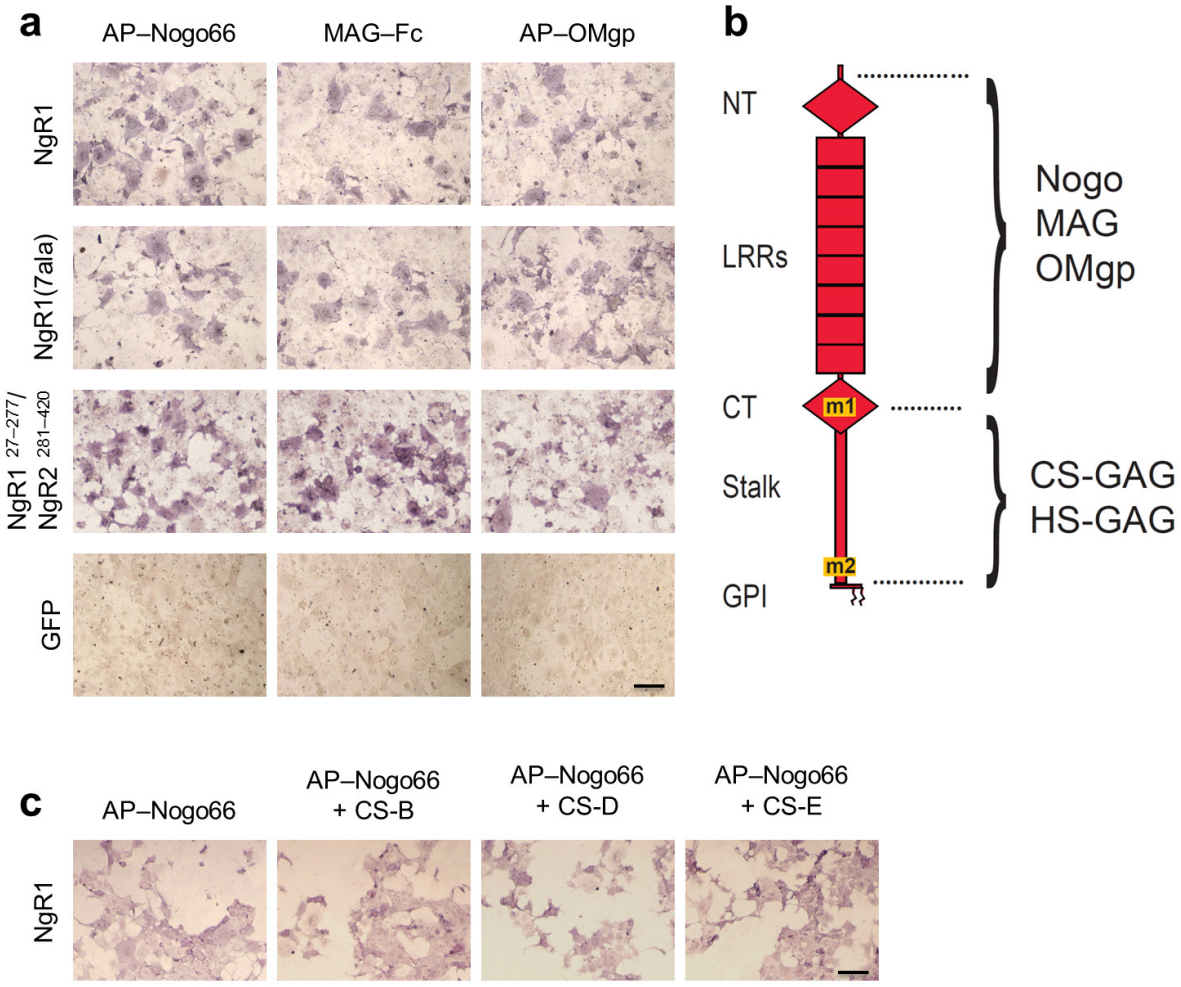

Figure 2.11: Binding sites for MAIs and CSPGs on NgR1 are distinct and dissociable. (**a**) In transiently transfected COS-7 cells, wild-type NgR1 and the GAG-binding-deficient mutant [NgR1(7ala)] show very similar binding of the MAIs AP-Nogo66, MAG-Fc, and AP-OMgp. The NgR1 fragment F278-E445 (AP-NgR1$^{\Delta 15CT+stalk}$) is sufficient for high-affinity binding to neural GAGs. When residues 278-445 in NgR1 are replaced with the corresponding sequences of NgR2, resulting in construct NgR1$^{C27\text{-}K277}$/NgR2$^{V281\text{-}L420}$, binding of MAIs is not diminished compared to wild-type NgR1. Ligand binding to GFP-transfected COS-7 cells is shown as a negative control. (**b**) Schematic of NgR1, showing the regions necessary for binding of MAIs and GAGs. The GAG-binding motifs m1 and m2 of NgR1 are distinct and dissociable from the Nogo-, MAG-, and OMgp-binding sequences. (**c**) In the presence of bath-applied CS-B, CS-D, or CS-E GAGs (1mg/ml), binding of AP-Nogo66 to NgR1-expressing COS-7 cells is not altered. Scale bar, 20μm.

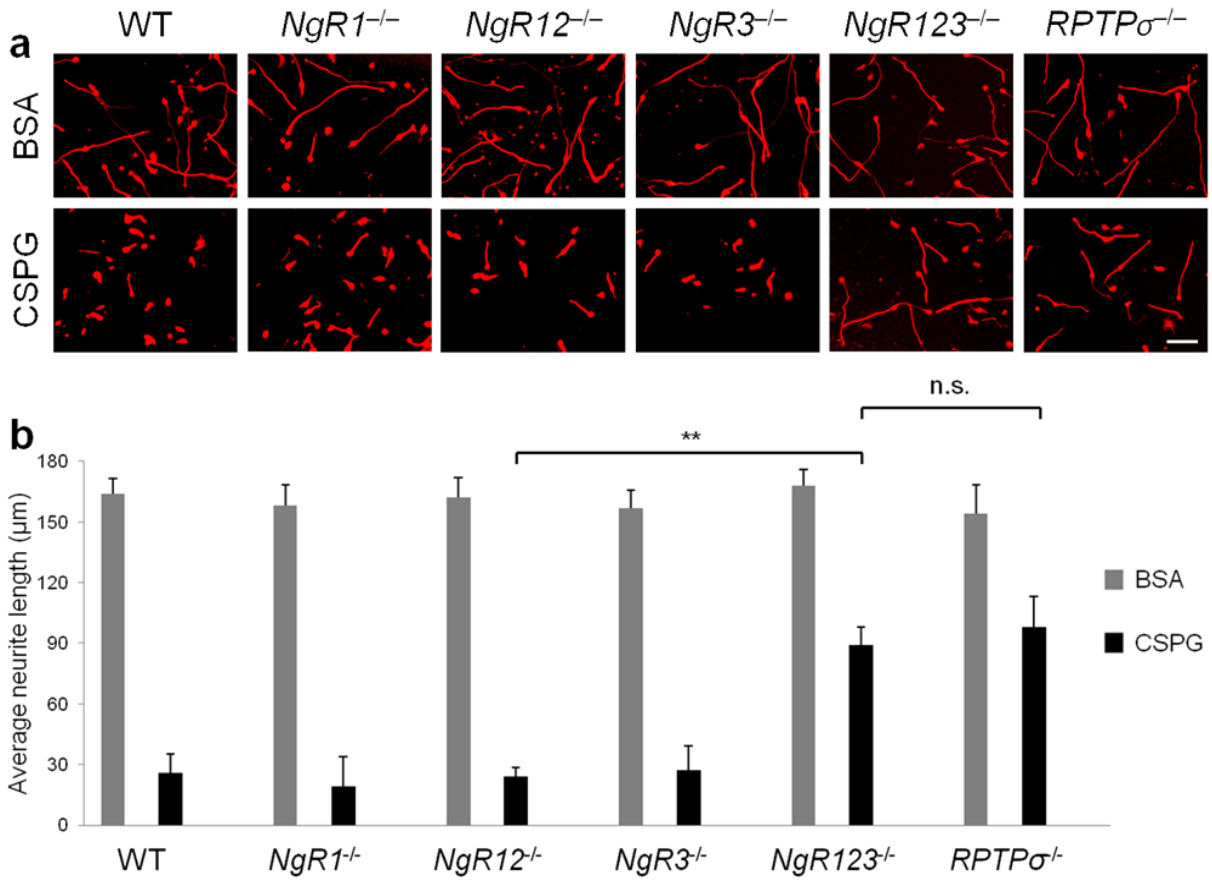

Figure 2.12: Nogo receptors mediate CSPG inhibition. (**a**) *In vitro*, WT P7 CGNs are strongly inhibited when plated on substrate-bound CSPGs (10µg/ml). Studies with CGNs from *NgR1*$^{-/-}$, *NgR12*$^{-/-}$, and *NgR3*$^{-/-}$ mutants revealed no substantial release of CSPG inhibition. Loss of all three NgRs (*NgR123*$^{-/-}$) or *RPTPσ* alone (*RPTPσ*$^{-/-}$) leads to a significant, yet incomplete release of CSPG inhibition. On a control substrate (BSA), neurite length of all six genotypes is comparable. (**b**) Quantification of neurite length. Gray bars (BSA); black bars (CSPGs). At least 300 neurites of TuJ1-labeled cells were counted per condition (n=8 independent experiments). Results are presented as mean ±SEMs. ** $P < 0.001$ (one-way ANOVA, Tukey's *post hoc*), n.s.= not significant. Scale bar, 70µm.

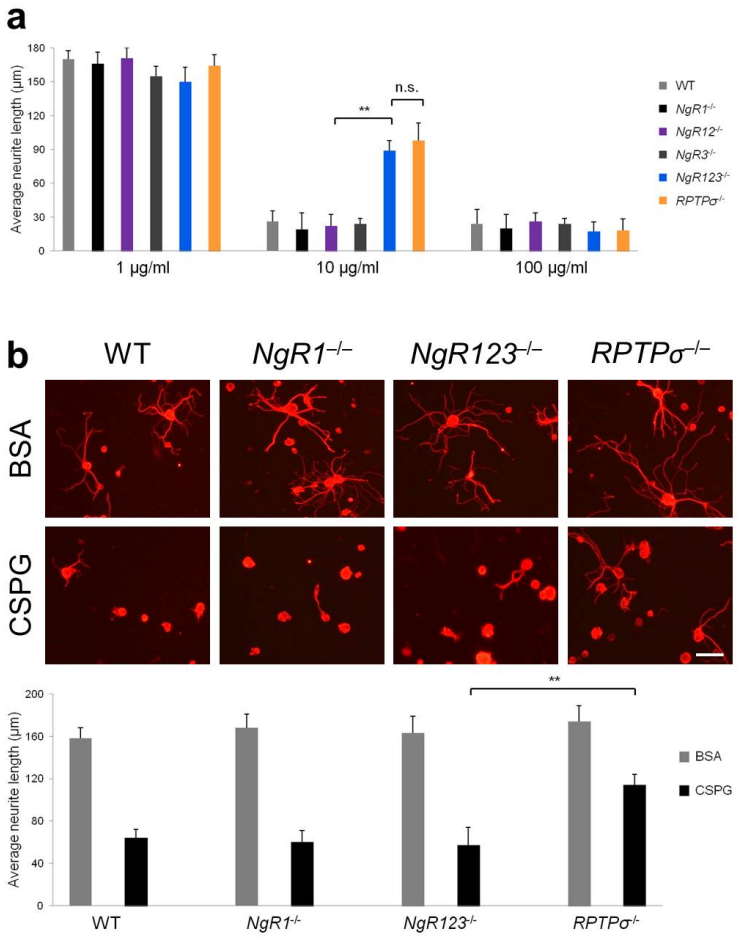

Figure 2.13: Evidence for Nogo receptor-independent mechanisms for CSPG inhibition. (**a**) CSPG dose-response effect on P7 CGN neurite outgrowth inhibition. When adsorbed to culture plates at 1µg/ml, CSPGs do not significantly inhibit neurite outgrowth. At 10µg/ml, neurite length is decreased in all genotypes; however, *NgR123*$^{-/-}$ and *RPTPσ*$^{-/-}$ neurites are significantly longer than WT, *NgR1*$^{-/-}$, *NgR12*$^{-/-}$, and *NgR3*$^{-/-}$ neurites. At 100µg/ml CSPG, *NgR123*$^{-/-}$ and *RPTPσ*$^{-/-}$ CGNs no longer show enhanced neurite growth compared to controls. Light gray bars (WT); black bars (*NgR1*$^{-/-}$); purple bars (*NgR12*$^{-/-}$); dark gray bars (*NgR3*$^{-/-}$); blue bars (*NgR123*$^{-/-}$); orange bars (*RPTPσ*$^{-/-}$). At least 300 neurites were counted per condition (n=4 independent experiments). Results are presented as mean ±SEMs. ** $P< 0.001$ (one-way ANOVA, Tukey's *post hoc*), n.s.=not significant. (**b**) WT, *NgR1*$^{-/-}$, and *NgR123*$^{-/-}$ P7 DRG neurons are strongly inhibited when plated on substrate-bound CSPGs (10µg/ml). *RPTPσ*$^{-/-}$ DRG neurons show a significant, yet incomplete release of CSPG inhibition. On a BSA control substrate, neurite length of all four genotypes is comparable. Gray bars (BSA); black bars (CSPGs). At least 300 neurites of TuJ1-labeled cells were counted per condition (n=4 independent experiments). Results are presented as mean ±SEMs. ** $P< 0.001$ (one-way ANOVA, Tukey's *post hoc*). Scale bar, 30µm.

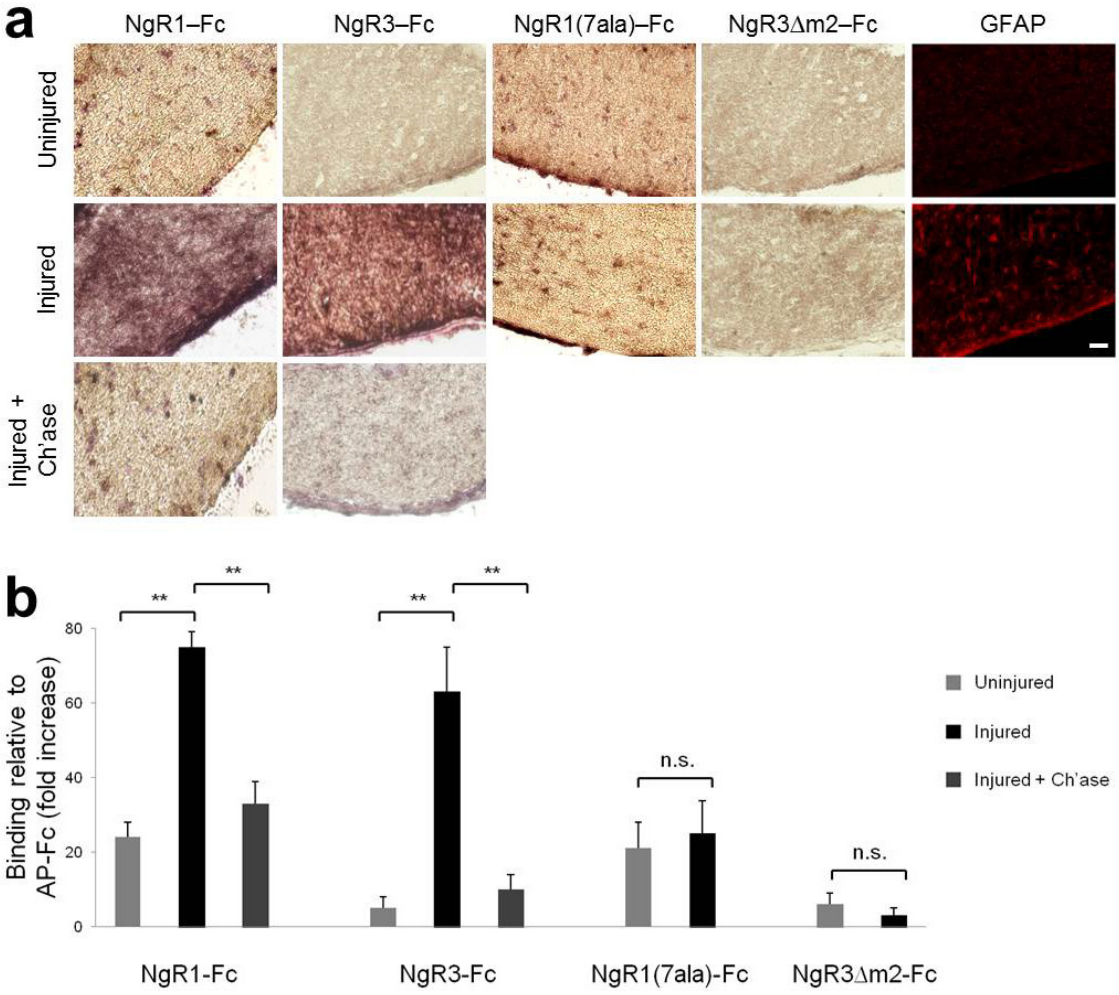

Figure 2.14: Binding of soluble NgR1-Fc and NgR3-Fc to optic nerve is enhanced by injury. (**a**) Longitudinal sections of uninjured and injured adult mouse optic nerve (7 days following retro-orbital nerve crush) were incubated with NgR1-Fc, NgR3-Fc, NgR1(7ala)-Fc, and NgR3Δm2-Fc. Soluble NgR1-Fc and NgR1(7ala)-Fc, but not NgR3-Fc or NgR3Δm2-Fc, bind weakly to uninjured optic nerve sections. Following injury, binding of NgR1-Fc and NgR3-Fc is strongly increased and depends on the presence of the proteoglycan-binding motif 2, as no increase was observed for NgR1(7ala)-Fc and NgR3Δm2-Fc . Treatment of injured optic nerve sections with 1unit/ml chondroitinase ABC (Ch'ase) strongly reduces NgR1-Fc and NgR3-Fc binding, suggesting that endogenous CSPGs participate in the binding of NgR1 and NgR3. (**b**) Quantification of binding to optic nerve sections. All binding is shown as a fold increase relative to AP-Fc. At least 20 sections were counted per condition (n=4 independent experiments). Light gray bars (Uninjured); black bars (Injured); dark gray bars (Injured + Ch'ase). Results are presented as mean ±SEMs. ** $P< 0.001$ (one-way ANOVA, Tukey's *post hoc*), n.s.= not significant. Scale bar, 30μm.

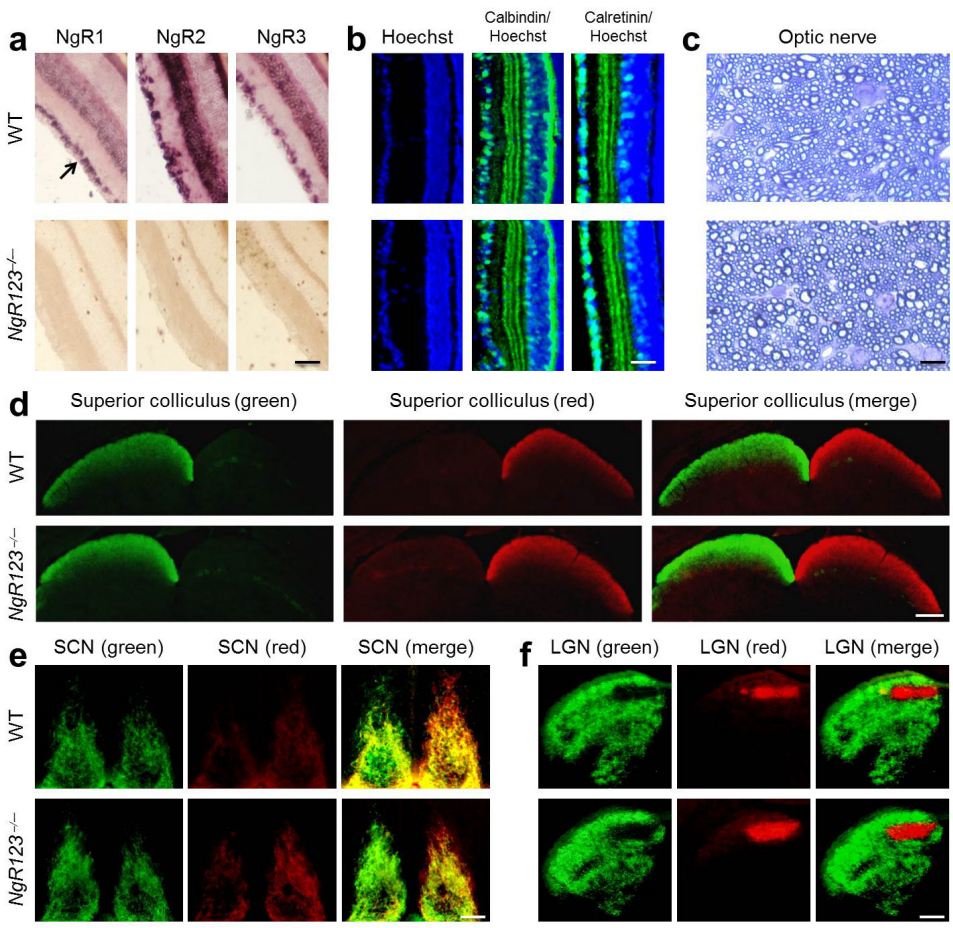

Figure 2.15: Retinal stratification, optic nerve myelination, and RGC central projections appear normal in *NgR123*$^{-/-}$ mice. (**a**) Sections of adult WT and Nogo receptor triple mutant (*NgR123*$^{-/-}$) mouse retina were subjected to *in situ* hybridization with digoxigenin-labeled cRNA probes specific for NgR1, NgR2, and NgR3 transcripts. All three receptors are strongly expressed in the ganglion cell layer (arrow) and the inner nuclear layer, but are absent from the outer nuclear layer of the retina. No signal was detected on parallel-processed sections of *NgR123*$^{-/-}$ retina. (**b**) Hoechst 33342 nuclear staining, as well as anti-calbindin and anti-calretinin immunolabeling, of adult WT and *NgR123*$^{-/-}$ retina did not reveal any noticeable differences in retinal organization among the two genotypes. (**c**) Toluidine Blue labeling of epon-embedded adult WT and *NgR123*$^{-/-}$ optic nerve cross sections reveals a comparable number of axons and degree of myelinated fibers. (**d-f**) The fidelity of RGC central projections in six-week-old WT and *NgR123*$^{-/-}$ mice was assessed by anterograde fiber tracing. Five days after injection of Alexa 594-conjugated Cholera Toxin β into the right eye and Alexa 488-conjugated Cholera Toxin β into the left eye, mice were sacrificed, perfused, and brain sections analyzed by fluorescence microscopy. Right eye (red) and left eye (green) RGC projections to the (**d**) superior colliculus, (**e**) suprachiasmatic nucleus and (**f**) lateral geniculate nucleus in *NgR123*$^{-/-}$ mice are indistinguishable from age-matched WT controls. Scale bar: a, b, 80µm; c, 5µm; d, 100µm; e, f, 60µm.

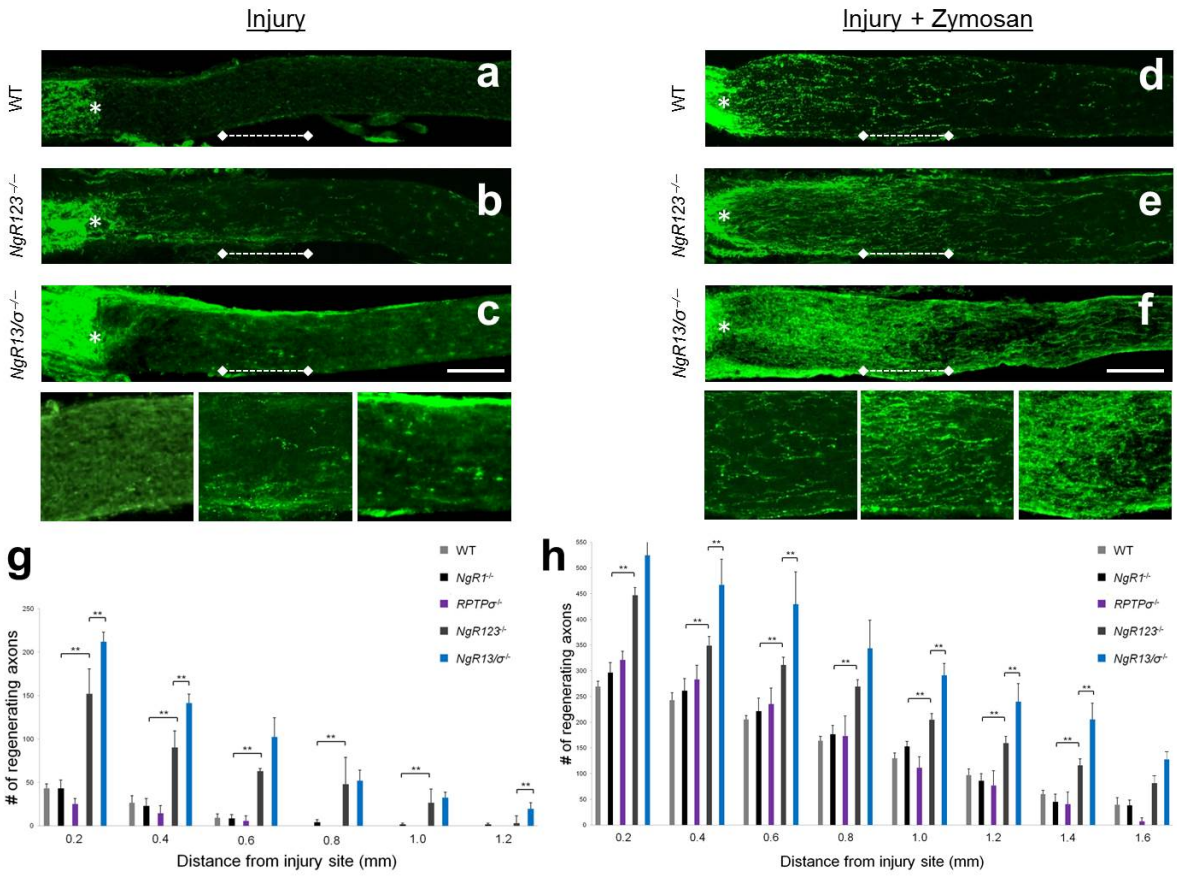

Figure 2.16: *NgR123*$^{-/-}$ and *NgR13/RPTPσ*$^{-/-}$ compound mutants show enhanced fiber regeneration following crush injury to the optic nerve. 2 weeks following injury, regenerating axons in optic nerve sections were visualized by anti-GAP-43 immunolabeling. The injury site is marked with an asterisk. (**a**) WT mice show very limited regenerative axonal growth following injury. (**b**) In *NgR123*$^{-/-}$ mice, many GAP-43-positive fibers grow beyond the lesion site. (**c**) In *NgR13/RPTPσ*$^{-/-}$ (*NgR13/σ*$^{-/-}$) mice, a further increase of GAP-43-positive fiber growth is observed. (**g**) Quantification of the number of GAP-43-positive axons at 0.2 to 1.2mm distal to the lesion site. Light gray bars (WT, n=6); black bars (*NgR1*$^{-/-}$, n=7); purple bars (*RPTPσ*$^{-/-}$, n=5); dark gray bars (*NgR123*$^{-/-}$, n=8); blue bars (*NgR13/σ*$^{-/-}$, n=4). (**d**) Intraocular injection of Zymosan enhances regenerative axonal growth in WT mice. A further increase is observed in (**e**) *NgR123*$^{-/-}$ mice, which is further enhanced in (**f**) *NgR13/σ*$^{-/-}$, mice. (**h**) Quantification of the number of GAP-43-positive axons at 0.2 to 1.6mm distal to the lesion site in Zymosan-injected mice. Light gray bars (WT + Zymosan, n=6); black bars (*NgR1*$^{-/-}$ + Zymosan, n=6); purple bars (*RPTPσ*$^{-/-}$ + Zymosan, n=4); dark gray bars (*NgR123*$^{-/-}$ + Zymosan, n=8); blue bars (*NgR13/σ*$^{-/-}$ + Zymosan, n=3). Results are presented as mean ±SEMs. ** $P< 0.05$ (one-way ANOVA, Tukey's *post hoc*). Scale bar, 200µm.

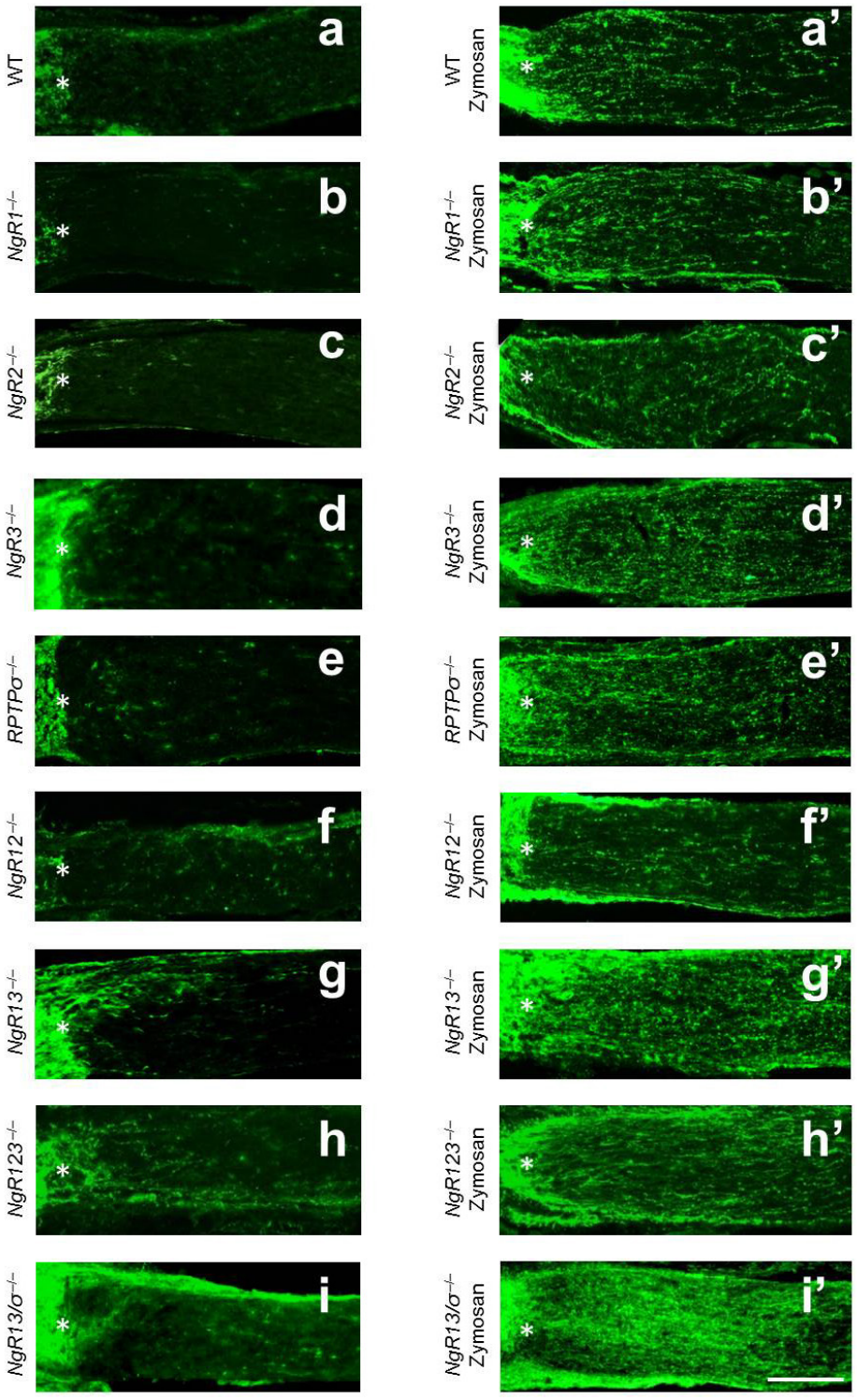

Figure 2.17: In adult mice, the combined loss of NgR1 and NgR3, but not NgR1 and NgR2, is sufficient to significantly enhance axon regeneration following retro-orbital optic nerve

crush injury. (**a-i**) 2 weeks following optic nerve injury, regenerative axonal growth was assessed by anti-GAP-43 immunolabeling of longitudinal optic nerve sections. (**a'-i'**) To assess whether RGCs in a growth-activated state show an additive growth effect when combined with genetic ablation of Nogo receptors, a separate group of animals received an intraocular injection (i.o.) of Zymosan at the time of optic nerve injury. Anti-GAP-43 immunolabeling of injured optic nerve from (**a**) WT, (**b**) *NgR1*$^{-/-}$, (**c**) *NgR2*$^{-/-}$, (**d**) *NgR3*$^{-/-}$, (**e**) *RPTPσ*$^{-/-}$, and (**f**) *NgR12*$^{-/-}$ mice fails to identify significant regenerative growth of axons beyond the lesion site (asterisk). (**g**) *NgR13*$^{-/-}$ and (**h**) *NgR123*$^{-/-}$ mice show increased and comparable axonal regeneration, which is further enhanced in (**i**) *NgR13/RPTPσ*$^{-/-}$ (*NgR13/σ*$^{-/-}$) triple mutant mice. Following i.o. Zymosan injection, (**b'**) *NgR1*$^{-/-}$, (**c'**) *NgR2*$^{-/-}$, (**d'**) *NgR3*$^{-/-}$, (**e'**) *RPTPσ*$^{-/-}$, and (**f'**) *NgR12*$^{-/-}$ mice do not show enhanced regeneration compared to (**a'**) WT mice with i.o. Zymosan. An additive effect of i.o. Zymosan with genetic manipulation was observed for (**g'**) *NgR13*$^{-/-}$ and (**h'**) *NgR123*$^{-/-}$ mice. (**i'**) Loss of NgR1, NgR3 and RPTPσ (*NgR13/σ*$^{-/-}$) combined with i.o. Zymosan resulted in a further increase of fiber growth. Scale bar, 200μm.

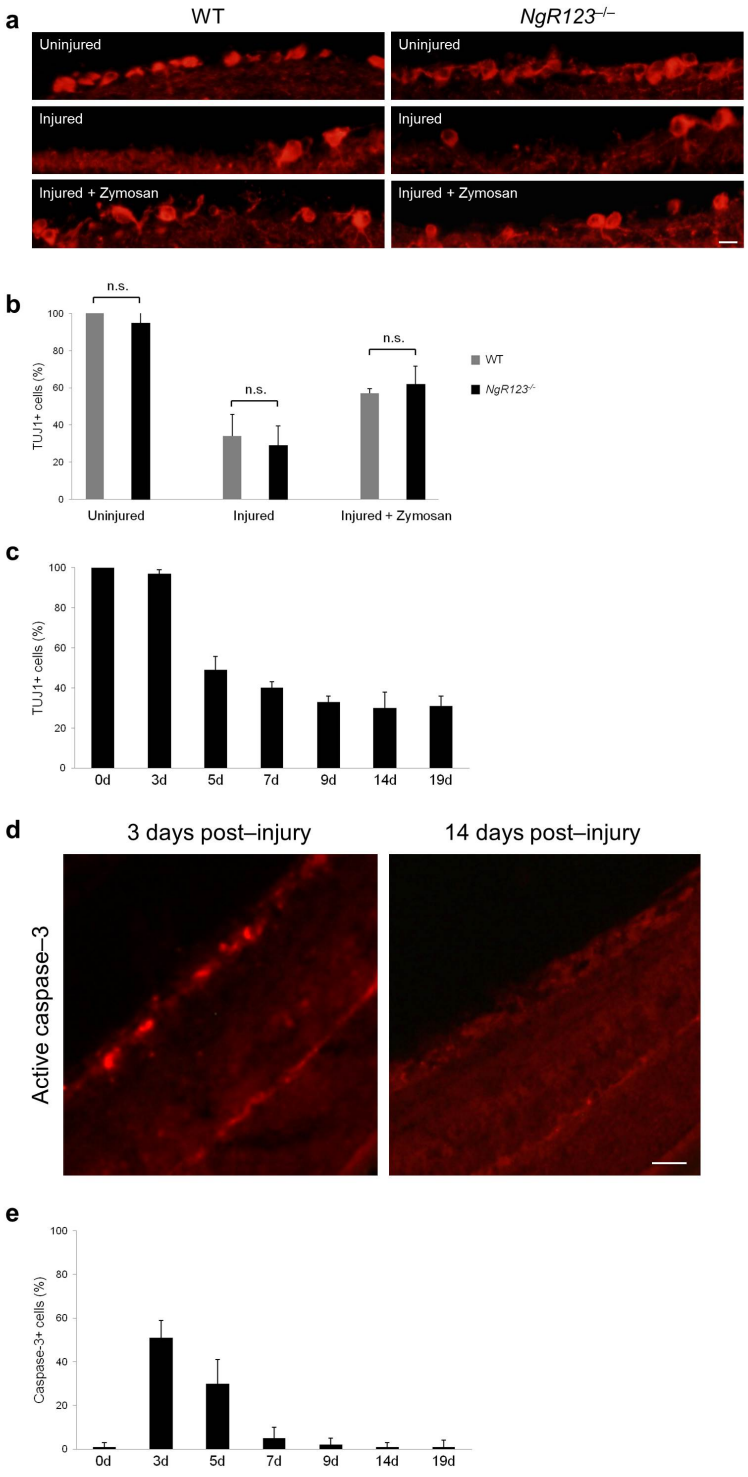

Figure 2.18: Optic nerve injury-induced retinal ganglion cell death is similar in WT and *NgR123*$^{-/-}$ triple mutants. (**a**) To assess cell loss in the RGC layer 14 days after nerve crush injury, coronal sections of WT and *NgR123*$^{-/-}$ retina were immunolabeled with TuJ1 and

compared to uninjured retina. Intraocular injection of Zymosan increased the density of TuJ1-labeled cells in the RGC layer; however, this effect was independent of the Nogo receptor genotype. (**b**) Quantification of the density of $TuJ1^+$ cells in the RGC layer per field of view as a percentage of the uninjured WT control. Cell counts were performed on at least 15 sections per condition (n=3 independent experiments). Gray bars (WT); black bars (*NgR123*$^{-/-}$). Results are presented as mean ±SEMs (one-way ANOVA, Tukey's *post hoc*), n.s.=not significant. (**c**) Time course of RGC death following optic nerve injury. Shown is the quantification of the density of $TuJ1^+$ cells in the RGC layer per field of view (at 0, 3, 5, 7, 9, 14, and 19 days following injury) as a percentage of the uninjured retina. The majority of cell death occurs by 7 days post-optic nerve injury. Cell counts were performed on at least 10 sections per condition. Results are presented as mean ±SEMs. (**d-e**) Time course of caspase-3 activation following optic nerve injury. The number of RGCs labeled for activated caspase-3 is shown as a percentage of the total number of cells (TUJ1-positive) per field of view at each time point (0, 3, 5, 7, 9, 14, and 19 days following injury). The peak of activated caspase-3 labeling is seen between 3 and 5 days post-injury. Cell counts were performed on at least 10 sections per condition. Results are presented as mean ±SEMs. Scale bar: a, 30μm; d, 60μm.

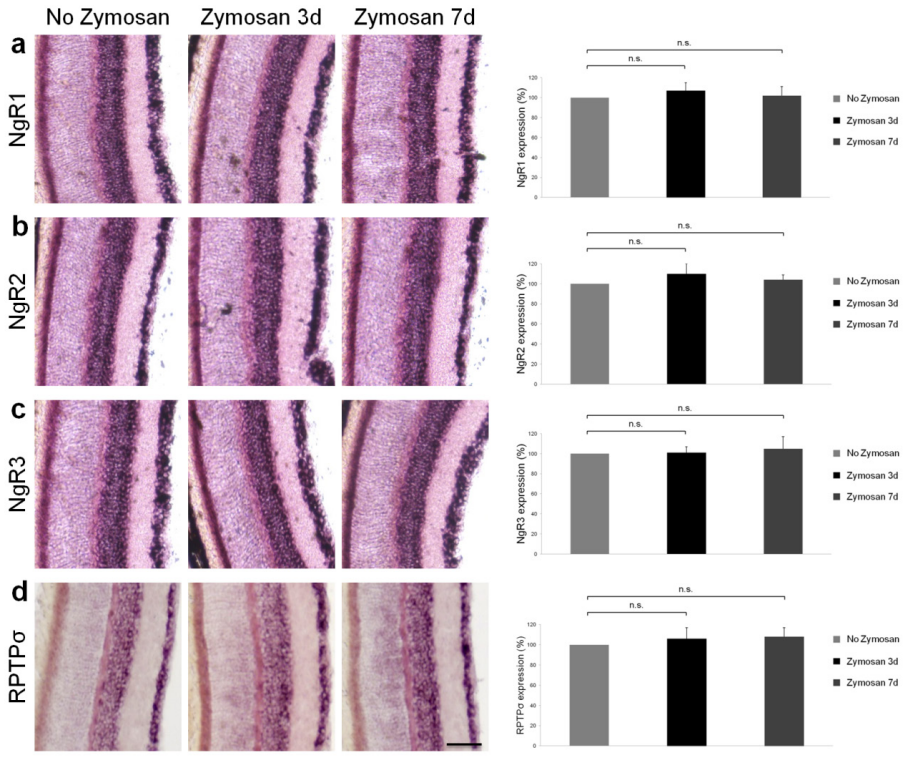

Figure 2.19: Intraocular Zymosan injection does not affect the expression of Nogo receptors or RPTPσ in the retinal ganglion cell layer. *In situ* hybridization on adult WT retina with digoxigenin-labeled cRNA probes specific for (**a**) NgR1, (**b**) NgR2, (**c**) NgR3, and (**d**) RPTPσ transcripts. Mice received either no Zymosan or intraocular Zymosan injection on day 0, followed by examination at 3 or 7 days post-injection. Zymosan injection does not result in any obvious changes in expression of NgRs or RPTPσ in the RGC layer or inner nuclear layer. For quantification of receptor expression in the RGC layer, all retinal sections were developed for the same amount of time. The expression of each receptor in the RGC layer is shown as a percentage of the "No Zymosan" control. At least 20 sections were assessed per condition (n=4 independent experiments). Light gray bars (No Zymosan); black bars (Zymosan 3d); dark gray bars (Zymosan 7d). Results are presented as mean ±SEMs (one-way ANOVA, Tukey's *post hoc*), n.s.= not significant. Scale bar, 80μm.

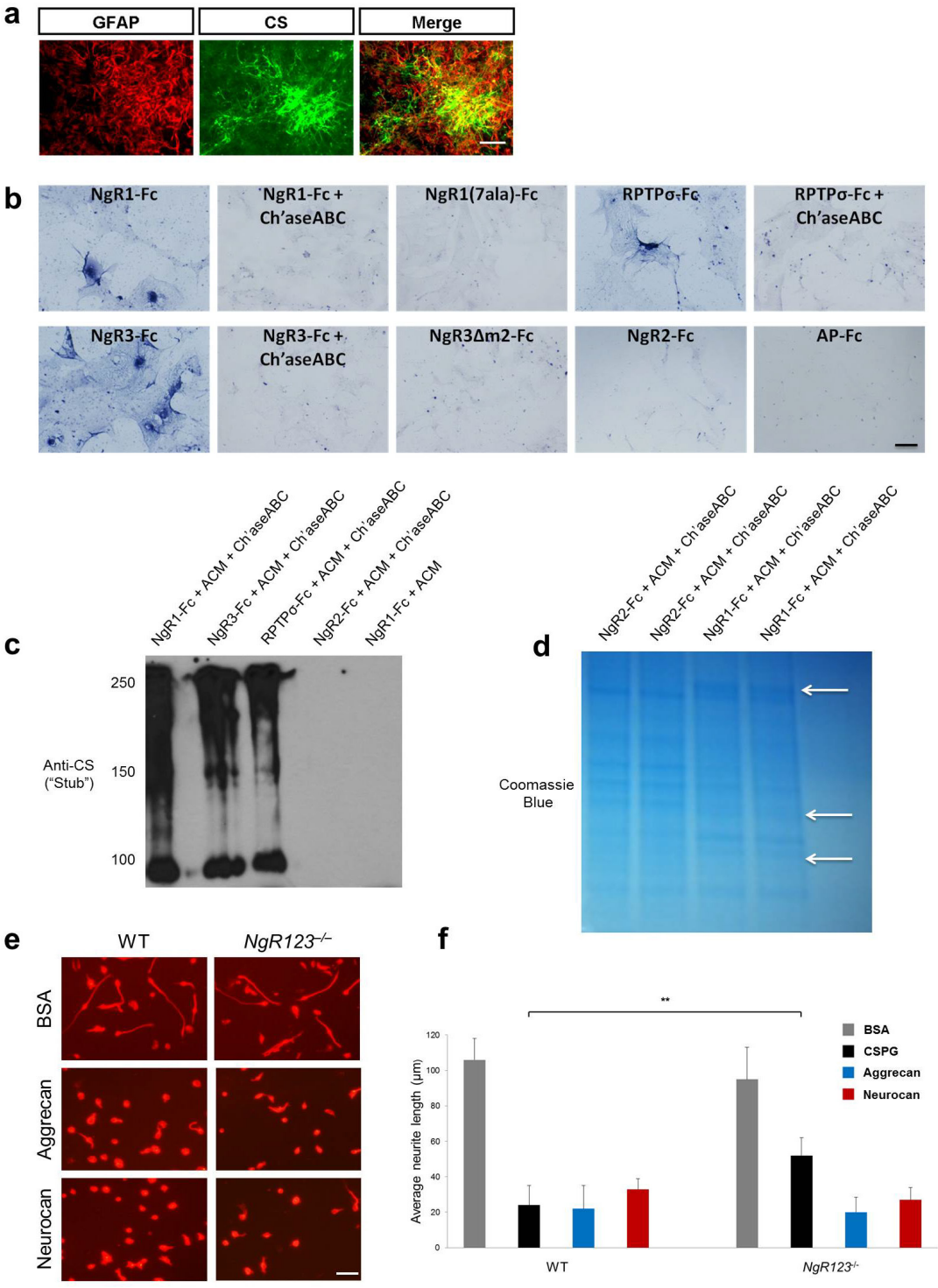

Figure 2.20: NgR1 and NgR3, but not NgR2, interact with astrocyte-released CSPGs. (**a**) P1 cortical astrocytes were cultured and treated with TGFβ1 (1μg/ml) for 7 days, prior to anti-GFAP and anti-CS immunolabeling to confirm reactivity. (**b**) Following TGFβ1 treatment,

astrocyte cultures were incubated with AP-Fc, NgR1-Fc, NgR2-Fc, NgR3-Fc, RPTPσ(Ig1-3)-Fc, NgR1(7ala)-Fc, or NgR3Δm2-Fc. Soluble NgR1-Fc, NgR3-Fc, and RPTPσ(Ig1-3)-Fc, but not NgR1(7ala)-Fc or NgR3Δm2-Fc, bind strongly to reactive astrocytes, suggesting that this interaction depends on the presence of the proteoglycan-binding motif 2. Treatment of astrocytes with 1unit/ml Ch'aseABC abolishes binding, suggesting that CSPGs participate in the binding of NgR1, NgR3, and RPTPσ. (**c**) ACM from TGFβ1-treated cultures was tumbled with either affinity-purified NgR1-Fc, NgR2-Fc, NgR3-Fc, or RPTPσ(Ig1-3)-Fc. Some of the precipitated immune complex was then incubated with Ch'aseABC (1unit/ml), before analysis by immunoblotting, using anti-chondroitin sulfate "stub". Following Ch'aseABC treatment of the NgR1, NgR3, and RPTPσ(Ig1-3)-Fc (but not NgR2) conditions, several bands are noted in the 100-250 kilodalton range. No bands are recognized by the "stub" antibody without Ch'aseABC treatment. (**d**) Some Ch'aseABC-treated precipitates were subjected to SDS-PAGE and stained with Coomassie Blue to identify protein bands. Coomassie Blue staining revealed distinct bands (in the 100-250 kilodalton range; white arrows) present in the NgR1, but not NgR2, conditions. (**e**) In CGNs, NgRs are not necessary for inhibition on substrate-bound aggrecan or neurocan (10μg/ml). P7 CGNs from WT and *NgR123*$^{-/-}$ pups are strongly and equally inhibited when plated on either CSPG protein core. On a BSA control substrate, neurite lengths of WT and *NgR123*$^{-/-}$ CGNs are comparable. (**f**) Quantification of neurite length. At least 200 neurites of TuJ1-labeled cells were counted per condition (n=5 independent experiments). Gray bars (BSA); black bars (CSPG); blue bars (Aggrecan); red bars (Neurocan). Results are presented as mean ±SEMs. ** $P< 0.001$ (one-way ANOVA, Tukey's *post hoc*). Scale bar: a, 30μm; b, 20μm; e, 50μm.

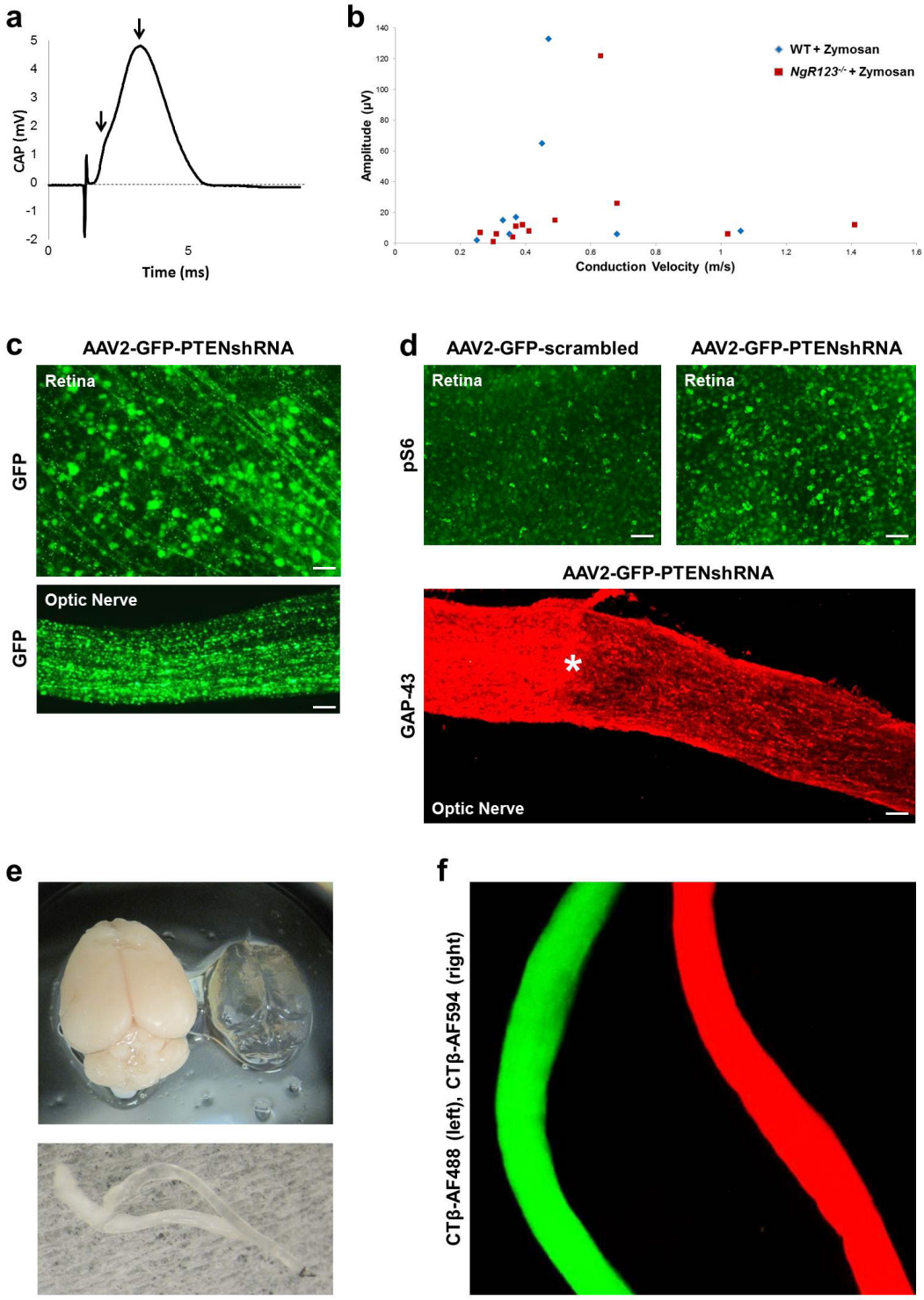

Figure 2.21: Future strategies for assessment of long-distance axonal regeneration and functional recovery. (**a**) Representative CAP recording from an adult mouse optic nerve, in which a large peak is seen with multiple components (black arrows). These components likely

represent the fast and slow myelinated fibers of the optic nerve. An uninjured, adult nerve has an average conduction velocity of 4m/s and average peak amplitude of 5mV. (**b**) A plot of the conduction velocities and peak amplitudes of optic nerves from WT and *NgR123*$^{-/-}$ animals with Zymosan administration, 3-11 weeks post-crush injury. With the exception of a few outliers that show marginal improvement, neither condition reveals any substantial functional recovery when compared to WT animals with crush injury. It should be noted that there is no correlation between the number of weeks passed before recording and the conduction velocity/peak amplitude. Blue triangles (WT + Zymosan, n=8 nerves); red squares (*NgR123*$^{-/-}$ + Zymosan, n=12 nerves). (**c**) Intraocular injection of AAV2-GFP-PTENshRNA results in efficient transduction of RGCs and their projections, as visualized by anti-GFP immunolabeling of the retina (top) and optic nerve (bottom). (**d**) pS6 levels are greatly increased in RGCs upon transduction with AAV2-GFP-PTENshRNA compared to the AAV2-GFP-scrambled control, as determined by anti-pS6 immunolabeling of the retina (top). Additionally, intraocular injection of AAV2-GFP-PTENshRNA results in substantial RGC fiber growth distal to the injury site in the optic nerve, 2 weeks following crush injury (bottom). The injury site is marked with an asterisk. (**e**) Representative images of the brain (top) and optic nerve (bottom), following THF-based chemical clearing. Uncleared tissues are also shown for comparison. (**f**) Five days after injection of Alexa 488-conjugated Cholera Toxin β into the left eye and Alexa 594-conjugated Cholera Toxin β into the right eye, mice were sacrificed, perfused, and optic nerves were chemically cleared. Strong levels of fluorescence are seen in both cleared optic nerves, without the need for any histological sectioning. Scale bar: c (top), 60μm; c (bottom), 50μm; d (top), 90μm; d (bottom), 50μm.

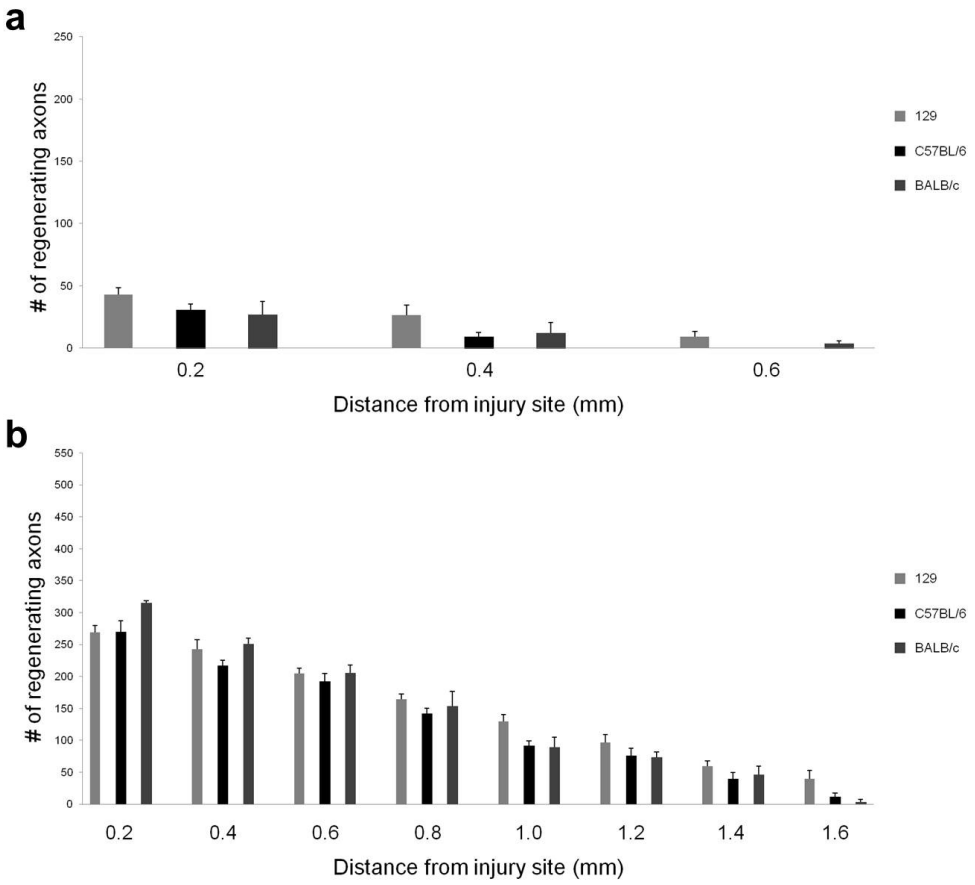

Figure 2.22: The genetic background of wild-type mice does not significantly influence RGC axon regeneration. (**a**) Quantification of the number of GAP-43-positive axons at 0.2 to 0.6mm distal to the lesion site in 129 (light gray bars, n=6), C57BL/6 (black bars, n= 6), and BALB/c (dark gray bars, n= 4) wild-type mice 2 weeks following optic nerve injury revealed no significant differences. (**b**) Quantification of the number of GAP-43-positive axons at 0.2 to 1.6mm distal to the lesion site following intraocular Zymosan injection in 129 (light gray bars, n=6), C57BL/6 (black bars, n=7), and BALB/c (dark gray bars, n=3) wild-type mice, 2 weeks following optic nerve injury. No significant differences at any distance were observed. Results are presented as mean ±SEMs (one-way ANOVA, Tukey's *post hoc*).

a *Injury*

Genotype	Number of Nerves	Significance vs. WT 0.2 mm	Significance vs. WT 0.4 mm
NgR123$^{-/-}$	8	***	***
NgR1$^{-/-}$	7	ns	ns
NgR2$^{-/-}$	3	ns	ns
NgR3$^{-/-}$	3	ns	ns
NgR12$^{-/-}$	3	ns	ns
NgR13$^{-/-}$	4	***	***
RPTPσ$^{-/-}$	5	ns	ns
NgR13/RPTPσ$^{-/-}$	4	***	***

b *Injury + Zymosan*

Genotype	Number of Nerves	Significance vs. WT 0.2 mm	Significance vs. WT 0.8 mm
NgR123$^{-/-}$	8	***	**
NgR1$^{-/-}$	6	ns	ns
NgR2$^{-/-}$	3	ns	ns
NgR3$^{-/-}$	3	ns	ns
NgR12$^{-/-}$	3	ns	ns
NgR13$^{-/-}$	3	***	**
RPTPσ$^{-/-}$	4	ns	ns
NgR13/RPTPσ$^{-/-}$	3	***	***

c *Injury*

Genotype	Number of Nerves	Significance vs. *NgR123*$^{-/-}$ 0.2 mm	Significance vs. *NgR123*$^{-/-}$ 0.4 mm
WT	6	***	***
NgR1$^{-/-}$	7	***	***
NgR2$^{-/-}$	3	***	***
NgR3$^{-/-}$	3	***	***
NgR12$^{-/-}$	3	***	***
NgR13$^{-/-}$	4	ns	ns
RPTPσ$^{-/-}$	5	***	***
NgR13/RPTPσ$^{-/-}$	4	***	**

d *Injury + Zymosan*

Genotype	Number of Nerves	Significance vs. *NgR123*$^{-/-}$ 0.2 mm	Significance vs. *NgR123*$^{-/-}$ 0.8 mm
WT	6	***	**
NgR1$^{-/-}$	6	***	**
NgR2$^{-/-}$	3	***	**
NgR3$^{-/-}$	3	***	**
NgR12$^{-/-}$	3	***	*
NgR13$^{-/-}$	3	ns	ns
RPTPσ$^{-/-}$	4	***	*
NgR13/RPTPσ$^{-/-}$	3	ns	ns

e

Genotype	P-value of K.B. vs. Y.K. data (0.4 mm)	P-value of K.B. vs. Y.K. data (1.0 mm)
WT (C57BL/6)	0.9181	n/a
WT (C57BL/6) with Zymosan	0.3643	0.5888
NgR1$^{-/-}$	0.7067	n/a
NgR1$^{-/-}$ with Zymosan	0.3845	0.0818
WT (129)	0.4323	n/a
WT (129) with Zymosan	0.9905	0.6718
NgR123$^{-/-}$	0.8359	0.3945
NgR123$^{-/-}$ with Zymosan	0.7162	0.2738

Table 2.1: Summary of optic nerve regeneration studies. (**a**) 2 weeks following injury, regeneration in *NgR123*$^{-/-}$, *NgR13*$^{-/-}$, and *NgR13/RPTPσ*$^{-/-}$ compound mutant mice is significantly increased compared to WT mice at 0.2 and 0.4mm distal to the injury site. Compared to WT mice, regeneration in *NgR1*$^{-/-}$, *NgR2*$^{-/-}$, *NgR3*$^{-/-}$, *NgR12*$^{-/-}$, or *RPTPσ*$^{-/-}$ at 0.2 and 0.4mm is not significantly enhanced. *** $P< 0.001$ (one-way ANOVA, Tukey's *post hoc*), n.s.= not significant. (**b**) Following intraorbital Zymosan injection, regeneration in *NgR123*$^{-/-}$, *NgR13*$^{-/-}$, and *NgR13/RPTPσ*$^{-/-}$ compound mutant mice is significantly enhanced compared to WT mice at 0.2 and 0.8mm distal to the injury site. There is no significant difference in axon regeneration between WT mice and *NgR1*$^{-/-}$, *NgR2*$^{-/-}$, *NgR3*$^{-/-}$, *NgR12*$^{-/-}$, or *RPTPσ*$^{-/-}$ mutant mice. *** $P< 0.001$, ** $P< 0.01$ (one-way ANOVA, Tukey's *post hoc*), n.s.= not significant. (**c**) 2 weeks following injury, regeneration in *NgR123*$^{-/-}$ mice is significantly increased compared to WT, *NgR1*$^{-/-}$, *NgR2*$^{-/-}$, *NgR3*$^{-/-}$, *NgR12*$^{-/-}$, and *RPTPσ*$^{-/-}$ mice, and decreased compared to *NgR13/RPTPσ*$^{-/-}$ mice, at 0.2 and 0.4mm distal to the injury site. There is no significant difference in the regeneration phenotype of *NgR123*$^{-/-}$ and *NgR13*$^{-/-}$ compound mutants. *** $P< 0.001$, ** $P< 0.01$ (one-way ANOVA, Tukey's *post hoc*), n.s.= not significant. (**d**) Following intraocular Zymosan injection, axon regeneration in *NgR123*$^{-/-}$ mice is significantly increased compared to WT, *NgR1*$^{-/-}$, *NgR2*$^{-/-}$, *NgR3*$^{-/-}$, *NgR12*$^{-/-}$, and *RPTPσ*$^{-/-}$ mice at 0.2 and 0.8mm distal to the injury site. There is no significant difference in axon regeneration between *NgR123*$^{-/-}$ and *NgR13*$^{-/-}$ or *NgR13/RPTPσ*$^{-/-}$ mutant mice (with intraocular Zymosan injection) at these distances. At distances 0.4, 0.6, 1.0, 1.2, and 1.4mm beyond the injury site, axon regeneration in *NgR13/RPTPσ*$^{-/-}$ mice is significantly greater than in *NgR123*$^{-/-}$ mice (with intraocular Zymosan injection). *** $P< 0.001$, ** $P< 0.01$, * $P< 0.05$ (one-way ANOVA, Tukey's *post hoc*), n.s.= not significant. (**e**) For an unbiased assessment of the optic nerve regeneration phenotype in Nogo receptor single and compound mutants, two independent data sets were generated by two independent surgeons: K. Baldwin (University of Michigan) and Y. Koriyama (visiting scientist from Kanazawa University). Both surgeons were originally trained in the laboratory of L. Benowitz. A total of 84 mice (K.B. - 51 mice, Y.K. - 33 mice) were operated on, and each surgeon performed crush injury on the following genotypes: WT, *NgR1*$^{-/-}$, and *NgR123*$^{-/-}$ mice. Only optic nerves from mice that showed no bleeding, infection, degeneration, or other complications of the operated eye were included for quantification of regenerating axons. The two data sets were then compared and analyzed for any significant differences between them, comparing the total number of GAP-43-positive axons for each genotype at two prespecified distances (0.4mm, 1.0mm) beyond the lesion site (unpaired *t* test). While there is some variation in the number of regenerating fibers, the principal findings of the two independently generated data sets are very comparable: WT mice (129 background or C57BL/6 background) show minimal regeneration of GAP-43-positive retinal ganglion cell axons. Regeneration in *NgR1*$^{-/-}$ mice is not enhanced compared to WT mice. Both data sets show a modest but significant increase in regenerating axons in *NgR123*$^{-/-}$ mice ($P< 0.001$, K.B; $P< 0.05$, Y.K.). WT mice that received Zymosan show greatly enhanced axon regeneration compared to WT mice that did not receive Zymosan. Notably, regeneration in Zymosan-treated WT mice is significantly enhanced compared to *NgR123*$^{-/-}$ mice without Zymosan ($P< 0.001$ for both data sets). Importantly, both data sets show significantly enhanced fiber growth at 0.2-1.4mm beyond the injury site in *NgR123*$^{-/-}$ mice with Zymosan compared to WT mice with Zymosan ($P< 0.05$ at 1.0, 1.2, and 1.4mm; $P< 0.01$ at 0.8mm; $P< 0.001$ at 0.2, 0.4, and 0.6mm - K.B.; $P< 0.05$ at 0.4 and 0.6mm; $P< 0.01$ at 0.2, 1.2, and 1.4mm; $P< 0.001$ at 0.8 and 1.0mm - Y.K.).

Identified Proteins (LC-MS/MS, Mus musculus)
M2-type pyruvate kinase
Heat shock protein HSP 90-beta
Alpha-tubulin isotype M-alpha-2
Glyceraldehyde-3-phosphate dehydrogenase-like isoform 1
Ribosomal protein, large, P0
40S ribosomal protein S3
Tubulin, beta 5
Protease, serine, 1 precursor
Vimentin
Annexin A2
Heat shock protein 90, beta (Grp94), member 1
Heat shock protein HSP 90-alpha
Chaperonin
T-complex protein 1 subunit beta
Tropomyosin alpha-3 chain isoform 4
Cullin-associated NEDD8-dissociated protein 1
Apolipoprotein E
mCG21063
Elongation factor 1-gamma
Protein disulfide isomerase associated 6
Spliceosome RNA helicase Ddx39b
T-complex polypeptide 1A
mCG129789
mCG118515
Complement C1q subcomponent subunit A precursor
F-actin-capping protein subunit beta isoform d
14-3-3
Exportin-2
Valosin containing protein
Capping protein (actin filament) muscle Z-line
Synaptic vesicle membrane protein VAT-1 homolog
T-complex protein 1 subunit eta
Annexin A3
Atp5b protein
Peptidylglycine alpha-amidating monooxygenase

Table 2.2: Summary of identified proteins from LC-MS/MS. LC-MS/MS analysis from NgR1-Fc/ACM/Ch'aseABC and NgR2-Fc/ACM/Ch'aseABC samples. All mouse proteins identified by LC-MS/MS were found in both groups (and at comparable levels). Additionally, NgR (rat), Fc (human), and Ch'aseABC (bacteria) components were identified by LC-MS/MS (data not shown).

Genotype	Amplitude (μV)	Conduction Velocity (m/s)	Number of Days Post-Crush
WT	133	0.47	21
WT	65	0.45	21
WT	17	0.37	21
WT	2	0.25	21
WT	15	0.33	22
NgR123$^{-/-}$	122	0.63	22
NgR123$^{-/-}$	6	0.31	22
NgR123$^{-/-}$	1	0.30	23
NgR123$^{-/-}$	12	0.39	23
NgR123$^{-/-}$	7	0.26	27
NgR123$^{-/-}$	6	1.02	27
WT	6	0.35	28
NgR123$^{-/-}$	12	1.41	28
NgR123$^{-/-}$	4	0.36	30
NgR123$^{-/-}$	11	0.37	40
NgR123$^{-/-}$	15	0.49	56
WT	8	1.06	56
WT	6	0.68	63
NgR123$^{-/-}$	26	0.68	63
NgR123$^{-/-}$	8	0.41	77

Table 2.3: Summary of optic nerve conduction recordings. Peak amplitudes (μV) and conduction velocities (m/s) of optic nerves from WT and *NgR123*$^{-/-}$ adult mice with Zymosan administration, 3-11 weeks post-crush injury. For reference purposes, uninjured optic nerves have an average peak amplitude of 5mV and average conduction velocity of 4m/s. Injured optic nerves have an average peak amplitude of 15μV and average conduction velocity of 0.5m/s. Neither experimental condition reveals any substantial functional recovery when compared to WT animals with crush injury. It should be noted that there is no correlation between the number of weeks passed before recording and the peak amplitude/conduction velocity.

2.9 Bibliography

Aricescu AR, McKinnell IW, Halfter W, Stoker AW (2002) Heparan sulfate proteoglycans are ligands for receptor protein tyrosine phosphatase sigma. Mol Cell Biol 22:1881-1892.

Atwal JK, Pinkston-Gosse J, Syken J, Stawicki S, Wu Y, Shatz C, Tessier-Lavigne M (2008) PirB is a functional receptor for myelin inhibitors of axonal regeneration. Science 322:967-970.

Barton WA, Liu BP, Tzvetkova D, Jeffrey PD, Fournier AE, Sah D, Cate R, Strittmatter SM, Nikolov DB (2003) Structure and axon outgrowth inhibitor binding of the Nogo-66 receptor and related proteins. EMBO J 22:3291-3302.

Bradbury EJ, Moon LD, Popat RJ, King VR, Bennett GS, Patel PN, Fawcett JW, McMahon SB (2002) Chondroitinase ABC promotes functional recovery after spinal cord injury. Nature 416:636-640.

Bregman BS, Kunkel-Bagden E, Schnell L, Dai HN, Gao D, Schwab ME (1995) Recovery from spinal cord injury mediated by antibodies to neurite growth inhibitors. Nature 378:498-501.

Briani C, Berger JS, Latov N (1998) Antibodies to chondroitin sulfate C: a new detection assay and correlations with neurological diseases. J Neuroimmunol 84:117-121.

Cafferty WB, Duffy P, Huebner E, Strittmatter SM (2010) MAG and OMgp synergize with Nogo-A to restrict axonal growth and neurological recovery after spinal cord trauma. J Neurosci 30:6825-6837.

Chivatakarn O, Kaneko S, He Z, Tessier-Lavigne M, Giger RJ (2007) The Nogo-66 receptor NgR1 is required only for the acute growth cone-collapsing but not the chronic growth-inhibitory actions of myelin inhibitors. J Neurosci 27:7117-7124.

Coles CH, Shen Y, Tenney AP, Siebold C, Sutton GC, Lu W, Gallagher JT, Jones EY, Flanagan JG, Aricescu AR (2011) Proteoglycan-specific molecular switch for RPTPσ clustering and neuronal extension. Science 332:484-488.

de Lima S, Koriyama Y, Kurimoto T, Oliveira JT, Yin Y, Li Y, Gilbert HY, Fagiolini M, Martinez AM, Benowitz L (2012). Full-length axon regeneration in the adult mouse optic nerve and partial recovery of simple visual behaviors. Proc Natl Acad Sci U S A 109:9149-9154.

Erturk A, Mauch CP, Hellal F, Forstner F, Keck T, Becker K, Jahrling N, Steffens H, Richter M, Hubener M, Kramer E, Kirchhoff F, Dodt HU, Bradke F (2011) Three-dimensional imaging of the unsectioned adult spinal cord to assess axon regeneration and glial responses after injury. Nat Med 18:166-171.

Fischer D, He Z, Benowitz LI (2004a) Counteracting the Nogo receptor enhances optic nerve regeneration if retinal ganglion cells are in an active growth state. J Neurosci 24:1646-1651.

Fischer D, Petkova V, Thanos S, Benowitz LI (2004b) Switching mature retinal ganglion cells to a robust growth state in vivo: gene expression and synergy with RhoA inactivation. J Neurosci 24:8726-8740.

Fisher D, Xing B, Dill J, Li H, Hoang HH, Zhao Z, Yang XL, Bachoo R, Cannon S, Longo FM, Sheng M, Silver J, Li S (2011) Leukocyte common antigen-related phosphatase is a functional receptor for chondroitin sulfate proteoglycan axon growth inhibitors. J Neurosci 31:14051-14066.

Fournier AE, GrandPre T, Strittmatter SM (2001) Identification of a receptor mediating Nogo-66 inhibition of axonal regeneration. Nature 409:341-346.
Fry EJ, Chagnon MJ, Lopez-Vales R, Tremblay ML, David S (2009) Corticospinal tract regeneration after spinal cord injury in receptor protein tyrosine phosphatase sigma deficient mice. Glia 58:423-433.
Fujita Y, Endo S, Takai T, Yamashita T (2011) Myelin suppresses axon regeneration by PIR-B/SHP-mediated inhibition of Trk activity. EMBO J 30:1389-1401.
Garcia-Alias G, Barkhuysen S, Buckle M, Fawcett JW (2009) Chondroitinase ABC treatment opens a window of opportunity for task-specific rehabilitation. Nat Neurosci 12:1145-1151.
Harvey DJ (2005) Proteomic analysis of glycosylation: structural determination of N- and O-linked glycans by mass spectrometry. Expert Rev Proteomics 2:87-101.
Houle JD, Tom VJ, Mayes D, Wagoner G, Phillips N, Silver J (2006) Combining an autologous peripheral nervous system "bridge" and matrix modification by chondroitinase allows robust, functional regeneration beyond a hemisection lesion of the adult rat spinal cord. J Neurosci 26:7405-7415.
Jones LL, Margolis RU, Tuszynski MH (2003) The chondroitin sulfate proteoglycans neurocan, brevican, phosphacan, and versican are differentially regulated following spinal cord injury. Exp Neurol 182:399-411.
Kadoya K, Tsukada S, Lu P, Coppola G, Geschwind D, Filbin MT, Blesch A, Tuszynski MH (2009) Combined intrinsic and extrinsic neuronal mechanisms facilitate bridging axonal regeneration one year after spinal cord injury. Neuron 64:165-172.
Kantor DB, Chivatakarn O, Peer KL, Oster SF, Inatani M, Hansen MJ, Flanagan JG, Yamaguchi Y, Sretavan DW, Giger RJ, Kolodkin AL (2004) Semaphorin 5A is a bifunctional axon guidance cue regulated by heparan and chondroitin sulfate proteoglycans. Neuron 44:961-975.
Karlen A, Karlsson TE, Mattsson A, Lundstromer K, Codeluppi S, Pham TM, Backman CM, Ogren SO, Aberg E, Hoffman AF, Sherling MA, Lupica CR, Hoffer BJ, Spenger C, Josephson A, Brene S, Olson L (2009) Nogo receptor 1 regulates formation of lasting memories. Proc Natl Acad Sci U S A 106:20476-20481.
Kim JE, Liu BP, Park JH, Strittmatter SM (2004) Nogo-66 receptor prevents raphespinal and rubrospinal axon regeneration and limits functional recovery from spinal cord injury. Neuron 44:439-451.
Lee H, Raiker SJ, Venkatesh K, Geary R, Robak LA, Zhang Y, Yeh HH, Shrager P, Giger RJ (2008) Synaptic function for the Nogo-66 receptor NgR1: regulation of dendritic spine morphology and activity-dependent synaptic strength. J Neurosci 28:2753-2765.
Lee JK, Geoffroy CG, Chan AF, Tolentino KE, Crawford MJ, Leal MA, Kang B, Zheng B (2010) Assessing spinal axon regeneration and sprouting in Nogo-, MAG-, and OMgp-deficient mice. Neuron 66:663-670.
Leibinger M, Muller A, Andreadaki A, Hauk TG, Kirsch M, Fischer D (2009) Neuroprotective and axon growth-promoting effects following inflammatory stimulation on mature retinal ganglion cells in mice depend on ciliary neurotrophic factor and leukemia inhibitory factor. J Neurosci 29:14334-14341.
Li S, Liu BP, Budel S, Li M, Ji B, Walus L, Li W, Jirik A, Rabacchi S, Choi E, Worley D, Sah DW, Pepinsky B, Lee D, Relton J, Strittmatter SM (2004) Blockade of Nogo-66, myelin-associated glycoprotein, and oligodendrocyte myelin glycoprotein by soluble Nogo-66

receptor promotes axonal sprouting and recovery after spinal injury. J Neurosci 24:10511-10520.
Liu BP, Cafferty WB, Budel SO, Strittmatter SM (2006) Extracellular regulators of axonal growth in the adult central nervous system. Philos Trans R Soc Lond B Biol Sci 361:1593-1610.
Liu K, Lu Y, Lee JK, Samara R, Willenberg R, Sears-Kraxberger I, Tedeschi A, Park KK, Jin D, Cai B, Xu B, Connolly L, Steward O, Zheng B, He Z (2010) PTEN deletion enhances the regenerative ability of adult corticospinal neurons. Nat Neurosci. 13:1075-1081.
Luo X, Salgueiro Y, Beckerman SR, Lemmon VP, Tsoulfas P, Park KK (2013) Three-dimensional evaluation of retinal ganglion cell axon regeneration and pathfinding in whole mouse tissue after injury. Exp Neurol S0014-4886:00084-00088.
Massey JM, Hubscher CH, Wagoner MR, Decker JA, Amps J, Silver J, Onifer SM (2006) Chondroitinase ABC digestion of the perineuronal net promotes functional collateral sprouting in the cuneate nucleus after cervical spinal cord injury. J Neurosci 26:4406-4414.
McGee AW, Yang Y, Fischer QS, Daw NW, Strittmatter SM (2005) Experience-driven plasticity of visual cortex limited by myelin and Nogo receptor. Science 309:2222-2226.
McKeon RJ, Hoke A, Silver J (1995) Injury-induced proteoglycans inhibit the potential for laminin-mediated axon growth on astrocytic scars. Exp Neurol 136:32-43.
Niederost BP, Zimmermann DR., Schwab ME, Bandtlow CE (1999) Bovine CNS myelin contains neurite growth-inhibitory activity associated with chondroitin sulfate proteoglycans. J Neurosci 19:8979-8989.
Ohlsson M, Mattsson P, Svensson M (2004) A temporal study of axonal degeneration and glial scar formation following a standardized crush injury of the optic nerve in the adult rat. Restor Neurol Neurosci 22:1-10.
Park KK, Liu K, Hu Y, Smith PD, Wang C, Cai B, Xu B, Connolly L, Kramvis I, Sahin M, He Z (2008) Promoting axon regeneration in the adult CNS by modulation of the PTEN/mTOR pathway. Science 322:963-966.
Pekny M, Nilsson M (2005) Astrocyte activation and reactive gliosis. Glia 50:427-434.
Pizzorusso T, Medini P, Berardi N, Chierzi S, Fawcett JW, Maffei L (2002) Reactivation of ocular dominance plasticity in the adult visual cortex. Science 298:1248-1251.
Powell EM, Mercado ML, Calle-Patino Y, Geller HM (2001) Protein kinase C mediates neurite guidance at an astrocyte boundary. Glia 33:288-297.
Raiker SJ, Lee H, Baldwin KT, Duan Y, Shrager P, Giger RJ (2010) Oligodendrocyte-myelin glycoprotein and Nogo negatively regulate activity-dependent synaptic plasticity. J Neurosci 30:12432-12445.
Rhodes KE, Fawcett JW (2004) Chondroitin sulphate proteoglycans: preventing plasticity or protecting the CNS? J Anat 204:33-48.
Robak LA, Venkatesh K, Lee H, Raiker SJ, Duan Y, Lee-Osbourne J, Hofer T, Mage RG, Rader C, Giger RJ (2009) Molecular basis of the interactions of the Nogo-66 receptor and its homolog NgR2 with myelin-associated glycoprotein: development of NgROMNI-Fc, a novel antagonist of CNS myelin inhibition. J Neurosci 29:5768-5783.
Sapieha PS, Duplan L, Uetani N, Joly S, Tremblay ML, Kennedy TE, Di Polo A (2005) Receptor protein tyrosine phosphatase sigma inhibits axon regrowth in the adult injured CNS. Mol Cell Neurosci 28:625-635.

Satoh J, Yamamura T, Arima K (2004) The 14-3-3 protein epsilon isoform expressed in reactive astrocytes in demyelinating lesions of multiple sclerosis binds to vimentin and glial fibrillary acidic protein in cultured human astrocytes. Am J Pathol 165:577-592.

Schiffer D, Giordana MT, Migheli A, Giaccone G, Pezzotta S, Mauro A (1986) Glial fibrillary acidic protein and vimentin in the experimental glial reaction of the rat brain. Brain Res 374:110-118.

Schweigreiter R, Walmsley AR, Niederost B, Zimmermann DR, Oertle T, Casademunt E, Frentzel S, Dechant G, Mir A, Bandtlow CE (2004) Versican V2 and the central inhibitory domain of Nogo-A inhibit neurite growth via p75NTR/NgR-independent pathways that converge at RhoA. Mol Cell Neurosci 27:163-174.

Shen Y, Tenney AP, Busch SA, Horn KP, Cuascut FX, Liu K, He Z, Silver J, Flanagan JG (2009) PTPsigma is a receptor for chondroitin sulfate proteoglycan, an inhibitor of neural regeneration. Science 326:592-596.

Shypitsyna A, Malaga-Trillo E, Reuter A, Stuermer CA (2010) Origin of Nogo-A by domain shuffling in an early jawed vertebrate. Mol Biol Evol 28:1363-1370.

Silver J, Miller JH (2004) Regeneration beyond the glial scar. Nat Rev Neurosci 5:146-156.

Sivasankaran R, Pei J, Wang KC, Zhang YP, Shields CB, Xu XM, He Z (2004) PKC mediates inhibitory effects of myelin and chondroitin sulfate proteoglycans on axonal regeneration. Nat Neurosci 7:261-268.

Sofroniew MV (2009) Molecular dissection of reactive astrogliosis and glial scar formation. Trends Neurosci 32:638-647.

Venkatesh K, Chivatakarn O, Lee H, Joshi PS, Kantor DB, Newman BA, Mage R, Rader C, Giger RJ (2005) The Nogo-66 receptor homolog NgR2 is a sialic acid-dependent receptor selective for myelin-associated glycoprotein. J Neurosci 25:808-822.

Wang H, Katagiri Y, McCann TE, Unsworth E, Goldsmith P, Yu ZX, Tan F, Santiago L, Mills EM, Wang Y, Symes AJ, Geller HM (2008) Chondroitin-4-sulfation negatively regulates axonal guidance and growth. J Cell Sci 121:3083-3091.

Williams G, Wood A, Williams EJ, Gao Y, Mercado ML, Katz A, Joseph-McCarthy D, Bates B, Ling HP, Aulabaugh A, Zaccardi J, Xie Y, Pangalos MN, Walsh FS, Doherty P (2008) Ganglioside inhibition of neurite outgrowth requires Nogo receptor function: identification of interaction sites and development of novel antagonists. J Biol Chem 283:16641-16652.

Winzeler AM, Mandemakers WJ, Sun MZ, Stafford M, Phillips CT, Barres BA (2011) The lipid sulfatide is a novel myelin-associated inhibitor of CNS axon outgrowth. J Neurosci 31:6481-6492.

Yamashita T, Fujitani M, Yamagishi S, Hata K, Mimura F (2005). Multiple signals regulate axon regeneration through the Nogo receptor complex. Mol Neurobiol 32:105-111.

Yin Y, Cui Q, Gilbert HY, Yang Y, Yang Z, Berlinicke C, Li Z, Zaverucha-do-Valle C, He H, Petkova V, Zack DJ, Benowitz LI (2009) Oncomodulin links inflammation to optic nerve regeneration. Proc Natl Acad Sci U S A 106:19587-19592.

Yu P, Wang H, Katagiri Y, Geller HM (2012) An in vitro model of reactive astrogliosis and its effect on neuronal growth. Methods Mol Biol 814:327-340.

Zagrebelsky M, Schweigreiter R, Bandtlow CE, Schwab ME, Korte M (2010) Nogo-A stabilizes the architecture of hippocampal neurons. J Neurosci 30:13220-13234.

Zhang L, Kuang X, Zhang J (2011) Nogo receptor 3, a paralog of Nogo-66 receptor 1 (NgR1), may function as a NgR1 co-receptor for Nogo-66. J Genet Genomics 38:515-523.

Zheng B, Atwal J, Ho C, Case L, He XL, Garcia KC, Steward O, Tessier-Lavigne M (2005) Genetic deletion of the Nogo receptor does not reduce neurite inhibition in vitro or promote corticospinal tract regeneration in vivo. Proc Natl Acad Sci U S A 102:1205-1210.

CHAPTER III:

LRP1 is a Sialic Acid-Independent Receptor for the Myelin-Associated Glycoprotein

3.1 Abstract

In the injured adult mammalian central nervous system (CNS), neuronal regeneration is inhibited by myelin-associated inhibitory proteins (MAIs), including myelin-associated glycoprotein (MAG), Nogo, and oligodendrocyte myelin glycoprotein (OMgp). Binding of MAIs to neuronal cell surface receptors leads to activation of RhoA, growth cone collapse, and neurite outgrowth inhibition. Herein, we identify the low-density lipoprotein receptor-related protein 1 (LRP1) as a high-affinity, endocytic receptor for MAG. Unlike previously identified MAG receptors, MAG binds to LRP1 directly and independently of terminal sialic acids. In primary neurons, functional inactivation of LRP1 is sufficient to significantly reverse both MAG- and myelin-mediated inhibition of neurite outgrowth. Mechanistic studies show that LRP1 and $p75^{NTR}$ associate in a MAG-dependent manner and that MAG-mediated activation of RhoA involves both of these receptors. Furthermore, purified LRP1 and derivatives that retain ligand-binding activity counteract the effects of MAG and myelin. Collectively, our studies identify LRP1 as a novel MAG receptor that functions in neurite outgrowth inhibition.

3.2 Introduction

Neuronal regeneration in the injured adult mammalian CNS is limited. The inhibitory nature of adult CNS myelin and glial scar tissue contribute to the regenerative failure of severed axons (Busch and Silver, 2007; Fawcett, 2009; Schwab et al., 1993). Several MAIs have been identified, including MAG, Nogo, and OMgp (Filbin, 2003; Schwab, 2010; Yiu and He, 2006). Nogo-A, the largest splice form of the Nogo/reticulon 4 gene, is comprised of at least two distinct growth-inhibitory regions: amino-Nogo and Nogo66 (Schwab, 2010). MAG is a sialic acid-recognizing, Ig-family lectin (Tang et al., 1997; Vinson et al., 2001; Vyas et al., 2002). Deletion of the lectin activity in MAG disrupts binding to gangliosides and to the Nogo receptor family members NgR1 and NgR2, yet does not abolish growth inhibition (Cao et al., 2007; Robak et al., 2009).

NgR1 is the ligand-binding portion of a tripartite receptor complex that includes Lingo-1 and $p75^{NTR}$ or TROY (Yiu and He, 2006). This receptor complex participates in growth cone collapse in response to MAG, Nogo66 and OMgp (Kim et al., 2004). Similar to NgR1, paired Ig-like receptor B (PirB) binds to Nogo66, MAG and OMgp. Loss of PirB, but not NgR1, leads to a significant, yet incomplete release of neurite outgrowth inhibition in response to substrate-bound inhibitors (Atwal et al., 2008; Chivatakarn et al., 2007; Zheng et al., 2005). Myelin inhibition can be released by pretreatment of neurons with BDNF or by blocking activation of RhoA (Cai et al., 1999; Schmandke and Strittmatter, 2007). In the presence of Nogo and MAG, association of $p75^{NTR}$ with the Rho-GDP dissociation inhibitor (Rho-GDI) is enhanced and this leads to the release and subsequent activation of RhoA (Yamashita and Tohyama, 2003). Loss of $p75^{NTR}$ in sensory neurons, but not in cerebellar neurons, attenuates MAG and myelin inhibition *in vitro*, suggesting the existence of neuronal cell type-specific signaling mechanisms (Mehta et al., 2007; Venkatesh et al., 2007; Zheng et al., 2005).

LRP1 is a type 1 transmembrane receptor that binds over forty structurally and functionally distinct ligands, mediating their endocytosis and delivery to lysosomes (Strickland et al., 2002). LRP1 also functions in phagocytosis of large particles, including degenerated myelin (Gaultier et al., 2009; Lillis et al., 2008). Neurons in both the CNS and PNS express LRP1 (Bu et al., 1994; Campana et al., 2006; Wolf et al., 1992), which is partially localized to neuronal growth cones, both in intracellular vesicles and at the cell surface (Steuble et al., 2010).

LRP1 regulates cell signaling in conjunction with co-receptors or by regulating the plasma membrane abundance of other receptors, including uPAR, TNFR1, PDGFR, Trk receptors, and Frizzled-1 (Boucher et al., 2003; Gaultier et al., 2008; Shi et al., 2009; Webb et al., 2001; Zilberberg et al., 2004). Given the diversity of LRP1 co-receptors, it is reasonable to hypothesize that the activity of LRP1 in cell signaling may be ligand- and cell type-specific. In neurons and neuron-like cell lines, binding of tissue-type plasminogen activator (tPA) or α_2-macroglobulin (α_2M) to LRP1 activates ERK and AKT to promote neurite outgrowth (Fuentealba et al., 2009; Hayashi et al., 2007; Mantuano et al., 2008; Qiu et al., 2004; Shi et al., 2009). This response requires Trk receptor transactivation downstream of phosphorylated c-Src (Shi et al., 2009).

Previous work demonstrating myelin phagocytosis by LRP1 (Gaultier et al., 2009) prompted us to examine the role of LRP1 in the mechanism by which MAIs inhibit axonal regeneration. In this study, we demonstrate that LRP1 is a high-affinity, endocytic MAG receptor, which is important for RhoA activation and inhibition of neurite outgrowth by MAG.

3.3 Results

MAG binds directly to LRP1

Full-length LRP1 is a 600-kDa, two-chain transmembrane receptor (Franchini and Montagnana, 2011). Two of the four clusters of complement-like repeats (CII and CIV) in the extracellular α-chain of LRP1 are responsible for most of the ligand-binding activity of this receptor (Willnow et al., 1994). To screen for proteins in CNS myelin that bind to LRP1, we expressed CII and CIV as separate Fc fusion proteins (**Figure 3.1a**). CNS myelin vesicles were purified from rat brain as previously described (Gaultier et al., 2009), solubilized in Triton X-100, and incubated with CII-Fc or CIV-Fc. Fc fusion proteins were precipitated with Protein A-Sepharose and associated proteins were identified by LC-MS/MS (Gaultier et al., 2010). MAG was identified as a candidate binding partner for CII-Fc and CIV-Fc, but not Fc alone (data not shown).

As a first approach to test whether MAG binds to full-length LRP1, the ectodomain of MAG was expressed as an Fc fusion protein (MAG-Fc) and incubated with extracts of mouse N2a neuroblastoma cells, which is a rich source of LRP1 (**Figure 3.1b**). LRP1 was readily detected in MAG-Fc affinity-precipitates using a polyclonal antibody that detects the 85-kDa LRP1 β chain. LRP1 did not co-precipitate with purified Fc, demonstrating specificity in the MAG-LRP1 interaction. Next, we prepared extracts of rat brain and tested whether endogenous MAG associates with LRP1. LRP1 co-immunoprecipitated (co-IPed) with MAG from brain extracts and MAG co-IPed with LRP1 (**Figure 3.1c**). To test whether MAG binds to LRP1 in a purified system, full-length LRP1 was purified from rat liver as previously described (Gorovoy et al., 2010) and incubated with MAG-Fc or Fc. LRP1 was detected in affinity precipitates with MAG-Fc but not Fc alone, providing evidence for a direct association of MAG with full-length LRP1 (**Figure 3.1d**).

Receptor-associated protein (RAP) is an LRP1 chaperone that binds to LRP1 and inhibits binding of other known LRP1 ligands (Strickland et al., 2002). To test whether RAP inhibits binding of MAG to LRP1, MAG-Fc was incubated with extracts from the N20.1 cell line, which is an abundant source of LRP1, in the presence of either GST or GST-RAP. MAG-Fc bound to LRP1 in N20.1 cell extracts and GST-RAP greatly reduced this interaction (**Figure 3.1e**). Additionally, MAG from CNS myelin affinity precipitated with CII-Fc and CIV-Fc, but not with Fc alone (**Figure 3.1f**), and MAG-Fc bound to immobilized CII-Fc and CIV-Fc in a purified system (**Figure 3.1g**). These results validate our LC-MS/MS results, demonstrating that Fc fusion proteins, which contain ligand-binding sequences from LRP1, bind MAG.

MAG shows high-affinity, sialic acid-independent binding to CII and CIV

In order to assess binding affinities for the MAG-LRP1 interaction, we utilized an established model system in which full-length MAG is expressed in COS-7 cells, as previously described (Dickendesher et al., 2012). CII-Fc and CIV-Fc bound to cell-surface MAG and the level of binding was similar to that observed with NgR^{OMNI}-Fc (**Figure 3.1h**). In NgR^{OMNI}-Fc, Fc is fused to a chimeric form of NgR1 and NgR2 that binds MAG with higher affinity than wild-type NgR1 (Robak et al., 2009). Purified Fc did not bind to MAG-expressing COS-7 cells, indicating that binding of CII-Fc and CIV-Fc is specific. As a control, we examined binding of CII-Fc and CIV-Fc to COS-7 cells that were transfected to express PirB, which, similar to MAG, is a member of the Ig superfamily. As expected, neither CII-Fc nor CIV-Fc bound to PirB-expressing cells (**Figure 3.2a**). Importantly, GST-RAP almost completely inhibited binding of CII-Fc and CIV-Fc to MAG-expressing cells, but had no effect on the binding of NgR^{OMNI}-Fc (**Figure 3.1i**).

To calculate binding affinities, MAG-expressing COS-7 cells were incubated with increasing concentrations of CII-Fc, CIV-Fc, and NgR^{OMNI}-Fc. In initial studies, the fusion proteins were precoupled to alkaline phosphatase (AP)-conjugated anti-Fc antibody, allowing direct analysis of binding. The results were most accurately fit by non-linear regression to sigmoidal curves, suggesting possible complexity in the binding interactions, beyond a simple single-site model (**Figure 3.3a**). To estimate binding constants, we determined the concentration of ligand that yielded half-maximal saturation (Kd). The Kds are as follows: NgR^{OMNI}-Fc - 5.7 ± 0.1nM, CII-Fc - 8.1 ± 0.2nM, and CIV-Fc - 7.4 ± 0.2nM. The equivalent data were also fit to rectangular hyperbolae, assuming a simple, single-site model. The Kd values were largely unchanged, ranging from 5-15nM for all three fusion proteins. Monomeric fusion protein binding (no precoupling) was also most accurately fit to sigmoidal curves, with Kds of 9.6 ± 0.3nM for CII-Fc and 17 ± 3nM for CIV-Fc (**Figure 3.2b-c**).

MAG is an Ig-family lectin, which binds to gangliosides and Nogo receptors in a sialic acid-dependent manner (Robak et al., 2009; Vyas et al., 2002). To test whether the interaction of MAG with LRP1 is sialic acid-dependent, CII-Fc, CIV-Fc, and NgR^{OMNI}-Fc were pretreated with *V. cholera* neuraminidase (VCN), which removes terminal sialic acids on the cell surface (Robak et al., 2009; Venkatesh et al., 2007). While pretreatment of NgR^{OMNI}-Fc with VCN abolished binding to MAG-expressing COS-7 cells, pretreatment of CII-Fc and CIV-Fc with VCN did not inhibit binding (**Figure 3.3b**). Next, we examined binding of CII-Fc, CIV-Fc, and NgR^{OMNI}-Fc to COS-7 cells that express MAG^{R118A}, a point mutation that greatly reduces lectin activity (Tang et al., 1997). MAG^{R118A} failed to bind NgR^{OMNI}-Fc, as previously demonstrated (Robak et al., 2009); however, robust binding was observed to CII-Fc and CIV-Fc (**Figure 3.3c**). These results indicate that the interaction of MAG with LRP1 is not sialic acid-dependent.

LRP1 mediates the endocytosis of MAG

As LRP1 is a known endocytic receptor (Franchini and Montagnana, 2011), we investigated the possibility of MAG being internalized. MAG-Fc was incubated at 4^{o}C with N2a cells in the presence of GST or GST-RAP, followed warming of the cells to 37^{o}C. To ensure that only internalized MAG-Fc would remain cell-associated, a mild acid wash (pH 3.0) was performed. Immunofluorescence microscopy revealed that MAG-Fc was internalized by the N2a cells and the degree of internalization was substantially reduced when GST-RAP was added (**Figure 3.4a**). To show that the interaction of MAG-Fc with LRP1 is specific, we expressed the first three Ig-like domains of receptor protein tyrosine phosphatase sigma as an Fc fusion protein (RPTP-Fc) and studied uptake of this protein by N2a cells, in the presence or absence of GST-RAP. Although RPTP-Fc was internalized by N2a cells, the extent of internalization was not affected by GST-RAP (**Figure 3.4a**). In additional control experiments, we incubated MAG-Fc with N2a cells at 4^{o}C, but did not increase the temperature to 37^{o}C before performing the mild acid wash. Under these conditions, MAG-Fc binding was not detected (data not shown).

To further assess the role of LRP1 in the endocytosis of MAG, we developed a stable cell line in which LRP1 is silenced with shRNA in N2a cells. By immunoblot analysis, LRP1 was undetectable in these cells (data not shown). MAG-Fc was incubated with N2a cells in which LRP1 was silenced or with N2a cells that had been transfected with empty vector. Following the mild acid wash, MAG-Fc internalization was much greater in the LRP1-expressing cells, compared with cells in which LRP1 was silenced. Importantly, LRP1 gene silencing did not inhibit internalization of RPTP-Fc (**Figure 3.4b-c**). Additionally, we examined the uptake of ^{125}I-labeled MAG-Fc by N2a cells, defined as the fraction of radioligand internalization inhibited by a fiftyfold molar excess of unlabeled MAG-Fc. N2a cells that were treated with ^{125}I-labeled

MAG-Fc internalized 44 ± 4fmol MAG-Fc/mg of cellular protein per hour. LRP1 gene silencing completely abolished specific internalization of ^{125}I-MAG-Fc, providing further evidence that LRP1 is necessary for the endocytosis of MAG (**Figure 3.4d**).

LRP1 is required for inhibition of neurite outgrowth by MAG

To test whether LRP1 is involved in the pathway by which MAG inhibits neurite outgrowth, PC12 pheochromocytoma cells and N2a cells were cultured on monolayers of CHO cells that express MAG or on control R2 CHO cells (Mukhopadhyay et al., 1994). MAG-expressing CHO cells strongly inhibited neurite outgrowth of both cell types and GST-RAP, but not GST, significantly reversed this inhibition (**Figure 3.5a**). Importantly, MAG expression levels were not affected by RAP, as determined by immunoblot analysis (data not shown). To confirm that LRP1 is required for inhibition of neurite outgrowth by MAG, we transiently silenced LRP1 gene expression in PC12 and N2a cells. Control cells were transfected with non-targeting control (NTC) siRNA. LRP1 gene silencing was 80% and 85% effective in PC12 cells and N2a cells, respectively, as determined by RT-PCR. Similar extents of gene silencing were evident by immunoblot analysis (data not shown). LRP1 gene silencing significantly reversed MAG-mediated neurite outgrowth inhibition, suggesting that LRP1 expression in neuron-like cells is important for growth-inhibitory responses by MAG (**Figure 3.5b**).

To further test this hypothesis, we conducted neurite outgrowth experiments using primary cultures of rat cerebellar granule neurons (CGNs). We took three approaches to neutralize LRP1 in CGNs that were plated on MAG-expressing or control R2 CHO cells. First, cells were cultured in the presence of GST or GST-RAP. Addition of GST-RAP, but not GST alone, significantly reversed MAG-mediated inhibition of primary CGNs (**Figure 3.6a**). Second,

LRP1 expression was robustly silenced in CGNs using siRNA. LRP1 protein levels were substantially decreased by gene silencing (data not shown), resulting in a significant reversal of neurite outgrowth inhibition on MAG-expressing CHO cells (**Figure 3.6b**). Finally, CGNs were isolated from mice in which loxP sites flank part of the LRP1 promoter and the first two exons (*LRP1*$^{loxP/loxP}$), allowing for Cre-mediated LRP1 gene deletion (Rohlmann et al., 1996). These CGNs were transduced with herpes simplex virus-1 that encodes GFP and Cre (HSV-1-GFP-Cre) or a HSV-1-GFP control. Immunoblot analysis showed that HSV-1-GFP-Cre transduction caused substantial LRP1 gene deletion and a significant increase in CGN neurite length on MAG-expressing CHO cells when compared to CGNs infected with HSV-1-GFP (**Figure 3.6c**). Collectively, three different approaches show that functional ablation of LRP1 in primary neurons is sufficient to significantly attenuate MAG inhibition.

B**inding of MAG to LRP1 recruits p75^{NTR} and activates RhoA**

RhoA activation is critical for MAI-induced neurite outgrowth inhibition in both neurons and neuron-like cells (Kozma et al., 1997; Kuhn et al., 1999; Madura et al., 2004; Yamashita et al., 2002). Blocking RhoA activation promotes neurite outgrowth (Jalink et al., 1994; Jeon et al., 2012), even in cells plated on inhibitory substrata (Fu et al., 2007; Niederost et al., 2002; Tan et al., 2007). To test the role of LRP1 in MAG-induced RhoA activation, N2a cells in which LRP1 was silenced with shRNA were treated with MAG-Fc or Fc alone. MAG-Fc significantly increased GTP-loaded RhoA in LRP1-expressing N2a cells; however, when LRP1 was silenced, MAG-Fc failed to induce this increase (**Figure 3.7a**). As RhoA activation by MAIs requires p75NTR or TROY in some cell types (Park et al., 2005; Wang et al., 2002; Yamashita et al., 2002; Yamashita and Tohyama, 2003;), we treated N2a cells with TAT-Pep5, a TAT fusion

peptide that binds to $p75^{NTR}$ and blocks Rho-GDI binding to $p75^{NTR}$ and $p75^{NTR}$-dependent RhoA activation (Yamashita and Tohyama, 2003). TAT-Pep5 blocked RhoA activation in response to MAG-Fc, suggesting that $p75^{NTR}$ and LRP1 may both contribute to MAG-induced RhoA activation (**Figure 3.7b**).

It has been reported that $p75^{NTR}$ is recruited into a complex with NgR1 or PirB when these receptors bind MAIs (Fujita et al., 2011; Shao et al., 2005; Wang et al., 2002). To determine whether $p75^{NTR}$ forms a complex with LRP1, we performed co-IP experiments. When N2a cells were treated with MAG-Fc, but not Fc alone, $p75^{NTR}$ was found to co-IP with LRP1 (**Figure 3.7c**). To test whether $p75^{NTR}$ regulates the binding of MAG to LRP1, $p75^{NTR}$ was partially silenced in N20.1 cells. Total levels of LRP1, as well as the association of LRP1 and MAG-Fc, were not affected by $p75^{NTR}$ gene silencing (**Figure 3.7d**). These results suggest that the binding of MAG to LRP1 does not require $p75^{NTR}$, consistent with the results presented in **Figure 3.1**.

LRP1 is required for myelin-mediated neurite outgrowth inhibition

Given that $p75^{NTR}$ can be recruited as a co-receptor following the binding of multiple MAIs (Wang et al., 2002), we next examined neurite outgrowth of CGNs plated on purified rat CNS myelin. As expected, neurite outgrowth was strongly inhibited on myelin, and GST-RAP (**Figure 3.8a**) or LRP1 gene silencing (**Figure 3.8b**) significantly reversed this inhibition. However, addition of GST-RAP failed to reverse the inhibitory effects of another major group of CNS growth inhibitors, the chondroitin sulfate proteoglycans (CSPGs) (**Figure 3.9**).

As purified CNS myelin contains multiple MAIs in addition to MAG, including Nogo and OMgp, we investigated the possibility of additional MAI binding partners for LRP1. Indeed,

Nogo-A and LRP1 show an endogenous interaction in rat brain extracts (**Figure 3.8c**), Nogo-A and OMgp from purified rat CNS myelin co-IP with CII-Fc and CIV-Fc, but not Fc alone (**Figure 3.8d-e**), and AP-conjugated Nogo66 and OMgp bind to immobilized CII-Fc and CIV-Fc in a purified system (**Figure 3.8f**). Overall, these qualitative binding studies demonstrate that LRP1 can interact with multiple MAIs, but further quantitative binding and functional studies will be necessary to understand the significance of these interactions.

Soluble forms of LRP1 reverse MAI-mediated neurite outgrowth inhibition

We hypothesized that purified LRP1 and derivatives of LRP1 that include its ligand-binding sites will compete with membrane-anchored LRP1 for MAI binding and therefore reverse the growth-inhibitory activity of MAIs. Purified LRP1 derivatives may also compete with other membrane-anchored, MAI-binding receptors. Indeed, purified, full-length LRP1 significantly reversed the inhibition of CGN outgrowth observed on both MAG-expressing CHO cells (**Figure 3.10a**) and purified rat CNS myelin (**Figure 3.10b**).

LRP1 is released from cells as a "shed" product by α-secretase and accumulates in the blood and cerebrospinal fluid (Liu et al., 2009). As shed LRP1 retains the entire α-chain, ligand-binding activity remains intact (Quinn et al., 1999). Shed LRP1 was purified from human plasma, as previously described (Gorovoy et al., 2010), and was able to reverse the inhibitory effects of CNS myelin on CGN outgrowth (**Figure 3.10c**). Furthermore, addition of either the CII-Fc or CIV-Fc fusion proteins significantly reversed MAG- and myelin-mediated neurite outgrowth inhibition of CGNs (**Figures 3.10d-e, 3.11**).

3.4 Discussion

A detailed understanding of the mechanisms by which MAIs inhibit neuronal growth is of considerable interest, both biologically and clinically. Previously, NgR1 was reported to bind MAG, Nogo66, OMgp, and CSPGs; however, NgR1 mutant neurons are not disinhibited when plated on substrate-bound ligands, suggesting some degree of mechanistic redundancy in how growth inhibition is signaled (Chivatakarn et al., 2007; Dickendesher et al., 2012; Zheng et al., 2005). Another study identified PirB as a promiscuous receptor for MAG, Nogo66, and OMgp. Antagonism of PirB leads to a significant, yet incomplete release of neurite outgrowth inhibition in the presence of substrate-bound inhibitors or crude CNS myelin (Atwal et al., 2008). The combined functional ablation of NgR1 and PirB is not sufficient to fully release MAG, Nogo66, or OMgp inhibition, suggesting the existence of other receptor mechanisms. In addition to NgR1 and PirB, MAG has been shown to bind to brain gangliosides, NgR2, and β1-integrins, and depending on the neuronal cell type examined, these interactions contribute to growth inhibition to various degrees (Goh et al., 2008; Mehta et al., 2007; Venkatesh et al., 2007; Worter et al., 2009).

Herein, we report the identification of LRP1 as a novel receptor for MAG. We initially identified MAG as an LRP1 binding partner from LC-MS/MS screening experiments. We subsequently determined that MAG binds LRP1 directly and independently of its lectin activity. This is important, as the inhibitory effects of membrane-associated MAG on neurite outgrowth are known to occur independently of sialic acid binding (Tang et al., 1997). To our knowledge, LRP1 is the first receptor to demonstrate this anticipated characteristic of a functional MAG receptor. The association of MAG with LRP1 recruits $p75^{NTR}$ into a receptor complex and is coupled to MAG endocytosis. In primary neurons, functional ablation of LRP1 attenuates MAG- and myelin-induced inhibition of neurite outgrowth. Similar to NgR1 and PirB, LRP1

supports interactions with Nogo66 and OMgp, although more detailed work will be necessary to elucidate whether these interactions are important for the mechanism by which myelin inhibits neurite outgrowth.

NgR1 and NgR2 are GPI-anchored proteins and depend on interactions with membrane-spanning receptors for cell signaling. Lingo-1 and two members of the TNF receptor family, $p75^{NTR}$ and TROY, form complexes with NgR1 (Yiu and He, 2006). A more recent study showed that PirB associates with $p75^{NTR}$ to signal growth inhibition (Fujita et al., 2011). Similar to NgR1 and PirB, we show that LRP1 associates with $p75^{NTR}$ in the presence of MAG. Because of the limited distribution of $p75^{NTR}$ in the mature CNS and the strong inhibition observed in MAI-treated $p75^{NTR-/-}$ neurons, additional signal transducing components remain to be discovered (Zheng et al., 2005, Venkatesh et al., 2007). In addition to $p75^{NTR}$, LRP1 may also associate with TROY or Lingo-1, and it will be interesting to examine whether NgRs, PirB, and LRP1 are part of a multicomponent receptor complex or if they function separately.

Binding of tPA and α_2M to neuronal LRP1, in the absence of MAIs, results in enhanced neurite outgrowth and neuronal survival (Hayashi et al., 2007; Qiu et al., 2004; Mantuano et al., 2008; Shi et al., 2009). These LRP1 ligands activate Src family kinases, transactivate Trk receptors, and stimulate ERK and AKT in a Trk-dependent manner (Shi et al., 2009). In addition to Trk receptors, NMDA receptors may also be involved in the pathway by which ERK is activated by tPA and α_2M (May et al., 2004). The signaling downstream of these LRP1 ligands is very different from that observed with MAIs and reported in this study. We propose a model in which the activity of LRP1 in cell signaling is highly dependent on the co-receptors that are recruited to LRP1 by specific ligands. We further propose that whether $p75^{NTR}$ or Trk receptors are recruited to LRP1 is ligand-dependent and represents an important checkpoint in neuronal LRP1 signaling.

Joset et al. (2010) demonstrated that Nogo-A activates RhoA by a mechanism that requires Pincher-dependent macroendocytosis. Although this pathway occurs independently of clathrin-coated pits, formation of the signalosome and vesicular transport of Nogo-A within the cell was pivotal for growth cone collapse. Endocytosis of MAG by LRP1, possibly in combination with $p75^{NTR}$ and other members of the MAG receptor complex, may provide a related pathway for intracellular trafficking of myelin products and RhoA activation. Interestingly, Steuble et al. (2010) found evidence of Nogo and LRP1 colocalization in early endosomes when growth cone vesicles were isolated.

Both purified LRP1 and shed LRP1 from human plasma attenuated the inhibitory effects of MAG and purified myelin on neurite outgrowth. We interpret these results to reflect competition with membrane-anchored LRP1 for MAI binding. Purified and shed LRP1 may also competitively block binding of MAIs to other receptors, such as NgR1, NgR2, and PirB. We propose that the activity of MAG and other MAIs may be neutralized by any soluble LRP1 derivative that retains ligand-binding activity. Shed LRP1 is generated by the α-secretase, ADAM17 (Gorovoy et al., 2010). Inflammation increases LRP1 shedding and promotes the accumulation of shed LRP1 in the plasma (Gorovoy et al., 2010). In CNS ischemia, shedding of LRP1 from perivascular astrocytes is significantly increased (Polavarapu et al., 2007). It is not clear whether LRP1 shedding from neurons is regulated; however, our results suggest that shed LRP1 may serve as an endogenous antagonist of the growth-inhibitory activity of MAG and possibly other MAIs. As such, LRP1 shedding in the brain may represent a previously unappreciated mechanism by which the body attempts to promote neuronal recovery after CNS insult.

3.5 Methods

Recombinant and purified proteins: CII, which includes amino acids 804-1185 of mature human LRP1; CIV, which includes amino acids 3331-3778; and full-length rat MAG were cloned into pFuse-rFc2 (Invivogen) and expressed as Fc fusion proteins in CHO-K1 cells. NgR^{OMNI}-Fc and RPTP-Fc are previously described (Dickendesher et al., 2012; Robak et al., 2009). Fc fusion proteins were purified from conditioned culture medium by affinity chromatography on Protein A-Sepharose (GE Healthcare). GST-RAP and GST were expressed in bacteria and purified as previously described (Gaultier et al., 2009). Shed LRP1 was purified from human plasma by RAP affinity chromatography and molecular exclusion chromatography (Gorovoy et al., 2010). Full-length LRP1 was purified from rat liver, as described (Gorovoy et al., 2010). Homogeneity and integrity of LRP1 preparations were assessed by SDS-PAGE. OMgp-AP, AP-Nogo66, and AP-Fc were expressed in HEK293T cells as previously described (Dickendesher et al., 2012). Conditioned medium was collected and used as a source of these fusion proteins.

Cell culture: CHO-K1 cells were cultured in high glucose Dulbecco's Modified Eagle's Medium (DMEM) with 10% fetal bovine serum (FBS) (Thermo Scientific), 10mg/L L-glutamine, and 10 mg/L non-essential amino acid solution (Gibco). For expression of recombinant proteins, transfected CHO-K1 cells were cultured in PowerCHO™ Chemically Defined Medium (Lonza). MAG-expressing and R2 CHO cells were a generous gift from Dr. Mark Tuszynski (University of California San Diego). These cells were maintained in DMEM with 10% FBS, 2mM glutamine, 40mg/L proline, 0.73mg/L thymidine, 1μM methotrexate, and 7.5mg/L glycine. COS-7 cells were transfected to express full-length MAG, MAG^{R118A}, PirB, or

GFP as described (Atwal et al., 2008; Robak et al., 2009). PC12 cells were cultured in DMEM supplemented with 10% FBS, 5% heat-inactivated horse serum (Thermo Scientific), and penicillin/streptomycin (P/S; Thermo Scientific). For neurite outgrowth experiments, PC12 cells were plated in serum-free medium (SFM) and treated with 50μg/ml NGF-β (R & D Systems). N2a cells were a generous gift from Dr. Katerina Akassoglou (Gladstone Institute of Neurological Disease, University of California San Francisco). N2a cells were cultured in DMEM with 10% FBS and P/S, and plated in SFM for neurite outgrowth experiments. Primary cultures of rat cerebellar granule neurons (CGNs) were isolated and cultured in DMEM with 50mM glucose, 10% FBS, 25mM KCl, and P/S. Primary cultures of mouse CGNs were isolated, purified in a discontinuous Percoll gradient, and cultured as previously described (Dickendesher et al., 2012). N20.1 cells were a generous gift from Dr. Anthony Campagnoni (University of California Los Angeles) and were cultured as previously described (Wight and Dobretsova, 1997).

Neurite outgrowth assays: MAG-expressing and R2 CHO cells were cultured on glass slides as previously described (Domeniconi et al., 2002). When CHO cells were confluent, rat CGNs, PC12 cells, or N2a cells were added and grown for 48 hours, unless otherwise specified. For some experiments, CGNs from *LRP1*$^{loxP/loxP}$ mice (JAX® Mice and Services) were cultured for 24 hours on poly-D-lysine hydrobromide (PDL; 50μg/ml) before transduction with either herpes simplex virus-1 (HSV-1)-GFP or HSV-1-GFP-Cre (Viral Gene Transfer Core, McGovern Institute for Brain Research, MIT). After an additional 72 hours, CGNs were either lysed directly in 2X SDS sample buffer (for immunoblotting with anti-LRP1 [Sigma] and anti-βIII-tubulin [Promega] to confirm Cre-mediated deletion of LRP1) or gently dislodged using

Cellstripper™ non-enzymatic cell dissociation solution (Corning) and re-plated on MAG-expressing or R2 CHO cells for 24 hours before fixation and staining (Dickendesher et al., 2012).

As an alternative to the CHO cell system, culture surfaces were coated with PDL (50μg/ml) and, in some cases, subsequently coated with 8μg/ml purified myelin in 30μM HEPES pH 7.4, 10μg/ml BSA, or 10μg/ml chondroitin sulfate proteoglycan (CSPG) mix (Millipore) before coating with 2μg/ml laminin for 2 hours at room temperature. When GST-RAP or GST (200nM) was added, these proteins were preincubated with the neural cells in suspension for 15 minutes at the indicated concentration prior to plating. For studies involving shed LRP1, purified LRP1, CII-Fc, or CIV-Fc, these proteins (or appropriate controls) were preincubated with the indicated substrate. Neurite outgrowth was determined by immunofluorescence to detect βIII-tubulin (Promega) and quantified using ImageJ software.

Gene silencing: PC12 cells were transfected with LRP1-specific siRNA (CGAGCGACCUCCUAUCUUUUU) or with non-targeting control (NTC) siRNA (Thermo Scientific) using the Amaxa rat neuron nucleofector kit, according to the manufacturer's instructions. LRP1 was silenced in rat CGNs and mouse N2a cells using ON-TARGETplus LRP1-specific siRNA or with NTC siRNA (Thermo Scientific) and Lipofectamine® 2000 (Invitrogen). Stable LRP1 gene silencing was achieved in N2a cells using our previously described LRP1-specific shRNA, cloned into pSUPER (Oligoengine; Gaultier et al., 2008). This construct (or empty vector) was transfected into N2a cells using Lipofectamine® 2000. Transfected cells were selected first with puromycin (1μg/ml) and then for 48 hours with Exotoxin A (200ng/ml; List Biological Laboratories; FitzGerald et al., 1995). LRP1 gene silencing was confirmed by RT-PCR and by immunoblot analysis. Silencing of $p75^{NTR}$ was

performed using ON-TARGETplus $p75^{NTR}$-specific siRNA or with NTC siRNA (Thermo Scientific) and Lipofectamine® 2000.

CNS myelin purification/mass spectrometry: Myelin vesicles were purified from mouse and rat brain, as described by Norton and Poduslo (Norton and Poduslo, 1973). Briefly, adult rodent brains were homogenized in 0.32M sucrose, layered over 0.85M sucrose, and subjected to sucrose density gradient ultracentrifugation. Myelin was then subjected to osmotic shock, recovered, and resuspended in 20mM sodium phosphate, 150mM NaCl, pH 7.4 (PBS). The purity of the preparation was determined by Coomassie Blue staining and by immunoblot analysis for myelin basic protein, as previously described (Gaultier et al., 2009).

Myelin-associated proteins were solubilized from purified myelin vesicles with RIPA buffer (100mM Tris-HCl, 150mM NaCl, 1% Triton X-100, 0.5% deoxycholate, 0.1% SDS supplemented with 1mM CaCl2, and protease inhibitor cocktail). Protein extracts (2mg) were incubated with 1μM CII-Fc, CIV-Fc, or Fc overnight at 4°C. The fusion proteins and associated proteins were recovered by incubation with Protein A-Sepharose for 1 hour at 20°C. After extensive washing with RIPA buffer, proteins were digested with trypsin in the presence of ProteaseMAX™ Surfactant as described by the manufacturer (Promega). Proteins associated with CII-Fc or CIV-Fc, but not with Fc, were identified as "specific interactors" by LC-MS/MS as previously described (Gaultier et al., 2010).

Immunoprecipitation analysis: Unless otherwise specified, protein extracts were prepared in 50mM HEPES pH 7.4, 1% Triton X-100, 150mM NaCl, 10% glycerol, 2mM EDTA, 1mM sodium orthovanadate, and protease inhibitor cocktail. For affinity precipitation studies,

CII-Fc, CIV-Fc, MAG-Fc, or Fc were immobilized on Protein A-Sepharose prior to adding ligands or protein extracts. In some studies, 200nM GST-RAP or GST was added to protein extracts prior to affinity precipitation. Following a preclearing step with non-immune IgG, LRP1 was affinity precipitated using an LRP1-specific antibody (Sigma) coupled to Protein A-Sepharose. Nogo-A, MAG, and OMgp were identified in affinity precipitates by immunoblot analysis using the indicated antibody (R & D Systems). $p75^{NTR}$ was detected using an antibody that recognizes the intracellular domain (Millipore).

For detection of endogenous LRP1 interactions, membrane preparations from adult rat brain were collected using sucrose gradient centrifugation, as previously described (Winters et al., 2011). Membranes were incubated in lysis buffer containing 20mM Tris-HCl pH 7.5, 150mM NaCl, 5mM EDTA, 1% NP-40, and protease inhibitor cocktail, before tumbling for 4 hours at 4°C with antibodies against either LRP1 (Sigma), MAG (custom; Winters et al., 2011), or Nogo-A (R & D Systems). Following precipitation with Protein G Plus/Protein A-Agarose overnight at 4°C, samples were rinsed six times with lysis buffer, and bound proteins were eluted with 2X SDS sample buffer. Precipitates were analyzed by immunoblotting.

Binding assays: Fc fusion proteins, which were preclustered with anti-human or anti-rabbit IgG, conjugated to alkaline phosphatase (AP), were incubated with COS-7 cells expressing MAG, MAG^{R118A}, PirB, or GFP for 75 minutes. Unbound fusion protein was removed by extensive rinsing with OptiMEM (Invitrogen). Cells were then fixed with 1% formaldehyde in 60% acetone solution, and rinsed three times in HEPES-buffered saline. Endogenous phosphatases were heat inactivated by incubation at 65°C for 90 minutes. Binding of fusion proteins was visualized by developing the AP reaction with nitro-blue tetrazolium and

5-bromo-4-chloro-3'-indolyphosphate (Sigma). In some experiments, ligands were pretreated with either *V. cholera* neuraminidase (1mU/ml; Robak et al., 2009) or with GST-RAP (200nM) for 1 hour at 37°C. Binding was quantified using ImageJ software. For monomeric binding studies with no preclustering, anti-human IgG-AP or anti-rabbit IgG-AP were applied to cells following fusion protein incubation. To determine binding isotherms, increasing concentrations of each Fc fusion protein were incubated with MAG-expressing COS-7 cells.

For dot blotting studies, 40pmol of CII-Fc, CIV-Fc, or Fc was immobilized on nitrocellulose (secured in a Bio-Rad Bio-Dot Apparatus). Membranes were then rinsed in PBS and blocked in PBS with 5% BSA, followed by incubation with the indicated protein for 1 hour at room temperature. After extensive washing in PBS, bound proteins were detected using the appropriate antibodies.

RhoA activation: N2a cells were cultured for 1 day and then serum starved for 1 hour. MAG-Fc or Fc was preincubated with an Fc-specific antibody (Jackson Immunoresearch Laboratories) at a 2:1 molar ratio and added to the N2a cells (20nM) for 10 minutes. Cell extracts were prepared and GTP-loaded RhoA was affinity precipitated using the Rho binding domain of Rhotekin, which was expressed as a GST fusion protein, according to the manufacturer's instructions (Millipore). The levels of affinity-precipitated active RhoA and total RhoA were determined by immunoblot analysis using a RhoA antibody (Cell Signaling). For quantification of RhoA activation in LRP1-expressing and -deficient N2a cells, the ratio of active/total RhoA was quantified by densitometric analysis. For experiments using TAT-Pep5 (Millipore), which binds to $p75^{NTR}$ and blocks $p75^{NTR}$-dependent RhoA activation (Yamashita

and Tohyama, 2003), cells were incubated with 500nM TAT-Pep5 for 30 minutes prior to the addition of MAG-Fc.

Endocytosis assays: LRP1-positive and -deficient N2a cells, as well as standard N2a cells in the presence of GST-RAP or GST (200nM), were plated on PDL-coated glass slides and allowed to grow overnight. Cells were then differentiated in SFM for 4 hours, before being treated with 1ug/ml of an Fc receptor blocking antibody (BD Biosciences) for 30 minutes at 4°C, followed by 25nM MAG-Fc, RPTP-Fc, or Fc control for 60 minutes at 4°C. For internalization, the cells were warmed to 37°C for 30 minutes. Surface-associated Fc fusion proteins were removed by treatment with acetic acid/sodium acetate pH 3.0 for 4 minutes. Cells were then rinsed with cold PBS, fixed with 4% paraformaldehyde in PBS for 10 minutes, permeabilized and blocked for non-specific binding by incubation with 0.1% Triton X-100 and 5% goat serum in PBS for 1 hour, and immunolabeled to detect the Fc tag of the fusion proteins. For immunoblot analysis, proteins were extracted in RIPA buffer as previously described (Mantuano et al., 2008). An equivalent amount of cellular protein (30µg per lane) was subjected to SDS-PAGE and immunoblot analysis to detect levels of the Fc tag and tubulin.

In additional experiments, MAG-Fc was radioiodinated with 1 mCi of $Na^{125}I$ using Iodination Beads (Pierce, Rockford, IL, USA) and separated from free $Na^{125}I$ by molecular exclusion chromatography. $1x10^5$ cells were plated in 12-well plates and equilibrated in DMEM with 25mM HEPES pH 7.4, 0.1% BSA, and an Fc receptor blocking antibody (BD Biosciences). ^{125}I-MAG-Fc (25nM) was incubated with cells for 2 hours at 37°C. Unlabeled MAG (1.25µM) was added to some wells. At the end of the incubation, cells were washed and treated with 0.25% Pronase (Roche) for 15 minutes to eliminate surface-associated ^{125}I-MAG-Fc. Cell

extracts were prepared in 0.1M NaOH and 1% SDS. Cell-associated radioactivity was determined using a Wallac Wizard 1470 Gamma Counter (Perkin Elmer), and cellular protein levels were determined by a bicinchoninic acid assay (Pierce). Specific MAG-Fc uptake was calculated as the fraction of total uptake that was inhibited by excess unlabeled MAG.

MAG expression analysis: To evaluate the effect of RAP treatment on the expression of MAG in MAG-CHO cells, confluent MAG-CHO cells were cultured with 200nM GST-RAP or GST for 24, 48, 72, or 96 hours. Proteins were then extracted in RIPA buffer as previously described (Mantuano et al., 2008). An equivalent amount of cellular protein was then subjected to SDS-PAGE and immunoblot analysis using an anti-MAG antibody (R & D Systems).

Data analysis: Data processing and statistical analysis were performed using GraphPad Prism 5.00 (GraphPad Software). Data sets were analyzed using one-way ANOVA followed by Tukey's *post hoc* comparisons. P values <0.01 were considered statistically significant.

3.6 Acknowledgments

Portions of this chapter have been published (see citation below) and permission was received from the editors to use this work as part of a dissertation:

Stiles TL*, **Dickendesher TL***, Gaultier A, Fernandez-Castaneda A, Mantuano E, Giger RJ, Gonias SL (2013) LDL receptor-related protein-1 is a sialic acid-independent receptor for myelin-associated glycoprotein (MAG) that functions in neurite outgrowth inhibition by MAG and CNS myelin. J Cell Sci 126:209-220.

* denotes equal contribution

This work was supported by the National Institutes of Health R01NS054671, R01HL060551 (Steven L. Gonias) and R21NS071347 (Alban Gaultier); the Dr. Miriam and Sheldon G. Adelson Medical Foundation on Neural Repair and Rehabilitation; and the US Department of Veterans Affairs Grant 1I01RX000229-01 (Roman J. Giger). We would like to thank Katerina Akassoglou for insightful discussions and N2a cells, Mark Tuszynski for MAG-expressing and R2 CHO cells, and Anthony Campagnoni for N20.1 cells.

3.7 Author Contributions

Travis L. Stiles (T.L.S.), Travis L. Dickendesher (T.L.D.), Roman J. Giger (R.J.G.), and Steven L. Gonias (S.L.G.) designed the experiments; T.L.S., T.L.D., Alban Gaultier, Anthony Fernandez-Castaneda, and Elisabetta Mantuano performed experiments; T.L.S. and T.L.D. contributed to data analysis and figure preparation; and T.L.S., T.L.D., R.J.G., and S.L.G. wrote the manuscript.

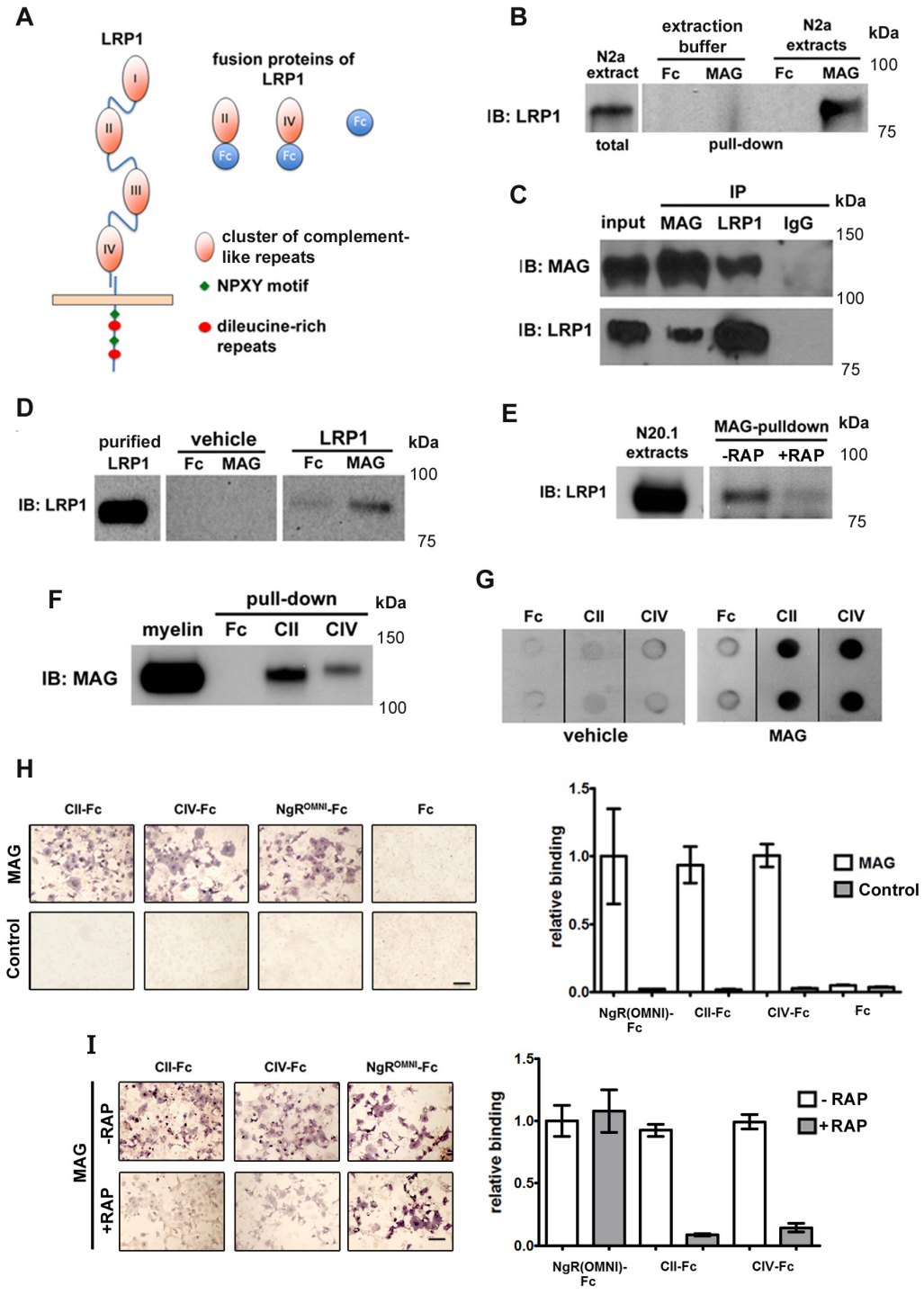

Figure 3.1: LRP1 is a MAG receptor. (**a**) Schematic diagram showing the relationship of the CII-Fc and CIV-Fc fusion proteins to the intact structure of LRP1. (**b**) N2a cell extracts (or extraction buffer only) were incubated with MAG-Fc or Fc, which were immobilized on Protein A-Sepharose beads. Precipitated proteins were subjected to immunoblot analysis for LRP1. (**c**)

Endogenous MAG and LRP1 were precipitated from adult rat membrane preparations using MAG- or LRP1-specific antibodies, followed by immunoblotting for both proteins. A non-specific IgG was used as a control. (**d**) Recombinant MAG-Fc or Fc were immobilized on Protein A-Sepharose and incubated with purified LRP1 or with vehicle (PBS). Affinity-precipitated proteins were subjected to immunoblot analysis for LRP1. (**e**) Protein extracts prepared from N20.1 cells were treated with 200nM GST-RAP (+RAP) or GST (-RAP) and then precipitated with MAG-Fc coupled to Protein A-Sepharose. Affinity-precipitated samples were subjected to immunoblot analysis for LRP1. (**f**) CII-Fc, CIV-Fc, or Fc were incubated with purified CNS myelin extracts followed by precipitation with Protein A-Sepharose. Immunoblot analysis was performed to detect MAG. (**g**) CII-Fc, CIV-Fc, or Fc (40pmol) were immobilized in duplicate on nitrocellulose membranes and incubated with MAG-Fc (10μg/ml) or vehicle (PBS). MAG binding was detected using a MAG-specific antibody. (**h**) COS-7 cells were transfected with either membrane-bound MAG or control (GFP), and then incubated with CII-Fc, CIV-Fc, NgR^{OMNI}-Fc, or Fc control. All fusion proteins were conjugated to alkaline phosphatase (AP), and bound proteins were detected by developing the AP reaction with nitro-blue tetrazolium and 5-bromo-4-chloro-3'-indolyphosphate (NBT/BCIP). The graph represents the degree of binding relative to NgR^{OMNI}-Fc (mean ±SEM, n=5 independent experiments). (**i**) COS-7 cells were transfected with membrane-bound MAG, and then incubated with CII-Fc, CIV-Fc, or NgR^{OMNI}-Fc in the presence of either 200nM GST-RAP (+RAP) or GST (-RAP). The graph represents the degree of binding relative to NgR^{OMNI}-Fc (mean ±SEM, n=4 independent experiments). Scale bars, 20μm.

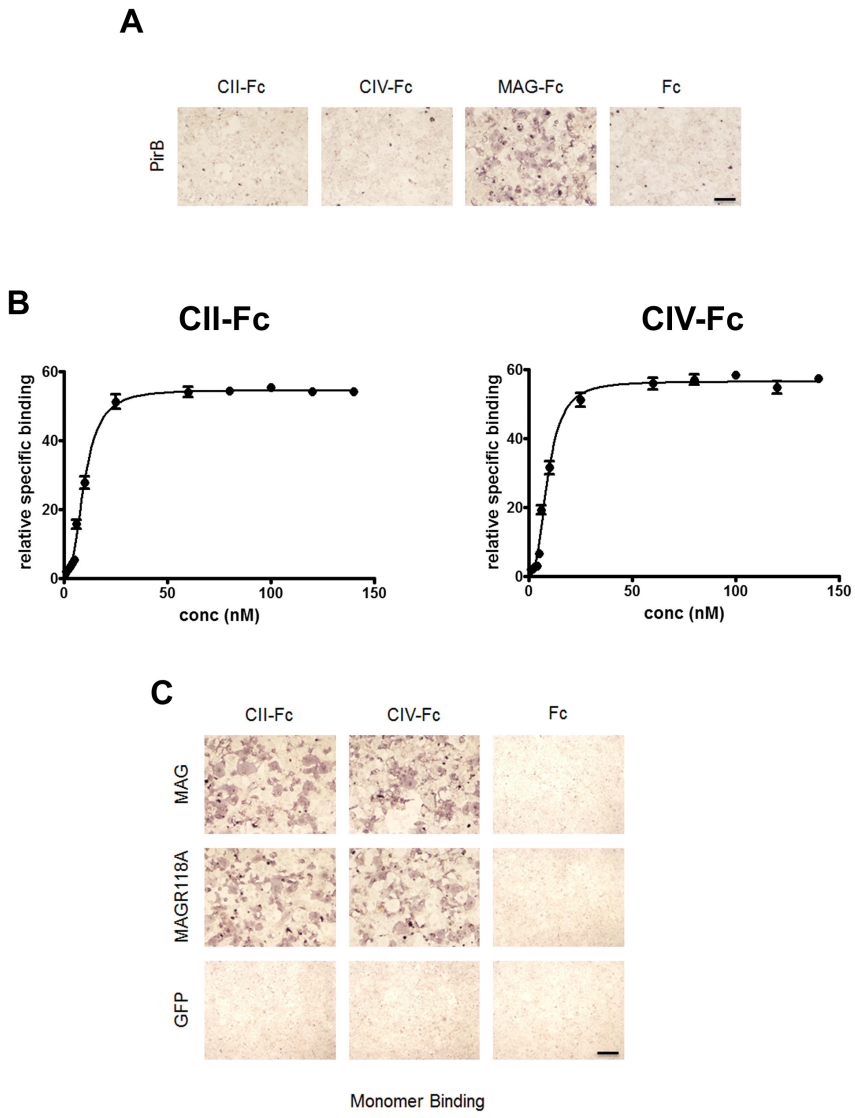

Figure 3.2: Monomeric CII-Fc and CIV-Fc bind with high affinity to MAG, but not PirB. (**a**) COS-7 cells were transfected with membrane-bound PirB, and then incubated with CII-Fc, CIV-Fc, MAG-Fc (positive control), or Fc (negative control). All fusion proteins were conjugated to AP, and bound proteins were detected by developing the AP reaction with NBT/BCIP. (**b**) COS-7 cells were transfected with membrane-bound MAG, and then incubated (at increasing concentrations) with monomers of CII-Fc or CIV-Fc. Following fusion protein incubation, anti-IgG-AP conjugate was applied and bound proteins were detected by developing the AP reaction with NBT/BCIP. Binding from 4 independent experiments was quantified using ImageJ software, and then averaged to yield the presented data points (mean ±SEM). A sigmoidal line of best fit was used to assess binding affinities. (**c**) COS-7 cells were transfected with membrane-bound MAG, MAG^{R118A} (a mutant with greatly reduced lectin activity), or control (GFP) before addition of monomers of CII-Fc, CIV-Fc, or Fc. Scale bars, 20µm.

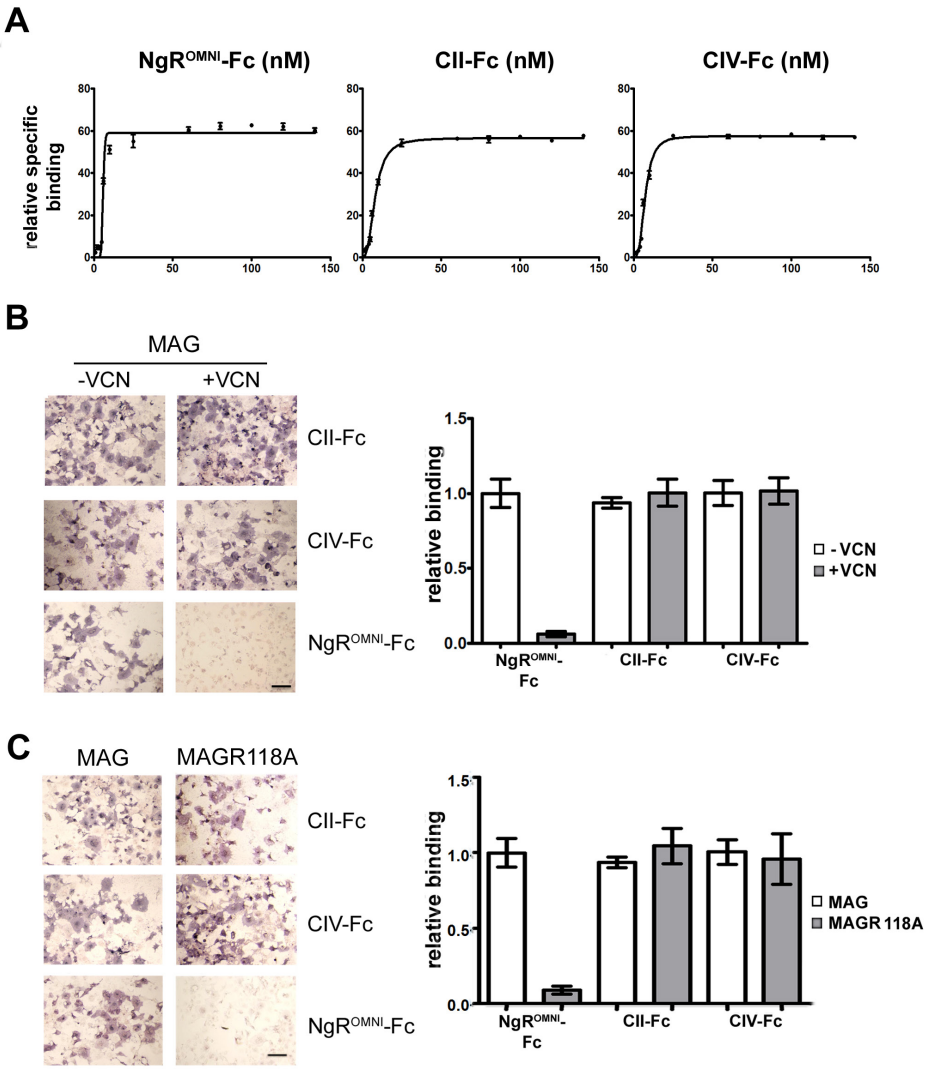

Figure 3.3: MAG binds to the CII and CIV domains of LRP1 in a sialic acid-independent manner. (**a**) COS-7 cells were transfected with membrane-bound MAG, and then incubated (at increasing concentrations) with CII-Fc, CIV-Fc, or NgR^{OMNI}-Fc. All fusion proteins were conjugated to AP, and bound proteins were detected by developing the AP reaction with NBT/BCIP. Binding from 5 independent experiments was quantified using ImageJ software, and then averaged to yield the presented data points (mean ±SEM). A sigmoidal line of best fit was used to assess binding affinities. (**b**) MAG-expressing COS-7 cells were incubated with CII-Fc, CIV-Fc, or NgR^{OMNI}-Fc. In some cases, ligands were pretreated with 1mU/ml *V. cholera* neuraminidase (+VCN) for 1 hour before incubation with COS-7 cells. The graph represents the degree of binding relative to NgR^{OMNI}-Fc (mean ±SEM, n=4 independent experiments). (**c**) COS-7 cells were transfected with either membrane-bound MAG or MAG^{R118A}, before addition of CII-Fc, CIV-Fc, or NgR^{OMNI}-Fc. The graph represents the degree of binding relative to NgR^{OMNI}-Fc (mean ±SEM, n=4 independent experiments). Scale bars, 20μm.

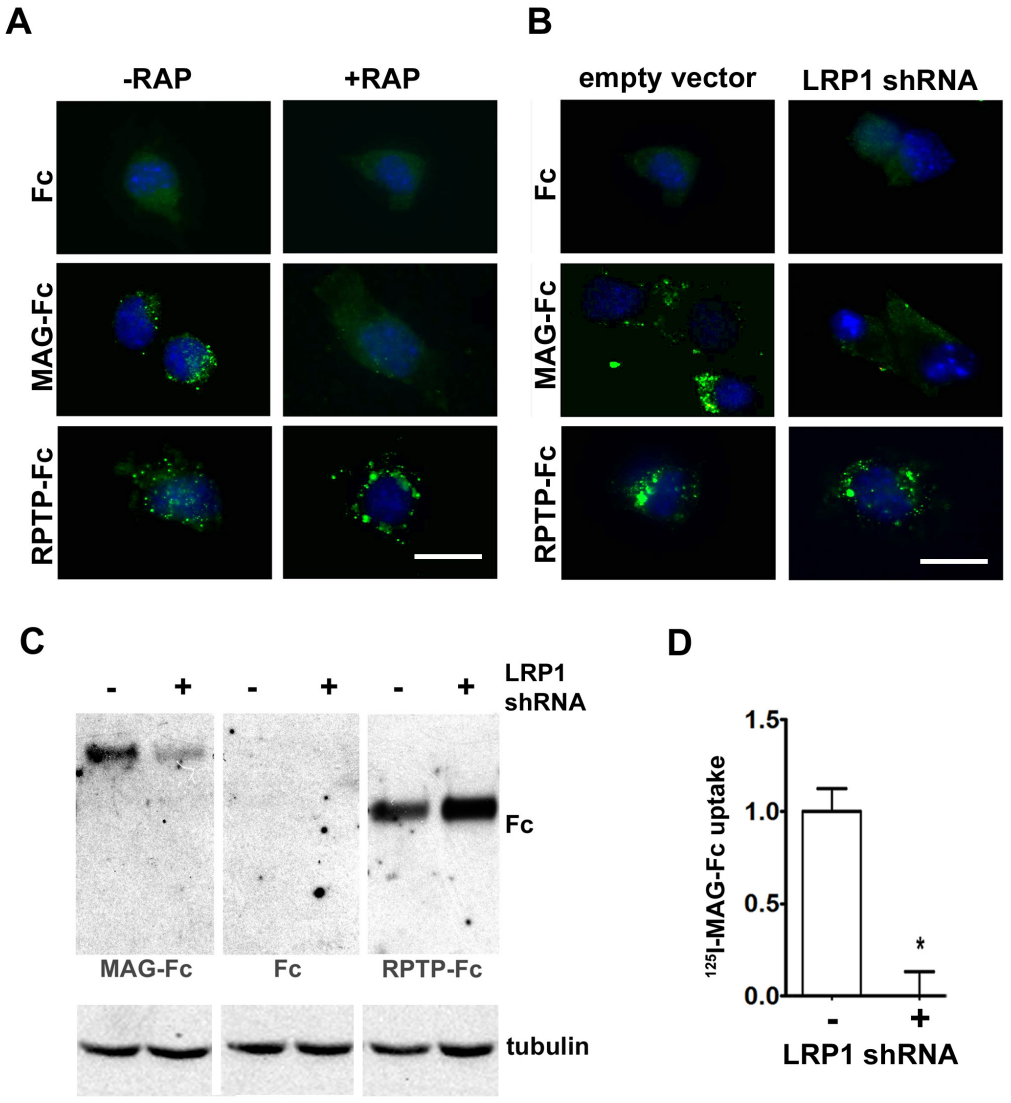

Figure 3.4: LRP1 is an endocytic receptor for MAG. (**a**) N2a cells were treated with 200nM GST-RAP (+RAP) or GST (-RAP) prior to addition of 25nM RPTP-Fc, MAG-Fc, or Fc control. Surface-associated proteins were removed by mild acid washing before visualization of the internalized protein by immunofluorescent detection of the Fc tag. (**b**) N2a cells stably transfected with LRP1-specific shRNA or empty vector were incubated with 25nM RPTP-Fc, MAG-Fc, or Fc control prior to mild acid washing and immunofluorescent detection. (**c**) N2a cells stably transfected with LRP1-specific shRNA or empty vector were incubated with 25nM of fusion proteins prior to mild acid washing. Protein extracts were prepared and immunoblotted for the Fc tag, as well as tubulin (loading control). (**d**) To quantify the differences in MAG endocytosis, N2a cells stably transfected with LRP1-specific shRNA or empty vector were incubated with 25nM ^{125}I-MAG-Fc, in the presence of a fiftyfold molar excess of unlabeled MAG-Fc. Specific MAG-Fc internalization was determined relative to the empty vector control (mean ±SEM, n=5 independent experiments, * $P< 0.01$). Scale bars, 20μm**.**

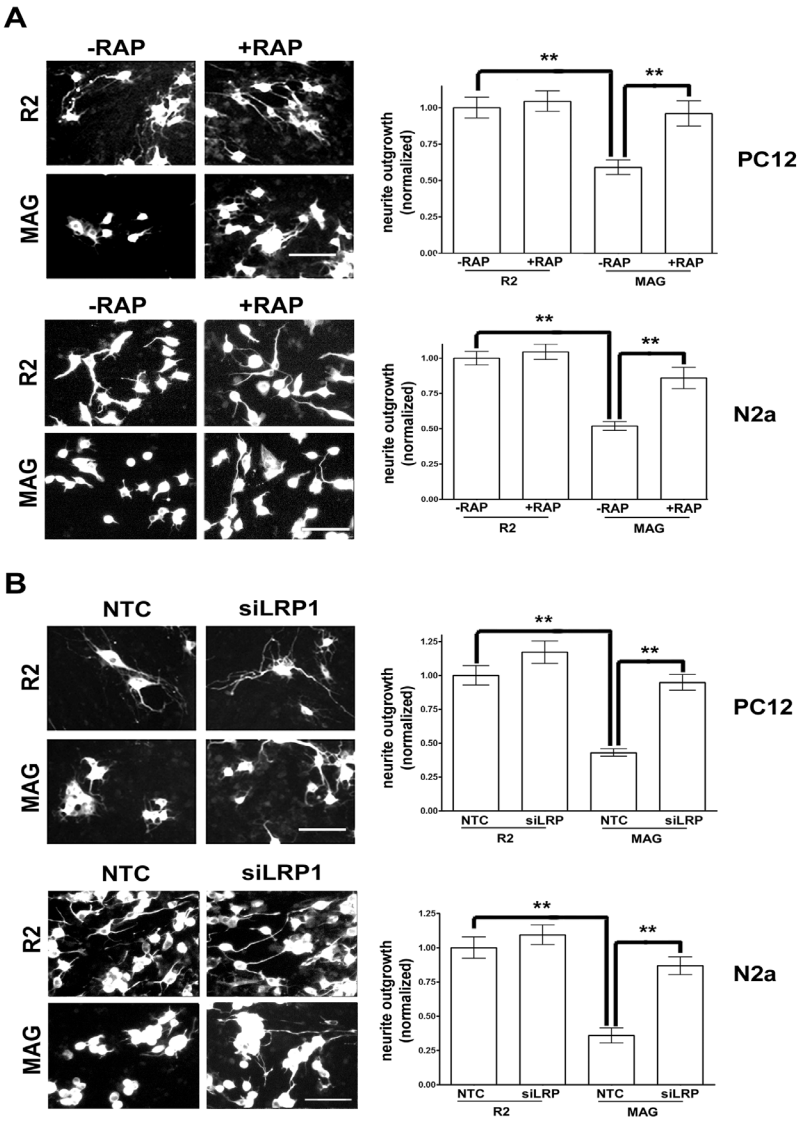

Figure 3.5: LRP1 inactivation enhances neurite outgrowth of neuron-like cells on MAG-expressing CHO cells. (**a**) PC12 cells (top) and N2a cells (bottom) were plated on R2 control or MAG-expressing CHO cells and allowed to grow for 48 hours in the presence of 200nM GST-RAP (+RAP) or GST (-RAP). Neurite outgrowth was detected by immunofluorescent imaging of βIII-tubulin. Results were normalized to outgrowth on R2 control CHO cells (mean ±SEM, n=4 independent experiments, ** $P< 0.01$). (**b**) PC12 cells (top) and N2a cells (bottom) were transfected with non-targeting control (NTC) or LRP1-specific (siLRP1) siRNA prior to plating on monolayers of R2 control or MAG-expressing CHO cells, and were allowed to grow for 48 hours. Neurite outgrowth was detected by immunofluorescent imaging of βIII-tubulin. Results were normalized to outgrowth on R2 control CHO cells (mean ±SEM, n=5 independent experiments, ** $P< 0.001$). Scale bars, 100μm**.**

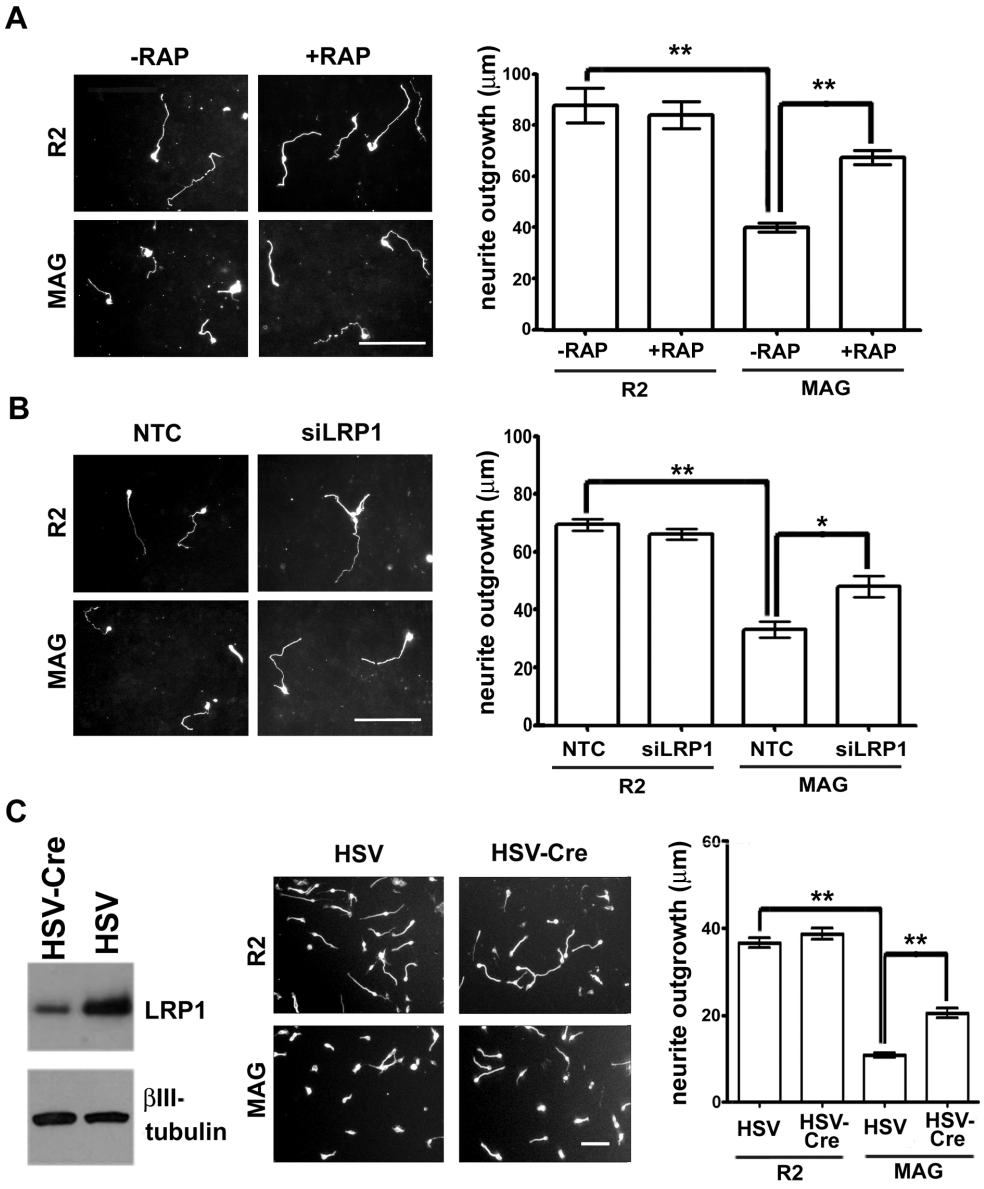

Figure 3.6: LRP1 inactivation enhances neurite outgrowth of primary cerebellar granule neurons on MAG-expressing CHO cells. (**a**) Cerebellar granule neurons (CGNs) pretreated with 200nM GST-RAP (+RAP) or GST (-RAP) were plated on monolayers of MAG-expressing or R2 control CHO cells and grown for 48 hours prior to immunofluorescent detection of βIII-tubulin. The graph represents the mean neurite outgrowth (±SEM) per condition (n=5 independent experiments, ** $P< 0.001$). (**b**) CGNs transfected with non-targeting control (NTC) or LRP1-specific (siLRP1) siRNA were plated on monolayers of MAG-expressing or R2 control CHO cells and grown for 48 hours prior to immunofluorescent detection of βIII-tubulin. The graph represents the mean neurite outgrowth (±SEM) per condition (n=4 independent experiments, * $P< 0.01$, ** $P< 0.001$). (**c**) Primary CGNs were isolated from *LRP1*$^{loxp/loxp}$ mice and were infected with either HSV-1-GFP (HSV) or HSV-1-GFP-Cre (HSV-Cre) prior to plating

on monolayers of MAG-expressing or R2 control CHO cells. CGNs were grown on CHO cell feeder layers for 24 hours prior to immunofluorescent detection of βIII-tubulin. The extent of silencing was demonstrated by immunoblotting of HSV- and HSV-Cre-infected CGN lysates for LRP1 and βIII-tubulin (loading control). The graph represents the mean neurite outgrowth (±SEM) per condition (n=5 independent experiments, ** $P< 0.001$). Scale bars, 100μm (**a**, **b**); 70μm (**c**)**.**

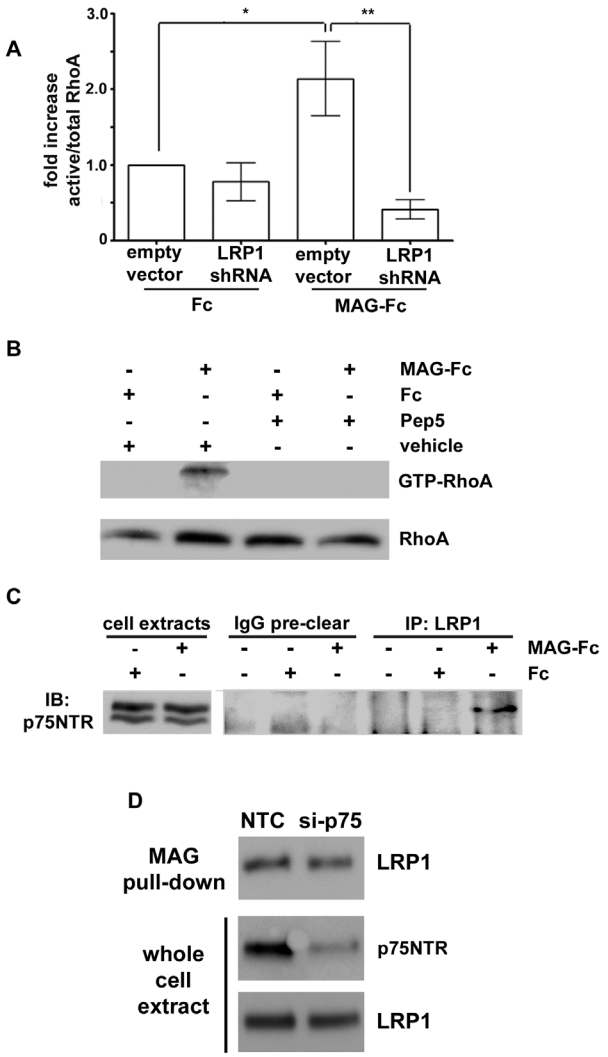

Figure 3.7: LRP1 and p75^{NTR} are required for MAG-mediated RhoA activation. (**a**) N2a cells in which LRP1 was stably silenced with shRNA, as well as cells transfected with empty vector, were treated with 20nM MAG-Fc or Fc. GTP-loaded RhoA was then affinity precipitated using the Rho binding domain of Rhotekin, and relative RhoA activity was determined as a ratio of GTP-loaded RhoA to total RhoA. The graph represents the relative RhoA activity normalized to Fc-treated control cells (mean ±SEM, n=5 independent experiments, * $P< 0.01$, ** $P< 0.001$). (**b**) N2a cells were pretreated with TAT-Pep5 or vehicle (PBS), followed by treatment with 20nM MAG-Fc or Fc. GTP-loaded and total RhoA levels were assessed by immunoblot. (**c**) N2a cells were treated with 20nM MAG-Fc or Fc, extracted, and sequentially immunoprecipitated with control IgG (IgG pre-clear) and then with a LRP1-specific antibody. Precipitated proteins were subjected to immunoblot analysis for p75^{NTR}. (**d**) N20.1 cells were transfected with p75^{NTR}-specific (si-p75) or non-targeting control (NTC) siRNA and analyzed 48 hours later by affinity precipitation of LRP1 with MAG-Fc from cell extracts. Whole cell extracts were subjected to immunoblot analysis to detect p75^{NTR} and LRP1.

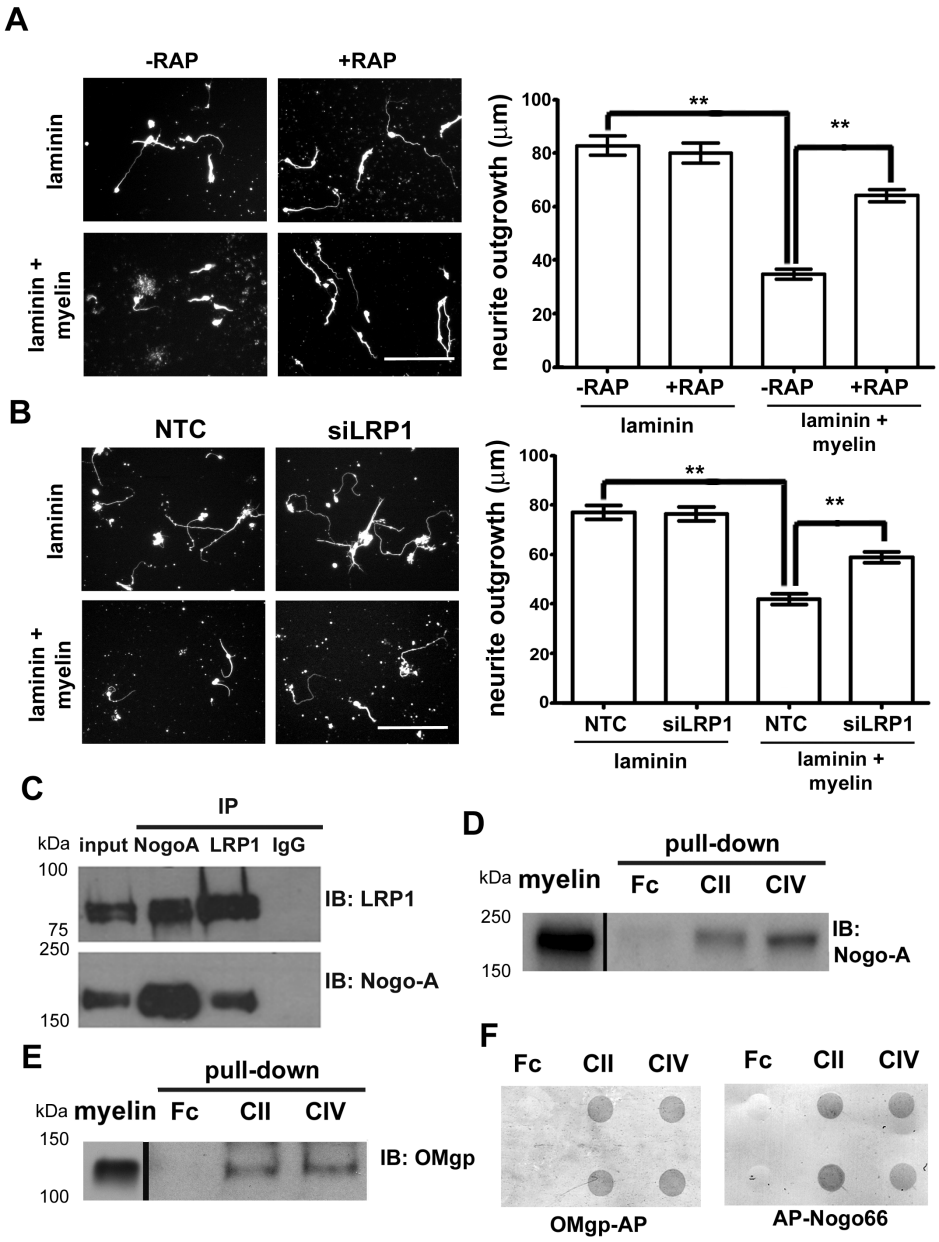

Figure 3.8: LRP1 inactivation enhances neurite outgrowth of primary cerebellar granule neurons on purified CNS myelin. (**a**) CGNs pretreated with 200nM GST-RAP (+RAP) or GST (-RAP) were plated on laminin or laminin + myelin (8μg/ml) and grown for 48 hours prior to immunofluorescent detection of βIII-tubulin. The graph represents the mean neurite outgrowth (±SEM) per condition (n=4 independent experiments, ** $P< 0.001$). (**b**) CGNs transfected with non-targeting control (NTC) or LRP1-specific (siLRP1) siRNA were plated on laminin or laminin + myelin and grown for 48 hours prior to βIII-tubulin labeling. The graph represents the mean neurite outgrowth (±SEM) per condition (n=5 independent experiments, ** $P< 0.001$). (**c**) Endogenous Nogo-A and LRP1 were precipitated from adult rat membrane preparations using

Nogo- or LRP1-specific antibodies, followed by immunoblotting for both proteins. A non-specific IgG was used as a control. (**d**, **e**) CII-Fc, CIV-Fc, or Fc were incubated with purified CNS myelin extracts followed by precipitation with Protein A-Sepharose. Immunoblot analysis was performed to detect (**d**) Nogo-A or (**e**) OMgp. (**f**) CII-Fc, CIV-Fc, or Fc (40pmol) were immobilized in duplicate on nitrocellulose membranes and incubated with OMgp-AP or AP-Nogo66. Binding was detected by developing the AP reaction with NBT/BCIP. Scale bars, 100μm**.**

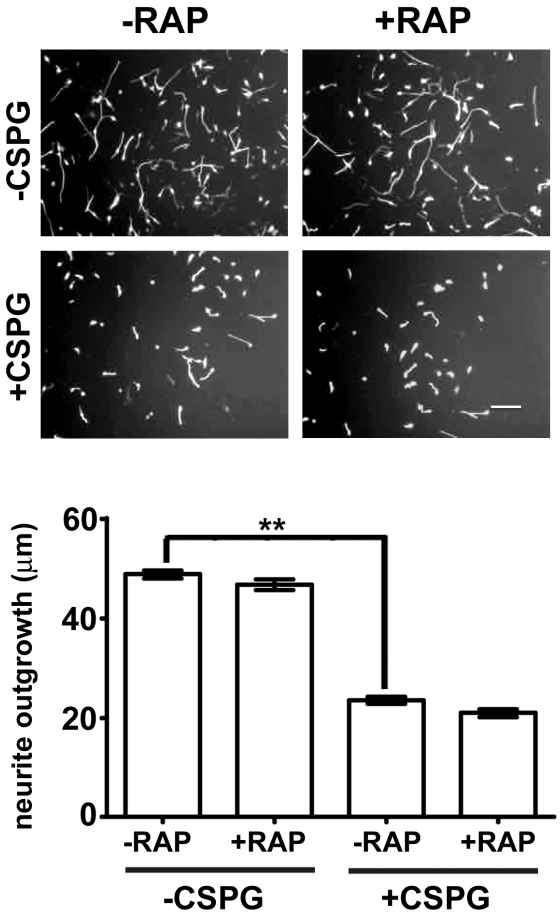

Figure 3.9: LRP1 is not required for CSPG-mediated neurite outgrowth inhibition of primary cerebellar granule neurons. Primary CGNs pretreated with 200nM GST-RAP (+RAP) or GST (-RAP) were plated on laminin + BSA (10μg/ml; -CSPG) or laminin + chondroitin sulfate proteoglycan (CSPG) mix (10μg/ml; +CSPG) and grown for 24 hours prior to immunofluorescent detection of βIII-tubulin. The graph represents the mean neurite outgrowth (±SEM) per condition (n=4 independent experiments, ** $P< 0.001$). Scale bar, 70μm.

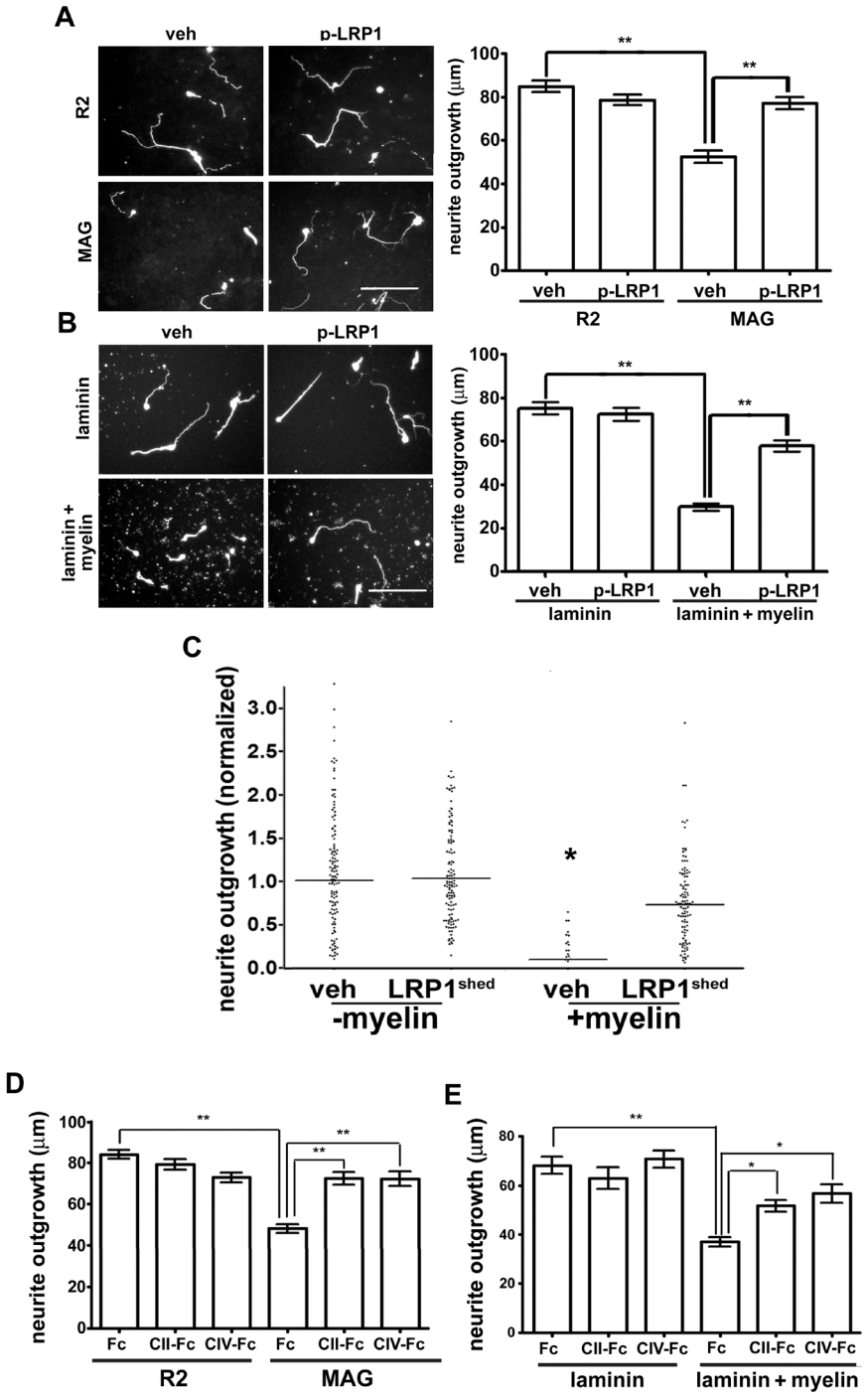

Figure 3.10: Soluble forms of LRP1 enhance neurite outgrowth of primary cerebellar granule neurons on myelin-associated inhibitors. (**a**) Monolayers of MAG-expressing and R2 control CHO cells were incubated for 15 minutes with purified LRP1 (p-LRP1) or vehicle control (PBS; veh) prior to addition of CGNs, which were grown for 48 hours before immunofluorescent staining for βIII-tubulin. The graph represents the mean neurite outgrowth

(±SEM) per condition (n=5 independent experiments, ** $P< 0.001$). (**b**) Surfaces coated with laminin or laminin + myelin (8μg/ml) were incubated for 15 minutes with purified LRP1 (p-LRP1) or vehicle control (PBS; veh) prior to addition of CGNs, which were grown for 48 hours before βIII-tubulin labeling. The graph represents the mean neurite outgrowth (±SEM) per condition (n=4 independent experiments, ** $P< 0.001$). (**c**) Surfaces coated with laminin (-myelin) or laminin + myelin (8μg/ml; +myelin) were incubated for 15 minutes with shed LRP1 (purified from human plasma; $LRP1^{shed}$) or vehicle control (PBS). CGNs were then plated and grown for 48 hours prior to immunofluorescent staining for βIII-tubulin. Neurite outgrowth was standardized to the vehicle control. The graph represents a scatter plot of neurite outgrowth per cell, with bars representing the mean neurite outgrowth per condition (* $P< 0.01$). (**d**) Monolayers of MAG-expressing and R2 control CHO cells were incubated for 15 minutes with 1μM CII-Fc, CIV-Fc or Fc, prior to addition of CGNs. CGNs were grown for 48 hours before βIII-tubulin labeling. The graph represents the mean neurite outgrowth (±SEM) per condition (n=4 independent experiments, ** $P< 0.001$). (**e**) Surfaces coated with laminin or laminin + myelin (8μg/ml) were incubated for 15 minutes with 1μM CII-Fc, CIV-Fc or Fc, prior to addition of CGNs. CGNs were grown for 48 hours prior to immunofluorescent staining for βIII-tubulin. The graph represents the mean neurite outgrowth (±SEM) per condition (n=4 independent experiments, * $P< 0.01$, ** $P< 0.001$). Scale bars, 100μm.

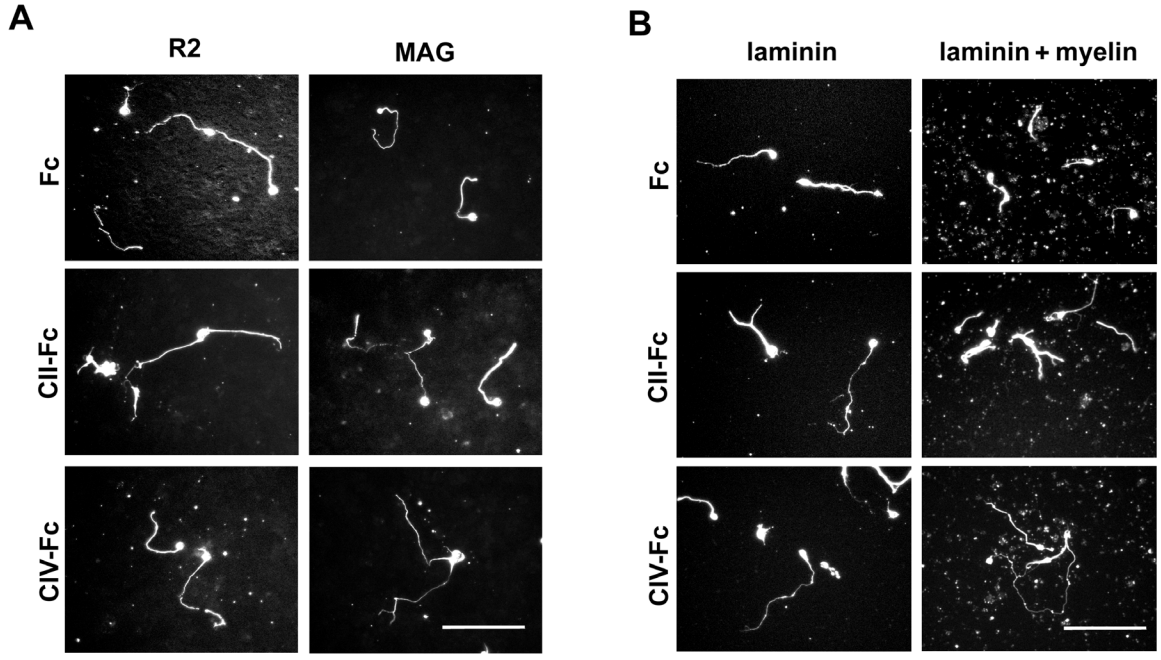

Figure 3.11: Soluble CII-Fc and CIV-Fc reverse both MAG- and myelin-mediated neurite outgrowth inhibition. Representative images from the graphs presented in **Figure 3.10d-e**. (**a**) Images that correspond to the graph in **Figure 3.10d**. (**b**) Images that correspond to the graph in **Figure 3.10e**. Scale bars, 100μm.

3.8 Bibliography

Atwal JK, Pinkston-Gosse J, Syken J, Stawicki S, Wu Y, Shatz C, Tessier-Lavigne M (2008) PirB is a functional receptor for myelin inhibitors of axonal regeneration. Science 322:967-970.

Boucher P, Gotthardt M, Li WP, Anderson RG, Herz J (2003) LRP: role in vascular wall integrity and protection from atherosclerosis. Science 300:329-332.

Bu G, Maksymovitch EA, Nerbonne JM, Schwartz AL (1994) Expression and function of the low density lipoprotein receptor-related protein (LRP) in mammalian central neurons. J Biol Chem 269:18521-18528.

Busch SA, Silver J (2007) The role of extracellular matrix in CNS regeneration. Curr Opin Neurobiol 17:120-127.

Cai D, Shen Y, De Bellard M, Tang S, Filbin MT (1999) Prior exposure to neurotrophins blocks inhibition of axonal regeneration by MAG and myelin via a cAMP-dependent mechanism. Neuron 22:89-101.

Campana WM, Li X, Dragojlovic N, Janes J, Gaultier A, Gonias SL (2006) The low-density lipoprotein receptor-related protein is a pro-survival receptor in Schwann cells: possible implications in peripheral nerve injury. J Neurosci 26:11197-11207.

Cao Z, Qiu J, Domeniconi M, Hou J, Bryson JB, Mellado W, Filbin MT (2007) The inhibition site on myelin-associated glycoprotein is within Ig-domain 5 and is distinct from the sialic acid binding site. J Neurosci 27:9146-9154.

Chivatakarn O, Kaneko S, He Z, Tessier-Lavigne M, Giger RJ (2007) The Nogo-66 receptor NgR1 is required only for the acute growth cone-collapsing but not the chronic growth-inhibitory actions of myelin inhibitors. J Neurosci 27:7117-7124.

Dickendesher TL, Baldwin KT, Mironova YA, Koriyama Y, Raiker SJ, Askew KL, Wood A, Geoffroy CG, Zheng B, Liepmann CD, Katagiri Y, Benowitz LI, Geller HM, Giger RJ (2012) NgR1 and NgR3 are receptors for chondroitin sulfate proteoglycans. Nat Neurosci 15:703-712.

Domeniconi M, Cao Z, Spencer T, Sivasankaran R, Wang K, Nikulina E, Kimura N, Cai H, Deng K, Gao Y, He Z, Filbin M (2002) Myelin-associated glycoprotein interacts with the Nogo66 receptor to inhibit neurite outgrowth. Neuron 35:283-290.

Fawcett J (2009) Molecular control of brain plasticity and repair. Prog Brain Res 175:501-509.

Filbin MT (2003) Myelin-associated inhibitors of axonal regeneration in the adult mammalian CNS. Nat Rev Neurosci 4:703-713.

FitzGerald DJ, Fryling CM, Zdanovsky A, Saelinger CB, Kounnas M, Winkles JA, Strickland D, Leppla S (1995) Pseudomonas exotoxin-mediated selection yields cells with altered expression of low-density lipoprotein receptor-related protein. J Cell Biol 129:1533-1541.

Franchini M, Montagnana M (2011) Low-density lipoprotein receptor-related protein 1: new functions for an old molecule. Clin Chem Lab Med 49:967-970.

Fu Q, Hue J, Li S (2007) Nonsteroidal anti-inflammatory drugs promote axon regeneration via RhoA inhibition. J Neurosci 27:4154-4164.

Fuentealba RA, Liu Q, Kanekiyo T, Zhang J, Bu G (2009) Low density lipoprotein receptor-related protein 1 promotes anti-apoptotic signaling in neurons by activating Akt survival pathway. J Biol Chem 284:34045-34053.

Fujita Y, Takashima R, Endo S, Takai T, Yamashita T (2011) The p75 receptor mediates axon growth inhibition through an association with PirB. Cell Death Dis 2:e198.

Gaultier A, Arandjelovic S, Niessen S, Overton CD, Linton MF, Fazio S, Campana WM, Cravatt BF, 3rd, Gonias SL (2008) Regulation of tumor necrosis factor receptor-1 and the IKK-NF-kappaB pathway by LDL receptor-related protein explains the antiinflammatory activity of this receptor. Blood 111:5316-5325.

Gaultier A, Wu X, Le Moan N, Takimoto S, Mukandala G, Akassoglou K, Campana WM, Gonias SL (2009) Low-density lipoprotein receptor-related protein 1 is an essential receptor for myelin phagocytosis. J Cell Sci 122:1155-1162.

Gaultier A, Simon G, Niessen S, Dix MM, Takimoto S, Cravatt BF, Gonias SL (2010) LDL receptor-related protein 1 regulates the abundance of diverse cell-signaling proteins in the plasma membrane proteome. J Proteome Res 9:6689-6695.

Goh EL, Young JK, Kuwako K, Tessier-Lavigne M, He Z, Griffin JW, Ming GL (2008) beta1-integrin mediates myelin-associated glycoprotein signaling in neuronal growth cones. Mol Brain 1:10.

Gorovoy M, Gaultier A, Campana WM, Firestein GS, Gonias SL (2010) Inflammatory mediators promote production of shed LRP1/CD91, which regulates cell signaling and cytokine expression by macrophages. J Leukoc Biol 88:769-778.

Hayashi H, Campenot RB, Vance DE, Vance JE (2007) Apolipoprotein E-containing lipoproteins protect neurons from apoptosis via a signaling pathway involving low-density lipoprotein receptor-related protein-1. J Neurosci 27:1933-1941.

Jalink K, van Corven EJ, Hengeveld T, Morii N, Narumiya S, Moolenaar WH (1994) Inhibition of lysophosphatidate- and thrombin-induced neurite retraction and neuronal cell rounding by ADP ribosylation of the small GTP-binding protein Rho. J Cell Biol 126:801-810.

Jeon CY, Moon MY, Kim JH, Kim HJ, Kim JG, Li Y, Jin JK, Kim PH, Kim HC, Meier KE, Kim YS, Park JB (2012) Control of neurite outgrowth by RhoA inactivation. J Neurochem 120:684-698.

Joset A, Dodd DA, Halegoua S, Schwab ME (2010) Pincher-generated Nogo-A endosomes mediate growth cone collapse and retrograde signaling. J Cell Biol 188:271-285.

Kim JE, Liu BP, Park JH, Strittmatter SM (2004) Nogo-66 receptor prevents raphespinal and rubrospinal axon regeneration and limits functional recovery from spinal cord injury. Neuron 44:439-451.

Kozma R, Sarner S, Ahmed S, Lim L (1997) Rho family GTPases and neuronal growth cone remodelling: relationship between increased complexity induced by Cdc42Hs, Rac1, and acetylcholine and collapse induced by RhoA and lysophosphatidic acid. Mol Cell Biol 17:1201-1211.

Kuhn TB, Brown MD, Wilcox CL, Raper JA, Bamburg JR (1999) Myelin and collapsin-1 induce motor neuron growth cone collapse through different pathways: inhibition of collapse by opposing mutants of rac1. J Neurosci 19:1965-1975.

Lillis AP, Greenlee MC, Mikhailenko I, Pizzo SV, Tenner AJ, Strickland DK, Bohlson SS (2008) Murine low-density lipoprotein receptor-related protein 1 (LRP) is required for phagocytosis of targets bearing LRP ligands but is not required for C1q-triggered enhancement of phagocytosis. J Immunol 181:364-373.

Liu Q, Zhang J, Tran H, Verbeek MM, Reiss K, Estus S, Bu G (2009) LRP1 shedding in human brain: roles of ADAM10 and ADAM17. Mol Neurodegener 4:17.

Madura T, Yamashita T, Kubo T, Fujitani M, Hosokawa K, Tohyama M (2004) Activation of Rho in the injured axons following spinal cord injury. EMBO Rep 5:412-417.

Mantuano E, Mukandala G, Li X, Campana WM, Gonias SL (2008) Molecular dissection of the human alpha2-macroglobulin subunit reveals domains with antagonistic activities in cell signaling. J Biol Chem 283:19904-19911.

May P, Rohlmann A, Bock HH, Zurhove K, Marth JD, Schomburg ED, Noebels JL, Beffert U, Sweatt JD, Weeber EJ, Herz J (2004) Neuronal LRP1 functionally associates with postsynaptic proteins and is required for normal motor function in mice. Mol Cell Biol 24:8872-8883.

Mehta NR, Lopez PH, Vyas AA, Schnaar RL (2007) Gangliosides and Nogo receptors independently mediate myelin-associated glycoprotein inhibition of neurite outgrowth in different nerve cells. J Biol Chem 282:27875-27886.

Mukhopadhyay G, Doherty P, Walsh FS, Crocker PR, Filbin MT (1994) A novel role for myelin-associated glycoprotein as an inhibitor of axonal regeneration. Neuron 13:757-767.

Niederost B, Oertle T, Fritsche J, McKinney RA, Bandtlow CE (2002) Nogo-A and myelin-associated glycoprotein mediate neurite growth inhibition by antagonistic regulation of RhoA and Rac1. J Neurosci 22:10368-10376.

Norton WT, Poduslo SE (1973) Myelination in rat brain: method of myelin isolation. J Neurochem 21:749-757.

Park JB, Yiu G, Kaneko S, Wang J, Chang J, He XL, Garcia KC, He Z (2005) A TNF receptor family member, TROY, is a coreceptor with Nogo receptor in mediating the inhibitory activity of myelin inhibitors. Neuron 45:345-351.

Polavarapu R, Gongora MC, Yi H, Ranganthan S, Lawrence DA, Strickland D, Yepes M (2007) Tissue-type plasminogen activator-mediated shedding of astrocytic low-density lipoprotein receptor-related protein increases the permeability of the neurovascular unit. Blood 109:3270-3278.

Qiu Z, Hyman BT, Rebeck GW (2004) Apolipoprotein E receptors mediate neurite outgrowth through activation of p44/42 mitogen-activated protein kinase in primary neurons. J Biol Chem 279:34948-34956.

Quinn KA, Pye VJ, Dai YP, Chesterman CN, Owensby DA (1999) Characterization of the soluble form of the low density lipoprotein receptor-related protein (LRP). Exp Cell Res 251:433-441.

Robak LA, Venkatesh K, Lee H, Raiker SJ, Duan Y, Lee-Osbourne J, Hofer T, Mage RG, Rader C, Giger RJ (2009) Molecular basis of the interactions of the Nogo-66 receptor and its homolog NgR2 with myelin-associated glycoprotein: development of NgROMNI-Fc, a novel antagonist of CNS myelin inhibition. J Neurosci 29:5768-5783.

Rohlmann A, Gotthardt M, Willnow TE, Hammer RE, Herz J (1996) Sustained somatic gene inactivation by viral transfer of Cre recombinase. Nat Biotechnol 14:1562-1565.

Schmandke A, Strittmatter SM (2007) ROCK and Rho: biochemistry and neuronal functions of Rho-associated protein kinases. Neuroscientist 13:454-469.

Schwab ME, Kapfhammer JP, Bandtlow CE (1993) Inhibitors of neurite growth. Annu Rev Neurosci 16:565-595.

Schwab ME (2010) Functions of Nogo proteins and their receptors in the nervous system. Nat Rev Neurosci 11:799-811.

Shao Z, Browning JL, Lee X, Scott ML, Shulga-Morskaya S, Allaire N, Thill G, Levesque M, Sah D, McCoy JM, Murray B, Jung V, Pepinsky RB, Mi S (2005) TAJ/TROY, an orphan TNF receptor family member, binds Nogo-66 receptor 1 and regulates axonal regeneration. Neuron 45:353-359.

Shi Y, Mantuano E, Inoue G, Campana WM, Gonias SL (2009) Ligand binding to LRP1 transactivates Trk receptors by a Src family kinase-dependent pathway. Sci Signal 2:ra18.

Steuble M, Gerrits B, Ludwig A, Mateos JM, Diep TM, Tagaya M, Stephan A, Schatzle P, Kunz B, Streit P, Sonderegger P (2010) Molecular characterization of a trafficking organelle: dissecting the axonal paths of calsyntenin-1 transport vesicles. Proteomics 10:3775-3788.

Strickland DK, Gonias SL, Argraves WS (2002) Diverse roles for the LDL receptor family. Trends Endocrinol Metab 13:66-74.

Tan EY, Law JW, Wang CH, Lee AY (2007) Development of a cell transducible RhoA inhibitor TAT-C3 transferase and its encapsulation in biocompatible microspheres to promote survival and enhance regeneration of severed neurons. Pharm Res 24:2297-2308.

Tang S, Shen YJ, DeBellard ME, Mukhopadhyay G, Salzer JL, Crocker PR, Filbin MT (1997) Myelin-associated glycoprotein interacts with neurons via a sialic acid binding site at ARG118 and a distinct neurite inhibition site. J Cell Biol 138:1355-1366.

Venkatesh K, Chivatakarn O, Sheu SS, Giger RJ (2007) Molecular dissection of the myelin-associated glycoprotein receptor complex reveals cell type-specific mechanisms for neurite outgrowth inhibition. J Cell Biol 177:393-399.

Vinson M, Strijbos PJ, Rowles A, Facci L, Moore SE, Simmons DL, Walsh FS (2001) Myelin-associated glycoprotein interacts with ganglioside GT1b. A mechanism for neurite outgrowth inhibition. J Biol Chem 276:20280-20285.

Vyas AA, Patel HV, Fromholt SE, Heffer-Lauc M, Vyas KA, Dang J, Schachner M, Schnaar RL (2002) Gangliosides are functional nerve cell ligands for myelin-associated glycoprotein (MAG), an inhibitor of nerve regeneration. Proc Natl Acad Sci U S A 99:8412-8417.

Wang KC, Kim JA, Sivasankaran R, Segal R, He Z (2002) p75 interacts with the Nogo receptor as a co-receptor for Nogo, MAG and OMgp. Nature 420:74-78.

Webb DJ, Thomas KS, Gonias SL (2001) Plasminogen activator inhibitor 1 functions as a urokinase response modifier at the level of cell signaling and thereby promotes MCF-7 cell growth. J Cell Biol 152:741-752.

Wight PA, Dobretsova A (1997) The first intron of the myelin proteolipid protein gene confers cell type-specific expression by a transcriptional repression mechanism in non-expressing cell types. Gene 201:111-117.

Willnow TE, Orth K, Herz J (1994) Molecular dissection of ligand binding sites on the low density lipoprotein receptor-related protein. J Biol Chem 269:15827-15832.

Winters JJ, Ferguson CJ, Lenk GM, Giger-Mateeva VI, Shrager P, Meisler MH, Giger RJ (2011) Congenital CNS hypomyelination in the Fig4 null mouse is rescued by neuronal expression of the PI(3,5)P(2) phosphatase Fig4. J Neurosci 31:17736-17751.

Wolf BB, Lopes MB, VandenBerg SR, Gonias SL (1992) Characterization and immunohistochemical localization of alpha 2-macroglobulin receptor (low-density lipoprotein receptor-related protein) in human brain. Am J Pathol 141:37-42.

Worter V, Schweigreiter R, Kinzel B, Mueller M, Barske C, Bock G, Frentzel S, Bandtlow CE (2009) Inhibitory activity of myelin-associated glycoprotein on sensory neurons is largely independent of NgR1 and NgR2 and resides within Ig-Like domains 4 and 5. PLoS One 4:e5218.

Yamashita T, Higuchi H, Tohyama M (2002) The p75 receptor transduces the signal from myelin-associated glycoprotein to Rho. J Cell Biol 157:565-570.

Yamashita T, Tohyama M (2003) The p75 receptor acts as a displacement factor that releases Rho from Rho-GDI. Nat Neurosci 6:461-467.

Yiu G, He Z (2006) Glial inhibition of CNS axon regeneration. Nat Rev Neurosci 7:617-627.

Zheng B, Atwal J, Ho C, Case L, He XL, Garcia KC, Steward O, Tessier-Lavigne M (2005) Genetic deletion of the Nogo receptor does not reduce neurite inhibition in vitro or promote corticospinal tract regeneration in vivo. Proc Natl Acad Sci U S A 102:1205-1210.

Zilberberg A, Yaniv A, Gazit A (2004) The low density lipoprotein receptor-1, LRP1, interacts with the human frizzled-1 (HFz1) and down-regulates the canonical Wnt signaling pathway. J Biol Chem 279:17535-17542.

CHAPTER IV:

Myelin-Associated Glycoprotein Utilizes Distinct Receptors and Signaling Pathways to Confer Growth Inhibition vs. Neuroprotection

4.1 Abstract

The regenerative potential of injured axons in the adult mammalian central nervous system (CNS) is very limited. Protein components associated with the damaged myelin sheath, including the myelin-associated glycoprotein (MAG), bind with high affinity to neuronal cell surface receptors and initiate signaling cascades that inhibit regrowth of these connections. In addition to its role in growth inhibition, MAG has recently been shown to protect neurons from axonal degeneration and excitotoxicity. Here we show that paired immunoglobulin (Ig)-like receptor B (PirB) and low-density lipoprotein receptor-related protein 1 (LRP1) mediate MAG-induced growth inhibition of cultured neurons, whereas the Nogo66 receptor-1 (NgR1) mediates MAG-induced neuroprotection. Loss of NgR1 results in increased vulnerability to acrylamide administration, as determined by rotarod performance and electrophysiological recordings of the sciatic nerve. *NgR1*$^{-/-}$ mice also show increased susceptibility to kainic acid-induced seizures. Additionally, we provide evidence that the PI3K-AKT-mTOR pathway is a major target for MAG growth inhibition and identify a novel connection between MAG and calpain-induced cleavage of the cytoskeleton during acute toxicity. Collectively, we have performed a

comprehensive dissection of the growth-inhibitory and neuroprotective functions of MAG and identified distinct receptor-signaling systems that mediate these functions.

4.2 Introduction

Following injury to the adult mammalian CNS, severed axons do not regenerate beyond the lesion site, often leading to permanent functional deficits. A number of growth-inhibitory molecules associated with CNS myelin and glial scar tissue contribute to the non-permissive environment of the injured CNS (Akbik et al., 2012; Fawcett et al., 2012; Silver and Miller, 2004). The best characterized myelin-associated inhibitors (MAIs) are Nogo, MAG, and oligodendrocyte myelin glycoprotein (OMgp). Nogo, which is a member of the reticulon family of proteins, exists in three isoforms (Nogo-A, -B, and -C), all of which contain an inhibitory 66 amino acid loop (Nogo66). Both NgR1 and PirB have been identified as functional receptors for Nogo66, MAG, and OMgp (Atwal et al., 2008; Domeniconi et al., 2002; Fournier et al., 2001; Liu et al., 2002; Wang et al., 2002).

MAG is a member of the sialic acid-binding Ig lectins, composed of an extracellular segment with five Ig-like domains, a transmembrane domain, and a cytoplasmic tail (Filbin, 2003). The lectin activity of MAG complexes with terminal sialic acids and critically depends on an arginine residue (Arg118) located in the first Ig-like domain (Kelm et al., 1994; Tang et al., 1997; Vyas and Schnaar, 2001). In addition to NgR1 and PirB, MAG interacts with NgR2, LRP1, the gangliosides GD1a and GT1b, and β1-integrin (Collins et al., 1997; Goh et al., 2008; Stiles et al., 2013; Venkatesh et al., 2005; Vyas et al., 2002; Yang et al., 1996). Structural studies have determined that while all known MAG interactors bind to Ig-like domains 1-3 (Goh et al., 2008; Robak et al., 2009; Vinson et al., 2001; unpublished observations), the growth-

inhibitory activity of MAG resides within Ig-like domain 5 (Cao et al., 2007; Robak et al., 2009; Tang et al., 1997).

While MAG is localized to the periaxonal membranes of Schwann cell and oligodendrocyte myelin sheaths, analysis of *MAG*$^{-/-}$ mice revealed that MAG is not necessary for myelination *in vivo* (Li et al., 1994; Montag et al., 1994; Quarles, 2007). However, as *MAG*$^{-/-}$ mice age, they exhibit a peripheral neuropathy that includes degeneration of myelinated axons, decreased axonal caliber, reduced phosphorylation of neurofilament proteins, and reduction of neurofilament spacing (Yin et al., 1998). In the CNS, progressive axonal degeneration, as well as decreases in axonal diameter and neurofilament spacing, has been noted in older *MAG*$^{-/-}$ mice (Loers et al., 2004; Pan et al., 2005; Nguyen et al., 2009). Other abnormalities in the absence of MAG have been reported, including an irregular distribution of sodium channels at the nodes of Ranvier, dystrophic oligodendrocytes, the formation of redundant myelin, and doubly myelinated axons (Bartsch, 1996; Marcus et al., 2002; Weiss et al., 2000).

These subtle phenotypes in aging *MAG*$^{-/-}$ mice have led to the hypothesis that MAG influences axonal maintenance and stability. Indeed, a recent study has shown that MAG promotes resistance to axonal injury and degeneration when confronted with a variety of stresses, including acrylamide, vincristine sulfate, and induction of experimental autoimmune encephalomyelitis (EAE), a mouse model of multiple sclerosis (Nguyen et al., 2009). This protective function of MAG extends to the neuronal cell body, as MAG guards neurons from excitotoxic insults, including kainic acid and NMDA (Lopez et al., 2011). Here we report on the identification of distinct receptors and novel signaling pathways that mediate the growth-inhibitory vs. neuroprotective functions of MAG.

4.3 Results

PirB and LRP1 participate in MAG-dependent growth inhibition

To determine the contribution of high-affinity MAG receptors to growth inhibition *in vitro*, primary neurons were cultured on either control CHO cells or CHO cells stably expressing MAG on the surface (Domeniconi et al., 2002). When plated on MAG-CHO monolayers, postnatal day 7 (P7) cortical neurons, hippocampal neurons, and DRG neurons from mice lacking NgR1 (*NgR1*$^{-/-}$) or PirB (*PirB*$^{-/-}$) do not show enhanced neurite growth compared to wild-type (WT) controls (**Figure 4.1**). Because there is evidence of functional redundancy among MAG receptors (Atwal et al., 2008; Venkatesh et al., 2007; Worter et al., 2009), we repeated our outgrowth assays using neurons from mice lacking all NgRs (*NgR123*$^{-/-}$) or from mice lacking NgR1, NgR2, and PirB combined (*NgR12*/*PirB*$^{-/-}$). Surprisingly, the combined loss of these receptors in cortical, hippocampal, and DRG neurons does not result in enhanced outgrowth (**Figure 4.1**). In P7 CGNs and RGCs, however, the loss of PirB, but not NgRs, results in a significant ($P< 0.01$, one-way ANOVA, Tukey's *post hoc*), yet incomplete release of growth inhibition (**Figure 4.2**).

As germline deletion of LRP1 results in embryonic lethality (Herz et al., 1992), we took three alternative approaches to disrupt LRP1 activity in primary neurons: (1) inhibition of MAG-LRP1 binding by the LRP1 antagonist, receptor-associated protein (RAP) (Stiles et al., 2013; Strickland et al., 2002); (2) Cre-mediated deletion of LRP1 in *LRP1*$^{f/f}$ neurons by herpes simplex virus-1 (HSV-1-GFP-Cre) transduction (Rohlmann et al., 1996; Stiles et al., 2013); and (3) tissue-specific deletion of LRP1 in differentiated neurons of *LRP1*$^{f/f}$ mice using Synapsin I-Cre (Syn-Cre) (May et al., 2004). In four of the five cell types tested (cortical neurons, hippocampal neurons, CGNs, and RGCs), antagonism of LRP1 with a GST-RAP fusion protein (**Figures 4.1,**

4.2), but not GST alone (Stiles et al., 2013; data not shown), enhances neurite outgrowth on MAG-CHO cells. In a similar vein, transduction of these neuronal cell types with HSV-1-GFP-Cre, but not HSV-1-GFP, results in increased neurite outgrowth on MAG-CHO cells (**Figure 4.3**). Only three of the cell types isolated from *LRP1*$^{f/f}$; Syn-Cre mice (cortical neurons, hippocampal neurons, RGCs) show significant ($P< 0.01$, one-way ANOVA, Tukey's *post hoc*) growth in the presence of MAG (**Figure 4.4a-e**). This is likely explained by the fact that strong Syn-Cre expression is noted in multiple layers of the cortex and regions of the hippocampus, as well as in the RGC layer of the retina; however, limited expression is seen in the cerebellum and in subsets of DRG neurons (**Figure 4.4f-m**). In total, these results argue for the existence of cell type-specific receptor mechanisms for MAG to exert its growth-inhibitory function (Mehta et al., 2007; Perdigoto et al., 2011; Venkatesh et al., 2007). Specifically, complete inhibition by MAG requires PirB and LRP1 in certain neuronal populations, but does not depend on the presence of NgR family members.

RGC axon regeneration is not enhanced following deletion of high-affinity MAG receptors

To assess whether the role of PirB and LRP1 in RGC growth inhibition *in vitro* extends to an *in vivo* CNS injury model, we performed retro-orbital optic nerve crush injury in adult *PirB*$^{-/-}$ and *NgR12*/*PirB*$^{-/-}$ mutant mice. Compared to injured wild-type controls, *PirB*$^{-/-}$ and *NgR12*/*PirB*$^{-/-}$ mice do not show any substantial RGC axon regeneration at two weeks post-injury (**Figure 4.5a,c**). To delete LRP1 in RGCs, we performed an intravitreal injection of adeno-associated virus 2 encoding GFP and Cre (AAV2-GFP-Cre) in adult *LRP1*$^{f/f}$ mice. Similar to a previous study (Park et al., 2008), this procedure results in an almost 80% transduction efficiency of RGCs (**Figure 4.6a-b**), strong expression of Cre recombinase in the RGC layer

(**Figure 4.6c**), and substantial knockdown of LRP1 protein levels in the retina, two weeks post-injection (**Figure 4.6d**). Two weeks post-injury, *LRP1*$^{f/f}$ mice with AAV2-GFP-Cre injection show no enhanced fiber regeneration compared to wild-type controls or *LRP1*$^{f/f}$ mice with AAV2-GFP injection (**Figure 4.5a,c**).

Because of the lack of optic nerve axon regeneration in *PirB*$^{-/-}$, *NgR12*/*PirB*$^{-/-}$, and *LRP1*$^{f/f}$; AAV2-GFP-Cre mutant mice (**Figure 4.5a,c**), as well as *NgR1*$^{-/-}$, *NgR2*$^{-/-}$, and *NgR12*$^{-/-}$ mutants (Dickendesher et al., 2012), we performed intravitreal injection of these mice with the yeast cell wall extract Zymosan to stimulate RGC growth potential (Leibinger et al., 2009; Yin et al., 2009). It has been demonstrated that there are additive effects when extrinsic inhibitory cues are blocked while intrinsic growth programs are simultaneously activated (Dickendesher et al., 2012; Fischer et al., 2004; Kadoya et al., 2009). Zymosan-induced RGC axon regeneration, however, was comparable between all genotypes (**Figure 4.5b,d**). Thus, there is a limited and/or redundant role for these receptors in growth inhibition following CNS injury *in vivo*.

NgR1 participates in MAG-dependent neuroprotection

As NgR1 and NgR2 are not required for MAG-mediated longitudinal neurite outgrowth inhibition, we hypothesized that these receptors may be critical for a second function of MAG: resistance to axonal injury and excitotoxic damage. To test this hypothesis, P7 mouse DRG explants were dissected and cultured for one week to allow extension of neurites, and subjected to vincristine treatment for 36 hours. As expected, vincristine sulfate, a microtubule-destabilizing drug broadly used as an anti-cancer treatment with peripheral neuropathy as a well-established side effect (Jaggi and Singh, 2012), induces severe axonal degeneration (**Figure 4.7a**). Consistent with a previous report (Nguyen et al., 2009), the addition of MAG-Fc to the

culture medium leads to significant ($P< 0.01$, one-way ANOVA, Tukey's *post hoc*), but partial, protection from degeneration, as assessed by class III β-tubulin labeling. To determine if any of the known, high-affinity MAG receptors mediate this protective effect, the assay was repeated with receptor mutant DRG explants. Strikingly, *NgR1*$^{-/-}$ DRG explants, but not *NgR2*$^{-/-}$ or *PirB*$^{-/}$ explants, show a significant ($P< 0.01$, one-way ANOVA, Tukey's *post hoc*) loss of MAG-induced axon protection (**Figure 4.7a**). This effect is not further enhanced in *NgR12*$^{-/-}$ or *NgR12*/*PirB*$^{-/-}$ explants, suggesting that NgR1 is the primary receptor to mediate MAG-induced protection from axonal degeneration. It should be noted that loss of NgR1 does not completely abolish MAG protection, likely due to the continued MAG-ganglioside interaction (Mehta et al., 2010; Nguyen et al., 2009). Furthermore, reduction of LRP1 levels by HSV-1-GFP-Cre transduction of *LRP1*$^{f/f}$ DRG explants does not substantially affect MAG-induced axon protection from vincristine (**Figure 4.8a**).

In addition to protection from axonal degeneration, MAG has also been implicated in the protection of neuronal cell bodies from excitotoxicity and cell death (Lopez et al., 2011). Indeed, bath application of MAG-Fc to cultured mouse hippocampal neurons partially protects them from kainic acid-induced excitotoxic cell death after 36 hours (**Figure 4.7b**). Loss of NgR1, but not NgR2, PirB, or LRP1, completely abolishes MAG-dependent protection (**Figures 4.7b, 4.8b**), providing strong evidence that MAG utilizes NgR1 for multiple protective functions following toxic insult. This effect is specific for MAG, as no protection from degeneration or cell death is seen with bath application of the MAIs Nogo-66 or OMgp (data not shown), or the structurally-related Ig lectin Siglec-3 (**Figure 4.7c-d**).

MAG Ig-like domains 1-3 are sufficient to confer neuroprotection

To further confirm the protective role of MAG-NgR1 from kainic acid-induced excitotoxicity, an alternative, membrane-bound source of MAG was provided. CHO cell lines expressing full-length L-MAG (MAG Ig1-5-CHO), MAG with Ig-like domains 4 and 5 deleted (MAG Ig1-3-CHO), and MAG with Ig-like domains 1 and 2 deleted (MAG Ig3-5-CHO) were established. Successful expression of the indicated MAG proteins was confirmed by immunoblotting of CHO cell line lysates with a custom-made MAG antibody directed against the L-MAG cytoplasmic portion (**Figure 4.9a**) (Winters et al., 2011), as well as immunostaining for surface-expressed MAG (**Figure 4.9b**). P7 mouse hippocampal neurons were strongly inhibited when grown for 24 hours on MAG Ig1-5-CHO and MAG Ig3-5-CHO cell monolayers, but not on MAG Ig1-3-CHO cell lines (**Figure 4.9b**). This is consistent with previous studies demonstrating that the growth-inhibitory activity of MAG resides within Ig-like domain 5 (Cao et al., 2007; Robak et al., 2009; Tang et al., 1997). Similar to experiments with soluble MAG-Fc (**Figures 4.7b, 4.8b**), culturing hippocampal neurons on MAG Ig1-5-CHO feeder layers partially protects them from kainic acid-induced excitotoxicity, an effect that is reversed to an equal degree in *NgR1*$^{-/-}$, *NgR12*$^{-/-}$, and *NgR12*/*PirB*$^{-/-}$ neurons (**Figure 4.9c**). Importantly, kainic acid does not induce cell death of the CHO feeder layers themselves (data not shown).

To determine the structural basis for MAG-mediated protection from excitotoxicity, hippocampal neurons were cultured on either MAG Ig1-5-CHO, MAG Ig1-3-CHO, or MAG Ig3-5-CHO cell lines, and treated with kainic acid for 36 hours. Both the MAG Ig1-5 and MAG Ig1-3 cell lines, but not the MAG Ig3-5 line, confer significant ($P< 0.01$, one-way ANOVA, Tukey's *post hoc*) and equal protection from cell death (**Figure 4.9d**). Similar results were obtained using soluble forms of these MAG structural mutants. Bath application of MAG Ig1-5-Fc and MAG Ig1-3-Fc, but not MAG Ig3-5-Fc, is sufficient to protect DRG explants from

vincristine-induced axonal degeneration (**Figure 4.10a**) and hippocampal neurons from kainic acid-induced excitotoxicity (**Figure 4.10b**). In total, these results suggest that the growth-inhibitory and protective functions of MAG can be dissociated, with the growth-inhibitory activity residing within Ig-like domain 5 (Cao et al., 2007; Robak et al., 2009; Tang et al., 1997) and the protective activity residing within Ig-like domains 1-3.

Loss of NgR1 increases vulnerability to acrylamide-induced axonal degeneration and kainic acid-induced seizures

Given the critical role for NgR1 in MAG-dependent protection *in vitro*, we set out to establish the importance of these receptors when confronted with toxic insults *in vivo*. To this end, adult mice were treated for two weeks with acrylamide, a neurotoxin that produces distal axonopathies of both sensory and motor nerves (Ko et al., 2000; Miller and Spencer, 1985). On a congenic C57BL/6 background, adult $MAG^{+/+}$ and $MAG^{+/-}$ mice display less severe gait abnormalities and hindlimb clasping behavior following acrylamide administration than age-matched $MAG^{-/-}$ mice (data not shown). Consistent with a previous study (Nguyen et al., 2009), administration of acrylamide to $MAG^{-/-}$ mice leads to a substantially lower retention time on the rotarod following a three day training period (**Figure 4.11a**). Strikingly, acrylamide administration in $NgR1^{-/-}$ mice, but not in $NgR2^{-/-}$ or $PirB^{-/-}$ mice on the same genetic background, results in a similar phenotype and significantly ($P< 0.01$, one-way ANOVA, Tukey's *post hoc*) impaired retention time on the rotarod (**Figure 4.11b**). $NgR1^{-/-}$, $NgR12^{-/-}$, $NgR1/PirB^{-/-}$, and $NgR12/PirB^{-/-}$ mice display comparable deficits in rotarod retention time, suggesting that NgR1 is the major contributor for this protective effect. Importantly, no significant ($P> 0.05$) changes in baseline rotatod retention time are noted for any of these mice before treatment with

acrylamide (**Figure 4.11a-b**). As an independent confirmation of the increased susceptibility of *MAG*$^{-/-}$ and *NgR1*$^{-/-}$ mice to acrylamide administration, mice were also subjected to a performance test on a grid apparatus, as a measure of behavioral impairment (Tillerson et al., 2003). Mice were lifted by their tail and placed in the center of the apparatus, before slow inversion of the grid to hang the mice upside down. Two weeks following acrylamide intoxication, *NgR1*$^{-/-}$, *NgR12*$^{-/-}$, *NgR1/PirB*$^{-/-}$, and *NgR12/PirB*$^{-/-}$ mice all show significant ($P< 0.01$, one-way ANOVA, Tukey's *post hoc*) and comparable decreases in their latency to fall from the grid apparatus (**Figure 4.11d**). While *MAG*$^{-/-}$ mice show a trend toward a decreased latency to fall compared to *MAG*$^{+/+}$ or *MAG*$^{+/-}$ controls, this difference is not significant ($P> 0.05$) (**Figure 4.11c**).

To identify any corresponding physiological alterations in sciatic nerve function of mice treated with acrylamide, compound action potentials (CAPs) were recorded from the tibial branch of the sciatic nerve of adult WT, *NgR1*$^{-/-}$, *NgR2*$^{-/-}$, *PirB*$^{-/-}$, and *NgR12/PirB*$^{-/-}$ mice. All mice show comparable CAP recordings of myelinated axons of the tibial branch (measured at 37°C) prior to treatment, with no differences in either conduction velocity (>15m/s) or peak amplitude (>2mV) (**Figure 4.12a,c,e-f**). Two weeks following acrylamide administration, *NgR2*$^{-/-}$ and *PirB*$^{-/-}$ mice display significant ($P< 0.01$, one-way ANOVA, Tukey's *post hoc*) reductions in both conduction velocity (<15m/s) and amplitude (<2mV), comparable to the reductions noted in WT mice (**Figure 4.12b,e-f**). *NgR1*$^{-/-}$ and *NgR12/PirB*$^{-/-}$ mice, on the other hand, show an even further reduction in peak amplitude (<1mV) (**Figure 4.12d-f**). Thus, administration of acrylamide on an *NgR1*$^{-/-}$ background results in a significant decrease of CAP amplitude, but not conduction velocity, when compared to WT controls, suggesting that NgR1 is protective through prevention of axonal degeneration rather than demyelination.

As an *in vivo* readout for susceptibility to excitotoxicity, $MAG^{+/+}$, $MAG^{+/-}$, and $MAG^{-/-}$ mice were given intraperitoneal injections of kainic acid, which is an epileptogenic and neuroexcitotoxic agent that acts as an agonist for ionotropic glutamate receptors. In this role, kainic acid causes severe seizures in mice and neuronal cell death in the CA1 and CA3 regions of the hippocampus (Jin et al., 2009; Zheng et al., 2011). Upon kainic acid injection, mouse seizure activity was recorded and then quantitatively scored on a 0-7 scale (Liu et al., 1999) for a period of seven hours. The seizure onset time is decreased in $MAG^{-/-}$ animals, and the severity and duration of the seizures is greatly increased compared to $MAG^{+/+}$ and $MAG^{+/-}$ mice (**Figure 4.13a-b**), as previously reported (Nguyen et al., 2009). $MAG^{-/-}$ animals reach higher seizure scores, including a 20% fatality rate, which is seen throughout the entire period of analysis.

Notably, $NgR1^{-/-}$ mice show an even greater response to kainic acid injection, with significantly ($P< 0.01$, one-way ANOVA, Tukey's *post hoc*) higher seizure scores, a 50% fatality rate, a decreased seizure onset time, and a longer duration of seizure activity compared to WT controls on the same background (**Figure 4.13c-d**). While $NgR2^{-/-}$ and $PirB^{-/-}$ mice show comparable seizure activity to WT controls, $NgR12^{-/-}$, $NgR1/PirB^{-/-}$, and $NgR12/PirB^{-/-}$ mice display similar activity to $NgR1^{-/-}$ mice. These results are further supported by electroencephalogram (EEG) recordings performed on $NgR1^{-/-}$ and WT control mice. Following kainic acid injection, the latency until the first sign of abnormal activity is decreased by more than half in $NgR1^{-/-}$ animals when compared to WT controls (average of 6 minutes vs. 16 minutes), with *NgR1-/-* mice displaying synchronized, high-voltage, fast-spiking, generalized seizures much earlier than WT mice (average of 18 minutes vs. 43 minutes; **Figure 4.13e**). Interestingly, baseline EEG recordings (no kainic acid administration) reveal that $NgR1^{-/-}$ animals display a higher frequency of semi-periodic epileptiform discharges (exceeding 750μV)

than WT controls (up to 11 discharges per hour vs. up to 1 discharge per hour; **Figure 4.13f**). In *NgR1*$^{-/-}$ animals, but not WT controls, these discharges are often associated with myoclonic jerks, suggesting a general level of hyperexcitability in *NgR1*$^{-/-}$ mice.

MAG antagonizes the PI3K-AKT-mTOR pathway to confer neurite outgrowth inhibition

Because MAG utilizes distinct receptors to mediate growth-inhibitory vs. protective responses, we examined whether this is also true for the downstream signaling pathways that are activated by MAG. The PI3K-AKT-mTOR pathway is negatively regulated by a number of growth-inhibitory ligands and receptors, including myelin-associated inhibitors (Fujita et al., 2011; Nie et al., 2010; Oinuma et al., 2010; Perdigoto et al., 2011; Raiker et al., 2010). To examine whether acute treatment of primary neurons with MAG leads to regulation of PI3K-AKT-mTOR, primary mouse CGNs were cultured for 14 days, followed by treatment with either AP-Fc or MAG-Fc for 30 minutes before cell lysis. Strikingly, MAG-Fc treatment results in a substantial decrease of both phospho (p)-AKT (Ser473) and p-p70 S6 kinase (Thr389), but not p-p44/42 ERK1/2 (Thr202/Tyr204), levels (**Figure 4.14a**). This suggests that MAG is indeed suppressing the PI3K-AKT-mTOR pathway in cultured primary neurons. To understand the functional relevance of MAG-mediated regulation of this pathway, primary CGNs were transfected with a siRNA construct targeting phosphatase and tensin homolog (PTEN), a negative regulator of PI3K, and subsequently analyzed for neurite outgrowth on CHO or MAG-CHO feeder layers. While knockdown of PTEN does not alter CGN growth on control CHO cells, it significantly ($P< 0.01$, one-way ANOVA, Tukey's *post hoc*), but only partially, releases MAG-CHO-mediated growth inhibition (**Figure 4.14b**). This effect depends on the mammalian target of rapamycin (mTOR), as rapamycin, a well-characterized mTOR inhibitor, blocks this

release of growth inhibition. As expected, transfection of CGNs with PTEN siRNA does reduce PTEN levels and increases p-p70 S6 kinase (Thr389) levels, a hallmark of increased mTOR activity (**Figure 4.14c**). Importantly, treatment of CGNs with rapamycin strongly reduces the levels of p-p70 S6 kinase below baseline.

Because knockdown of PTEN influences a wide spectrum of downstream signaling pathways and is not specific to regulation of mTOR, we repeated our neurite outgrowth assay using a constitutively active form of the GTPase Rheb1 (CA Rheb1), which remains in its GTP-bound state and drives sustained levels of mTOR and p-p70 S6 kinase (**Figure 4.15b**; Henry et al., 2012). Similar to knockdown of PTEN, transfection of CGNs with CA Rheb1 significantly ($P< 0.01$, one-way ANOVA, Tukey's *post hoc*) releases MAG inhibition in a rapamycin-sensitive manner (**Figure 4.15a**). Thus, the growth-inhibitory activity of MAG depends on the negative regulation of the PI3K-AKT-mTOR pathway. To test if the same is true for MAG-mediated protection from excitotoxicty, primary mouse hippocampal neurons, transfected with either PTEN siRNA or CA Rheb 1, were subjected to kainic acid treatment in the presence of AP-Fc or MAG-Fc. While knockdown of PTEN alone or treatment with MAG-Fc alone both reduce the levels of kainic acid-induced cell death to a similar degree, there is no additive effect (**Figure 4.15c**). Furthermore, despite being actively expressed in hippocampal neurons (Henry et al., 2012; data not shown), CA Rheb 1 has no effect on kainic acid-induced cell death under any of the conditions tested (**Figure 4.15d**). As the reduction of cell death with PTEN knockdown is not sensitive to rapamycin treatment (**Figure 4.15c**) and CA Rheb 1 expression does not alter cell death levels (**Figure 4.15d**), it is likely that mTOR-independent pathways that are downstream of PI3K (and are not regulated by MAG) have protective activity (Asomugha et al., 2010; Gary and Mattson, 2002; Zhang et al., 2007). In total, these results suggest that

regulation of the PI3K-AKT-mTOR pathway by MAG is important for its growth-inhibitory, but not protective, function.

We next wanted to explore the mechanism by which MAG negatively regulates the PI3K-AKT-mTOR pathway in primary neurons. Studies in non-neuronal cells have shown that PTEN is directly phosphorylated and activated by ROCK (Li et al., 2005). It is well established that ROCK and its small GTPase activator, RhoA, are converging points for the majority of growth inhibitors, and that blockade of ROCK with a pharmalogical inhibitor, Y-27632, releases myelin-induced growth inhibition (McKerracher et al., 2012; Tonges et al., 2011). We thus hypothesized that inhibition of mTOR activity will prevent the release of MAG-mediated growth inhibition seen with Y-27632 treatment in primary neurons. Indeed, primary mouse CGNs are strongly inhibited on MAG-CHO feeder layers, an effect that is partially reversed in the presence of Y-27632 (**Figure 4.16**). Concurrent treatment of CGNs with Y-27632 and rapamycin, however, completely blocks this reversal of MAG inhibition, suggesting a potential mechanism for MAG-mediated growth inhibition that involves the downstream activation of ROCK, which directly stimulates PTEN and thus negatively regulates PI3K-AKT-mTOR.

MAG prevents calpain-induced cleavage of the cytoskeleton in an NgR1-dependent manner

In an effort to identify downstream components regulated by MAG in the context of protection during axonal degeneration and excitotoxicity, proteins known to be involved in both processes were investigated. Of particular interest is the intracellular cysteine protease, calpain, which is activated by increased intracellular calcium levels and has the ability to cleave a number of substrates, including α-fodrin/spectrin (Nath et al., 1996), tubulin (Billger et al., 1988), NMDA receptor subunits (Guttmann et al., 2002; Simpkins et al., 2003), p53 (Pariat et al., 1997),

and p35 (Patrick et al., 1999). Calpain has been shown to mediate vincristine-induced axonal degeneration (Wang et al., 2000) and excitotoxic cell death in response to kainate receptor activation (Sanchez-Gomez et al., 2011). Additionally, inhibition of calpains has been linked to neuronal protection from injury-induced death *in vitro* and *in vivo* (McKernan et al., 2007; Ryu et al., 2012). To test whether calpain activity is altered in the presence of MAG, primary mouse hippocampal neurons were cultured for 14 days, pretreated with either Siglec-3-Fc or MAG-Fc for 30 minutes, and then subjected to kainic acid for 4 hours before cell lysis. As expected, the cleavage product of a known calpain substrate and component of the cytoskeleton, α-fodrin, is substantially increased when treated with kainic acid (**Figure 4.17a-b**). In the presence of MAG-Fc, however, cleavage of α-fodrin is largely abrogated, with a corresponding increase in the larger, unprocessed form. Importantly, kainic acid-induced, α-fodrin cleavage is mostly prevented with pretreatment of the neurons with PD150606, a cell-permeable, non-competitive calpain inhibitor (**Figure 4.17b**), suggesting that MAG prevents α-fodrin cleavage by inhibiting the activity of calpain. In addition, pretreatment of the neurons with the ROCK inhibitor Y-27632 does not alter MAG-mediated prevention of α-fodrin cleavage (**Figure 4.17b**). Thus, while ROCK is necessary for MAG-mediated protection from axonal degeneration and excitotoxicity (**Figure 4.17c-d**; Lopez et al., 2011; Mehta et al., 2010), it is likely not acting by inhibiting calpain activity. Similar results were obtained when vincristine sulfate was used to induce degeneration in these cultures (data not shown).

To determine which high-affinity receptor is critical for MAG-mediated prevention of cytoskeletal breakdown, the assay was repeated in *NgR1*$^{-/-}$, *NgR2*$^{-/-}$, *PirB*$^{-/-}$, *NgR12*$^{-/-}$, *NgR1/PirB*$^{-/-}$, *NgR2/PirB*$^{-/-}$ and *NgR12/PirB*$^{-/-}$ hippocampal neurons. Strikingly, cleavage of α-fodrin is largely restored in the presence of MAG-Fc when *NgR1*$^{-/-}$, *NgR12*$^{-/-}$, *NgR1/PirB*$^{-/-}$, or

NgR12/PirB$^{-/-}$ neurons are used (**Figure 4.17a**), suggesting that a MAG-NgR1 pathway is responsible for inhibiting calpain activity in the presence of toxic insults. While it remains to be tested if MAG inhibition of calpain activity is responsible for MAG-mediated protection from axonal degeneration and excitotoxicity, inhibition of calpain does significantly ($P< 0.01$, one-way ANOVA, Tukey's *post hoc*) reduce axonal degeneration and excitotoxic cell death to a similar degree as treatment with MAG-Fc, with no additive effect when MAG-Fc treatment and calpain inhibition are combined (**Figure 4.17c-d**). As expected, inhibition of calpain has no effect on the ability of MAG to inhibit neurite outgrowth (data not shown).

4.4 Discussion

In this study, we show that the growth-inhibitory and neuroprotective activities of MAG can be dissociated (**Figure 4.18**). The neuroprotective activity resides within the N-terminal and the growth-inhibitory activity within the C-terminal portion of the MAG ectodomain. Moreover, MAG-mediated neurite outgrowth inhibition of CGNs and RGCs depends, at least in part, on the presence of PirB and LRP1, but is independent of NgR1 and NgR2. The neuroprotective function of MAG in hippocampal and DRG neurons is mediated by NgR1 and independent of NgR2, PirB, and LRP1. Biochemical studies further reveal that MAG blocks activation of calpains and that direct inhibition of calpains mimics the MAG neuroprotective function toward acrylamide or vincristine. Together these studies provide novel mechanistic insights into how MAG exerts neuroprotection and suggest that the growth-inhibitory and protective activity of MAG can be targeted separately for therapeutic applications following nervous system injury or disease.

MAG employs multiple receptors in a cell type-specific manner to inhibit neurite outgrowth

While there are a relatively small number of CNS growth-inhibitory ligands, it is becoming abundantly clear that their neuronal cell surface receptors are far more diverse and complex (Akbik et al., 2012; Fawcett et al., 2012). MAG is known to participate in high-affinity interactions with NgR1, NgR2, PirB, and LRP1 (Atwal et al., 2008; Domeniconi et al., 2002; Liu et al., 2002; Stiles et al., 2013; Venkatesh et al., 2005); thus, we set out to explore which of these receptors mediate the growth-inhibitory function of MAG in cultures of primary mouse neurons. In CGNs and RGCs, the loss of PirB or LRP1 partially releases MAG inhibition, whereas in cortical and hippocampal neurons, only LRP1 plays a substantial role. To our surprise, the loss of these receptors has no effect on MAG-mediated growth inhibition of DRG neurons. These results support the growing notion that inhibitory ligands utilize multiple receptor complexes to signal inhibition, depending on the cell type (Mehta et al., 2007; Perdigoto et al., 2011; Venkatesh et al., 2007). Our neurite outgrowth inhibition assays also reveal a limited role for members of the Nogo receptor family in longitudinal outgrowth inhibition by membrane-bound MAG. This is consistent with previous reports (Chivatakarn et al., 2007; Venkatesh et al., 2007) that suggest a role for NgR1 in MAG-induced growth cone collapse but not inhibition of neurite extension, implying distinct receptor mechanisms for these two actions.

Because total release of MAG inhibition is not achieved with the loss of any receptor, and DRG neurons remain completely inhibited under all conditions, it is likely that (1) a substantial degree of functional redundancy exists between MAG receptors (Atwal et al., 2008; Venkatesh et al., 2007; Worter et al., 2009), and/or (2) additional MAG receptors have yet to be identified. As gangliosides have interactions with MAG for growth inhibition in a cell type-specific manner

(Mehta et al., 2007; Vyas et al., 2002), it is possible that the continued MAG-ganglioside relationship in our neuronal cultures prevents a total release of MAG inhibition. It is also possible that there is an additive effect with deletion of multiple MAG receptors, as might be the case with the combined loss of PirB and LRP1 in CGNs and RGCs. Still, structure/function analysis of MAG has demonstrated that Ig-like domain 5 is sufficient to convey growth inhibition (Cao et al., 2007; Robak et al., 2009), whereas NgR1, NgR2, gangliosides, and β1-integrin all bind to Ig-like domains 1-3 (Goh et al., 2008; Robak et al., 2009; Vinson et al., 2001). Furthermore, we have found that PirB and LRP1 bind to MAG Ig-like domains 1-3 (unpublished observations), implying the existence of a novel, neuronal binding partner for the MAG inhibitory site located in Ig-like domain 5. Studies are currently underway to use MAG Ig1-5-, MAG Ig1-3-, and MAG Ig3-5-CHO cell lines as molecular handles to co-immunoprecipitate, identify, and characterize novel MAG interactors.

A novel, protective role for NgR1 in degeneration and excitotoxicity

In stark contrast to growth inhibition, MAG-mediated protection from axonal degeneration and neuronal excitotoxicity is conferred through Ig-like domains 1-3 and dependent on NgR1, but not NgR2, PirB, or LRP1. Compared to controls, *MAG*$^{-/-}$ and *NgR1*$^{-/-}$ mice both show worsened performances on the rotarod when subjected to acrylamide intoxication and higher seizure scores when given injections of kainic acid. However, *NgR1*$^{-/-}$ mice develop even greater deficiencies than *MAG*$^{-/-}$ mice when analyzed on the grid apparatus and higher fatality rates when seizures are induced. Unfortunately, a direct comparison between *MAG*$^{-/-}$ and *NgR1*$^{-/-}$ mice cannot be made due to the fact that the mice are on different genetic backgrounds, an important factor for these types of studies (McKhann et al., 2003; Zheng et al., 2011). However,

if *MAG/NgR1*$^{-/-}$ mice display a more severe phenotype than *MAG*$^{-/-}$ mice, it is tempting to speculate that other NgR1 ligands, such as Nogo66, OMgp, or chondroitin sulfate proteoglycans (CSPGs) (Dickendesher et al., 2012; Fournier et al., 2001; Wang et al., 2002), also mediate protection. Indeed, Nogo and CSPGs have already been implicated in protection from toxin-induced cell death (Okamoto et al., 1994a; Okamoto et al., 1994b; Teng and Tang, 2013).

Distinct downstream signaling components for MAG growth inhibition vs. neuroprotection

Genetic manipulations that lead to increased mTOR activation, such as deletion of PTEN, are known to promote robust axon regeneration in both the injured optic nerve and spinal cord (Liu et al., 2010; Park et al., 2008). It is thus believed that the PI3K-AKT-mTOR pathway is a key regulator of a "dormant" neuron intrinsic growth program in the adult mammalian CNS, but how this pathway itself is regulated upon injury is still not well understood. Recent reports have shown that ephrins, semaphorins, and MAIs negatively regulate the PI3K-AKT-mTOR pathway to inhibit neurite outgrowth (Nie et al., 2010; Oinuma et al., 2010; Perdigoto et al., 2011). More generally, MAIs and their receptors have the ability to antagonize the signaling pathways (including PI3K-AKT-mTOR) that are activated by growth factors (Fujita et al., 2011; Raiker et al., 2010), suggesting a pro-/anti-growth balancing act between these opposing protein systems.

Here we show that MAG reduces mTOR activation in primary neurons, and that increasing mTOR activity can partially override MAG-mediated growth inhibition, but not MAG-mediated protection from toxic insult. Additionally, we provide evidence for the first time of a functional link between mTOR and the RhoA/ROCK pathway in cultured neurons. As virtually all CNS growth inhibitors signal via RhoA/ROCK, and PTEN is known to be activated by ROCK (Li et al., 2005; McKerracher et al., 2012; Tonges et al., 2011), it is likely that these

inhibitors negatively regulate the PI3K-AKT-mTOR pathway by means of their activation of ROCK, which directly activates PTEN. Given that inhibition of ROCK, but not activation of mTOR, attenuates MAG-induced protection, it is probable that additional ROCK targets beyond PTEN are involved. Future studies in primary neurons will need to be performed to elucidate the full connections and complexity of this signaling cascade.

We have also identified a novel role for MAG, by means of NgR1, in the prevention of calpain-induced cleavage of the neuronal cytoskeleton, a critical cellular response in both degeneration and excitotoxicity (Sanchez-Gomez et al., 2011; Wang et al., 2000; Wang et al., 2012). While further experiments are needed to determine if MAG protects from degeneration and excitotoxicity through inhibition of calpain activity, it remains a likely scenario as both MAG treatment and calpain inhibition (1) provide comparable levels of protection from axon degeneration and cell death to cultured neurons, and (2) stabilize components of the neuronal cytoskeleton (Dashiell et al., 2002; Lopez-Picon et al., 2006; Nguyen et al., 2009; Yin et al., 1998). Interestingly, vincristine-treated DRG explants in the presence of MAG show a substantial delay, but not a complete prevention, of axonal degeneration (**Figure 4.7c**), similar to effects noted with the Wallerian degeneration slow (WldS) transgene (Wang et al., 2012). As axons isolated from the WldS mouse show resistance to calpain-mediated degradation of the cytoskeleton (Bernier et al., 1999), it remains an intriguing possibility that MAG- and WldS-mediated protection are functioning through similar pathways.

Implications for nervous system injury and disease

A wide spectrum of central and peripheral nervous system disorders (including traumatic, chronic inflammatory, demyelinating, and neurodegenerative diseases) ultimately present with

the fundamental problem of axonal degeneration and dropout. These disorders include amyotrophic lateral sclerosis, Charcot-Marie-Tooth disease, Guillain-Barré syndrome, and multiple sclerosis (Lingor et al., 2012). Similarly, excitotoxicity-induced cell death poses a major clinical problem, particularly for neurodegenerative diseases such as Alzheimer's disease, Huntington's disease, and Parkinson's disease (Dong et al., 2009). While these disorders have a wide array of aetiologies and pathological diversity, it is likely that there are common molecular mechanisms that can be therapeutically targeted. Because MAG is strikingly protective for neurons in the context of both degeneration and excitotoxicity, a better understanding of its receptor interactions and signaling pathways is warranted. As with any potential therapeutic, however, it is crucial to examine all aspects of MAG function, in both the healthy and injured nervous system.

Here we have identified specific receptors and signaling components that mediate MAG growth inhibition vs. neuroprotection. Our *in vivo* analysis of axon regeneration following optic nerve injury in MAG receptor mutants, coupled with recent regeneration studies in MAI or MAI receptor mutants (Cafferty et al., 2010; Fujita et al., 2011; Lee et al., 2010), suggests that targeting of these extrinsic inhibitors provides minimal axon growth following CNS injury. If multiple inhibitory ligands or receptors are deleted, however, or if this approach is coupled with strategies to increase the intrinsic growth potential of the neuron, substantial growth may be achieved (de Lima et al., 2012; Dickendesher et al., 2012; Fischer et al., 2004; Winzeler et al., 2011). In this context, the growth-inhibitory function of MAG needs to be deleted while the protective function preserved, so as to not increase degeneration of the already injured axons. A similar line of thinking needs to be applied in the context of introducing MAG or MAG receptor-signaling components as protective cues against degeneration or excitotoxicity. Collectively, our

identification of distinct receptor-signaling systems for two critical MAG functions sheds light on fundamental pathways for nervous system injury and disease, and sets the foundation for future studies that will further unravel the triggers, connections, and targets of these pathways.

4.5 Methods

Transgenic mice: All animal handling and surgical procedures were performed in compliance with local and national animal care guidelines, and were approved by the University of Michigan Committee on Use and Care of Animals (UCUCA). *LRP1*$^{f/f}$ mice (Jackson Laboratory, 012604) were kindly provided by Steven L. Gonias (University of California, San Diego), *MAG*$^{-/-}$ mice (Li et al., 1994) were kindly provided by Ronald L. Schnaar (Johns Hopkins School of Medicine), *NgR1*$^{-/-}$ mice (Zheng et al., 2005) were kindly provided by Marc Tessier-Lavigne (Rockefeller University), *PirB*$^{-/-}$ mice (Ujike et al., 2002) were kindly provided by Marc E. Rothenberg (Cincinnati Children's Hospital Medical Center), ROSA reporter mice (Jackson Laboratory, 003474) were kindly provided by Andrew P. Lieberman (University of Michigan Medical School), and Synapsin I-Cre mice (Jackson Laboratory, 003966) were kindly provided by Geoffrey G. Murphy (University of Michigan Medical School). *NgR2*$^{-/-}$ and *NgR3*$^{-/-}$ mice have been previously described (Dickendesher et al., 2012). Mice listed above were bred together to generate the following genotypes: *NgR12*$^{-/-}$, *NgR123*$^{-/-}$, *NgR1/PirB*$^{-/-}$, *NgR2/PirB*$^{-/-}$, *NgR12/PirB*$^{-/-}$, *LRP1*$^{f/f}$; Synapsin I-Cre, and ROSA; Synapsin I-Cre. For all experiments, control mice were of the exact same age and genetic background as mutant mice.

Neurite outgrowth assays: To assay MAG inhibition, 96-well plates were covered with monolayers of either CHO cells or CHO cells expressing recombinant MAG on their surface

(MAG-CHO; Mukhopadhyay et al., 1994). CHO and MAG-CHO cells were cultured in DMEM (Invitrogen) with 10% dialyzed fetal bovine serum (FBS), 2mM glutamine, 40mg/L proline, 0.73mg/L thymidine, and 7.5mg/L glycine. After 24 hours, P7 mouse cortical neurons, hippocampal neurons, DRG neurons, CGNs, or RGCs (from control or mutant mice) were plated on top of the confluent CHO feeder layers at a density of 8,000 cells/well. For some experiments, GST or GST-RAP (200nM), the ROCK inhibitor Y-27632 (15μM; Millipore), or rapamycin (25nM; Cell Signaling) were added to the wells at the time of plating. Cells were cultured for 24 hours at 37°C in the appropriate neuronal medium (see below), and then fixed with 4% paraformaldehyde, blocked in 1% horse serum and 0.1% Triton X-100 in PBS, and stained with anti-class III β-tubulin (TuJ1; Promega). Alexa Fluor-conjugated secondary antibodies (Invitrogen) were used for fluorescent labeling, and images were taken using an inverted microscope (IX71; Olympus) attached to a digital camera (DP72; Olympus). To quantify neurite outgrowth, UTHSCSA ImageTool for Windows was used, and processes equal or longer to one cell body diameter were measured.

Primary neurons were isolated as follows: (1) P7 mouse cerebral cortex or hippocampus (with meninges removed) was dissected in Neurobasal medium (Invitrogen) on ice, trypsinized for 15 minutes and gently washed/triturated, and resuspended in Neurobasal medium with B-27® supplement (Invitrogen), glutamine, and penicillin/streptomycin. (2) P7 mouse DRG neurons were dissected, incubated in 0.05% trypsin and 0.1% collagenase for 40 minutes, and triturated before resuspension in Neurobasal medium with B-27® supplement, glutamine, penicillin/streptomycin, and 15ng/ml nerve growth factor (Venkatesh et al., 2005). (3) P7 mouse cerebellum was dissected, trypsinized for 15 minutes/triturated, and CGNs were purified in a discontinuous Percoll gradient before resuspension in Neurobasal medium with B-27®

supplement, glutamine, glucose, and penicillin/streptomycin (Venkatesh et al., 2005). (4) P7 mouse retina was dissected, digested in papain (MP Biomedicals) for 30 minutes, washed, and plated onto 60mm culture dishes (Corning) that were precoated with goat anti-mouse IgM (Millipore) and anti-Thy1.2 (Sigma). After 1 hour at room temperature, unbound cells were removed by several rinses in PBS, and bound cells were lifted using 0.125% trypsin/EDTA, washed, and resuspended in Neurobasal medium with B-27® supplement, glutamine, glucose, and penicillin/streptomycin (Venkatesh et al., 2007).

In vitro **degeneration and excitotoxicity assays:** To assess levels of axonal degeneration, 96-well plates were coated with poly-D-lysine hydrobromide (50µg/ml; Sigma) overnight, rinsed in water, and air dried. P7 mouse DRG explants (from control or mutant mice) were then dissected and placed in the middle of each well (1 explant per well) in a minimal amount of medium (Neurobasal medium with B-27® supplement, glutamine, penicillin/streptomycin, and 15ng/ml nerve growth factor), allowing the explants to attach. After an overnight incubation at 37°C, additional medium was added to the wells, and the explants were allowed to extend neurites for 7 days. Some explants were then treated with 50nM vincristine sulfate (Sigma), as well as 50nM preclustered AP-Fc, Siglec-3-Fc, MAG-Fc, MAG Ig1-5-Fc, MAG Ig1-3-Fc, or MAG Ig3-5-Fc fusion proteins (Dickendesher et al., 2012; Robak et al., 2009), for 12-96 hours before all explants were fixed/stained for TuJ1/imaged as described above. For certain experiments, explants were treated with the ROCK inhibitor Y-27632 (15µM) or the membrane-permeable calpain inhibitor, PD150606 (10µM; Sigma). The percentage of axons with signs of degeneration (fragmentation or "blebbing" of the axon) was determined for each condition.

To assess levels of excitotoxicity-induced cell death, P7 mouse hippocampal neurons (from control or mutant mice) were cultured on poly-D-lysine hydrobromide-coated plates (50μg/ml) for 4 days at 37°C, in Neurobasal medium with B-27® supplement (Invitrogen), glutamine, and penicillin/streptomycin. Some neurons were then treated with 200μM kainic acid (A.G. Scientific), as well as 50nM preclustered AP-Fc, Siglec-3-Fc, MAG-Fc, MAG Ig1-5-Fc, MAG Ig1-3-Fc, or MAG Ig3-5-Fc fusion proteins, for 12-96 hours. For certain experiments, neurons were treated with Y-27632 (15μM) or PD150606 (10μM). Medium from all cultures was then replaced with fresh medium containing 10μg/ml propidium iodide (Invitrogen) for 40 minutes, and neurons were fixed/stained for TuJ1/imaged as described above. The percentage of live cells (positive for TuJ1, negative for propidium iodide) was determined for each condition. For some experiments, neurons were cultured for 2 days on feeder layers of CHO cell lines (see below), as opposed to poly-D-lysine-coated plates. These cultures did not receive treatment with Fc-fusion proteins.

Gene silencing/overexpression: To silence LRP1, *LRP1*$^{f/f}$ neurons/explants were cultured on poly-D-lysine hydrobromide-coated plates (50μg/ml) for 1 day (for neurite outgrowth assays, excitotoxicity assays) or 4 days (for degeneration assays) before transduction with either herpes simplex virus-1 (HSV-1)-GFP or HSV-1-GFP-Cre (Viral Gene Transfer Core, McGovern Institute for Brain Research, MIT). Virus was removed 2 days post-transduction and, at 3 days post-transduction, one group of neurons/explants were lysed in 2X SDS sample buffer and subjected to immunoblotting with anti-LRP1 (Sigma) and anti-TuJ1 to confirm Cre-mediated deletion of LRP1 (data not shown; also performed in Stiles et al., 2013). A second group of neurons/explants were subjected to excitotoxicity or degeneration assays (see above),

while a third group of neurons were gently dislodged using Cellstripper™ non-enzymatic cell dissociation solution (Corning) and re-plated on CHO or MAG-CHO cells for 24 hours (see above).

For knockdown of PTEN, CGNs or hippocampal neurons were transfected with siRNA targeted against mouse PTEN (siGENOME SMARTpool; Thermo Scientific) or with non-targeting control siRNA (Thermo Scientific), using the Amaxa Nucelofector™ Kit for mouse neurons, according to the manufacturer's instructions. Transfected neurons were grown for 3 days before (1) being lysed with 2X SDS sample buffer and subjected to immunoblotting with anti-PTEN (Cell Signaling), anti-p-p70 S6 kinase (Thr389; Cell Signaling), and anti-β-actin (Sigma) to confirm knockdown of PTEN and its activity, (2) being subjected to excitotoxicity assays (see above), or (3) being dislodged by Cellstripper™ (Corning) and re-plated on CHO or MAG-CHO cells for 24 hours (see above). Overexpression of Rheb1 was achieved in a similar manner, using either a plasmid containing a constitutively active form of Rheb1 (RhebQ64L; Henry et al., 2012) or a control plasmid containing GFP. Immunoblotting was performed using anti-p-p70 S6 kinase (Thr389; Cell Signaling), and anti-β-actin to confirm Rheb1 activity. All immunoblots were quantified by densitometric analysis (using ImageJ software - from a total of 4 independent experiments), normalized to β-actin levels, and graphed as a percentage of the control.

Construction of cell lines: Standard PCR cloning using the Tth-DNA polymerase (Applied Biosystems) was performed to produce the following structural variants of rat MAG: MAG Ig1-5, MAG Ig1-3, and MAG Ig3-5. Specifically, MAG Ig1-5 was created by amplifying the beginning of Ig-like domain 1 (S17) until one amino acid prior to the stop codon (K626). For

MAG Ig1-3, the region from S17 until the end of Ig-like domain 3 (A325) was fused to the beginning of the transmembrane domain (K513) until K626. For MAG Ig3-5, the region from the beginning of Ig-like domain 3 (L234) until K626 was amplified. KpnI and BamHI restriction sites were introduced at the beginning and the end, respectively, of all variants to allow cloning into the multiple cloning site of the pSecTag2A vector (Invitrogen). This vector allows proteins to receive the murine Ig κ-chain leader sequence at the N-terminus and the c-myc epitope and six tandem histidine residues (6HIS) at the C-terminus. Following successful cloning into pSecTag2A, all MAG variants (with the Ig κ-chain leader sequence, c-myc epitope, and 6HIS residues included) were cloned into the pIRES2-EGFP vector (BD Biosciences) by introducing SacII and XmaI restriction sites.

After sequencing analysis, CHO cells were then transfected with these plasmids, using Lipofectamine® 2000 (Invitrogen), and multiple treatments with 400μg/ml of G418 sulfate (Invitrogen) were performed to select for stably-transfected cells. To generate clonal cells, individual, EGFP-positive cells were picked and cultured in DMEM with 10% FBS, 2mM glutamine, 40mg/L proline, 0.73mg/L thymidine, and 7.5mg/L glycine. This process was repeated several times to obtain ~95% clonal purity. Fluorescence-activated cell sorting (FACS) was then performed on all cell lines, using anti-MAG, clone 513 (Millipore) for MAG Ig1-5-CHO and MAG Ig1-3-CHO cell lines, or anti-MAG, extracellular (a generous gift from James L. Salzer) for MAG Ig3-5-CHO cell lines. The top 3% of MAG-expressing cells for each cell line were collected, expanded, and continually maintained with 200μg/ml of G418 sulfate. To confirm successful MAG expression and proper molecular weight of all MAG variants, the newly created CHO cell lines were lysed with 2X SDS sample buffer and subjected to immunoblotting with custom-made, anti-MAG (Winters et al., 2011). Furthermore, cell-surface

expression of MAG was verified by immunostaining (without Triton X-100) with anti-MAG, clone 513 for MAG Ig1-5-CHO and MAG Ig1-3-CHO cell lines, or anti-MAG, extracellular for MAG Ig3-5-CHO cell lines. To check the functionality of all cell lines, neurite outgrowth assays with P7 mouse hippocampal neurons were performed (see above).

Optic nerve injury: Adult mice (control or mutant; 6-8 weeks of age) were anesthetized with an intraperitoneal injection of Ketamine (100mg/kg; Fort Dodge Animal Health) and Xylazine (10mg/kg; Akorn, Inc.). Without damaging the ophthalmic artery, the optic nerve was exposed and compressed for 10 seconds with angle jeweler's forceps (Dumont #5; Fine Science Tools) at approximately 1mm behind the eyeball. For intravitreal injection of Zymosan, 5µl of a suspension (12.5µg/µl in sterile PBS; Sigma) was injected using a Hamilton syringe with a 30 gauge removable needle. Following surgery, eyes were rinsed with sterile PBS and ophthalmic ointment was applied (Butler AHS). All surgeries were performed under aseptic conditions (Dickendesher et al., 2012). For deletion of LRP1 in *LRP1*$^{f/f}$ mouse RGCs, 2µl of AAV2-GFP (Vector Biolabs) was injected into the left eye and 2µl of AAV2-GFP-Cre (Vector Biolabs) was injected into the right eye, 14 days prior to optic nerve injury.

14 days following optic nerve injury, mice were given a lethal dose of anesthesia and perfused with PBS/4% paraformaldehyde. Eyes with optic nerves attached were dissected, post-fixed overnight at 4°C, and cryoprotected in 30% sucrose. Optic nerves were then embedded in OCT Tissue-Tek Medium (Sakura Finetek) and 14µm longitudinal sections were stained with anti-GAP-43 (a generous gift from Larry I. Benowitz). Alexa Fluor-conjugated secondary antibodies were used for fluorescent labeling, slides were mounted with Fluoromount-G™ (Southern Biotech), and images were taken. To quantify axonal growth, the number of GAP-43-

positive axons at prespecified distances from the injury site was counted in at least 3 sections per nerve. These numbers were converted into the number of regenerating axons per nerve as previously described (Fischer et al., 2004).

Histochemical studies: To evaluate expression levels of Cre recombinase under the Synapsin I promoter, 3-week-old ROSA; Synapsin I-Cre mice were perfused with PBS/4% paraformaldehyde, and the following tissues were dissected, post-fixed (overnight), and cryoprotected: eye, brain, spinal cord, and DRGs. Tissues were embedded and cryosectioned (20μm sections), and slides were washed for 15 minutes with PBS + 0.02% NP-40 (repeated two additional times). Stain solution [5mM $K_3Fe(CN)_6$, 5mM $K_4Fe(CN)_6$, 2mM $MgCl_2$, 0.01% sodium deoxycholate, 0.02% NP-40, and 1mg/ml X-Gal (Sigma) in PBS] was added to the slides for an overnight incubation at room temperature. Slides were then post-fixed in 4% paraformaldehyde for 20 minutes, washed, and mounted with Fluoromount-G™ before imaging. For expression analysis of AAV2-GFP-Cre, 6-week-old ROSA reporter mice received intravitreal injections of AAV2-GFP in the left eye and AAV2-GFP-Cre in the right eye. 14 days later, mice were perfused and retina was stained with X-Gal as described above.

To confirm successful injection of AAV2-GFP and AAV2-GFP-Cre into *LRP1*$^{f/f}$ mice, these mice were perfused with PBS/4% paraformaldehyde at 14 days post-injection. Eyes were removed and post-fixed overnight at 4°C, and retinal "cups" were dissected out and fixed in 4% paraformaldehyde for 30 minutes at 4°C. Retinas were washed with PBS, blocked in 10% goat serum and 0.2% Triton X-100 for 1 hour, incubated with primary antibodies (anti-GFP, Invitrogen; anti-TuJ1) for 1-2 days at 4°C, and washed with PBS. Following overnight incubation with the appropriate Alexa Fluor-conjugated secondary antibodies and another round

of washing, retinas were mounted onto slides for imaging. Transduction efficiency was calculated as the percentage of GFP/TuJ1-double positive cells, divided by the total number of TuJ1-positive cells.

Biochemical analysis: P7 mouse CGNs were cultured at a high density (800,000 cells/well) on poly-D-lysine hydrobromide-coated (50µg/ml), 6-well plates. After 14 days of growth in Neurobasal medium with B-27® supplement, glutamine, glucose, and penicillin/streptomycin medium, cultures were treated for 30 minutes with 50nM of preclustered AP-Fc or MAG-Fc in OptiMEM (Invitrogen). Cells were lysed for 30 minutes on ice using Brij lysis buffer (10mM potassium phosphate, pH 7.2; 1mM EDTA; 10mM magnesium chloride; 50mM β-glycerophosphate; 0.5% NP-40; 0.1% Brij® 35; 1mM Na_3V0_4; and 1:100 protease inhibitor cocktail - Sigma), followed by centrifugation at 4°C (Raiker et al., 2010). Supernatants were collected and protein concentration was determined using the BCA Protein Assay Kit (Thermo Scientific). For immunoblot analysis, 10µg of protein lysate was loaded, separated by SDS-PAGE, transferred onto nitrocellulose membranes, and probed for p-AKT (Ser473; Cell Signaling), total AKT (Cell Signaling), p-p70 S6 kinase (Thr389; Cell Signaling), total p70 S6 kinase (Cell Signaling), p-p44/42 ERK1/2 (Thr202/Tyr204; Cell Signaling), total p44/42 ERK1/2 (Cell Signaling), and anti-β-actin (Sigma). This experiment was repeated four times, with both treatments performed in duplicate for each experiment.

To assess levels of calpain activation, P7 mouse hippocampal neurons (from control or mutant mice) were cultured in a similar fashion for 14 days, followed by pretreatment for 30 minutes with 50nM of preclustered Siglec-3-Fc or MAG-Fc, with or without Y-27632 (15µM) or PD150606 (10µM). Some cells were treated with 50nM vincristine sulfate or 200µM kainic acid

for 4 hours, and then all cells were lysed and subjected to immunblotting as mentioned above. Membranes were probed for α-fodrin (Enzo Life Sciences) and TuJ1. Results were confirmed from 3-5 independent experiments, depending on the conditions.

To confirm reduction of LRP1 in *LRP1*$^{f/f}$ mice with AAV2-GFP-Cre (but not AAV2-GFP) injection, retinas were dissected from these mice at 14 days post-injection. Retinas were lysed (on ice) in RIPA Buffer (Sigma) with 1mM Na_3V0_4 and 1:100 protease inhibitor cocktail for 30 minutes, followed by centrifugation at 4°C and supernatant collection. For immunoblot analysis, 10μg of lysate was loaded, and blots were probed for LRP1 and β-actin. Quantification of relative protein levels was determined by densitometric analysis (using ImageJ software - from a total of 4 independent experiments), normalized to β-actin levels, and graphed as a percentage of the AAV2-GFP control.

Rotarod/grid apparatus performance: Adult mice (control or mutant; 6-8 weeks of age) were trained for 3 consecutive days (1 trial per day) on an accelerating rotarod (Ugo Basile), using a protocol that starts at 1 rotation per 38 seconds and ends at 1 rotation per 2 seconds. On the fourth day, the rotarod performance was recorded and mice began to receive acrylamide (400 parts per million; Sigma) in their drinking water for 2 weeks. 11 days into the treatment, mice were trained on the rotarod for another 3 days (1 trial per day), and the performance was recorded on the fourth day (14 days into acrylamide treatment). For all rotarod experiments, the retention time before falling (in seconds) was measured, beginning at the start of the acceleration. A "fall" was considered either (1) an actual fall from the accelerating rod, or (2) a complete rotation of the rod without the mouse running against it.

In a separate set of experiments, adult mice (control or mutant; 6-8 weeks of age) were tested for 1 day (3 trials - spaced 2 hours apart) on a grid apparatus (Tillerson et al., 2003), before receiving 2 weeks of acrylamide treatment. 14 days into the treatment, mice were again tested. To perform the test, a mouse was lifted by its tail and placed in the center of the apparatus. Once the mouse comfortably gripped the horizontal grid mesh, the apparatus was slowly inverted, thus hanging the mouse upside down. At this point, the latency of the mouse to fall from the apparatus (in seconds) was measured. Importantly, the apparatus was constructed to the specifications of the original study (Tillerson et al., 2003). For all rotarod and grid apparatus experiments, the tester was blind to the genotypes.

Electrophysiology: 6-8-week-old mice (control or mutant; with or without 2 weeks of acrylamide treatment) were killed by CO_2 inhalation. Both sciatic nerves were dissected on ice and immediately transferred to a temperature-controlled recording chamber held at 37 ± 0.4°C, with oxygenated artificial CSF (ACSF). Nerves less than 10mm in length were not used. ACSF contains the following: 125mM NaCl, 1.25mM NaH_2PO_4, 25mM glucose, 25mM $NaHCO_3$, 2.5mM $CaCl_2$, 1.3mM $MgCl_2$, and 2.5mM KCl (saturated with 95% O_2/5% CO_2). Each end of the nerve was drawn into the tip of a suction pipette electrode. The stimulating electrode was connected to a constant-current stimulus isolation unit (WPI) driven by Axon™ pClamp® 10.3 software, and a stimulating pulse (50μs) was applied to the proximal (toward the spinal cord) end of the nerve. The recording electrode was applied to the distal (tibial branch) end of the nerve and connected to the input of a differential alternating current amplifier (custom-made). In addition, the other amplifier input was connected to a pipette that was placed near the recording pipette but not in contact with the nerve. This electrode served to subtract most of the stimulus

artifact from the recordings. Signals were sampled at 100 kHz and fed into the data acquisition system (Axon™ Digidata 1440A, Axon™ pClamp® 10.3). All recordings were done blind to the genotype.

The resistance of the recording pipette was measured before (R1) and after (R2) the nerve was inserted. Similar to CAP area (Stys et al., 1991), we have found that CAP amplitude is a linear function of R2. We have also determined that the amplitude of the signal is independent of the glass pipette used (to within ~5%) if the CAP is measured with the ratio R2/R1 constant. Therefore, in order to normalize the data, all amplitude measurements were made with R2/R1=1.7. Data analysis was performed using Clampfit software, with conduction velocity taken as the length of the nerve divided by the time-to-peak.

Kainic acid-induced seizures/electroencephalogram recordings: Adult mice (control or mutant; 6-8 weeks of age) were given an intraperitoneal injection of kainic acid (25mg/kg in PBS) and were monitored for 7 hours, in order to assess their seizure onset/duration and seizure severity score. Seizure severity scores are based upon a 0-7 scale (Liu et al., 1999), and can be summarized as follows: (0) normal behavior; (1) exploring, sniffing, and grooming have ceased and the animal is motionless; (2) forelimb and/or tail extension, giving the appearance of a rigid posture; (3) myoclonic jerks of the head and neck, with brief twitching or repetitive movements; (4) forelimb clonus and partial rearing; (5) forelimb clonus, rearing, and falling; (6) generalized tonic-clonic activity; and (7) death. For all experiments, the tester was blind to the genotypes.

For EEG recordings, six electrodes were properly positioned (two frontal electrodes, two parietal electrodes, one ground electrode, and one reference electrode) using a mounting screw and socket (PlasticsOne). The sockets were fitted into an electrode pestal, connected to an

electrode holder, and a head cap was made using dental cement. After a recovery period of 5 days, mice were recorded using EEG hardware (Bio-Logic) for 48 hours to obtain baseline activity. Following an intraperitoneal injection of kainic acid (15mg/kg in PBS), mice were recorded for an additional 24 hours (or until death). Recordings were sampled at 400 Hz and filtered at 1Hz (high-pass)/70Hz (low-pass). Concurrent video was obtained and analyzed together with the EEG recordings by an observer blind to the genotypes.

Statistical analysis: With the exception of **Figure 4.6d** (unpaired *t*-test), data were analyzed using one-way analysis of variance followed by Tukey's *post hoc* comparisons. All statistics were performed using SigmaStat 3.5 for Windows (Systat Software), and $P < 0.01$ was considered significant.

4.6 Acknowledgments

This work was supported by the Neuroscience Training Grant T32EY017878, the University of Michigan Rackham Merit Fellowship (Travis L. Dickendesher), the Cellular and Molecular Biology Training Grant T32GM007315 (Katherine T. Baldwin and Yevgeniya A. Mironova), the Dr. Miriam and Sheldon G. Adelson Medical Foundation on Neural Repair and Rehabilitation, and the National Institute of Neurological Disorders and Stroke R01NS081281 (Roman J. Giger). We thank Larry I. Benowitz (Harvard Medical School) for the GAP-43 antibody, Marie T. Filbin (Hunter College) for CHO and MAG-CHO cell lines, Steven L. Gonias (University of California, San Diego) for GST and GST-RAP, Ken Inoki (University of Michigan Medical School) for the RhebQ64L construct, Brian A. Pierchala (University of

Michigan Medical School) for the HSV-1-GFP and HSV-1-GFP-Cre, and James L. Salzer (New York University Medical Center) for the MAG antibody.

We also thank Heather M. Grifka-Walk (University of Michigan Medical School) for her assistance with the FACS equipment, Stephanie A. Jimenez-Temme (University of Michigan Medical School) for training on the rotarod, Peter G. Shrager (University of Rochester Medical Center) for his invaluable assistance and expertise in the setup and analysis of sciatic nerve CAP recordings, and Corinne Weisheit (University of Michigan Medical School) for use of the grid apparatus. Additionally, we are grateful to the following investigators for sending us mice (details can be found in the methods section): Steven L. Gonias (University of California, San Diego), Andrew P. Lieberman (University of Michigan Medical School), Geoffrey G. Murphy (University of Michigan Medical School), Marc E. Rothenberg (Cincinnati Children's Hospital Medical Center), Ronald L. Schnaar (Johns Hopkins School of Medicine), and Marc Tessier-Lavigne (Rockefeller University).

4.7 Author Contributions

Travis L. Dickendesher (T.L.D.) and Roman J. Giger (R.J.G.) conceived the study; T.L.D., Matthew J. Korn (M.J.K.), Jack M. Parent, and R.J.G. designed the experiments; and T.L.D., M.J.K., Katherine T. Baldwin, and Yevgeniya A. Mironova performed experiments and data analysis.

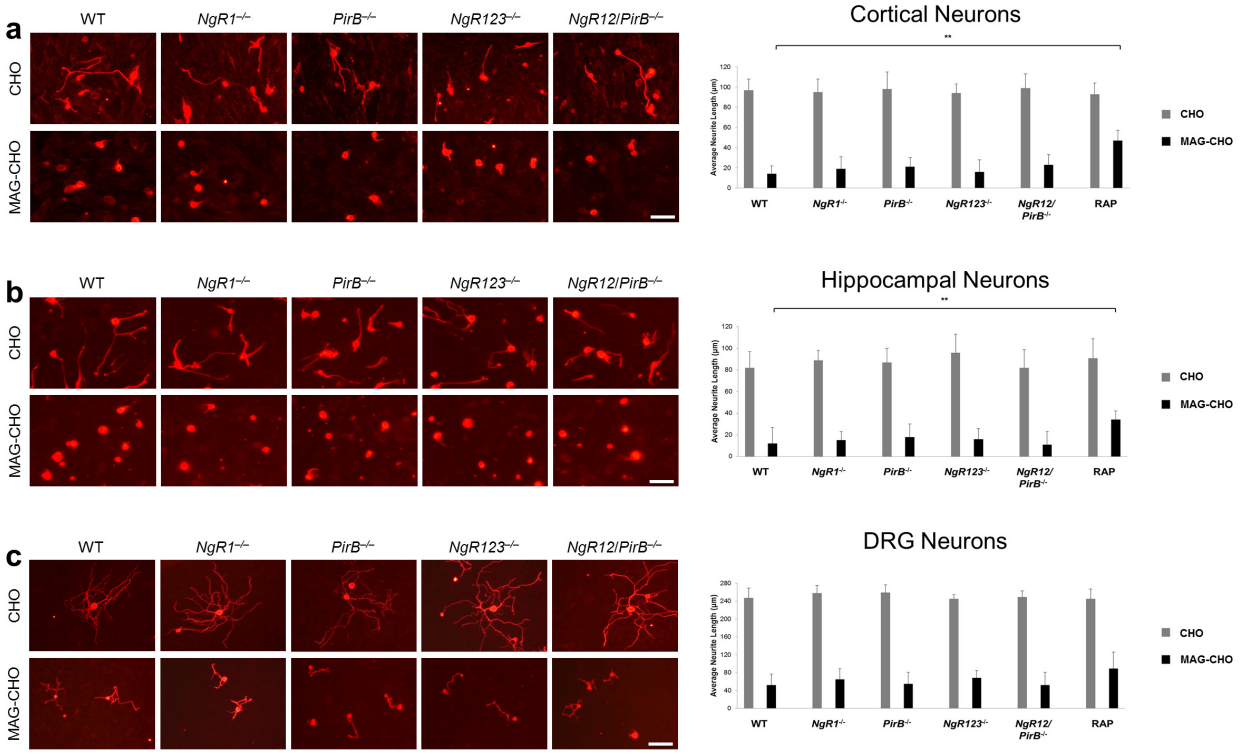

Figure 4.1: Antagonism of LRP1 partially releases MAG growth inhibition of cortical and hippocampal, but not DRG, neurons. (**a**) *In vitro*, WT P7 cortical neurons are strongly inhibited when plated on MAG-CHO cell feeder layers. *NgR1*$^{-/-}$, *PirB*$^{-/-}$, *NgR123*$^{-/-}$, and *NgR12/PirB*$^{-/-}$ cortical neurons show no substantial release of MAG inhibition; however, addition of GST-RAP (200nM) leads to a significant, yet incomplete release of growth inhibition. On control CHO cells, neurite length of all groups is comparable. (**b**) Similar to cortical neurons, WT, *NgR1*$^{-/-}$, *PirB*$^{-/-}$, *NgR123*$^{-/-}$, and *NgR12/PirB*$^{-/-}$ P7 hippocampal neurons are equally inhibited on MAG-CHO cells. Addition of GST-RAP (200nM), however, partially releases growth inhibition. (**c**) For DRG neurons, all groups are equally inhibited on MAG-CHO cells. Importantly, addition of 200nM GST has no effect on neurite outgrowth when these cell types are plated on CHO or MAG-CHO cells (data not shown). At least 150 neurites of TuJ1-labeled cells were counted per condition (n=5 independent experiments for cortical neurons, n=5 experiments for hippocampal neurons, n=7 experiments for DRG neurons). Results are presented as mean ±SEMs. ** $P< 0.01$ (one-way ANOVA, Tukey's *post hoc*). Gray bars (CHO); black bars (MAG-CHO). Scale bar: a, 60µm; b, 50µm; c, 80µm.

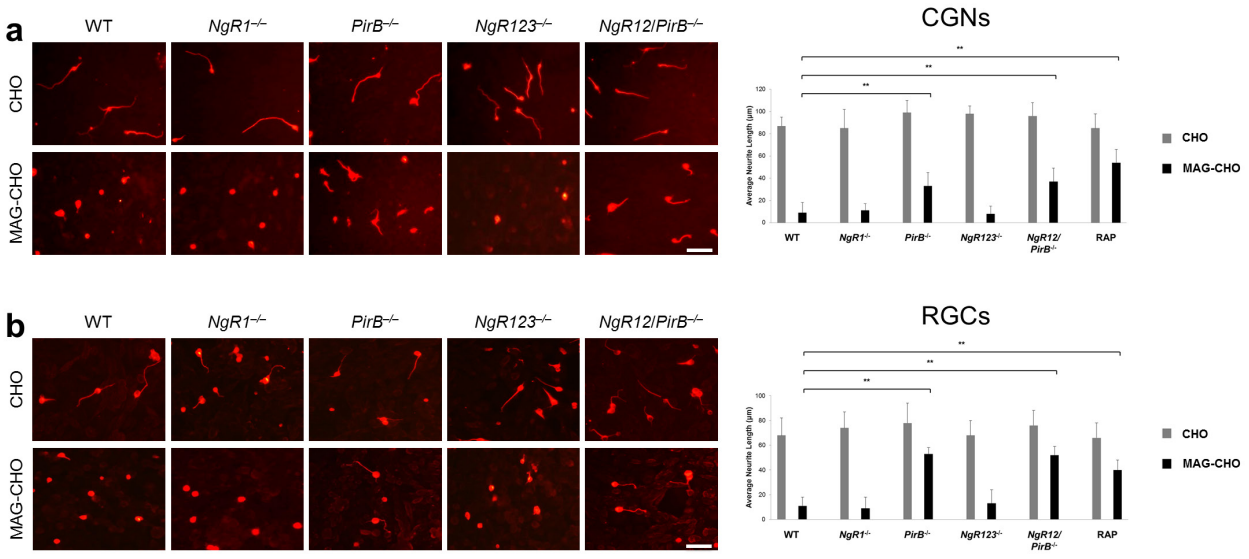

Figure 4.2: Antagonism of LRP1 or genetic deletion of PirB partially releases MAG growth inhibition of CGNs and RGCs. (**a**) *In vitro*, WT P7 CGNs are inhibited when plated on MAG-CHO cell feeder layers. *NgR1*$^{-/-}$ and *NgR123*$^{-/-}$ CGNs show no release of MAG inhibition; however, loss of PirB (*PirB*$^{-/-}$, *NgR12/PirB*$^{-/-}$) or addition of GST-RAP (200nM) leads to a significant, yet incomplete release of growth inhibition. On control CHO cells, neurite length of all groups is comparable. (**b**) Similar to CGNs, WT, *NgR1*$^{-/-}$, and *NgR123*$^{-/-}$ P7 RGCs are equally inhibited on MAG-CHO cells. Loss of PirB (*PirB*$^{-/-}$, *NgR12/PirB*$^{-/-}$) or addition of GST-RAP (200nM), however, partially releases growth inhibition. Importantly, addition of 200nM GST has no effect on neurite outgrowth when these cell types are plated on CHO or MAG-CHO cells (data not shown). At least 150 neurites of TuJ1-labeled cells were counted per condition (n=8 independent experiments for CGNs, n=6 experiments for RGCs). Results are presented as mean ±SEMs. ** $P< 0.01$ (one-way ANOVA, Tukey's *post hoc*). Gray bars (CHO); black bars (MAG-CHO). Scale bar, 60µm.

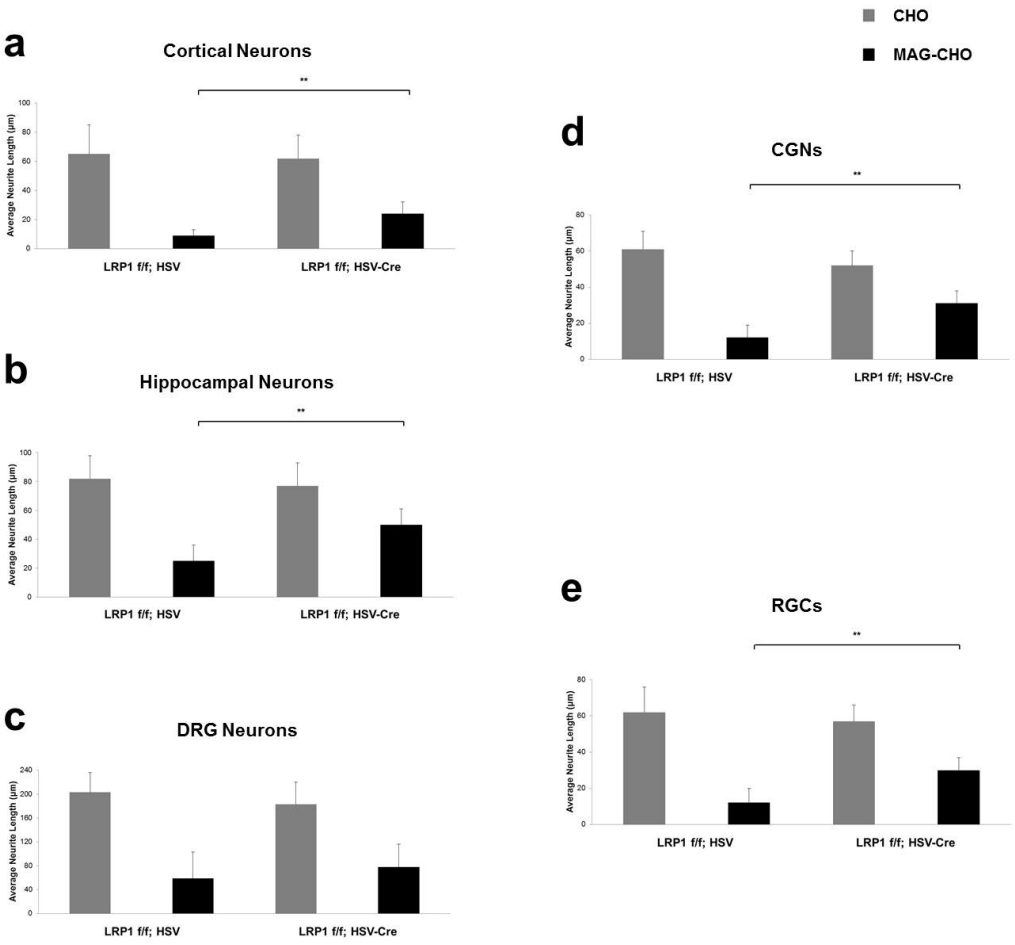

Figure 4.3: HSV-Cre transduction of *LRP1*$^{f/f}$ neurons releases MAG inhibition in a cell type-specific manner. (**a**) When infected with HSV-1-GFP-Cre, LRP1 floxed cortical neurons (*LRP1*$^{f/f}$; HSV-Cre) show a significant release of MAG-mediated growth inhibition compared to neurons infected with HSV-1-GFP (*LRP1*$^{f/f}$; HSV). On control CHO cells, neurite length of both groups is comparable. Similar results are seen in (**b**) hippocampal neurons, (**d**) CGNs, and (**e**) RGCs. (**c**) *LRP1*$^{f/f}$ DRG neurons, however, are as equally inhibited on MAG with HSV-1-GFP-Cre infection as with HSV-1-GFP infection. Importantly, LRP1 levels are substantially decreased in all five cell types when HSV-1-GFP-Cre is added (data not shown). At least 80 neurites of TuJ1-labeled cells were counted per condition (n=4 independent experiments for cortical neurons, n=3 experiments for hippocampal neurons, n=4 experiments for DRG neurons, n=4 experiments for CGNs, n=3 experiments for RGCs). Results are presented as mean ±SEMs. ** $P< 0.01$ (one-way ANOVA, Tukey's *post hoc*). Gray bars (CHO); black bars (MAG-CHO).

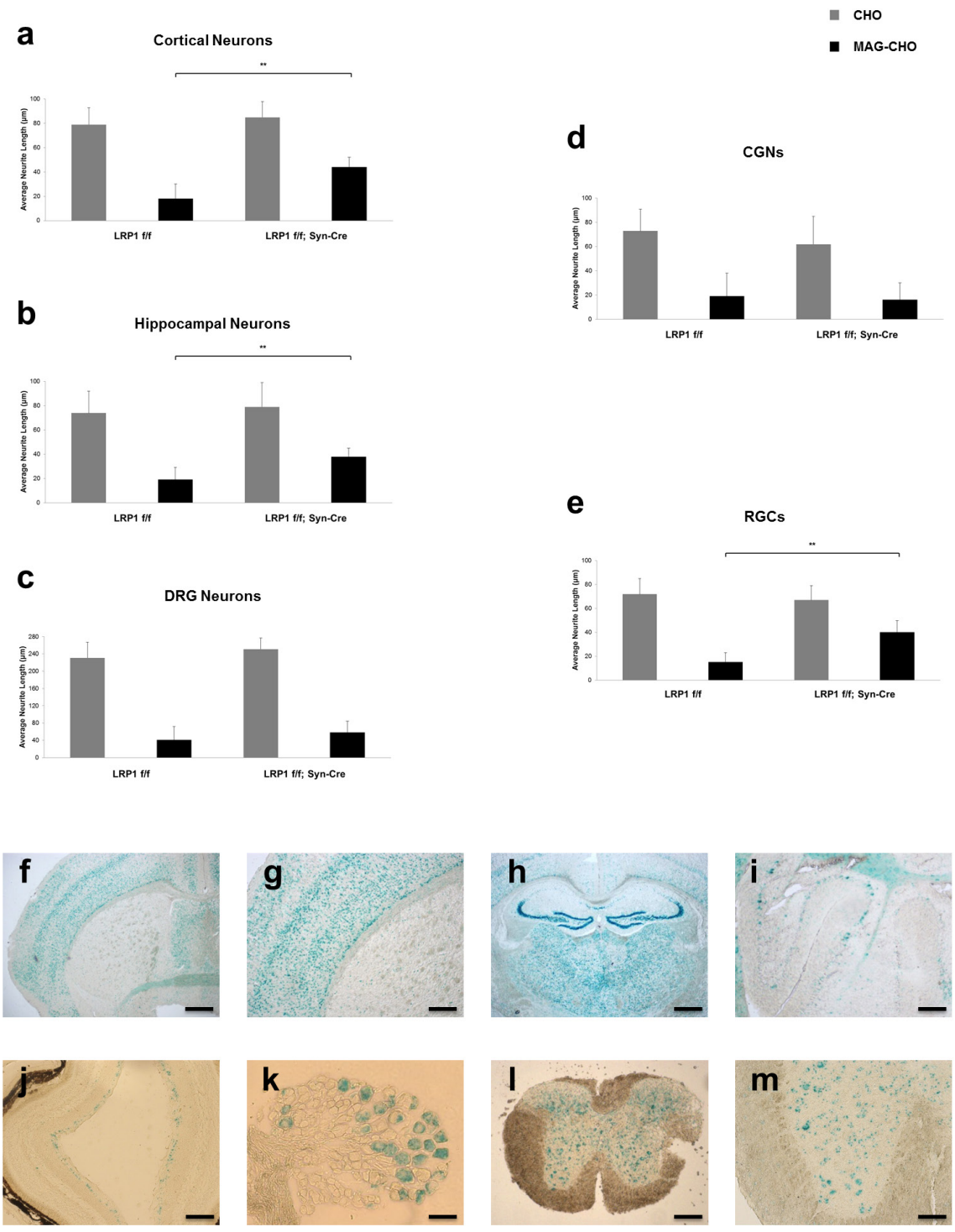

Figure 4.4: *LRP1*$^{f/f}$; Syn-Cre neurons show release of MAG inhibition in a cell type-specific manner. (**a**) Cortical neurons from *LRP1*$^{f/f}$ mice expressing Cre under the Synapsin I promoter

(*LRP1*$^{f/f}$; Syn-Cre) show a significant release of MAG growth inhibition compared to *LRP1*$^{f/f}$ control neurons. On control CHO cells, neurite length of both groups is comparable. Similar results are seen in (**b**) hippocampal neurons and (**e**) RGCs, but not in (**c**) DRG neurons or (**d**) CGNs. At least 100 neurites of TuJ1-labeled cells were counted per condition (n=4 independent experiments for cortical neurons, n=4 experiments for hippocampal neurons, n=3 experiments for DRG neurons, n=4 experiments for CGNs, n=3 experiments for RGCs). Results are presented as mean ±SEMs. ** $P< 0.01$ (one-way ANOVA, Tukey's *post hoc*). Gray bars (CHO); black bars (MAG-CHO). (**f-m**) X-Gal labeling of tissue from 3-week-old ROSA; Synapsin I-Cre mice reveals strong Cre expression in coronal sections of the brain, including (**f-g**) multiple layers of the cortex and (**h**) the dentate gyrus and CA3 regions of the hippocampus. Note the lack of expression in the white matter; in particular, the corpus callosum. (**i**) Strikingly, the cerebellum shows miminal levels of Cre expression. (**j**) The RGC layer of the retina, (**k**) a small subset of DRG neurons, and (**l-m**) a large number of cells in the gray matter of the spinal cord [including motor neurons of the anterior horn – best visualized in (**m)**] show expression as well. Scale bar: f, 500μm; g, 200μm; h, 500μm; i, 500μm; j, 500μm; k, 50μm; l, 500μm; m, 200μm.

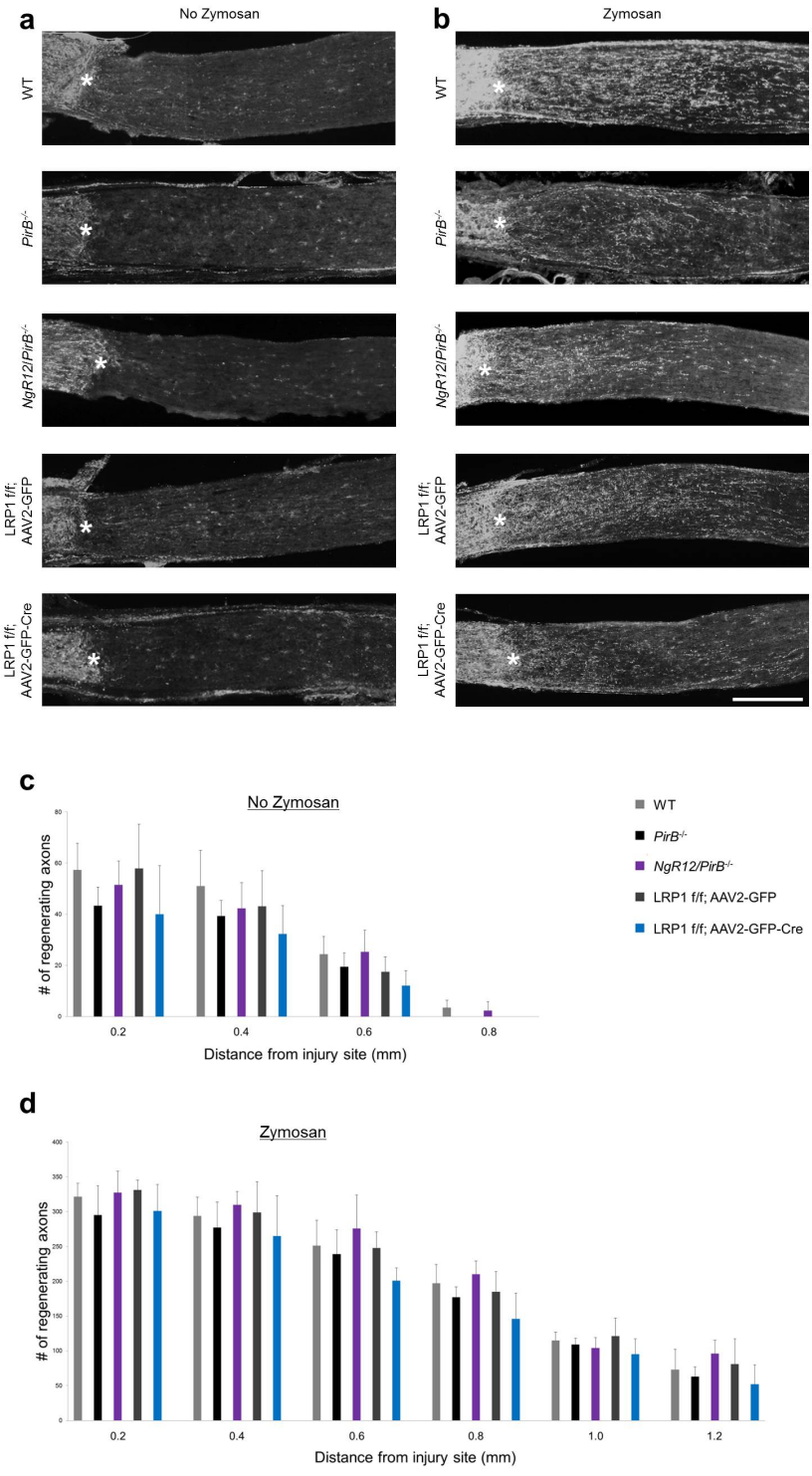

Figure 4.5: Loss of multiple MAG receptors is not sufficient to enhance axon regeneration following retro-orbital optic nerve crush injury. (**a**) 2 weeks following optic nerve injury, regenerative axonal growth was assessed by GAP-43 immunolabeling of longitudinal optic nerve

sections. GAP-43 immunolabeling of injured optic nerve from WT, *PirB*$^{-/-}$, and *NgR12/PirB*$^{-/-}$ mice fails to identify regenerative growth of axons beyond the lesion site (asterisk). Similarly, *LRP1*$^{f/f}$ mice with intravitreal injections of AAV2-GFP or AAV2-GFP-Cre show no substantial axon regeneration. (**b**) To test whether growth-activated RGCs show an additive regenerative effect when combined with genetic ablation of MAG receptors, a separate group of animals received an intravitreal injection of Zymosan at the time of optic nerve injury. Following Zymosan injection, *PirB*$^{-/-}$, *NgR12/PirB*$^{-/-}$ *LRP1*$^{f/f}$; AAV2-GFP, and *LRP1*$^{f/f}$; AAV2-GFP-Cre mice do not show enhanced regeneration compared to WT mice with Zymosan. (**c**) Quantification of the number of GAP-43-positive axons at 0.2 to 0.8mm distal to the lesion site. Light gray bars (WT, n=5); black bars (*PirB*$^{-/-}$, n=6); purple bars (*NgR12/PirB*$^{-/-}$, n=5); dark gray bars (*LRP1*$^{f/f}$; AAV2-GFP, n=6); blue bars (*LRP1*$^{f/f}$; AAV2-GFP-Cre, n=6). (**d**) Quantification of the number of GAP-43-positive axons at 0.2 to 1.2mm distal to the lesion site in Zymosan-injected mice. Light gray bars (WT, n=5); black bars (*PirB*$^{-/-}$, n=5); purple bars (*NgR12/PirB*$^{-/-}$, n=5); dark gray bars (*LRP1*$^{f/f}$; AAV2-GFP, n=6); blue bars (*LRP1*$^{f/f}$; AAV2-GFP-Cre, n=5). Results are presented as mean ±SEMs. Scale bar, 200μm.

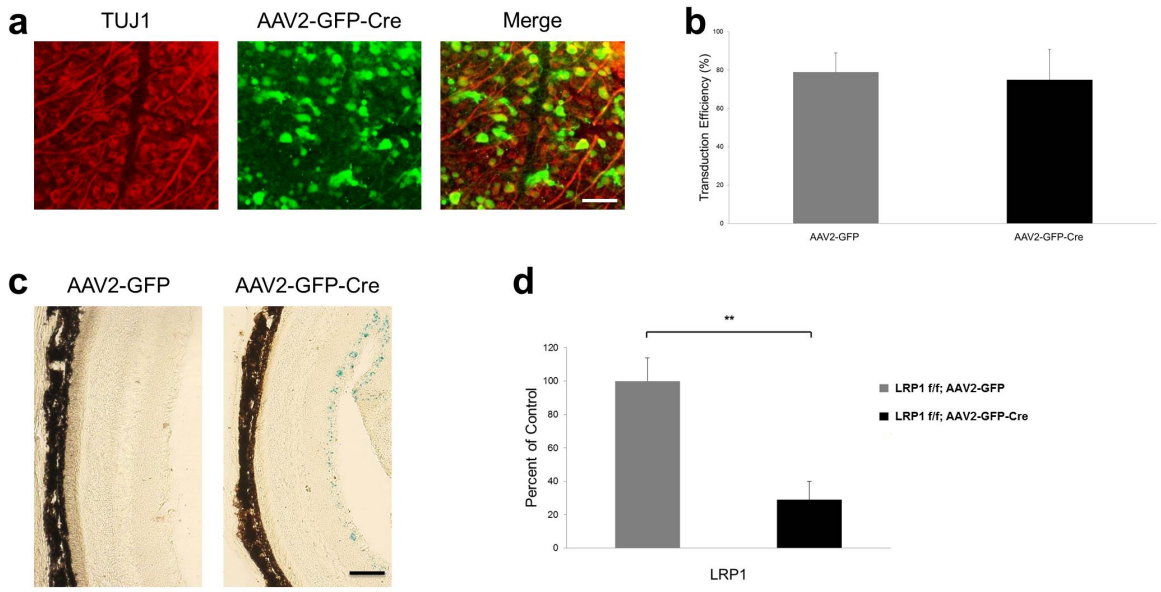

Figure 4.6: Intravitreal injection of AAV2-GFP-Cre reduces LRP1 levels in *LRP1*$^{f/f}$ mice. (**a**) 2 weeks following intravitreal injection of AAV2-GFP-Cre, retinal whole-mount preparations of *LRP1*$^{f/f}$ mice reveal several TuJ1-positive RGCs that are also GFP-positive. (**b**) Quantification of the RGC transduction efficiency of AAV2-GFP (gray bar) and AAV2-GFP-Cre (black bar). Transduction efficiency is calculated as the percentage of GFP/TuJ1-double positive cells, divided by the total number of TuJ1-positive cells. At least 500 TuJ1-labeled cells were counted per condition (n=4 eyes for AAV2-GFP, n=4 eyes for AAV2-GFP-Cre). Results are presented as mean ±SEMs. (**c**) X-Gal labeling of retina from *LRP1*$^{f/f}$ mice reveals strong Cre expression in the RGC layer when AAV2-GFP-Cre, but not AAV2-GFP, is injected into the eye. (**d**) Quantification of LRP1 protein levels in retinas from *LRP1*$^{f/f}$ mice receiving intravitreal injection of either AAV2-GFP (gray bar) or AAV2-GFP-Cre (black bar). Densitometric analysis of LRP1 bands was performed from 4 independent experiments and then normalized to β-actin levels. Results are presented as mean ±SEMs, and are shown as a percentage of the AAV2-GFP control. ** $P< 0.01$ (unpaired *t*-test). Scale bar: a, 60μm; c, 200μm.

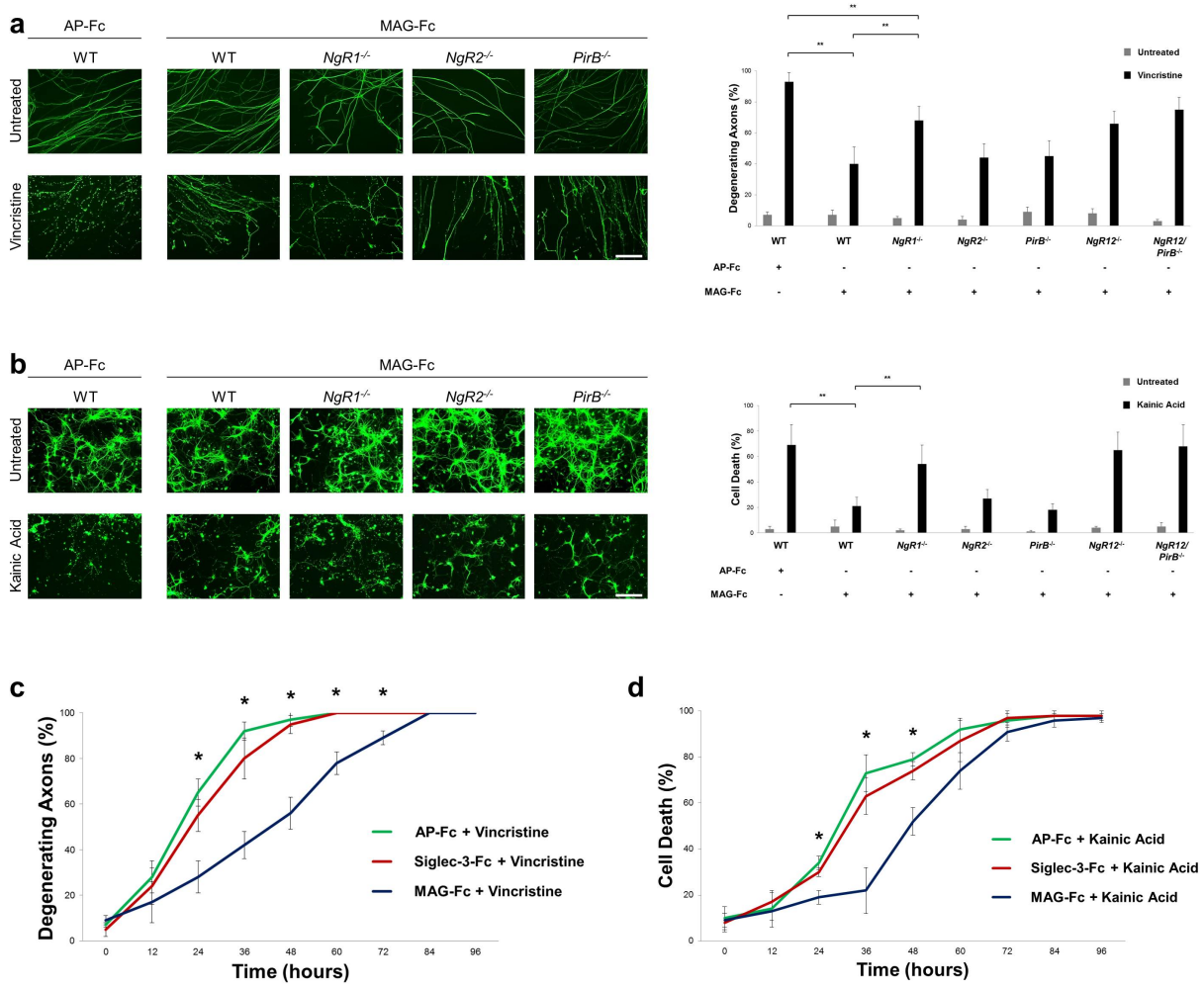

Figure 4.7: NgR1 mediates MAG protection from axonal degeneration and excitotoxicity. (**a**) 36 hours following treatment with 50nM vincristine sulfate, TuJ1-labeled DRG explants show signs of substantial axonal degeneration. In the presence of preclustered MAG-Fc, degeneration is significantly reduced in WT, *NgR2*$^{-/-}$, and *PirB*$^{-/-}$ explants. *NgR1*$^{-/-}$, *NgR12*$^{-/-}$, and *NgR12/PirB*$^{-/-}$ explants, however, are partially resistant to MAG-induced protection. The graph represents the percentage of axons with signs of degeneration (fragmentation or "blebbing"). At least 140 axons were counted per condition (n=6 independent experiments). Results are presented as mean ±SEMs. ** $P< 0.01$ (one-way ANOVA, Tukey's *post hoc*). Gray bars (Untreated); black bars (Vincristine). (**b**) 36 hours following treatment with 200μM kainic acid, TuJ1-labeled hippocampal neurons show signs of excitotoxicity and cell death. Neurons are also visualized for incorporation of propidium iodide (not shown). In the presence of preclustered MAG-Fc, cell death is significantly reduced in WT, *NgR2*$^{-/-}$, and *PirB*$^{-/-}$ neurons. *NgR1*$^{-/-}$, *NgR12*$^{-/-}$, and *NgR12/PirB*$^{-/-}$ neurons, however, are partially resistant to MAG-induced protection from cell death. The percentage of live cells (positive for TuJ1, negative for propidium iodide) was determined for each condition. At least 300 cells were counted per condition (n=5 independent experiments). Results are presented as mean ±SEMs. ** $P< 0.01$ (one-way

ANOVA, Tukey's *post hoc*). Gray bars (Untreated); black bars (Kainic Acid). Importantly, all genotypes show comparable levels of (**a**) vincristine-induced degeneration and (**b**) kainic acid-induced excitotoxicity in the presence of AP-Fc (data not shown). (**c**) Time course of vincristine-mediated axonal degeneration (50nM concentration) from 0-96 hours, in the presence of either preclustered AP-Fc, Siglec-3-Fc, or MAG-Fc. While there is no significant difference in degeneration between the AP-Fc and Siglec-3-Fc conditions, the addition of MAG-Fc is protective from 24-72 hours post-treatment with vincristine. At least 80 axons were counted per condition (n=4 independent experiments). Results are presented as mean ±SEMs. * $P< 0.01$ (one-way ANOVA, Tukey's *post hoc*; comparison between AP-Fc + Vincristine and MAG-Fc + Vincristine). Green line (AP-Fc + Vincristine); red line (Siglec-3-Fc + Vincristine); blue line (MAG-Fc + Vincristine). (**d**) Time course of kainic acid-mediated cell death (200μM concentration) from 0-96 hours, in the presence of either preclustered AP-Fc, Siglec-3-Fc, or MAG-Fc. While there is no significant difference in cell death between the AP-Fc and Siglec-3-Fc conditions, the addition of MAG-Fc is protective from 24-48 hours post-treatment with kainic acid. At least 150 cells were counted per condition (n=4 independent experiments). Results are presented as mean ±SEMs. * $P< 0.01$ (one-way ANOVA, Tukey's *post hoc*; comparison between AP-Fc + Vincristine and MAG-Fc + Vincristine). Green line (AP-Fc + Kainic Acid); red line (Siglec-3-Fc + Kainic Acid); blue line (MAG-Fc + Kainic Acid). Scale bar, 120μm.

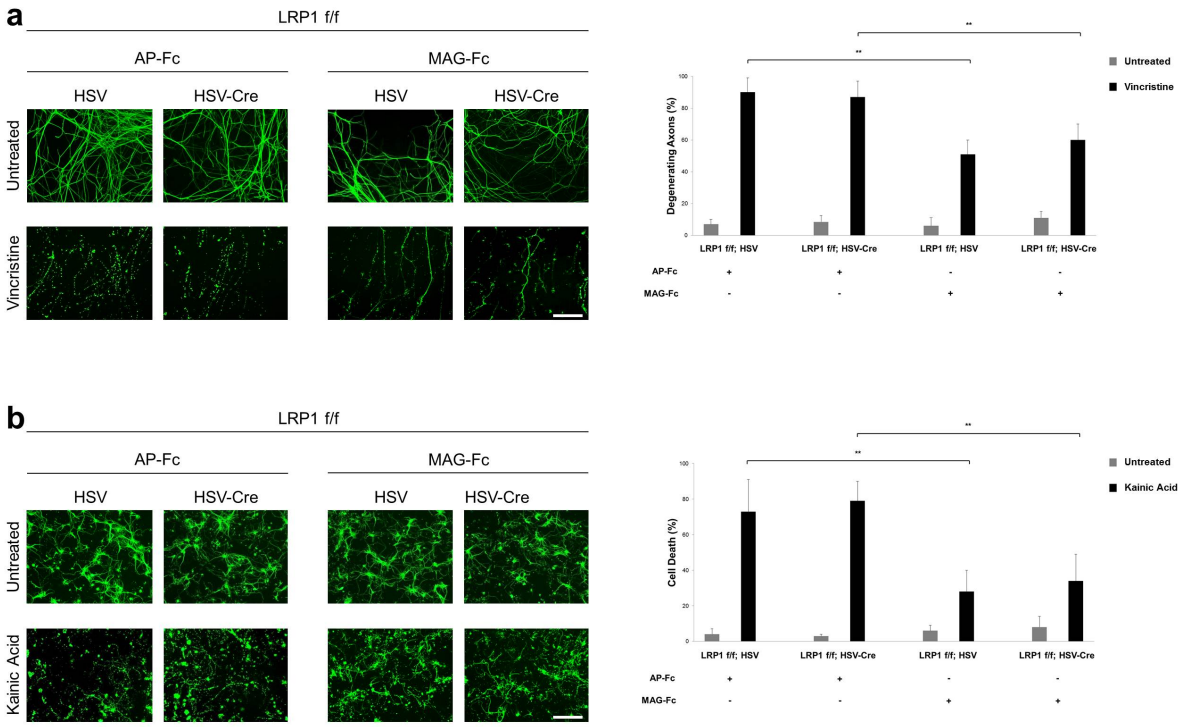

Figure 4.8: LRP1 is not necessary for MAG-mediated protection from axonal degeneration and excitotoxicity. (**a**) 36 hours following treatment with 50nM vincristine sulfate, LRP1 floxed DRG explants infected with HSV-1-GFP (*LRP1*$^{f/f}$; HSV) or HSV-1-GFP-Cre (*LRP1*$^{f/f}$; HSV-Cre) show comparable levels of degeneration. The addition of preclustered MAG-Fc reduces degeneration to a similar extent for both groups. The graph represents the percentage of axons with signs of degeneration (fragmentation or "blebbing"). At least 100 axons were counted per condition (n=4 independent experiments). Results are presented as mean ±SEMs. ** $P< 0.01$ (one-way ANOVA, Tukey's *post hoc*). Gray bars (Untreated); black bars (Vincristine). (**b**) 36 hours following treatment with 200μM kainic acid, *LRP1*$^{f/f}$; HSV and *LRP1*$^{f/f}$; HSV-Cre hippocampal neurons show comparable levels of cell death. The addition of preclustered MAG-Fc reduces cell death to a similar extent for both groups. The percentage of live cells (positive for TuJ1, negative for propidium iodide) was determined for each condition. At least 200 cells were counted per condition (n=4 independent experiments). Results are presented as mean ±SEMs. ** $P< 0.01$ (one-way ANOVA, Tukey's *post hoc*). Gray bars (Untreated); black bars (Kainic Acid). Scale bar, 120μm.

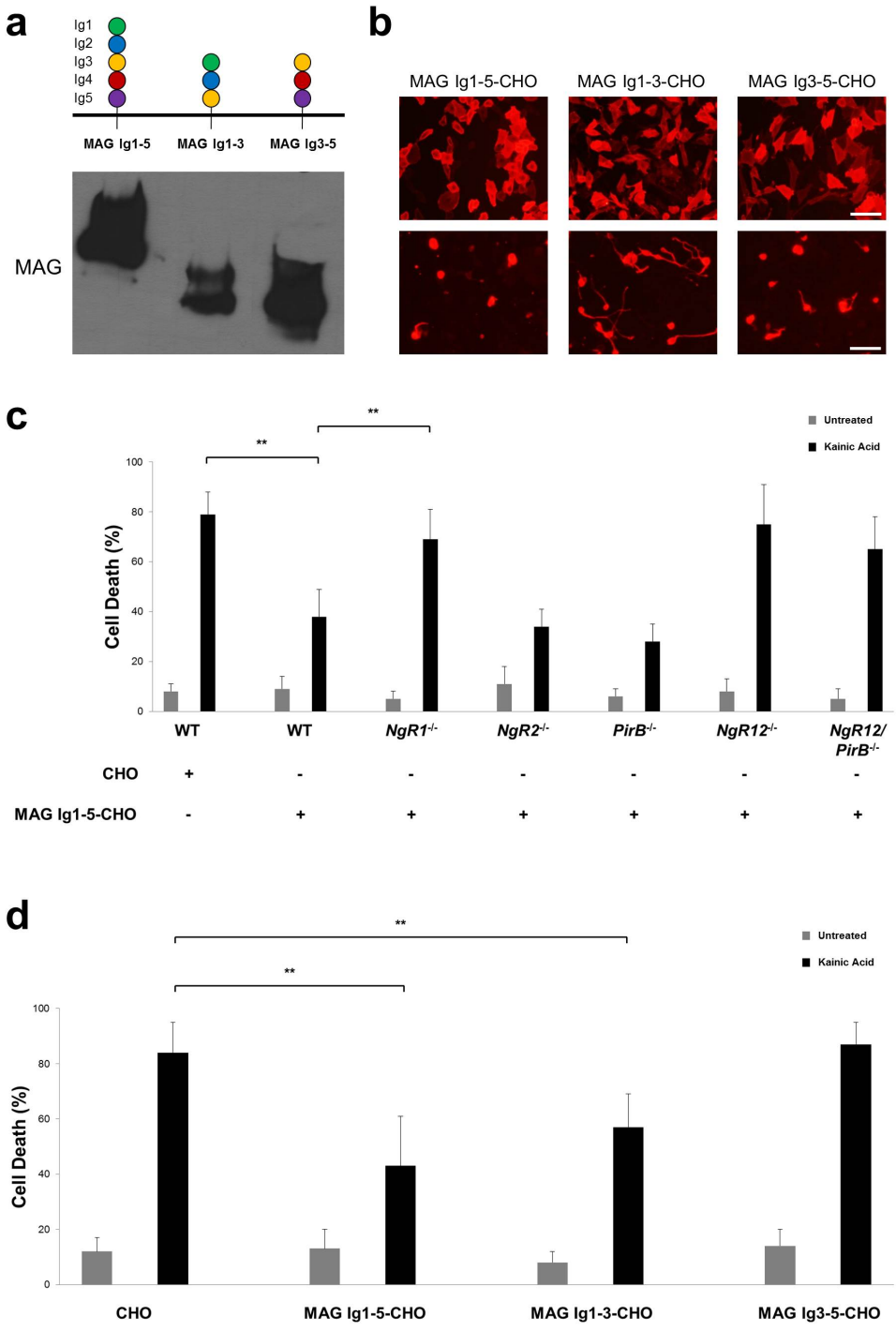

Figure 4.9: CHO cells expressing MAG Ig-like domains 1-5 or 1-3 confer protection from excitotoxicity. (**a**) Confirmation of MAG protein in CHO cell lines expressing variants of membrane-bound MAG. Immunoblotting of CHO cell lysates with a custom-made MAG antibody reveals a substantial drop in molecular weight when MAG Ig1-3-CHO and MAG Ig3-

5-CHO cell lysates are compared to the MAG Ig1-5-CHO cell lysates. Green circle (Ig-like domain 1); blue circle (Ig-like domain 2); orange circle (Ig-like domain 3); red circle (Ig-like domain 4); purple circle (Ig-like domain 5). (**b**) (Top) High levels of MAG are expressed on the surface of all CHO cell lines, as revealed by MAG immunostaining in the absence of Triton X-100. (Bottom) MAG Ig1-5-CHO and MAG Ig3-5-CHO cells, but not MAG Ig1-3-CHO cells, substantially inhibit outgrowth of TuJ1-labeled, P7 mouse hippocampal neurons. (**c**) When grown on MAG Ig1-5-CHO (but not CHO) feeder layers, kainic acid-induced cell death is significantly reduced in WT, *NgR2*$^{-/-}$, and *PirB*$^{-/-}$ hippocampal neurons. *NgR1*$^{-/-}$, *NgR12*$^{-/-}$, and *NgR12/PirB*$^{-/-}$ neurons, however, are completely resistant to MAG-induced protection from cell death. The percentage of live cells (positive for TuJ1, negative for propidium iodide) was determined for each condition. At least 200 cells were counted per condition (n=3 independent experiments). Results are presented as mean ±SEMs. ** $P< 0.01$ (one-way ANOVA, Tukey's *post hoc*). Gray bars (Untreated); black bars (Kainic Acid). (**d**) WT hippocampal neurons grown on MAG Ig1-5-CHO and MAG Ig1-3-CHO cells, but not CHO or MAG Ig3-5-CHO cells, are equally protected from kainic acid-induced cell death. The percentage of live cells (positive for TuJ1, negative for propidium iodide) was determined for each condition. At least 250 cells were counted per condition (n=3 independent experiments). Results are presented as mean ±SEMs. ** $P< 0.01$ (one-way ANOVA, Tukey's *post hoc*). Gray bars (Untreated); black bars (Kainic Acid). Scale bar, 50μm.

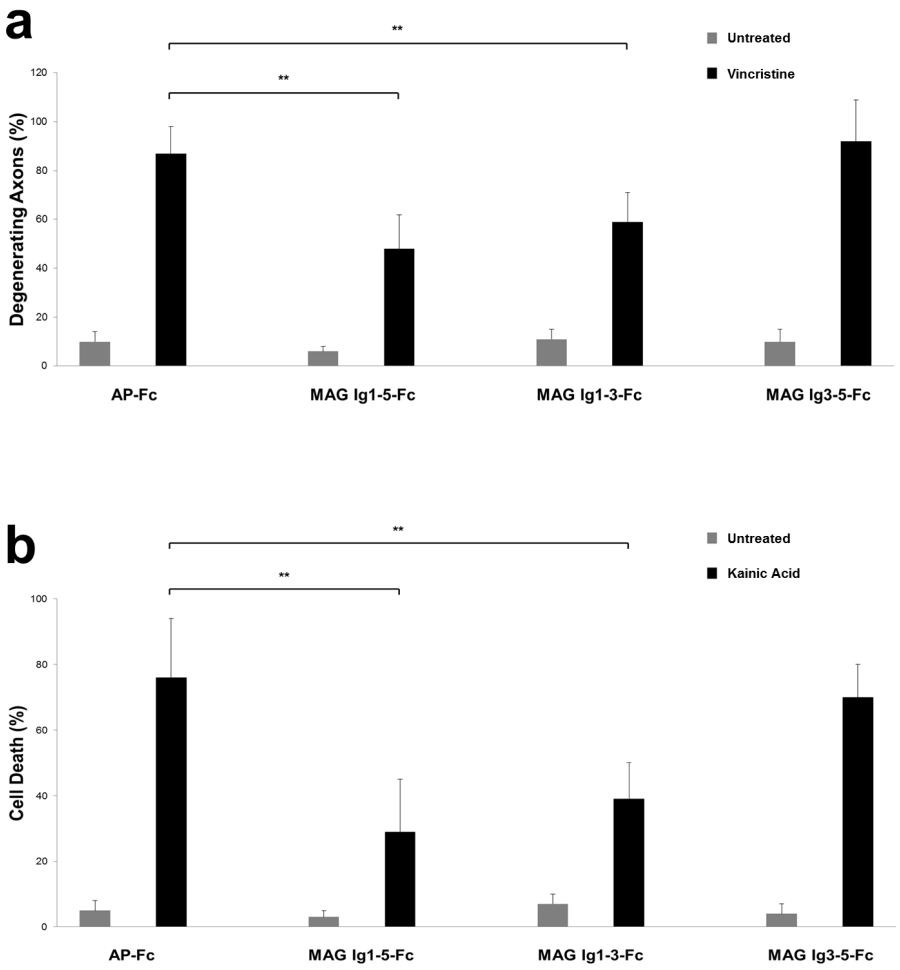

Figure 4.10: MAG Ig-like domains 1-5 and 1-3, but not 3-5, are sufficient to confer protection from axonal degeneration and excitotoxicity. (**a**) WT DRG explants treated with MAG Ig1-5-Fc or MAG Ig1-3-Fc, but not AP-Fc or MAG Ig3-5-Fc, are equally protected from vincristine sulfate-induced axonal degeneration. At least 100 axons were counted per condition (n=4 independent experiments). Results are presented as mean ±SEMs. ** $P< 0.01$ (one-way ANOVA, Tukey's *post hoc*). Gray bars (Untreated); black bars (Vincristine). (**b**) WT hippocampal neurons treated with MAG Ig1-5-Fc or MAG Ig1-3-Fc, but not AP-Fc or MAG Ig3-5-Fc, are equally protected from kainic acid-induced cell death. The percentage of live cells (positive for TuJ1, negative for propidium iodide) was determined for each condition. At least 200 cells were counted per condition (n=3 independent experiments). Results are presented as mean ±SEMs. ** $P< 0.01$ (one-way ANOVA, Tukey's *post hoc*). Gray bars (Untreated); black bars (Kainic Acid).

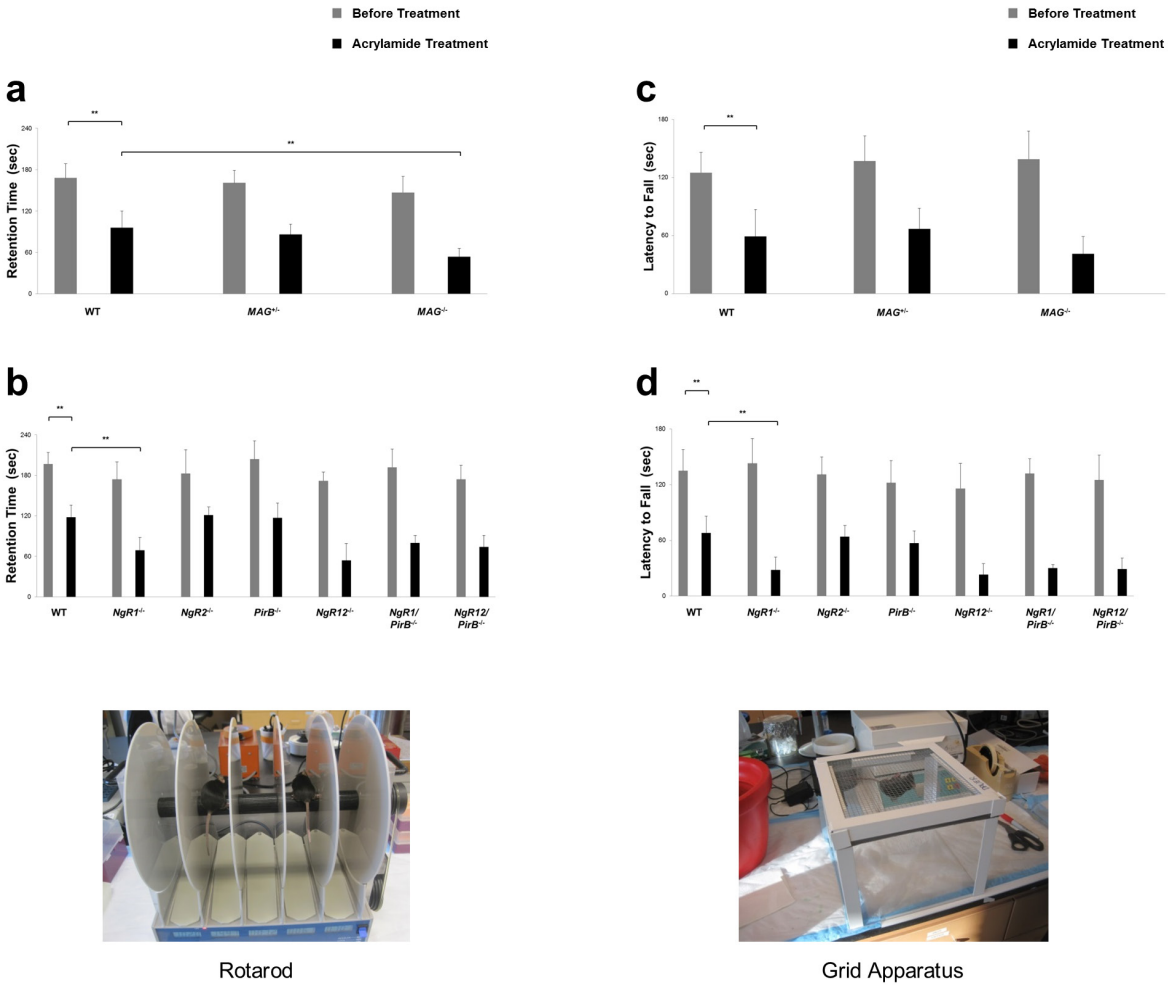

Figure 4.11: *MAG*$^{-/-}$ and *NgR1*$^{-/-}$ mice show increased susceptibility to acrylamide-induced behavioral deficits. (**a**) *MAG*$^{-/-}$ (but not *MAG*$^{+/+}$ or *MAG*$^{+/-}$) mice display substantially reduced retention times on an accelerating rotarod (post-training), following 2 weeks of acrylamide administration (400 parts per million). *MAG*$^{+/+}$ (WT): n=7 mice, *MAG*$^{+/-}$: n=5 mice, *MAG*$^{-/-}$: n=9 mice. (**b**) Similarly, *NgR1*$^{-/-}$, *NgR12*$^{-/-}$, *NgR1/PirB*$^{-/-}$, and *NgR12/PirB*$^{-/-}$ mice, but not *NgR2*$^{-/-}$ or *PirB*$^{-/-}$ mice, display reduced retention times following acrylamide treatment when compared to WT controls. WT: n=8 mice, *NgR1*$^{-/-}$: n=11 mice, *NgR2*$^{-/-}$: n=8 mice, *PirB*$^{-/-}$: n=10 mice, *NgR12*$^{-/-}$: n=7 mice, *NgR1/PirB*$^{-/-}$: n=11 mice, *NgR12/PirB*$^{-/-}$: n=4 mice. Results are presented as mean ±SEMs. ** $P< 0.01$ (one-way ANOVA, Tukey's *post hoc*). Gray bars (Before Treatment); black bars (Acrylamide Treatment). (**c**) *MAG*$^{+/+}$, *MAG*$^{+/-}$, and *MAG*$^{-/-}$ mice have comparable performances on the grid apparatus (measured as the latency to fall), following 2 weeks of acrylamide administration. It should be noted, however, that *MAG*$^{-/-}$ mice show a trend toward a decreased latency to fall. *MAG*$^{+/+}$ (WT): n=6 mice, *MAG*$^{+/-}$: n=7 mice, *MAG*$^{-/-}$: n=9 mice. (**d**) *NgR1*$^{-/-}$, *NgR12*$^{-/-}$, *NgR1/PirB*$^{-/-}$, and *NgR12/PirB*$^{-/-}$ mice, but not *NgR2*$^{-/-}$ or *PirB*$^{-/-}$ mice, show a decreased latency to fall from the grid apparatus following acrylamide treatment when compared to WT controls. WT: n=7 mice, *NgR1*$^{-/-}$: n=9 mice, *NgR2*$^{-/-}$: n=7 mice, *PirB*$^{-/-}$: n=8 mice,

NgR12$^{-/-}$: n=7 mice, *NgR1/PirB*$^{-/-}$: n=9 mice, *NgR12/PirB*$^{-/-}$: n=5 mice. Results are presented as mean ±SEMs. ** $P< 0.01$ (one-way ANOVA, Tukey's *post hoc*). Gray bars (Before Treatment); black bars (Acrylamide Treatment). In (**a-d**), there are no differences between the genotypes before treatment with acrylamide.

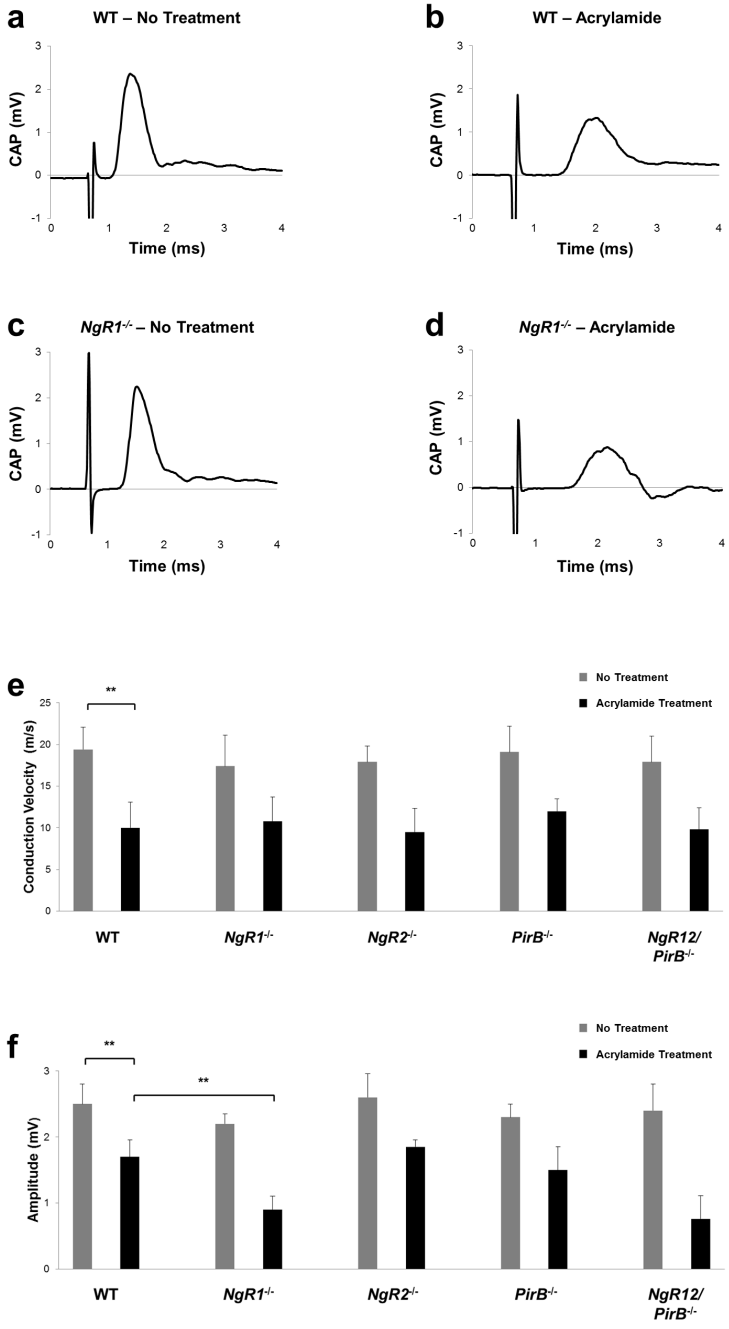

Figure 4.12: *NgR1*$^{-/-}$ mice show increased susceptibility to acrylamide-induced degeneration of the sciatic nerve. (**a-d**) Representative compound action potential (CAP) recordings of the sciatic nerve (tibial branch) from a (**a**) WT mouse, (**b**) WT mouse with 2 weeks of acrylamide treatment (400 parts per million), (**c**) *NgR1*$^{-/-}$ mouse, and (**d**) *NgR1*$^{-/-}$ mouse with acrylamide treatment. The first spike represents the artifact, while the major peak represents the myelinated component of the nerve. (**e**) While a significant decrease in conduction velocity is seen in all animals treated with acrylamide, there is no additional decrease in any of the mutant mice.

Conduction velocity is calculated as the length of the nerve divided by the time-to-peak. (**f**) All animals show a significant decrease in peak amplitude with acrylamide administration; however, *NgR1*$^{-/-}$ and *NgR12/PirB*$^{-/-}$ mice, but not *NgR2*$^{-/-}$ or *PirB*$^{-/-}$ mice, display an even further reduction than WT controls. At least 3 animals were used for every condition (1 or 2 nerves recorded per mouse). No Treatment - WT: n=4 nerves, *NgR1*$^{-/-}$: n=4 nerves, *NgR2*$^{-/-}$: n=3 nerves, *PirB*$^{-/-}$: n=4 nerves, *NgR12/PirB*$^{-/-}$: n=4 nerves. Acrylamide Treatment - WT: n=4 nerves, *NgR1*$^{-/-}$: n=5 nerves, *NgR2*$^{-/-}$: n=3 nerves, *PirB*$^{-/-}$: n=4 nerves, *NgR12/PirB*$^{-/-}$: n=3 nerves. Results are presented as mean ±SEMs. ** $P< 0.01$ (one-way ANOVA, Tukey's *post hoc*). Gray bars (No Treatment); black bars (Acrylamide Treatment).

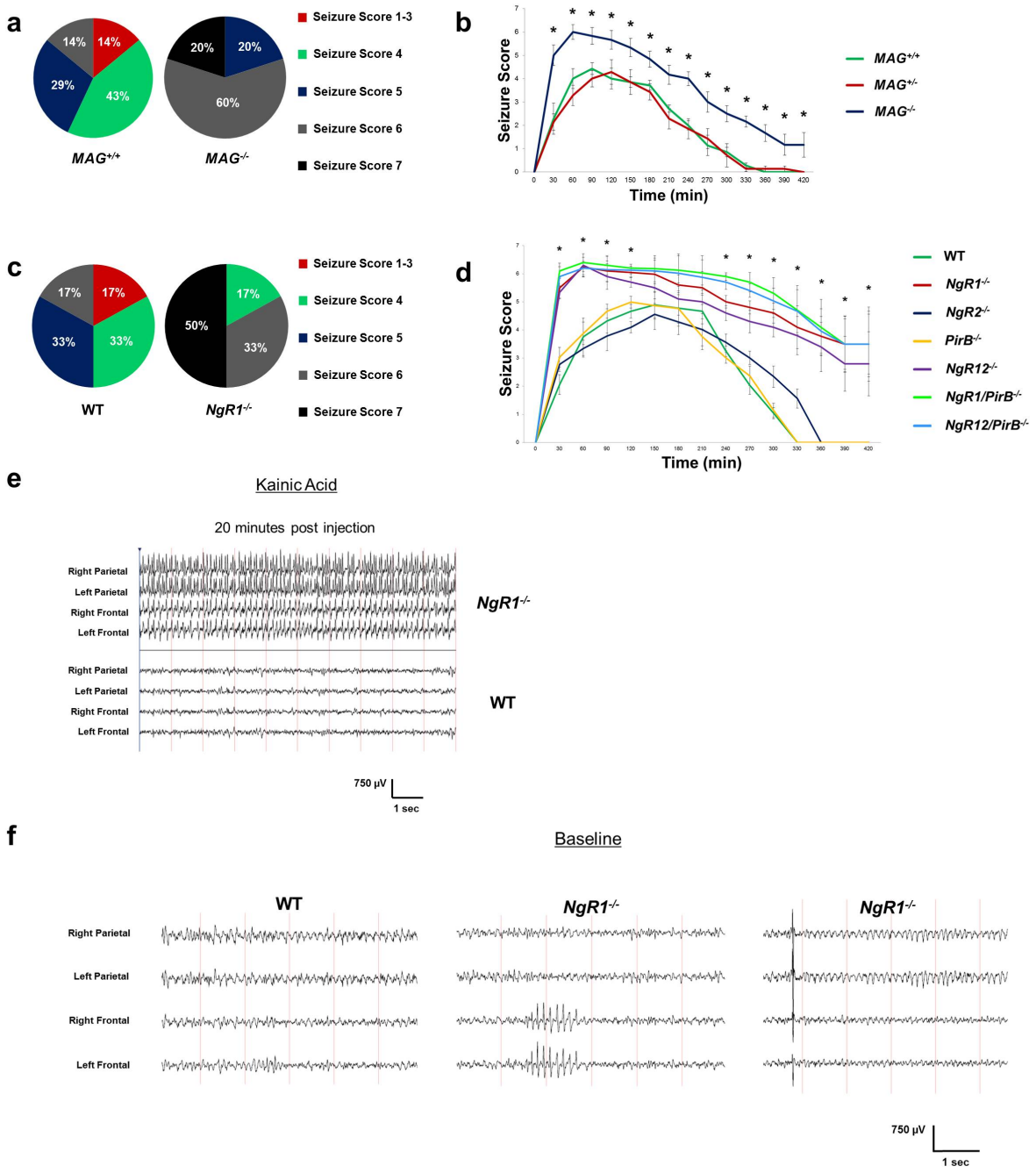

Figure 4.13: *MAG*$^{-/-}$ and *NgR1*$^{-/-}$ mice show increased susceptibility to kainic acid-induced seizures. (**a**) Following intraperitoneal injection of 25mg/kg kainic acid, *MAG*$^{-/-}$ mice (n=10) develop higher seizure severity scores than *MAG*$^{+/+}$ mice (n=14). The percentage of mice that reach a given seizure score as their maximum is shown. Scores are rated as follows: (0) normal behavior; (1 - red) exploring, sniffing, and grooming have ceased and the animal is motionless; (2 - red) forelimb and/or tail extension, giving the appearance of a rigid posture; (3 - red) myoclonic jerks of the head and neck, with brief twitching or repetitive movements; (4 - green)

forelimb clonus and partial rearing; (5 - blue) forelimb clonus, rearing, and falling; (6 - gray) generalized tonic-clonic activity; and (7 - black) death. (**b**) Comparison of seizure scores for the period of 7 hours following 25mg/kg kainic acid injection. *MAG*$^{-/-}$ mice (blue line, n=10) show a significant increase in seizure scores at multiple time points when compared to *MAG*$^{+/+}$ (green line, n=14) or *MAG*$^{+/-}$ mice (red line, n=8). Results are presented as mean ±SEMs. * $P< 0.01$ (one-way ANOVA, Tukey's *post hoc*; comparison between *MAG*$^{-/-}$ mice and *MAG*$^{+/+}$ mice). (**c**) Following injection of kainic acid, *NgR1*$^{-/-}$ mice (n=12) develop higher seizure severity scores than WT controls (n=12). (**d**) Comparison of seizure scores for the period of 7 hours following 25mg/kg kainic acid injection. *NgR1*$^{-/-}$ (red line, n=11), *NgR12*$^{-/-}$ (purple line, n=8), *NgR1/PirB*$^{-/-}$ (light green line, n=12), and *NgR12/PirB*$^{-/-}$ mice (light blue line, n=9), but not *NgR2*$^{-/-}$ (blue line, n=11) or *PirB*$^{-/-}$ mice (orange line, n=12), show a significant increase in seizure scores at multiple time points when compared to WT controls (green line, n=12). Results are presented as mean ±SEMs. * $P< 0.01$ (one-way ANOVA, Tukey's *post hoc*; comparison between *NgR1*$^{-/-}$ mice and WT mice). (**e**) Representative EEG traces from an *NgR1*$^{-/-}$ and WT control mouse, 20 minutes following injection of 15mg/kg kainic acid. The *NgR1*$^{-/-}$ animal, but not the WT control, displays synchronized, high-voltage (>750μV), fast-spiking waves (generalized seizures). (**f**) Representative, baseline EEG traces from an *NgR1*$^{-/-}$ and WT control mouse. The *NgR1*$^{-/-}$ animal displays semi-periodic epileptiform discharges exceeding 750μV (second and third traces), often associated with myoclonic jerks.

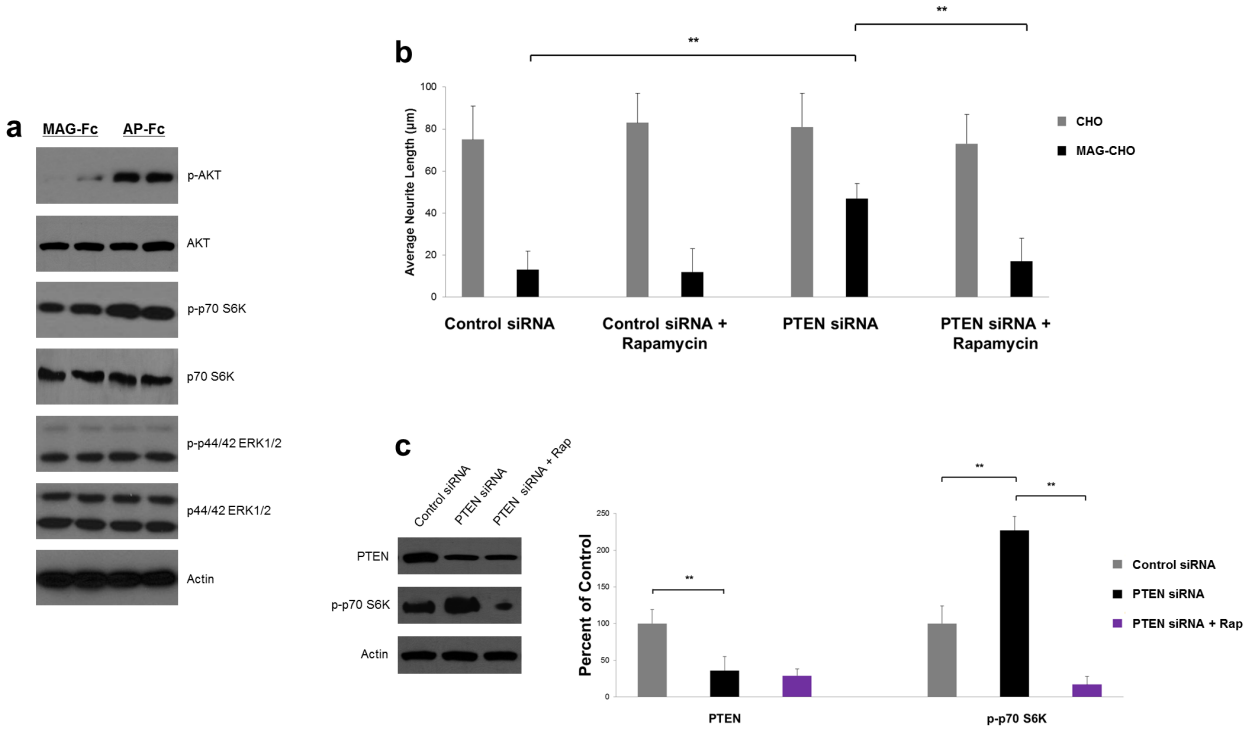

Figure 4.14: Silencing of PTEN significantly releases MAG-mediated inhibition of CGNs. (**a**) Treatment of primary mouse CGNs (cultured *in vitro* for 14 days) with MAG-Fc results in a substantial decrease of p-AKT (Ser473) and p-p70 S6 kinase (Thr389) levels, but not p-p44/42 ERK1/2 (Thr202/Tyr204) levels. Total levels of these proteins remain unchanged. β-actin is shown as a loading control for all CGN lysates. This experiment was repeated four times, with both treatments performed in duplicate for each experiment. (**b**) CGNs expressing PTEN siRNA, but not CGNs expressing a non-targeting control siRNA, show a significant release of MAG inhibition when plated on MAG-CHO feeder layers, an effect that is reversed with rapamycin treatment (25nM). All groups show comparable growth on control CHO feeder layers. At least 200 neurites of TuJ1-labeled cells were counted per condition (n=5 independent experiments). Results are presented as mean ±SEMs. ** $P< 0.01$ (one-way ANOVA, Tukey's *post hoc*). Gray bars (CHO); black bars (MAG-CHO). (**c**) Immunoblotting analysis from CGN lysates confirms that PTEN siRNA-transfected cells show a significant decrease in PTEN levels and subsequent increase in p-p70 S6 kinase levels. While rapamycin (Rap) treatment does not affect PTEN levels, it does significantly decrease p-p70 S6 kinase levels. For quantification, densitometric analysis of PTEN bands and p-p70 S6 kinase bands from 4 independent experiments was performed and then normalized to β-actin levels. Results are presented as mean ±SEMs, and are shown as a percentage of the control siRNA condition. ** $P< 0.01$ (one-way ANOVA, Tukey's *post hoc*). Gray bars (Control siRNA); black bars (PTEN siRNA); purple bars (PTEN siRNA + Rap).

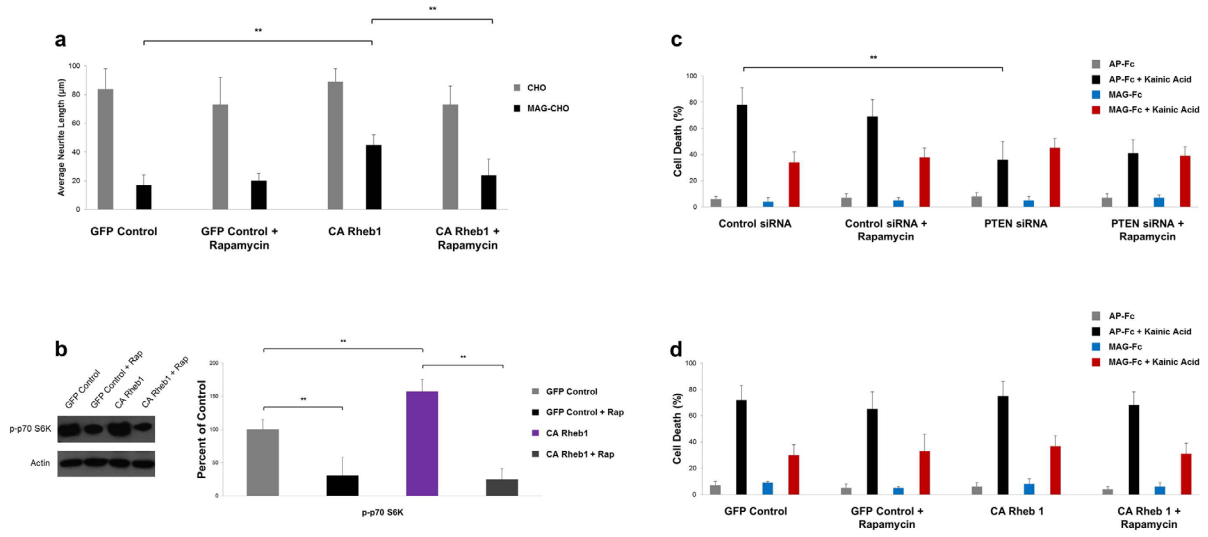

Figure 4.15: MAG negatively regulates the PI3K-AKT-mTOR pathway to inhibit neurite outgrowth, but not to protect from excitotoxicity. (**a**) CGNs expressing a constitutively active form of Rheb1 (CA Rheb1), but not CGNs expressing a GFP control, show a significant release of MAG inhibition when plated on MAG-CHO feeder layers, an effect that is reversed with rapamycin treatment (25nM). All groups show comparable growth on control CHO feeder layers. At least 150 neurites of TuJ1-labeled cells were counted per condition (n=4 independent experiments). Results are presented as mean ±SEMs. ** $P< 0.01$ (one-way ANOVA, Tukey's *post hoc*). Gray bars (CHO); black bars (MAG-CHO). (**b**) Immunoblotting analysis from CGN lysates confirms that CA Rheb1-transfected cells show a significant increase in p-p70 S6 kinase levels, while rapamycin (Rap) treatment significantly decreases p-p70 S6 kinase levels. For quantification, densitometric analysis of p-p70 S6 kinase bands from 4 independent experiments was performed and then normalized to β-actin levels. Results are presented as mean ±SEMs, and are shown as a percentage of the GFP control condition. ** $P< 0.01$ (one-way ANOVA, Tukey's *post hoc*). Gray bars (GFP Control); black bars (GFP Control + Rap); purple bars (CA Rheb1); dark gray bars (CA Rheb1 + Rap). (**c**) In the presence of MAG-Fc, kainic acid-induced cell death of mouse hippocampal neurons is significantly reduced. Similarly, hippocampal neurons expressing PTEN siRNA show a significant reduction in cell death, which is not additive with MAG-Fc or affected by rapamycin treatment (25nM). The percentage of live cells (positive for TuJ1, negative for propidium iodide) was determined for each condition. At least 200 cells were counted per condition (n=4 independent experiments). Results are presented as mean ±SEMs. ** $P< 0.01$ (one-way ANOVA, Tukey's *post hoc*). Gray bars (AP-Fc); black bars (AP-Fc + Kainic Acid); blue bars (MAG-Fc); red bars (MAG-Fc + Kainic Acid). (**d**) Hippocampal neurons expressing CA Rheb show no change in kainic acid-induced cell death. The percentage of live cells (positive for TuJ1, negative for propidium iodide) was determined for each condition. At least 200 cells were counted per condition (n=4 independent experiments). Results are presented as mean ±SEMs. Gray bars (AP-Fc); black bars (AP-Fc + Kainic Acid); blue bars (MAG-Fc); red bars (MAG-Fc + Kainic Acid).

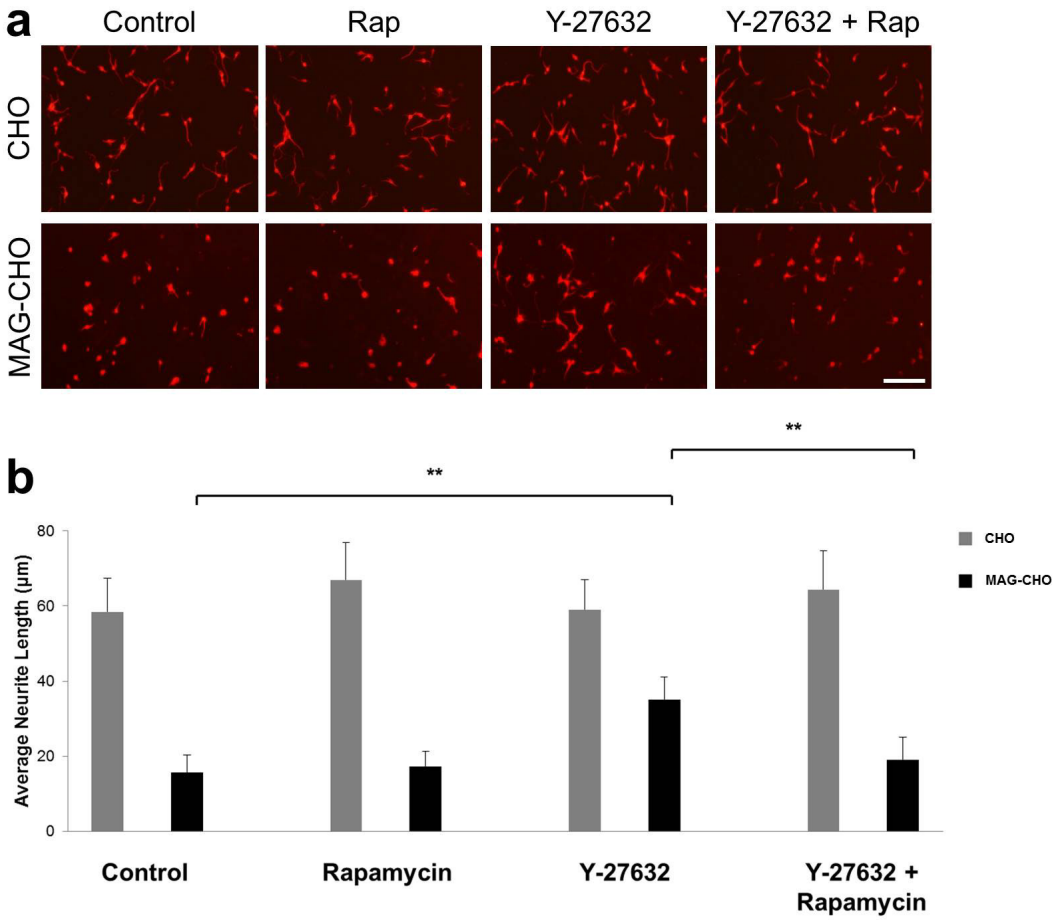

Figure 4.16: Rapamycin treatment blocks the release of MAG growth inhibition by Y-27632. (**a**) WT P7 CGNs are strongly inhibited when plated on MAG-CHO cell feeder layers; however, addition of the ROCK inhibitor Y-27632 (15µM) leads to a substantial release of growth inhibition. Concurrent treatment with rapamycin (Rap; 25nM) completely blocks this release. On control CHO cells, neurite length of all groups is comparable. (**b**) Quantification of neurite length. At least 200 neurites of TuJ1-labeled cells were counted per condition (n=6 independent experiments). Results are presented as mean ±SEMs. ** $P< 0.01$ (one-way ANOVA, Tukey's *post hoc*). Gray bars (CHO); black bars (MAG-CHO). Scale bar, 100µm.

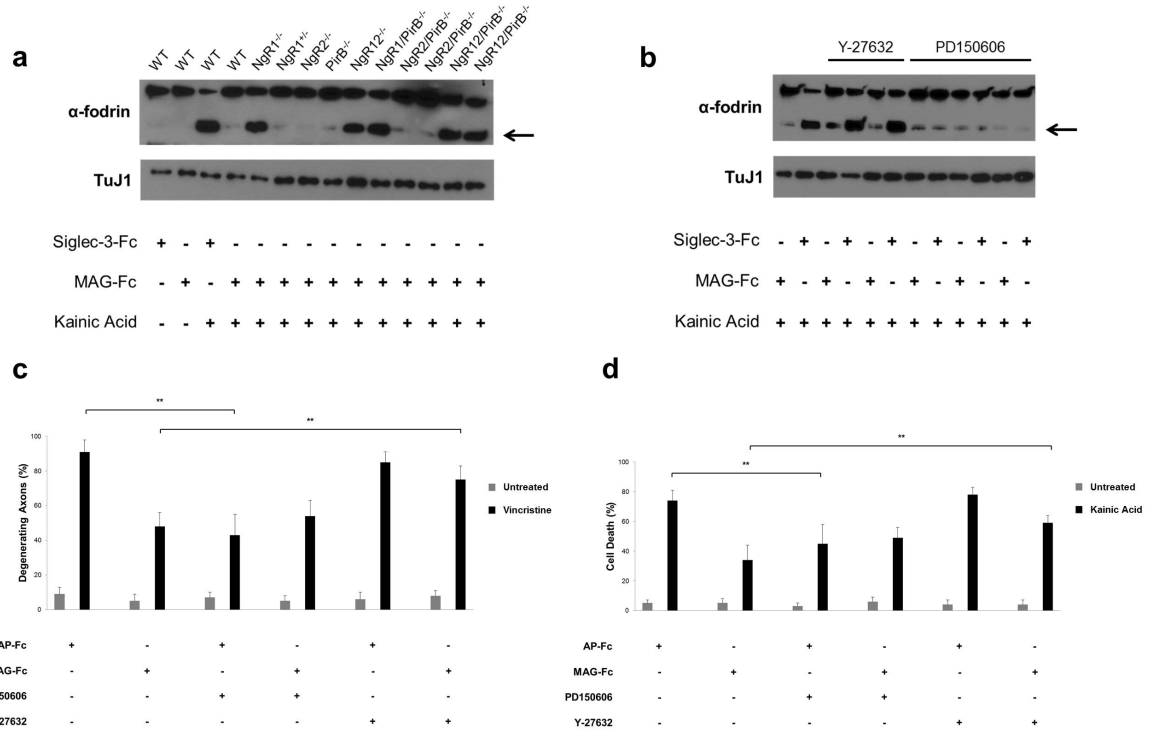

Figure 4.17: MAG inhibits calpain-induced cleavage of α-fodrin during toxic insult. (**a**) Treatment of primary mouse hippocampal neurons (cultured *in vitro* for 14 days) with 200μM kainic acid for 4 hours results in substantial cleavage of α-fodrin (arrow). Pretreatment of neurons with MAG-Fc for 30 minutes, however, largely prevents cleavage, leaving more of the unprocessed form (top band). *NgR1*$^{-/-}$, *NgR12*$^{-/-}$, *NgR1/PirB*$^{-/-}$, and *NgR12/PirB*$^{-/-}$ hippocampal neurons, but not *NgR1*$^{+/-}$, *NgR2*$^{-/-}$, *PirB*$^{-/-}$, or *NgR2/PirB*$^{-/-}$ neurons, show substantial restoration of α-fodrin cleavage in the presence of MAG-Fc. (**b**) Inhibition of calpain with 10μM PD150606 largely prevents kainic acid-induced cleavage of α-fodrin. Inhibition of ROCK with 15μM Y-27632, however, has no effect on MAG-mediated prevention of α-fodrin cleavage. TuJ1 is shown as a loading control for all hippocampal neuron lysates. The results shown in (**a**) were confirmed from 3 independent experiments, and the results shown in (**b**) were confirmed from 5 independent experiments. (**c**) Treatment of WT DRG explants with 10μM PD150606 significantly reduces vincristine-induced axonal degeneration, similar to treatment with MAG-Fc. MAG-Fc-mediated protection, however, is largely abrogated with addition of 15μM Y-27632 to the cultures. The graph represents the percentage of axons with signs of degeneration (fragmentation or "blebbing"). At least 100 axons were counted per condition (n=4 independent experiments). Results are presented as mean ±SEMs. ** $P< 0.01$ (one-way ANOVA, Tukey's *post hoc*). Gray bars (Untreated); black bars (Vincristine). (**d**) Similar results to (**c**) are seen when these experiments are repeated in the context of kainic acid-induced cell death of WT hippocampal neurons. The percentage of live cells (positive for TuJ1, negative for propidium iodide) was determined for each condition. At least 200 cells were counted per condition (n=4 independent experiments). Results are presented as mean ±SEMs. ** $P< 0.01$ (one-way ANOVA, Tukey's *post hoc*). Gray bars (Untreated); black bars (Kainic Acid).

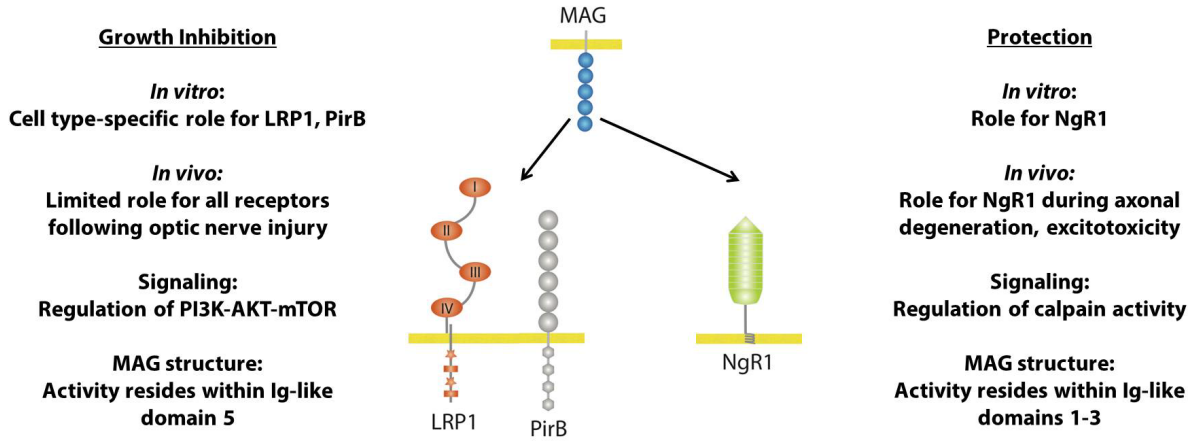

Figure 4.18: Summary of findings. Our studies have revealed that MAG utilizes distinct receptor systems and signaling pathways to mediate neuronal growth inhibition vs. protection from toxic insults. While LRP1 and PirB have cell type-specific roles for MAG growth inhibition *in vitro*, there is a limited role for these receptors in the context of axon regeneration following CNS injury. NgR1 has a role in MAG protection against axonal degeneration and excitotoxicity *in vitro*, and also plays a substantial role in protection against acrylamide-induced degeneration and kainic acid-induced seizures *in vivo*. Additionally, MAG antagonizes the PI3K-AKT-mTOR pathway to mediate growth inhibition, while it prevents calpain-dependent cleavage of the cytoskeleton during degenerative or excitotoxic insults. While it is known that the growth-inhibitory activity of MAG resides in the 5th Ig-like domain of the extracellular region, we have identified the protective activity to reside in Ig-like domains 1-3. Although previous studies have suggested that gangliosides and β1-integrin also mediate these MAG-dependent functions, our results show a limited role for NgR2. Note - This illustration was generously provided by Yevgeniya A. Mironova, and was modified for the purpose of this figure. The original figure appeared in: Mironova YA, Giger RJ (2013) Where no synapses go: gatekeepers of circuit remodeling and synaptic strength. Trends Neurosci 36:363-73.

4.8 Bibliography

Akbik F, Cafferty WB, Strittmatter SM (2012) Myelin associated inhibitors: a link between injury-induced and experience-dependent plasticity. Exp Neurol 235:43-52.

Asomugha CO, Linn DM, Linn CL (2010) ACh receptors link two signaling pathways to neuroprotection against glutamate-induced excitotoxicity in isolated RGCs. J Neurochem 112:214-226.

Atwal JK, Pinkston-Gosse J, Syken J, Stawicki S, Wu Y, Shatz C, Tessier-Lavigne M (2008) PirB is a functional receptor for myelin inhibitors of axonal regeneration. Science 322:967-970.

Bartsch U (1996) Myelination and axonal regeneration in the central nervous system of mice deficient in the myelin-associated glycoprotein. J Neurocytol 25:303-313.

Bernier B, Castejon S, Culver DG, Glass JD (1999) Axonal neurofilaments are resistant to calpain-mediated degradation in the WLD(S) mouse. Neuroreport 10:1423-1426.

Billger M, Wallin M, Karlsson JO (1988) Proteolysis of tubulin and microtubule-associated proteins 1 and 2 by calpain I and II. Difference in sensitivity of assembled and disassembled microtubules. Cell Calcium 9:33-44.

Cafferty WB, Duffy P, Huebner E, Strittmatter SM (2010) MAG and OMgp synergize with Nogo-A to restrict axonal growth and neurological recovery after spinal cord trauma. J Neurosci 30:6825-6837.

Chivatakarn O, Kaneko S, He Z, Tessier-Lavigne M, Giger RJ (2007) The Nogo-66 receptor NgR1 is required only for the acute growth cone-collapsing but not the chronic growth-inhibitory actions of myelin inhibitors. J Neurosci 27:7117-7124.

Collins BE, Yang LJ, Mukhopadhyay G, Filbin MT, Kiso M, Hasegawa A, Schnaar RL (1997) Sialic acid specificity of myelin-associated glycoprotein binding. J Biol Chem 272:1248-1255.

Cao Z, Qiu J, Domeniconi M, Hou J, Bryson JB, Mellado W, Filbin MT (2007) The inhibition site on myelin-associated glycoprotein is within Ig-domain 5 and is distinct from the sialic acid binding site. J Neurosci 27:9146-9154.

Dashiell SM, Tanner SL, Pant HC, Quarles RH (2002) Myelin-associated glycoprotein modulates expression and phosphorylation of neuronal cytoskeletal elements and their associated kinases. J Neurochem 81:1263-1272.

de Lima S, Koriyama Y, Kurimoto T, Oliveira JT, Yin Y, Li Y, Gilbert HY, Fagiolini M, Martinez AM, Benowitz L (2012). Full-length axon regeneration in the adult mouse optic nerve and partial recovery of simple visual behaviors. Proc Natl Acad Sci U S A 109:9149-9154.

Dickendesher TL, Baldwin KT, Mironova YA, Koriyama Y, Raiker SJ, Askew KL, Wood A, Geoffroy CG, Zheng B, Liepmann CD, Katagiri Y, Benowitz LI, Geller HM, Giger RJ (2012) NgR1 and NgR3 are receptors for chondroitin sulfate proteoglycans. Nat Neurosci 15:703-712.

Domeniconi M, Cao Z, Spencer T, Sivasankaran R, Wang K, Nikulina E, Kimura N, Cai H, Deng K, Gao Y, He Z, Filbin M (2002) Myelin-associated glycoprotein interacts with the Nogo66 receptor to inhibit neurite outgrowth. Neuron 35:283-290.

Dong XX, Wang Y, Qin ZH (2009) Molecular mechanisms of excitotoxicity and their relevance to pathogenesis of neurodegenerative diseases. Acta Pharmacol Sin 30:379-387.

Fawcett JW, Schwab ME, Montani L, Brazda N, Muller HW (2012) Defeating inhibition of regeneration by scar and myelin components. Handb Clin Neurol 109:503-522.
Filbin MT (2003) Myelin-associated inhibitors of axonal regeneration in the adult mammalian CNS. Nat Rev Neurosci 4:703-713.
Fischer D, He Z, Benowitz LI (2004) Counteracting the Nogo receptor enhances optic nerve regeneration if retinal ganglion cells are in an active growth state. J Neurosci 24:1646-1651.
Fournier AE, GrandPre T, Strittmatter SM (2001) Identification of a receptor mediating Nogo-66 inhibition of axonal regeneration. Nature 409:341-346.
Fujita Y, Endo S, Takai T, Yamashita T (2011) Myelin suppresses axon regeneration by PIR-B/SHP-mediated inhibition of Trk activity. EMBO J 30:1389-1401.
Gary DS, Mattson MP (2002) PTEN regulates Akt kinase activity in hippocampal neurons and increases their sensitivity to glutamate and apoptosis. Neuromolecular Med 2:261-269.
Goh EL, Young JK, Kuwako K, Tessier-Lavigne M, He Z, Griffin JW, Ming GL (2008) Beta1-integrin mediates myelin-associated glycoprotein signaling in neuronal growth cones. Mol Brain 1:10.
Guttmann RP, Sokol S, Baker DL, Simpkins KL, Dong Y, Lynch DR (2002) Proteolysis of the N-methyl-d-aspartate receptor by calpain in situ. J Pharmacol Exp Ther 302:1023-1030.
Henry FE, McCartney AJ, Neely R, Perez AS, Carruthers CJ, Stuenkel EL, Inoki K, Sutton MA (2012) Retrograde changes in presynaptic function driven by dendritic mTORC1. J Neurosci 32:17128-17142.
Herz J, Clouthier DE, Hammer RE (1992) LDL receptor-related protein internalizes and degrades uPA-PAI-1 complexes and is essential for embryo implantation. Cell 71:411-421.
Jaggi AS, Singh N (2012) Mechanisms in cancer-chemotherapeutic drugs-induced peripheral neuropathy. Toxicology 291:1-9.
Jin Y, Lim CM, Kim SW, Park JY, Seo JS, Han PL, Yoon SH, Lee JK (2009) Fluoxetine attenuates kainic acid-induced neuronal cell death in the mouse hippocampus. Brain Res 1281:108-116.
Kadoya K, Tsukada S, Lu P, Coppola G, Geschwind D, Filbin MT, Blesch A, Tuszynski MH (2009) Combined intrinsic and extrinsic neuronal mechanisms facilitate bridging axonal regeneration one year after spinal cord injury. Neuron 64:165-172.
Kelm S, Pelz A, Schauer R, Filbin MT, Tang S, de Bellard ME, Schnaar RL, Mahoney JA, Hartnell A, Bradfield P, Crocker PR (1994) Sialoadhesin, myelin-associated glycoprotein and CD22 define a new family of sialic acid-dependent adhesion molecules of the immunoglobulin superfamily. Curr Biol 4:965-972.
Ko MH, Chen WP, Hsieh ST (2000) Cutaneous nerve degeneration induced by acrylamide in mice. Neurosci Lett 293:195-198.
Lee JK, Geoffroy CG, Chan AF, Tolentino KE, Crawford MJ, Leal MA, Kang B, Zheng B (2010) Assessing spinal axon regeneration and sprouting in Nogo- , MAG-, and OMgp-deficient mice. Neuron 66:663-670.
Leibinger M, Muller A, Andreadaki A, Hauk TG, Kirsch M, Fischer D (2009) Neuroprotective and axon growth-promoting effects following inflammatory stimulation on mature retinal ganglion cells in mice depend on ciliary neurotrophic factor and leukemia inhibitory factor. J Neurosci 29:14334-14341.

Li C, Tropak MB, Gerlai R, Clapoff S, Abramow-Newerly W, Trapp B, Peterson A, Roder J (1994) Myelination in the absence of myelin-associated glycoprotein. Nature 369:747-750.

Li Z, Dong X, Wang Z, Liu W, Deng N, Ding Y, Tang L, Hla T, Zeng R, Li L, Wu D (2005) Regulation of PTEN by Rho small GTPases. Nat Cell Biol 7:399-404.

Lingor P, Koch JC, Tonges L, Bahr M (2012) Axonal degeneration as a therapeutic target in the CNS. Cell Tissue Res 349:289-311.

Liu BP, Fournier A, GrandPre T, Strittmatter SM (2002) Myelin-associated glycoprotein as a functional ligand for the Nogo-66 receptor. Science 297:1190-1193.

Liu H, Cao Y, Basbaum AI, Mazarati AM, Sankar R, Wasterlain CG (1999) Resistance to excitotoxin-induced seizures and neuronal death in mice lacking the preprotachykinin A gene. Proc Natl Acad Sci U S A 96:12096-12101.

Liu K, Lu Y, Lee JK, Samara R, Willenberg R, Sears-Kraxberger I, Tedeschi A, Park KK, Jin D, Cai B, Xu B, Connolly L, Steward O, Zheng B, He Z (2010) PTEN deletion enhances the regenerative ability of adult corticospinal neurons. Nat Neurosci. 13:1075-1081.

Loers G, Aboul-Enein F, Bartsch U, Lassmann H, Schachner M (2004) Comparison of myelin, axon, lipid, and immunopathology in the central nervous system of differentially myelin-compromised mutant mice: a morphological and biochemical study. Mol Cell Neurosci 27:175-189.

Lopez PH, Ahmad AS, Mehta NR, Toner M, Rowland EA, Zhang J, Dore S, Schnaar RL (2011) Myelin-associated glycoprotein protects neurons from excitotoxicity. J Neurochem 116:900-908.

Lopez-Picon FR, Kukko-Lukjanov TK, Holopainen IE (2006) The calpain inhibitor MDL-28170 and the AMPA/KA receptor antagonist CNQX inhibit neurofilament degradation and enhance neuronal survival in kainic acid-treated hippocampal slice cultures. Eur J Neurosci 23:2686-2694.

Marcus J, Dupree JL, Popko B (2002) Myelin-associated glycoprotein and myelin galactolipids stabilize developing axo-glial interactions. J Cell Biol 156:567-577.

May P, Rohlmann A, Bock HH, Zurhove K, Marth JD, Schomburg ED, Noebels JL, Beffert U, Sweatt JD, Weeber EJ, Herz J (2004). Neuronal LRP1 functionally associates with postsynaptic proteins and is required for normal motor function in mice. Mol Cell Biol 24:8872-8883.

McKernan DP, Guerin MB, O'Brien CJ, Cotter TG (2007) A key role for calpains in retinal ganglion cell death. Invest Ophthalmol Vis Sci 48:5420-5430.

McKerracher L, Ferraro GB, Fournier AE (2012) Rho signaling and axon regeneration. Int Rev Neurobiol 105:117-140.

McKhann GM 2nd, Wenzel HJ, Robbins CA, Sosunov AA, Schwartzkroin PA (2003) Mouse strain differences in kainic acid sensitivity, seizure behavior, mortality, and hippocampal pathology. Neuroscience 122:551-561.

Mehta NR, Lopez PH, Vyas AA, Schnaar RL (2007) Gangliosides and Nogo receptors independently mediate myelin-associated glycoprotein inhibition of neurite outgrowth in different nerve cells. J Biol Chem 282:27875-27886.

Mehta NR, Nguyen T, Bullen JW Jr, Griffin JW, Schnaar RL (2010) Myelin-associated glycoprotein (MAG) protects neurons from acute toxicity using a ganglioside-dependent mechanism. ACS Chem Neurosci 1:215-222.

Miller MS, Spencer PS (1985) The mechanisms of acrylamide axonopathy. Annu Rev Pharmacol Toxicol 25:643-666.

Montag D, Giese KP, Bartsch U, Martini R, Lang Y, Bluthmann H, Karthigasan J, Kirschner DA, Wintergerst ES, Nave KA, Zielasek J, Toyka KV, Lipp H, Schachner M (1994) Mice deficient for the myelin-associated glycoprotein show subtle abnormalities in myelin. Neuron 13:229-246.

Mukhopadhyay G, Doherty P, Walsh FS, Crocker PR, Filbin MT (1994) A novel role for myelin-associated glycoprotein as an inhibitor of axonal regeneration. Neuron 13:757-767.

Nath R, Raser KJ, Stafford D, Hajimohammadreza I, Posner A, Allen H, Talanian RV, Yuen P, Gilbertsen RB, Wang KK (1996) Non-erythroid alpha-spectrin breakdown by calpain and interleukin 1 beta-converting-enzyme-like protease(s) in apoptotic cells: contributory roles of both protease families in neuronal apoptosis. Biochem J 319:683-690.

Nie D, Di Nardo A, Han JM, Baharanyi H, Kramvis I, Huynh T, Dabora S, Codeluppi S, Pandolfi PP, Pasquale EB, Sahin M (2010) Tsc2-Rheb signaling regulates EphA-mediated axon guidance. Nat Neurosci 13:163-172.

Nguyen T, Mehta NR, Conant K, Kim KJ, Jones M, Calabresi PA, Melli G, Hoke A, Schnaar RL, Ming GL, Song H, Keswani SC, Griffin JW (2009) Axonal protective effects of the myelin-associated glycoprotein. J Neurosci 29:630-637.

Oinuma I, Ito Y, Katoh H, Negishi M (2010) Semaphorin 4D/plexin-B1 stimulates PTEN activity through R-Ras GAP activity, inducing growth cone collapse in hippocampal neurons. J Biol Chem 285:28200-28209.

Okamoto M, Mori S, Endo H (1994a) A protective action of chondroitin sulfate proteoglycans against neuronal cell death induced by glutamate. Brain Res 637:57-67.

Okamoto M, Mori S, Ichimura M, Endo H (1994b) Chondroitin sulfate proteoglycans protect cultured rat's cortical and hippocampal neurons from delayed cell death induced by excitatory amino acids. Neurosci Lett 172:51-54.

Pan B, Fromholt SE, Hess EJ, Crawford TO, Griffin JW, Sheikh KA, Schnaar RL (2005) Myelin-associated glycoprotein and complementary axonal ligands, gangliosides, mediate axon stability in the CNS and PNS: neuropathology and behavioral deficits in single- and double-null mice. Exp Neurol 195:208-217.

Pariat M, Carillo S, Molinari M, Salvat C, Debüssche L, Bracco L, Milner J, Piechaczyk M (1997) Proteolysis by calpains: a possible contribution to degradation of p53. Mol Cell Biol 17:2806-2815.

Park KK, Liu K, Hu Y, Smith PD, Wang C, Cai B, Xu B, Connolly L, Kramvis I, Sahin M, He Z (2008) Promoting axon regeneration in the adult CNS by modulation of the PTEN/mTOR pathway. Science 322:963-966.

Patrick GN, Zukerberg L, Nikolic M, de la Monte S, Dikkes P, Tsai LH (1999) Conversion of p35 to p25 deregulates Cdk5 activity and promotes neurodegeneration. Nature 402:615-622.

Perdigoto AL, Chaudhry N, Barnes GN, Filbin MT, Carter BD (2011) A novel role for PTEN in the inhibition of neurite outgrowth by myelin-associated glycoprotein in cortical neurons. Mol Cell Neurosci 46:235-244.

Quarles RH (2007) Myelin-associated glycoprotein: past, present and beyond. J Neurochem 100:1431-1448.

Raiker SJ, Lee H, Baldwin KT, Duan Y, Shrager P, Giger RJ (2010) Oligodendrocyte-myelin glycoprotein and Nogo negatively regulate activity-dependent synaptic plasticity. J Neurosci 30:12432-12445.

Robak LA, Venkatesh K, Lee H, Raiker SJ, Duan Y, Lee-Osbourne J, Hofer T, Mage RG, Rader C, Giger RJ (2009) Molecular basis of the interactions of the Nogo-66 receptor and its homolog NgR2 with myelin-associated glycoprotein: development of NgROMNI-Fc, a novel antagonist of CNS myelin inhibition. J Neurosci 29:5768-5783.

Rohlmann A, Gotthardt M, Willnow TE, Hammer RE, Herz J (1996) Sustained somatic gene inactivation by viral transfer of Cre recombinase. Nat Biotechnol 14:1562-1565.

Ryu M, Yasuda M, Shi D, Shanab AY, Watanabe R, Himori N, Omodaka K, Yokoyama Y, Takano J, Saido T, Nakazawa T (2012) Critical role of calpain in axonal damage-induced retinal ganglion cell death. J Neurosci Res 90:802-815.

Sanchez-Gomez MV, Alberdi E, Perez-Navarro E, Alberch J, Matute C (2011) Bax and calpain mediate excitotoxic oligodendrocyte death induced by activation of both AMPA and kainate receptors. J Neurosci 31:2996-3006.

Silver J, Miller JH (2004) Regeneration beyond the glial scar. Nat Rev Neurosci 5:146-156.

Simpkins KL, Guttmann RP, Dong Y, Chen Z, Sokol S, Neumar RW, Lynch DR (2003) Selective activation induced cleavage of the NR2B subunit by calpain. J Neurosci 23:11322-11331.

Stiles TL, Dickendesher TL, Gaultier A, Fernandez-Castaneda A, Mantuano E, Giger RJ, Gonias SL (2013) LDL receptor-related protein-1 is a sialic acid-independent receptor for myelin-associated glycoprotein (MAG) that functions in neurite outgrowth inhibition by MAG and CNS myelin. J Cell Sci 126:209-220.

Strickland DK, Gonias SL, Argraves WS (2002) Diverse roles for the LDL receptor family. Trends Endocrinol Metab 13:66-74.

Stys PK, Ransom BR, Waxman SG (1991) Compound action potential of nerve recorded by suction electrode: a theoretical and experimental analysis. Brain Res 546:18-32.

Tang S, Shen YJ, DeBellard ME, Mukhopadhyay G, Salzer JL, Crocker PR, Filbin MT (1997) Myelin-associated glycoprotein interacts with neurons via a sialic acid binding site at ARG118 and a distinct neurite inhibition site. J Cell Biol 138:1355-1366.

Teng FY, Tang BL (2013) Nogo/RTN4 isoforms and RTN3 expression protect SH-SY5Y cells against multiple death insults. Mol Cell Biochem [Epub ahead of print].

Tillerson JL, Miller GW (2003) Grid performance test to measure behavioral impairment in the MPTP-treated-mouse model of parkinsonism. J Neurosci Methods 123:189-200.

Tonges L, Koch JC, Bähr M, Lingor P (2011) ROCKing regeneration: Rho kinase inhibition as molecular target for neurorestoration. Front Mol Neurosci 4:39.

Ujike A, Takeda K, Nakamura A, Ebihara S, Akiyama K, Takai T (2002) Impaired dendritic cell maturation and increased T(H)2 responses in PIR-B(-/-) mice. Nat Immunol 3:542-548.

Venkatesh K, Chivatakarn O, Lee H, Joshi PS, Kantor DB, Newman BA, Mage R, Rader C, Giger RJ (2005) The Nogo-66 receptor homolog NgR2 is a sialic acid-dependent receptor selective for myelin-associated glycoprotein. J Neurosci 25:808-822.

Venkatesh K, Chivatakarn O, Sheu SS, Giger RJ (2007) Molecular dissection of the myelin-associated glycoprotein receptor complex reveals cell type-specific mechanisms for neurite outgrowth inhibition. J Cell Biol 177:393-399.

Vinson M, Strijbos PJ, Rowles A, Facci L, Moore SE, Simmons DL, Walsh FS (2001) Myelin-associated glycoprotein interacts with ganglioside GT1b. A mechanism for neurite outgrowth inhibition. J Biol Chem 276:20280-20285.

Vyas AA, Schnaar RL (2001) Brain gangliosides: functional ligands for myelin stability and the control of nerve regeneration. Biochimie 83:677-682.

Vyas AA, Patel HV, Fromholt SE, Heffer-Lauc M, Vyas KA, Dang J, Schachner M, Schnaar RL (2002) Gangliosides are functional nerve cell ligands for myelin-associated glycoprotein (MAG), an inhibitor of nerve regeneration. Proc Natl Acad Sci U S A 99:8412-8417.

Wang JT, Medress ZA, Barres BA (2012) Axon degeneration: molecular mechanisms of a self-destruction pathway. J Cell Biol 196:7-18.

Wang KC, Koprivica V, Kim JA, Sivasankaran R, Guo Y, Neve RL, He Z (2002) Oligodendrocyte-myelin glycoprotein is a Nogo receptor ligand that inhibits neurite outgrowth. Nature 417:941-944.

Wang MS, Wu Y, Culver DG, Glass JD (2000) Pathogenesis of axonal degeneration: parallels between Wallerian degeneration and vincristine neuropathy. J Neuropathol Exp Neurol 59:599-606.

Weiss MD, Hammer J, Quarles RH (2000) Oligodendrocytes in aging mice lacking myelin-associated glycoprotein are dystrophic but not apoptotic. J Neurosci Res 62:772-780.

Winters JJ, Ferguson CJ, Lenk GM, Giger-Mateeva VI, Shrager P, Meisler MH, Giger RJ (2011) Congenital CNS hypomyelination in the Fig4 null mouse is rescued by neuronal expression of the PI(3,5)P(2) phosphatase Fig4. J Neurosci 31:17736-17751.

Winzeler AM, Mandemakers WJ, Sun MZ, Stafford M, Phillips CT, Barres BA (2011) The lipid sulfatide is a novel myelin-associated inhibitor of CNS axon outgrowth. J Neurosci 31:6481-6492.

Worter V, Schweigreiter R, Kinzel B, Mueller M, Barske C, Bock G, Frentzel S, Bandtlow CE (2009) Inhibitory activity of myelin-associated glycoprotein on sensory neurons is largely independent of NgR1 and NgR2 and resides within Ig-Like domains 4 and 5. PLoS One 4:e5218.

Yang LJ, Zeller CB, Shaper NL, Kiso M, Hasegawa A, Shapiro RE, Schnaar RL (1996) Gangliosides are neuronal ligands for myelin-associated glycoprotein. Proc Natl Acad Sci U S A 93:814-818.

Yin X, Crawford TO, Griffin JW, Tu P, Lee VM, Li C, Roder J, Trapp BD (1998) Myelin-associated glycoprotein is a myelin signal that modulates the caliber of myelinated axons. J Neurosci 18:1953-1962.

Yin Y, Cui Q, Gilbert HY, Yang Y, Yang Z, Berlinicke C, Li Z, Zaverucha-do-Valle C, He H, Petkova V, Zack DJ, Benowitz LI (2009) Oncomodulin links inflammation to optic nerve regeneration. Proc Natl Acad Sci U S A 106:19587-19592.

Zhang QG, Wu DN, Han D, Zhang GY (2007) Critical role of PTEN in the coupling between PI3K/Akt and JNK1/2 signaling in ischemic brain injury. FEBS Lett 581:495-505.

Zheng B, Atwal J, Ho C, Case L, He XL, Garcia KC, Steward O, Tessier-Lavigne M (2005) Genetic deletion of the Nogo receptor does not reduce neurite inhibition in vitro or promote corticospinal tract regeneration in vivo. Proc Natl Acad Sci U S A 102:1205-1210.

Zheng XY, Zhang HL, Luo Q, Zhu J (2011) Kainic acid-induced neurodegenerative model: potentials and limitations. J Biomed Biotechnol 2011:457079.

CHAPTER V:

General Discussion

Taken together, the work presented in this dissertation provides new insights into the molecular and cellular mechanisms that inhibit long-distance axon regeneration of injured neurons in the adult mammalian CNS. Most relevant to the field of nervous system injury and repair is our (1) identification of novel ligand-receptor interactions that function in neuronal growth inhibition, (2) innovative approach of deleting receptors for extrinsic growth-inhibitory cues combined with boosting the intrinsic growth potential of neurons to promote axon regeneration, and (3) discovery of distinct receptor mechanisms and signaling pathways that differentiate the multiple functions of CNS regeneration inhibitors. These points, along with a frank assessment of the current state of the field of CNS repair and its future, are further discussed below.

Is blockade of extrinsic inhibitory barriers enough to promote long-distance axonal regeneration following injury?

While the growth-inhibitory properties of injured adult mammalian CNS tissue are well established, the underlying molecular mechanisms of neuronal growth inhibition (ligands, receptors, signaling pathways) have only recently started to come to light. Santiago Ramón y Cajal first reported in 1928 that axons of the mammalian PNS, but not the CNS, show regrowth

following injury. However, when injured CNS axons of the optic nerve are presented with a peripheral graft from the sciatic nerve, these axons are now able to regenerate (Ramón y Cajal, 1928). Over sixty years later, Albert Aguayo and colleagues confirmed that specific populations of adult CNS fiber tracts have the capacity to regenerate for several centimeters into peripheral nerve grafts, while injured axons of the sciatic nerve are not able to grow through grafts of the optic nerve (Aguayo et al., 1978; Aguayo et al., 1981; David and Aguayo, 1981; Richardson et al., 1980). These seminal experiments established the founding principles of the field of mammalian axon regeneration: the PNS environment, but not the CNS environment, is favorable for regrowth of injured adult axons. Furthermore, the intrinsic ability to regrow axons is found in at least some populations of adult CNS neurons.

As discussed extensively in this dissertation, we now have a much clearer, but still incomplete, picture of the inhibitory proteins that are present in the injured CNS environment, including the myelin-associated inhibitors (MAIs) and chondroitin sulfate proteoglycans (CSPGs). Here we have identified two members of the Nogo receptor family, NgR1 and NgR3, as high-affinity receptor components for CSPGs (**Chapter II; Figure 5.1**). As NgR1 is a well-established receptor for multiple MAIs (Domeniconi et al., 2002; Fournier et al., 2001; Liu et al., 2002; Wang et al., 2002), our results show for the first time that MAIs and CSPGs utilize common receptor components for neuronal inhibition, thus suggesting common pathways for therapeutic targeting. Indeed, our in-depth analysis reveals a functionally redundant role for these receptors in growth inhibition of select populations of primary neurons *in vitro*, as well as in limiting axon regeneration following optic nerve injury *in vivo*. Because Nogo receptors are GPI-anchored proteins, further work is still needed to identify the signal-transducing components of this CSPG receptor complex. We have found that NgR1 and NgR3 co-immunoprecipitate in

the presence of CSPG ligands, and preliminary evidence from our laboratory suggests that NgR1 and NgR3 also interact with RPTPσ, another established CSPG receptor (personal communication with Yevgeniya A. Mironova). It thus remains a possibility that RPTPσ is the transmembrane co-receptor for NgR1 and NgR3 to convey CSPG inhibition, and that growth-inhibitory ligands mediate their activity through large, multi-component signaling platforms.

Additionally, we have identified a novel interaction between MAG (a known MAI) and LRP1 (**Chapter III; Figure 5.1**). While this interaction is high affinity and has a functional consequence for neurite outgrowth inhibition *in vitro*, the *in vivo* significance for axon regeneration is underwhelming (**Chapter IV**). In fact, the majority of mouse genetic studies from the past decade have pointed to a somewhat disappointing conclusion: the targeting of growth inhibitors or their receptors individually is not sufficient to promote substantial, long-distance axon regeneration in the injured adult mammalian CNS (Ji et al., 2008; Kim et al., 2004; Nakamura et al., 2011; Zheng et al., 2003; Zheng et al., 2005). While acute blockage of myelin inhibitors with anti-Nogo-A or soluble NgR(310)-Fc, as well as degradation of CSPG side chains with chondroitinase ABC (Ch'aseABC), leads to a modest but significant increase in axonal growth (Bradbury et al., 2002; Harvey et al., 2009; MacDermid et al., 2004; Moon et al., 2001; Peng et al., 2009; Wang et al., 2006; Zorner and Schwab, 2010), claims of long-distance regeneration and functional recovery following CNS injury in genetic targeting studies have been highly controversial and not consistently reproducible (Cafferty et al., 2007; Kim et al., 2003; Simonen et al., 2003; Steward et al., 2007; Zheng et al., 2003). For this reason, studies with combined deletions of multiple inhibitory ligands have been conducted, but have also been largely ineffective in mammalian spinal cord injury (SCI) models (Cafferty et al., 2010; Lee et al., 2010). Our studies are the first to genetically delete multiple inhibitory receptors and assess

regeneration *in vivo*. While we found that *NgR13*$^{-/-}$, *NgR123*$^{-/-}$, and *NgR13/RPTPσ*$^{-/-}$ mice show significant regeneration following optic nerve crush (**Chapter II**), the same is not true for *NgR12*$^{-/-}$ and *NgR12/PirB*$^{-/-}$ mice (**Chapter II, Chapter IV**). In total, it is possible that (1) there is substantial functional redundancy for growth inhibition, (2) injured axons also need intrinsic growth programs to turn back on, and (3) these receptors are critical for other functions of CNS growth inhibitors, as discussed below.

Combined manipulations of extrinsic and intrinsic factors to boost regenerative potential

In addition to blockade of growth-inhibitory factors, another approach to increasing regenerative growth is to change the intrinsic growth state of the neuron. Following arrival of axons to their proper targets during development, CNS neurons downregulate the majority of growth pathways to allow for the proper formation of synaptic connections (Yang and Yang, 2012). As a result, injured adult CNS neurons are at an immediate disadvantage, as the critical signaling cascades that helped them grow and navigate during development are no longer active. Furthermore, injury to peripheral nerve axons induces transcription-dependent changes that promote regeneration by enhancing the intrinsic growth capacity of these neurons (Abe and Cavalli, 2008). Pathways including JAK/STAT, PI3K-AKT-mTOR, and cAMP/PKA/CREB are active in injured PNS neurons, in stark contrast to injured CNS neurons (Abe and Cavalli, 2008; Hannila and Filbin, 2008; Park et al., 2008; Qiu et al., 2005; Yang and Yang, 2012). Thus, it is not surprising that manipulations which lead to increased activation of these pathways in CNS neurons result in robust axon regeneration following injury (de Lima et al., 2012; Park et al., 2008; Sun et al., 2011).

A particularly elegant example of this difference in intrinsic growth potential is found in the dorsal root ganglion (DRG) neuron, which has both a peripheral branch (that does regenerate) and a central branch (that does not regenerate). Interestingly, if the peripheral branch is injured before the central branch, both branches will show regeneration (Neumann and Woolf, 1999). This effect is known as the conditioning lesion, as the peripheral branch injury increases the intrinsic state of the DRG neuron and thus drives regeneration of the central branch. It is important to mention that while the initial experiments of Ramón y Cajal and Aguayo showed that certain populations of injured CNS axons have some intrinsic growth potential, this is limited to a small subset of CNS neurons (Aguayo et al., 1978; Aguayo et al., 1981; David and Aguayo, 1981; Ramón y Cajal, 1928; Richardson et al., 1980).

A central finding of our studies is that the combination of (1) genetic deletion of multiple extrinsic inhibitory receptors and (2) activation of intrinsic growth programs by intraorbital injection of the yeast cell wall extract Zymosan has a substantial additive effect on regeneration of injured retinal ganglion cell (RGC) axons following optic nerve injury (**Chapter II**). Zymosan, which is a mixture of proteins, lipids, carbohydrates, and metabolites, is known to promote an inflammatory response in the vitreous of the eye and increase the regenerative state of RGCs (Yin et al., 2003). Specifically, it has been proposed that Zymosan administration leads to the release of growth-promoting factors, including oncomodulin (Yin et al., 2009), ciliary neurotrophic factor, and leukemia inhibitory factor (Leibinger et al., 2009), which act directly on RGCs to increase their intrinsic growth potential. While genetic deletion of multiple CSPG receptors had a significant but relatively minor effect on RGC regeneration, Zymosan injection resulted in substantially more RGC growth. The effect of combining these two manipulations, however, was striking. These results suggest that combined extrinsic/intrinsic targeting holds a

great deal of promise for future studies. It will be of great interest to examine RGC axon regeneration in *NgR13/RPTPσ*$^{-/-}$ mice with Zymosan (or with knockdown of PTEN - see **Chapter II**) at longer time points following injury, to determine if there is a limit to the regenerative growth of these fibers. Of more clinical relevance is to administer Zymosan at the time of, or a day after, optic nerve crush to see if robust regeneration is still observed, as well as to try these strategies in a SCI model. Furthermore, functional assays to measure compound action potentials in regenerating RGC fibers need to continued (see **Chapter II**), in the hope of demonstrating that these combined strategies result in both anatomical and functional regeneration. Ultimately, our findings and other recent studies (de Lima et al., 2012; Lu et al., 2012; Sun et al., 2011) suggest that a combination approach to axon regeneration has a great deal of potential. These combinations include (1) neutralization of extrinsic growth inhibitors, their receptors, or signaling pathways, (2) activation of intrinsic growth programs, (3) application of growth factor cocktails, and (4) grafting of neural stem cells.

The optic nerve as a CNS injury model

Throughout this dissertation, the optic nerve crush injury model is used as an *in vivo* assessment of axon regeneration in the mammalian CNS. This model is becoming an increasingly popular alternative to rodent SCI models, as it offers a simpler approach that is easier to interpret, while still maintaining the most essential properties of injured axons in the spinal cord (Benowitz and Yin, 2008). Importantly, the optic nerve is a part of the CNS, the RGCs that send their axons through the nerve have similar properties to other CNS axons, and the post-injury environment of the optic nerve is comparable to the spinal cord. Specifically, a glial scar forms at the injury site, consisting of an influx of reactive astrocytes and enhanced

CSPG production. Damaged oligodendrocytes are also present, exposing MAIs to cell surface receptors on injured RGCs (Ohlsson et al., 2004). Most critically, injured RGC axons fail to regenerate past the lesion site, similar to the injured spinal cord (Tuszynski and Steward, 2012).

The advantages of the optic nerve injury model all stem from its simplicity. Unlike the spinal cord, which contains numerous ascending and descending fibers at every level, the optic nerve consists of one set of axonal fibers. Additionally, the injured axons are in close proximity to their retinal cell bodies and it is relatively easy to achieve a complete crush of all fibers (Benowitz and Yin, 2008). Thus, unlike the spinal cord, where significant controversies have erupted over the possibility of spared fibers or fibers from other tracts being misinterpreted as regenerating axons (Cafferty et al., 2007; Steward et al., 2007), there is little question if axons are regenerating in the injured optic nerve. This is a major benefit to the model, as a definitive answer on regenerative potential can be given within a few weeks of the injury. Furthermore, the ease of access to the eye and optic nerve allows for minimally invasive methods to manipulate the system; for example, growth-promoting compounds or fluorescent tracers can be introduced by intravitreal injection, drugs can be directly applied to the optic nerve through the use of gelfoam, etc (Barry et al., 2008; Benowitz and Yin, 2008).

While these are substantial advantages, the simplicity of the optic nerve crush injury model is also its downside. One of the greatest challenges for almost all CNS injuries, including spinal cord injury, is the complexity of the injury site and the fact that axons have to navigate through long distances of inappropriate targets before arriving at the correct one. Additionally, spinal cord injury models have established measures of functional recovery, including the Basso-Beattie-Bresnahan (BBB) locomotor rating scale and electrophysiological measurements (Tuszynski and Steward, 2012). Currently, only one study using the optic nerve injury model

has proposed functional assessments of RGC axon regeneration, including the optomotor response, depth perception, and circadian photoentrainment (de Lima et al., 2012). Thus, the optic nerve is a great model for trying to decipher the molecular and cellular mechanisms that underlie CNS growth inhibition (as we have done in our studies), but ultimately the identified targets of these studies will need to be tested in SCI models before proceeding to any type of clinical setting.

CNS growth inhibitors as multifunctioning molecules in physiology and pathology

While most attention has focused on the role of MAIs (including Nogo, MAG, and OMgp) and CSPGs in growth inhibition, increasing evidence suggests that these proteins and their receptors have critical roles in a variety of other physiological and pathological processes. Nogo and CSPGs, as well as NgR1 and PirB, have been shown to be key components for the maintenance of neuronal networks that occurs after experience-dependent refinement in the visual cortex (the critical period) is completed (McGee et al., 2005; Pizzorusso et al., 2002; Syken et al., 2006). Additionally, Nogo, OMgp, and CSPGs are expressed on or near neurons and localize to the synapse, as do their receptors (Mironova and Giger, 2013). Their synaptic roles are complex, and include the regulation of dendrite complexity and spine morphology/density (Lee et al., 2008; Wills et al., 2012; Zagrebelsky et al., 2010), the inhibition of synaptogenesis (Wills et al., 2012), and influence over Hebbian forms of synaptic plasticity (Delekate et al., 2011; Lee et al., 2008; Raiker et al., 2010). MAG, on the other hand, has been shown to mediate axonal maintenance and stability over time, as well as protect neurons and their processes from a variety of toxic insults (Lopez et al., 2011; Nguyen et al., 2009). Here we performed a detailed characterization of these two major functions of MAG: growth inhibition

and protection (**Chapter IV**). We identified distinct receptors and signaling pathways for these functions, suggesting the possibility of targeting one without influencing the other. In the context of injury or disease, the ability to introduce therapeutic agents that are as specific as possible and have minimal side effects is essential.

Of particular interest is our finding that MAG negatively regulates the mTOR pathway for its growth-inhibitory, but not protective, activity (**Chapter IV**). Mounting evidence suggests that CNS growth inhibitors and neurotrophic factors have an antagonistic relationship, in which the inhibitors restrict levels of synaptogenesis and synaptic plasticity in order to limit exuberant growth during development, while the neurotrophic factors promote these processes (Mironova and Giger, 2013). One potential pathway to mediate these effects is the PI3K-AKT-mTOR pathway, as growth inhibitors and neurotrophic factors have opposite effects on the regulation of mTOR-dependent protein translation (Fortin et al., 2012; Peng et al., 2011). Furthermore, the dramatic increases in AKT and mTOR activation that are seen with neurotrophic factor application, such as brain-derived neurotrophic factor (BDNF), are strongly attenuated in the presence of either crude myelin or the Nogo66 (Raiker et al., 2010). This antagonistic relationship also applies directly to growth inhibition, as pretreatment of primary neurons with BDNF substantially reduces neurite outgrowth inhibition by myelin (Cai et al., 1999). In the context of both development and axonal injury, a delicate balance needs to be struck between allowing enough time for sufficient growth or regrowth of axons and preventing an excess of growth or sprouting. Indeed, without the necessary restrictions on synapse formation and plasticity, severe consequences for neurologic function may result, including epilepsy, memory deficits, and mental health disorders (Mironova and Giger, 2013).

Final thoughts and future strategies for SCI repair

Considering the biological complexity of a SCI, the development of new strategies that promote nervous system tissue regeneration and lead to a significant reduction of injury-inflicted disabilities remains a challenging task. A major goal of SCI research is to develop therapeutic strategies that lead to greatly improved behavioral outcomes in spinal cord-injured rodents and non-human primates. Subsequently, the most promising strategies are tested in clinical trials for their therapeutic efficacy in human subjects suffering from SCI.

Reproducibility of these strategies, however, has been problematic, as evidenced by a recent program by the National Institute of Neurological Disorders and Stroke, called Facilities of Research Excellence - Spinal Cord Injury (FORE-SCI) (Steward et al., 2012). The purpose of the FORE-SCI program was to replicate the most promising reports related to regeneration. Of the 11 studies that were replicated, only 1 confirmed the original findings, while 6 of the studies resulted in a complete failure of replication. Given the incredible cost in time, effort, and money to test these potential therapeutics at the primate level or for clinical trials, this is a worrisome trend. Future studies must be held accountable for their validity, robustness, choice of animal models, proper controls, blinded analyses, and delivery strategies, targets, and doses.

Successful repair of damaged nervous tissue depends on a series of critical steps. Following moderate to severe injury of the spinal cord, some degree of axonal growth will be necessary to achieve substantial repair. While enormous progress has been made in our understanding of how neuronal growth is regulated, long-distance axonal growth in an injured adult mammalian CNS remains a challenge. If axons regenerate in significant numbers, their growth needs to be directed, appropriate targets recognized, and new synapses formed. Meaningful synapses will have to be stabilized while others will need to be eliminated. It is

likely that task-specific training will be necessary to shape the connectivity of newly formed networks in a meaningful manner. Indeed, mounting evidence suggests that experience-dependent plasticity in the juvenile nervous system and injury-induced neuronal plasticity are regulated by similar mechanisms. Furthermore, neuronal networks will need to be supported by glia. Newly grown axons need to be myelinated to ensure axonal health and allow for rapid propagation of electrical impulses.

Additionally, scalability may become a problem when some of the most exciting findings in the rodent SCI field are translated to non-human primates and human patients. The first step, growth of new axons, takes weeks in rodent SCI models. If long-distance axonal regeneration can be achieved in human patients, it may take months to years in order to re-innervate distal targets in the injured spinal cord. Any future treatment will likely have to be combined with some form of exercise or skilled training in order to "teach" newly formed networks in an experience-dependent manner. There will be no "simple fix" for SCI; however, the greatly accelerated pace of which our mechanistic understanding of neuronal repair is growing raises optimism that the burdens of SCI can be substantially lowered.

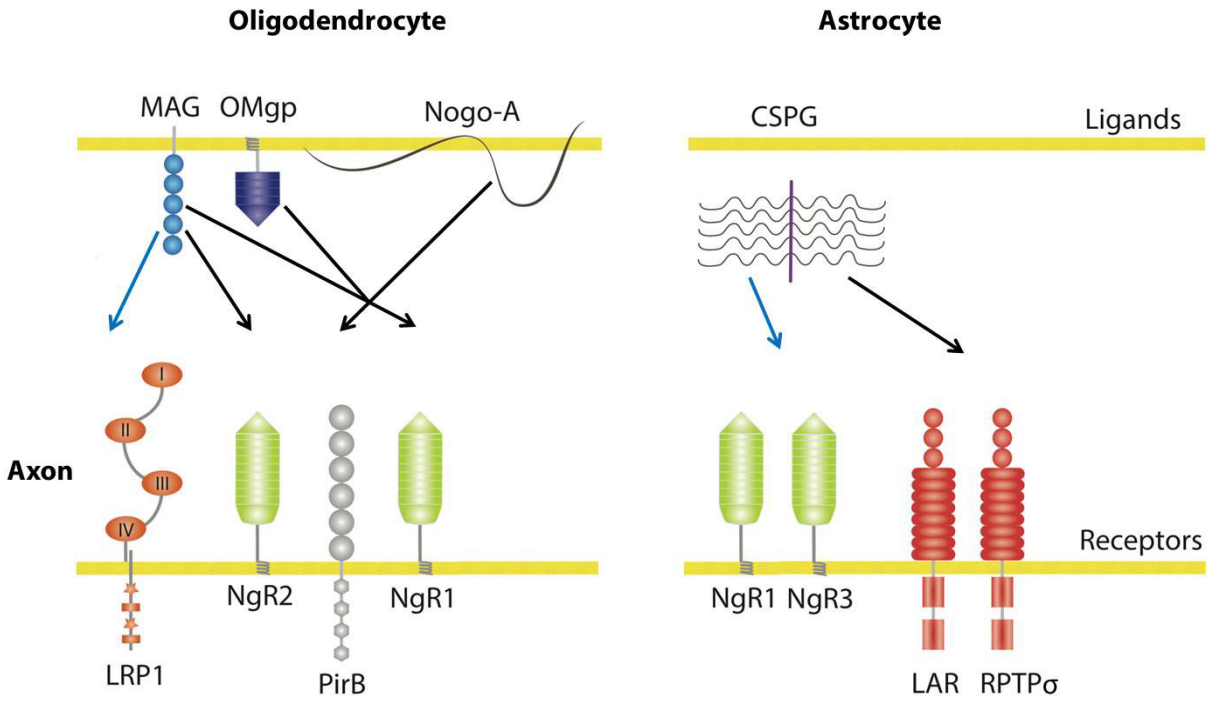

Figure 5.1: The major ligand-receptor interactions for axonal growth inhibition in the injured CNS. Arrows in black refer to established ligand-receptor interactions, while arrows in blue refer to the novel interactions identified during the course of this dissertation. Note - This illustration was generously provided by Yevgeniya A. Mironova, and was modified for the purpose of this figure. The original figure appeared in: Mironova YA, Giger RJ (2013) Where no synapses go: gatekeepers of circuit remodeling and synaptic strength. Trends Neurosci 36:363-73.

Bibliography

Abe N, Cavalli V (2008) Nerve injury signaling. Curr Opin Neurobiol 18:276-283.

Aguayo AJ, Dickson R, Trecarten J, Attiwell M, Bray GM, Richardson P (1978) Ensheathment and myelination of regenerating PNS fibres by transplanted optic nerve glia. Neurosci Lett 9:97-104.

Aguayo AJ, David S, Bray GM (1981) Influences of the glial environment on the elongation of axons after injury: Transplantation studies in adult rodents. J Exp Biol 95:231-240.

Benowitz L, Yin Y (2008) Rewiring the injured CNS: lessons from the optic nerve. Exp Neurol 209:389-398.

Berry M, Ahmed Z, Lorber B, Douglas M, Logan A (2008) Regeneration of axons in the visual system. Restor Neurol Neurosci 26:147-174.

Bradbury EJ, Moon LD, Popat RJ, King VR, Bennett GS, Patel PN, Fawcett JW, McMahon SB (2002) Chondroitinase ABC promotes functional recovery after spinal cord injury. Nature 416:636-640.

Cafferty WB, Kim JE, Lee JK, Strittmatter SM (2007) Response to correspondence: Kim et al., "axon regeneration in young adult mice lacking Nogo-A/B." Neuron 38, 187-199. Neuron 54:195-199.

Cafferty WB, Duffy P, Huebner E, Strittmatter SM (2010) MAG and OMgp synergize with Nogo-A to restrict axonal growth and neurological recovery after spinal cord trauma. J Neurosci 30:6825-6837.

Cai D, Shen Y, De Bellard M, Tang S, Filbin MT (1999) Prior exposure to neurotrophins blocks inhibition of axonal regeneration by MAG and myelin via a cAMP-dependent mechanism. Neuron 22:89-101.

David S, Aguayo AJ (1981) Axonal elongation into peripheral nervous system "bridges" after central nervous system injury in adult rats. Science 214:931-933.

Delekate A, Zagrebelsky M, Kramer S, Schwab ME, Korte M (2011) NogoA restricts synaptic plasticity in the adult hippocampus on a fast time scale. Proc Natl Acad Sci U S A 108:2569-2574.

de Lima S, Koriyama Y, Kurimoto T, Oliveira JT, Yin Y, Li Y, Gilbert HY, Fagiolini M, Martinez AM, Benowitz L (2012). Full-length axon regeneration in the adult mouse optic nerve and partial recovery of simple visual behaviors. Proc Natl Acad Sci U S A 109:9149-9154.

Domeniconi M, Cao Z, Spencer T, Sivasankaran R, Wang K, Nikulina E, Kimura N, Cai H, Deng K, Gao Y, He Z, Filbin M (2002) Myelin-associated glycoprotein interacts with the Nogo66 receptor to inhibit neurite outgrowth. Neuron 35:283-290.

Fortin DA, Srivastava T, Dwarakanath D, Pierre P, Nygaard S, Derkach VA, Soderling TR (2012) Brain-derived neurotrophic factor activation of CaM-kinase kinase via transient receptor potential canonical channels induces the translation and synaptic incorporation of GluA1-containing calcium-permeable AMPA receptors. J Neurosci 32:8127-8137.

Fournier AE, GrandPre T, Strittmatter SM (2001) Identification of a receptor mediating Nogo-66 inhibition of axonal regeneration. Nature 409:341-346.

Hannila SS, Filbin MT (2008) The role of cyclic AMP signaling in promoting axonal regeneration after spinal cord injury. Exp Neurol 209:321-332.

Harvey PA, Lee DH, Qian F, Weinreb PH, Frank E (2009) Blockade of Nogo receptor ligands promotes functional regeneration of sensory axons after dorsal root crush. J Neurosci 29:6285-6295.

Ji B, Case LC, Liu K, Shao Z, Lee X, Yang Z, Wang J, Tian T, Shulga-Morskaya S, Scott M, He Z, Relton JK, Mi S (2008) Assessment of functional recovery and axonal sprouting in oligodendrocyte-myelin glycoprotein (OMgp) null mice after spinal cord injury. Mol Cell Neurosci 39:258-267.

Kim JE, Li S, GrandPre T, Qiu D, Strittmatter SM (2003) Axon regeneration in young adult mice lacking Nogo-A/B. Neuron 38:187-199.

Kim JE, Liu BP, Park JH, Strittmatter SM (2004) Nogo-66 receptor prevents raphespinal and rubrospinal axon regeneration and limits functional recovery from spinal cord injury. Neuron 44:439-451.

Lee H, Raiker SJ, Venkatesh K, Geary R, Robak LA, Zhang Y, Yeh HH, Shrager P, Giger RJ (2008) Synaptic function for the Nogo-66 receptor NgR1: regulation of dendritic spine morphology and activity-dependent synaptic strength. J Neurosci 28:2753-2765.

Lee JK, Geoffroy CG, Chan AF, Tolentino KE, Crawford MJ, Leal MA, Kang B, Zheng B (2010) Assessing spinal axon regeneration and sprouting in Nogo- , MAG-, and OMgp-deficient mice. Neuron 66:663-670.

Leibinger M, Muller A, Andreadaki A, Hauk TG, Kirsch M, Fischer D (2009) Neuroprotective and axon growth-promoting effects following inflammatory stimulation on mature retinal ganglion cells in mice depend on ciliary neurotrophic factor and leukemia inhibitory factor. J Neurosci 29:14334-14341.

Liu BP, Fournier A, GrandPre T, Strittmatter SM (2002) Myelin-associated glycoprotein as a functional ligand for the Nogo-66 receptor. Science 297:1190-1193.

Lopez PH, Ahmad AS, Mehta NR, Toner M, Rowland EA, Zhang J, Dore S, Schnaar RL (2011) Myelin-associated glycoprotein protects neurons from excitotoxicity. J Neurochem 116:900-908.

Lu P, Wang Y, Graham L, McHale K, Gao M, Wu D, Brock J, Blesch A, Rosenzweig ES, Havton LA, Zheng B, Conner JM, Marsala M, Tuszynski MH (2012) Long-distance growth and connectivity of neural stem cells after severe spinal cord injury. Cell 150:1264-1273.

MacDermid VE, McPhail LT, Tsang B, Rosenthal A, Davies A, Ramer MS (2004) A soluble Nogo receptor differentially affects plasticity of spinally projecting axons. Eur J Neurosci 20:2567-2579.

McGee AW, Yang Y, Fischer QS, Daw NW, Strittmatter SM (2005) Experience-driven plasticity of visual cortex limited by myelin and Nogo receptor. Science 309:2222-2226.

Mironova YA, Giger RJ (2013) Where no synapses go: gatekeepers of circuit remodeling and synaptic strength. Trends Neurosci 36:363-73.

Moon LD, Asher RA, Rhodes KE, Fawcett JW (2001) Regeneration of CNS axons back to their target following treatment of adult rat brain with chondroitinase ABC. Nat Neurosci 4:465-466.

Nakamura Y, Fujita Y, Ueno M, Takai T, Yamashita T (2011) Paired immunoglobulin-like receptor B knockout does not enhance axonal regeneration or locomotor recovery after spinal cord injury. J Biol Chem 286:1876-1883.

Neumann S, Woolf CJ (1999) Regeneration of dorsal column fibers into and beyond the lesion site following adult spinal cord injury. Neuron 23:83-91.

Nguyen T, Mehta NR, Conant K, Kim KJ, Jones M, Calabresi PA, Melli G, Hoke A, Schnaar RL, Ming GL, Song H, Keswani SC, Griffin JW (2009) Axonal protective effects of the myelin-associated glycoprotein. J Neurosci 29:630-637.

Ohlsson M, Mattsson P, Svensson M (2004) A temporal study of axonal degeneration and glial scar formation following a standardized crush injury of the optic nerve in the adult rat. Restor Neurol Neurosci 22:1-10.

Park KK, Liu K, Hu Y, Smith PD, Wang C, Cai B, Xu B, Connolly L, Kramvis I, Sahin M, He Z (2008) Promoting axon regeneration in the adult CNS by modulation of the PTEN/mTOR pathway. Science 322:963-966.

Peng X, Zhou Z, Hu J, Fink DJ, Mata M (2009) Soluble nogo receptor down-regulates expression of neuronal Nogo-A to enhance axonal regeneration. J Biol Chem 285:2783-2795.

Peng X, Kim J, Zhou Z, Fink DJ, Mata M (2011) Neuronal Nogo-A regulates glutamate receptor subunit expression in hippocampal neurons. J Neurochem 119:1183-1193.

Pizzorusso T, Medini P, Berardi N, Chierzi S, Fawcett JW, Maffei L (2002) Reactivation of ocular dominance plasticity in the adult visual cortex. Science 298:1248-1251.

Qiu J, Cafferty WB, McMahon SB, Thompson SW (2005) Conditioning injury-induced spinal axon regeneration requires signal transducer and activator of transcription 3 activation. J Neurosci 25:1645-1653.

Raiker SJ, Lee H, Baldwin KT, Duan Y, Shrager P, Giger RJ (2010) Oligodendrocyte-myelin glycoprotein and Nogo negatively regulate activity-dependent synaptic plasticity. J Neurosci 30:12432-12445.

Ramón y Cajal, S (1928) Degeneration and regeneration of the nervous system. Haffner Publishing Co. New York, New York, USA.

Richardson PM, McGuinness UM, Aguayo AJ (1980) Axons from CNS neurones regenerate into PNS grafts. Nature 284:264-265.

Simonen M, Pedersen V, Weinmann O, Schnell L, Buss A, Ledermann B, Christ F, Sansig G, van der Putten H, Schwab ME (2003) Systemic deletion of the myelin-associated outgrowth inhibitor Nogo-A improves regenerative and plastic responses after spinal cord injury. Neuron 38:201-211.

Steward O, Zheng B, Banos K, Yee KM (2007) Response to: Kim et al., "axon regeneration in young adult mice lacking Nogo-A/B." Neuron 38, 187-199. Neuron 54:191-195.

Steward O, Popovich PG, Dietrich WD, Kleitman N (2012) Replication and reproducibility in spinal cord injury research. Exp Neurol 233:597-605.

Sun F, Park KK, Belin S, Wang D, Lu T, Chen G, Zhang K, Yeung C, Feng G, Yankner BA, He Z (2011) Sustained axon regeneration induced by co-deletion of PTEN and SOCS3. Nature 480:372-375.

Syken J, Grandpre T, Kanold PO, Shatz CJ (2006) PirB restricts ocular-dominance plasticity in visual cortex. Science 313:1795-1800.

Tuszynski MH, Steward O (2012) Concepts and methods for the study of axonal regeneration in the CNS. Neuron 74:777-791.

Wang KC, Koprivica V, Kim JA, Sivasankaran R, Guo Y, Neve RL, He Z (2002) Oligodendrocyte-myelin glycoprotein is a Nogo receptor ligand that inhibits neurite outgrowth. Nature 417:941-944.

Wang X, Baughman KW, Basso DM, Strittmatter SM (2006) Delayed Nogo receptor therapy improves recovery from spinal cord contusion. Ann Neurol 60:540-549.

Wills ZP, Mandel-Brehm C, Mardinly AR, McCord AE, Giger RJ, Greenberg ME (2012) The nogo receptor family restricts synapse number in the developing hippocampus. Neuron 73:466-481.

Yang P, Yang Z (2012) Enhancing intrinsic growth capacity promotes adult CNS regeneration. J Neurol Sci 312:1-6.

Yin Y, Cui Q, Li Y, Irwin N, Fischer D, Harvey AR, Benowitz LI (2003) Macrophage-derived factors stimulate optic nerve regeneration. J Neurosci 23:2284-2293.

Yin Y, Cui Q, Gilbert HY, Yang Y, Yang Z, Berlinicke C, Li Z, Zaverucha-do-Valle C, He H, Petkova V, Zack DJ, Benowitz LI (2009) Oncomodulin links inflammation to optic nerve regeneration. Proc Natl Acad Sci U S A 106:19587-19592.

Zagrebelsky M, Schweigreiter R, Bandtlow CE, Schwab ME, Korte M (2010) Nogo-A stabilizes the architecture of hippocampal neurons. J Neurosci 30:13220-13234.

Zheng B, Ho C, Li S, Keirstead H, Steward O, Tessier-Lavigne M (2003) Lack of enhanced spinal regeneration in Nogo-deficient mice. Neuron 38:213-224.

Zheng B, Atwal J, Ho C, Case L, He XL, Garcia KC, Steward O, Tessier-Lavigne M (2005) Genetic deletion of the Nogo receptor does not reduce neurite inhibition in vitro or promote corticospinal tract regeneration in vivo. Proc Natl Acad Sci U S A 102:1205-1210.

Zorner B, Schwab ME (2010) Anti-Nogo on the go: from animal models to a clinical trial. Ann N Y Acad Sci 1198:E22-34.

APPENDIX I:

Analysis of Tmem125: A Novel Oligodendrocyte-Specific Membrane Protein

Multiple lines of evidence show that demyelination causes alterations in axonal transport, axonal degeneration, and axonal loss (Chandran et al., 2008; Quarles, 2007). Examples include a number of heritable demyelinating diseases of the central and peripheral nervous systems (Trapp and Nave, 2008; Zhou and Griffin, 2003). Remyelination is often incomplete in demyelinating diseases such as multiple sclerosis (MS), a cause of neurological disability that primarily affects young adults (Franklin and Ffrench-Constant, 2008). Mechanistic insights into the process of developmental myelination, as well as remyelination following injury or disease, are thus of critical importance to help understand why remyelination fails in MS and in other demyelinating diseases and how it might be enhanced therapeutically. Here we have taken a genetic approach to study the function of a novel, CNS myelin-specific protein called transmembrane protein 125 (Tmem125) *in vivo*.

To study cell type-specific gene expression profiles in the CNS, the laboratory of our collaborator, Ben A. Barres, isolated different cell types to high purity between postnatal day 1 (P1) and P30 from mouse forebrain (Cahoy et al., 2008). Affymetrix GeneChip Arrays with a total of more than 20,000 genes were used to identify gene products expressed in cell type-specific patterns. Data sets from these studies are available publically and were used for

comparative analysis of the transcriptome of acutely isolated neurons, oligodendrocytes, and astrocytes (Cahoy et al., 2008).

Genes regulated during oligodendrocyte differentiation are of particular interest for processes such as myelination, the biology of axon-glia interactions, myelin sheath stability, and white matter disorders in general. To study gene expression in the oligodendrocyte lineage, oligodendrocyte progenitor cells (OPCs), newly differentiated oligodendrocytes, and myelinating oligodendrocytes were isolated and subjected to GeneChip analysis. While a number of oligodendrocyte lineage-specific genes have been previously characterized, several novel genes that are expressed in an oligodendrocyte-specific manner were identified (Cahoy et al., 2008). Many of these genes are presumptive membrane-associated proteins, perhaps not surprising given the highly specialized function of these cells in the formation of myelin membranes.

Genes that are likely to be important for myelination, remyelination, or myelin stability are expected to be (1) strongly expressed in myelinating and mature oligodendrocytes (but not OPCs), (2) associated with the cell membrane, and (3) not expressed in neurons or astrocytes. As an additional search criterion, we focused on genes that do not have structurally-related family members, thus reducing the risk for potential compensatory mechanisms following germline ablation of the gene of interest. Given these search criteria, *Tmem125* stands out from the transcriptome analysis, as it is exceptionally abundant in myelinating oligodendrocytes (with comparable levels to myelin basic protein, myelin-associated glycoprotein, and proteolipid protein) but is also a completely novel gene.

Tmem125 (also known as 6330530A05Rik) is a protein consisting of 220 amino acid residues, with 4 predicted transmembrane domains and several regions that are highly conserved throughout vertebrate evolution. Moreover, NCBI database searches for Tmem125-related

molecules did not identify any potential Tmem125 family members in human, rat, mouse, or chicken, suggesting that it has a unique function. In the nervous system, Tmem125 is selectively expressed by myelinating and mature oligodendrocytes (Cahoy et al., 2008).

To address the functional significance of Tmem125 *in vivo*, we targeted the mouse *Tmem125* locus to generate germline mutants. The mouse *Tmem125* gene is composed of four exons. The open reading frame is encoded by exon 4; thus, it was deleted (along with exon 3) by homologous recombination using the targeting vector shown (**Figure A1.1a**). To identify embryonic stem (ES) cells that underwent homologous recombination at the *Tmem125* locus, Southern blot analysis was performed, using probes that distinguish between the *Tmem125* wild-type and mutant locus (**Figure A1.1a-b**). Successfully targeted ES cells were injected into a host blastocyst, embryos were transferred to a pseudopregnant recipient female mouse, and the resulting chimeric mice were bred with wild-type mice to achieve germline transmission. PCR genotyping from tail DNA confirms that *Tmem125*$^{-/-}$ mice were generated (**Figure A1.1c**).

To our surprise, *Tmem125*$^{-/-}$ mice do not display any noticeable phenotypes suggestive of defective myelin development or stability, such as generalized tremors, seizures, impaired motor coordination, or shortened lifespan, as has been noted for several mutants that are incapable of proper myelination (Chow et al., 2007; Ikenaka and Kagawa, 1995; Readhead and Hood, 1990). However, on a mixed genetic background (129/C57BL/6), *Tmem125*$^{-/-}$ mice show a striking "excessive grooming" behavior, resulting in a substantial loss of fur along their face and back (**Figure A1.1d**). This type of behavior has been linked to mouse models of obsessive-compulsive disorder, a neuropsychiatric disorder characterized by intrusive thoughts and ritualistic behaviors (Yang and Lu, 2011). Our analysis shows that *Tmem125*$^{-/-}$ mice, but not *Tmem125*$^{+/+}$ or *Tmem125*$^{+/-}$ mice, excessively groom themselves, as well as their littermates,

beginning around ~6 weeks of age and continuing throughout their life. Interestingly, a number of studies have suggested that deficiencies in myelination are related to various neuropsychiatric disorders (reviewed in Bartzokis, 2012).

Ongoing work in our laboratory is aimed at characterizing these behavioral abnormalities of *Tmem125*$^{-/-}$ mice. As the mice are on a mixed background, they are first being backcrossed onto a C57BL/6 background for behavioral studies. Additionally, commercial antibodies for Tmem125 are currently being tested by immunoblot analysis, to confirm deletion of the Tmem125 protein in *Tmem125*$^{-/-}$ mice. Immunoblot analysis is also being used to determine levels of myelin marker proteins (myelin basic protein, myelin-associated glycoprotein, proteolipid protein, etc.) in *Tmem125*$^{-/-}$ mice, during and after the process of CNS myelination. Similarly, myelin structure and axon density are being assessed by Toluidine Blue staining and electron microscopy. Preliminary evidence suggests that there are no major differences in the number of myelinated axons or the thickness of the myelin sheath (at 6 months of age) in *Tmem125*$^{-/-}$ mice, when compared to *Tmem125*$^{+/+}$ control littermates. This appears to be true in the sciatic nerve (as expected, given that *Tmem125* is not expressed in the peripheral nervous system - data not shown), the spinal cord, and the optic nerve (**Figure A1.1e-f**; data not shown). It is possible that, similar to the myelin-associated glycoprotein (see **Chapter IV**), *Tmem125*$^{-/-}$ mice do not display substantial deficits in developmental myelination, but instead show a loss of myelin stability over time or when subjected to injury or insult. Thus, we are also investigating myelin structure and axonal dropout in older *Tmem125*$^{-/-}$ mice, as well as the levels of demyelination (and remyelination) induced by cuprizone, lysolecithin, and experimental autoimmune encephalomyelitis (the mouse model of MS) in these mice.

Acknowledgments

This work was supported by the Neuroscience Training Grant T32EY017878, the University of Michigan Rackham Merit Fellowship (Travis L. Dickendesher), the Dr. Miriam and Sheldon G. Adelson Medical Foundation on Neural Repair and Rehabilitation, and the National Institute of Neurological Disorders and Stroke R01NS047333 (Roman J. Giger). We thank Ben A. Barres (Stanford School of Medicine) for thoughtful discussions, Lin Gan and Zunyi Zhang (University of Rochester Medical Center) for generation of the *Tmem125*$^{-/-}$ mice, and the University of Michigan Microscopy and Image Analysis Laboratory (Chris Edwards, Manager) for assistance in Toluidine Blue staining.

Author Contributions

Travis L. Dickendesher (T.L.D.), Xiujun Pi (X.P.), and Roman J. Giger designed the experiments; and T.L.D. and X.P. performed experiments.

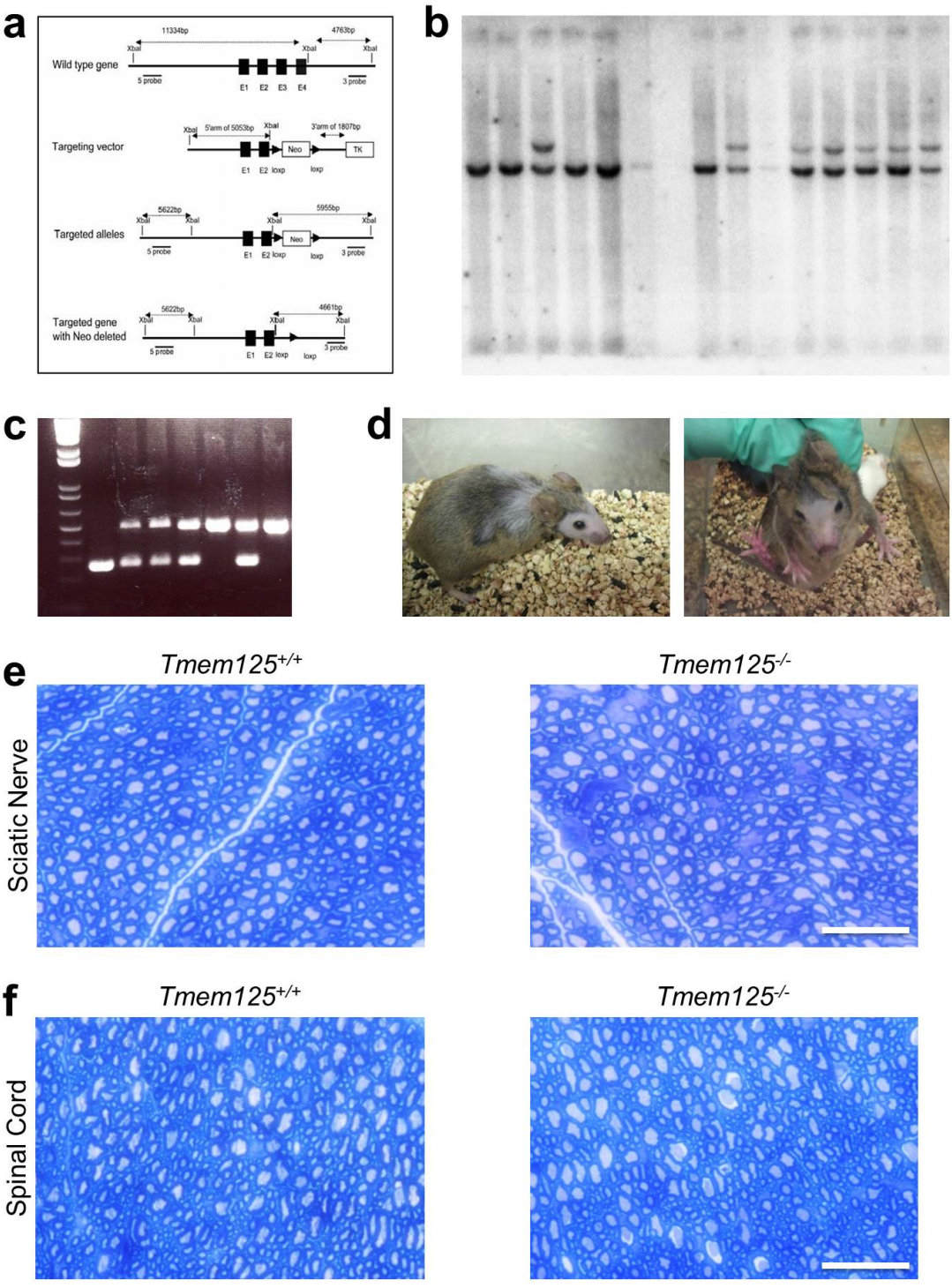

Figure A1.1: Generation and preliminary analysis of *Tmem125*$^{-/-}$ mice. (**a**) Targeting strategy for the mouse *Tmem125* gene. The gene is composed of four exons (E1-E4), and the

position of DNA probes (5' and 3' probes) and XbaI restriction sites used for Southern blotting are shown. The targeting vector is designed to delete E3 and E4 of the *Tmem125* locus. After gene targeting, ES cells were subjected to positive (Neo; neomycin) and negative (TK; thymidine kinase) selection. ES cells that underwent homologous recombination were identified by Southern blotting, and the properly targeted gene was subjected to Cre-mediated recombination to delete the Neo cassette. (**b**) Southern blot analysis of several ES cells, using XbaI digestion and the 3' probe. Many successfully targeted ES cells were identified. (**c**) PCR genotyping of tail DNA from *Tmem125*$^{+/+}$ (lane 2), *Tmem125*$^{+/-}$ (lanes 3, 4, 5, 7), and *Tmem125*$^{-/-}$ (lanes 6, 8) mice. Primers were designed to produce a ~250bp wild-type allele product and a ~525bp null allele product. (**d**) Representative examples of adult *Tmem125*$^{-/-}$ mice with substantial loss of their fur, as a result of excessive grooming. (**e-f**) At 6 months of age, Toluidine Blue labeling of epon-embedded *Tmem125*$^{+/+}$ and *Tmem125*$^{-/-}$ (**e**) sciatic nerve and (**f**) spinal cord cross sections reveals a comparable number of axons and degree of myelinated fibers. Scale bar, 10μm.

Bibliography

Bartzokis G (2012) Neuroglialpharmacology: myelination as a shared mechanism of action of psychotropic treatments. Neuropharmacology 62:2137-2153.

Cahoy JD, Emery B, Kaushal A, Foo LC, Zamanian JL, Christopherson KS, Xing Y, Lubischer JL, Krieg PA, Krupenko SA, Thompson WJ, Barres BA (2008) A transcriptome database for astrocytes, neurons, and oligodendrocytes: a new resource for understanding brain development and function. J Neurosci 28:264-278.

Chandran S, Hunt D, Joannides A, Zhao C, Compston A, Franklin RJ (2008) Myelin repair: the role of stem and precursor cells in multiple sclerosis. Philos Trans R Soc Lond B Biol Sci 363:171-183.

Chow CY, Zhang Y, Dowling JJ, Jin N, Adamska M, Shiga K, Szigeti K, Shy ME, Li J, Zhang X, Lupski JR, Weisman LS, Meisler MH (2007) Mutation of FIG4 causes neurodegeneration in the pale tremor mouse and patients with CMT4J. Nature 448:68-72.

Franklin RJ, Ffrench-Constant C (2008) Remyelination in the CNS: from biology to therapy. Nat Rev Neurosci 9:839-855.

Ikenaka K, Kagawa T (1995) Transgenic systems in studying myelin gene expression. Dev Neurosci 17:127-136.

Quarles RH (2007) Myelin-associated glycoprotein (MAG): past, present and beyond. J Neurochem 100:1431-1448.

Readhead C, Hood L (1990) The dysmyelinating mouse mutations shiverer (shi) and myelin deficient (shimld). Behav Genet 20:213-234.

Trapp BD, Nave KA (2008) Multiple sclerosis: an immune or neurodegenerative disorder? Annu Rev Neurosci 31:247-269.

Yang XW, Lu XH (2011) Molecular and cellular basis of obsessive-compulsive disorder-like behaviors: emerging view from mouse models. Curr Opin Neurol 24:114-118.

Zhou L, Griffin JW (2003) Demyelinating neuropathies. Curr Opin Neurol 16:307-313.

APPENDIX II:

Development of a Transgenic Mouse to Investigate Semaphorin3A Function

Semaphorins are a large family of evolutionally conserved glycoproteins, best known for their repulsive (and sometimes attractive, depending on the context) roles in developmental axon guidance (Pasterkamp and Giger, 2009). The secreted semaphorin, Sema3A, was the first vertebrate semaphorin to be described, and has powerful repellent and growth gone collapsing activities toward a number of peripheral and central nervous system neurons (Luo et al., 1993; Pasterkamp and Kolodkin, 2003). These include populations of sympathetic neurons, sensory neurons, motoneurons, cortical neurons, and hippocampal neurons (reviewed in Raper, 2000). *In vivo*, loss of Sema3A has been reported to result in a multitude of phenotypes, including inappropriate projections of trigeminal, facial, vagus, accessory, and glossopharyngeal nerves (Taniguchi et al., 1997). Improper orientation of pyramidal neurons in the neocortex and axon defasciculation of several neuronal populations has also been noted in *Sema3A*$^{-/-}$ mice (Behar et al., 1996; Polleux et al., 1998; Taniguchi et al., 1997). To exert its function, Sema3A requires Neuropilin-1 (Npn1) as a co-receptor in order to signal through its transmembrane receptors, any member of the class A plexins (PlexinA1, PlexinA2, PlexinA3, or PlexinA4) (Pasterkamp and Giger, 2009).

While Sema3A has been extensively investigated for its roles in axon guidance, its expression continues long beyond the time of neuronal outgrowth and target navigation, suggesting roles in other cellular processes. Indeed, Sema3A has been implicated in the

regulation of dendritic spine density, coordination of synaptic transmission in the CA1 region of the hippocampus, and inhibition of axon regeneration following injury (reviewed in Pasterkamp and Giger, 2009). Furthermore, roles for Sema3A in other tissues, including the bone, kidney and heart, have been suggested (Behar et al., 1996; Reidy and Tufro, 2011). A major goal of our laboratory is to understand the plethora of functions that canonical axon guidance molecules perform (beyond axon guidance), using mouse genetic tools and gain- or loss-of-function approaches. Thus, as a tool for future studies, we generated a transgenic mouse to allow overexpression of Sema3A in a cell type-specific and/or temporal fashion.

In order to visualize the cells that are overexpressing Sema3A, we constructed a tdTomato-Semaphorin3A (tdT-Sema3A) fusion protein using sequences from tdT and rat Sema3A (**Figure A2.1a**). The entire tdT sequence was fused to Sema3A with a HindIII restriction site and then cloned into the pSecTag2A vector (Invitrogen). More specifically, the end of tdT (the lysine residue immediately preceding the stop codon) was fused to the beginning of Sema3A (the 23rd residue - alanine - following the start codon). As a control, a second protein was constructed in the exact same manner, except that the tdT stop codon was included. Thus, this protein (referred to as tdT) consists of an expressed tdT and non-expressed Sema3A.

tdT-Sema3A and tdT expression were confirmed in transiently transfected HEK293T cells. Conditioned cell culture supernatants were collected and concentrated using centrifugal filter units. The expression levels and size of tdT-Sema3A and tdT in cell lysates were assessed by immunoblotting using anti-DsRed antibody (Clontech), as well as anti-β-actin (Sigma) as a loading control. Indeed, tdT-Sema3A and tdT are expressed at the correct molecular weight (**Figure A2.1b**) and produce bright red fluorescence in HEK293T cells (**Figure A2.1c**). To confirm the functionality of the tdT-Sema3A fusion protein, HEK293T cells were transiently

transfected with either pIRES-EGFP (GFP) or full-length rat Neuropilin-1 in pIRES-EGFP (GFP-Npn1). 24 hours later, the cells were incubated with 5nM of either tdT or tdT-Sema3A for 90 minutes, before washing and fixation. As expected, the tdT-Sema3A fusion protein shows robust binding (based on red fluorescence) to GFP-Npn1, but not to GFP only (**Figure A2.1d**).

To assess the bioactivity of tdT-Sema3A, a neurite repulsion assay with embryonic day 18 dorsal root ganglion (DRG) explants was performed. HEK293T cells were transiently transfected with either tdT-Sema3A or tdT. 24 hours later, the cells were trypsinized and collected in "hanging droplets", and the droplets were incubated for 5 hours at 37°C to form cell aggregates. In a collagen matrix, a DRG explant was placed in close proximity to aggregated HEK293T cells, and the co-cultures were incubated at 37°C for 48 hours. The cultures were then fixed, washed, and immunolabeled with 2H3 anti-neurofilament antibody (Developmental Studies Hybridoma Bank, University of Iowa). While DRGs exposed to tdT-expressing HEK293T cells grew long processes directly into the cells, DRGs exposed to tdT-Sema3A-expressing cells were significantly repulsed ($P< 0.001$, unpaired *t*-test) (**Figure A2.1e-f**).

Following successful confirmation of tdT-Sema3A expression and activity (see above), we next cloned the entire tdT-Sema3A construct (with the Ig κ-chain leader sequence from pSecTag2A included) into the STOP-eGFP-ROSA26TV vector (Stratagene). This vector contains loxP sites surrounding a STOP cassette, which is followed by the gene of interest. Thus, tdT-Sema3A will only be expressed when Cre is present and the STOP cassette is removed, allowing overexpression of the fusion protein in select cell types and/or at specific times of development or adulthood. This final construct was then used for development of a transgenic mouse expressing tdt-Sema3A following Cre recombination. PCR genotyping has confirmed the presence of the transgene (data not shown) in tdT-Sema3A transgenic mice and

studies are currently underway to confirm expression of tdT-Sema3A in mice that are also expressing nestin-Cre or in mice that have received intraorbital injection of AAV2-GFP-Cre.

Acknowledgments

As a result of an ongoing collaboration with the laboratory of Brian A. Pierchala (University of Michigan Medical School), portions of this material (describing the generation of the tdT-Sema3A fusion protein) are currently under review for publication (see citation below):

Abdesselem H, **Dickendesher TL**, Wehner AB, Giger RJ, Pierchala BA. Semaphorin 3A retrograde signaling triggers apoptotic cell death in sympathetic neurons (under review).

This work was supported by the Neuroscience Training Grant T32EY017878, the University of Michigan Rackham Merit Fellowship (Travis L. Dickendesher), the Dr. Miriam and Sheldon G. Adelson Medical Foundation on Neural Repair and Rehabilitation, and the National Institute of Neurological Disorders and Stroke R01NS047333 (Roman J. Giger). We thank Lin Gan (University of Rochester Medical Center) for generation of the tdT-Sema3A transgenic mice and Samuel L. Pfaff (Salk Institute for Biological Studies) for providing the original tdT plasmid.

Author Contributions

Travis L. Dickendesher (T.L.D.) and Roman J. Giger designed the experiments; and T.L.D. performed experiments and data analysis.

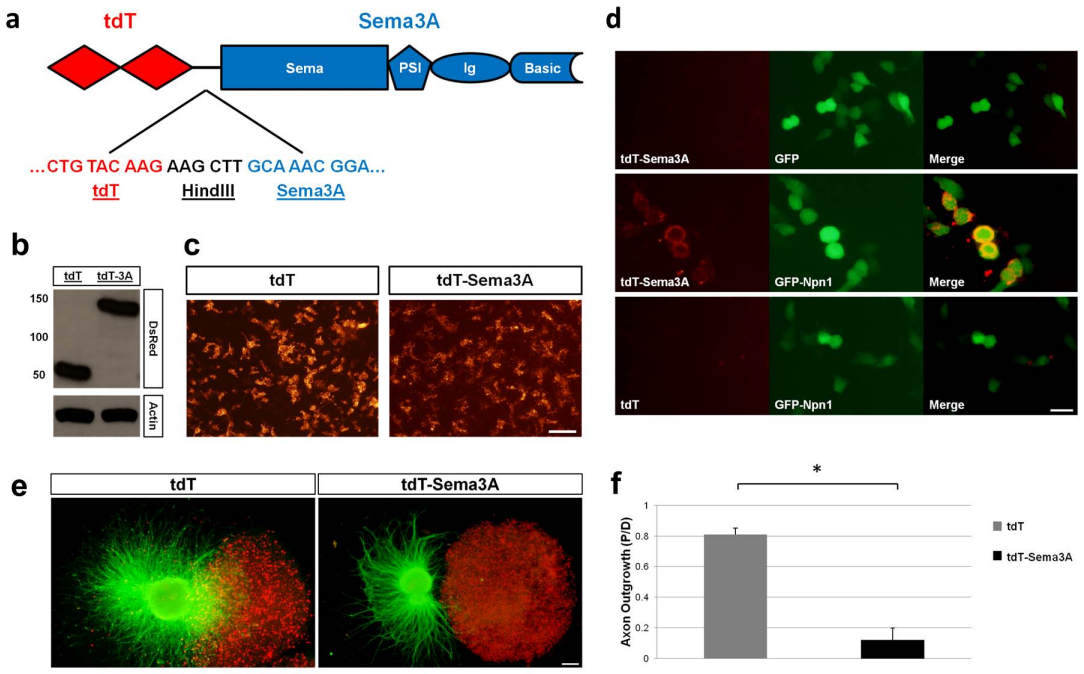

Figure A2.1: Expression and functionality of a tdTomato-Semaphorin3A fusion protein. (**a**) Schematic of the tdTomato-Semaphorin3A secreted fusion protein (tdT-Sema3A). The end of tdTomato (1 amino acid before the stop codon - red) was fused to the beginning of rat Sema3A (23 amino acids after the start codon - blue) by inserting a HindIII restriction site (black) and cloning into the psectag2A vector. Sema=amino-terminal semaphorin domain, PSI=plexin-semaphorin-integrin domain, Ig=immunoglobulin-like domain, Basic=basic C-terminal domain. (**b-c**) Confirmation of tdT-Sema3A expression in HEK293T cells. In (**b**), western blotting using conditioned media from HEK293T cells transfected with either tdT or tdT-Sema3A revealed the expected protein sizes when probed with an anti-DsRed antibody (actin shown as a loading control). In (**c**), HEK293T cells transfected with either tdT or tdT-Sema3A display strong tdT fluorescence. (**d-f**) Confirmation of tdT-Sema3A functionality. In (**d**), HEK293T cells were transfected with either GFP or GFP-Neuropilin-1 (GFP-Npn1), and binding of tdT or tdT-Sema3A was assessed 24 hours later. Binding is only observed between the tdT-Sema3A fusion protein and GFP-Npn1-transfected cells. In (**e**), E18 rat DRG explants were co-cultured in a collagen matrix with HEK293T cells expressing either tdT or tdT-Sema3A and grown for 48 hours. DRG axonal projections were labeled with 2H3 anti-neurofilament antibody. DRG axons are repelled by the tdT-Sema3A-expressing HEK293Ts, but not by the tdT-expressing cells. (**f**) Quantification of the repulsion assay shown in (**e**). The length of axonal projections on the proximal (P) and distal (D) sides of the DRG explant was measured and used to calculate the P/D value. 16 explants were analyzed for each condition (from 3 independent experiments). Gray bar (tdT); black bar (tdT-Sema3A). Results are presented as mean ± SEM. * $P< 0.001$ (unpaired *t*-test). Scale bar: c, 70µm; d, 30µm; e, 200µm.

Bibliography

Behar O, Golden JA, Mashimo H, Schoen FJ, Fishman MC (1996) Semaphorin III is needed for normal patterning and growth of nerves, bones and heart. Nature 383:525-528.

Luo Y, Raible D, Raper JA (1993) Collapsin: a protein in brain that induces the collapse and paralysis of neuronal growth cones. Cell 75:217-227.

Pasterkamp RJ, Kolodkin AL (2003) Semaphorin junction: making tracks toward neural connectivity. Curr Opin Neurobiol 13:79-89.

Pasterkamp RJ, Giger RJ (2009) Semaphorin function in neural plasticity and disease. Curr Opin Neurobiol 19:263-274.

Polleux F, Giger RJ, Ginty DD, Kolodkin AL, Ghosh A (1998) Patterning of cortical efferent projections by semaphorin-neuropilin interactions. Science 282:1904-1906.

Raper JA (2000) Semaphorins and their receptors in vertebrates and invertebrates. Curr Opin Neurobiol 10:88-94.

Reidy K, Tufro A (2011) Semaphorins in kidney development and disease: modulators of ureteric bud branching, vascular morphogenesis, and podocyte-endothelial crosstalk. Pediatr Nephrol 26:1407-1412.

Taniguchi M, Yuasa S, Fujisawa H, Naruse I, Saga S, Mishina M, Yagi T (1997) Disruption of semaphorin III/D gene causes severe abnormality in peripheral nerve projection. Neuron 19:519-530.

APPENDIX III:

VEGF Shows Its Attractive Side at the Midline

The following commentary was written as a preview for two articles appearing in a 2011 issue of Neuron:

The assembly of a highly organized network of neuronal connections is a key developmental process and essential for all neural function, ranging from simple movement to complex cognitive processes. Research focused on the cellular strategies and molecular mechanisms that orchestrate neural network assembly led to the discovery of a wide variety of axon guidance molecules and receptors (Kolodkin and Tessier-Lavigne, 2010). Many guidance molecules are evolutionarily conserved and, based on their mode of action, are categorized into short- or long-range guidance cues that influence growth cone steering in a positive (attractive) or negative (repulsive/inhibitory) manner. We now know that the activity of an individual guidance cue is not absolute, but instead interpreted by the neuronal growth cone in a context-dependent manner. Important conceptual advances in deciphering the molecular language of axon guidance and network assembly include the discovery of hierarchies among guidance cues, the identification of molecular switches that when flipped turn an attractive cue into an inhibitory one (or vice versa), and the existence of diverse receptor complexes that facilitate cell type-specific responses to a specific guidance cue. The discovery of general principles underlying the

wiring of the developing nervous system provides insight into the molecular logic that allows a relatively small set of guidance cues to initiate the assembly of complex neural networks with myriad interconnected circuits. In this issue of Neuron, Erskine et al. (2011) and Ruiz de Almodovar et al. (2011) now provide new evidence that a key angiogenic factor, VEGF-A, exhibits angiogenesis-independent chemoattractive effects on spinal commissural and retinal ganglion cell axons at the CNS midline.

It is not by chance that analysis of nervous system midline development has been particularly successful in the discovery of guidance cues and the elucidation of axon pathfinding mechanisms. Axons extending toward the CNS midline during development must make an important decision: to cross and find a synaptic partner on the contralateral side of the nervous system (relative to their cell body) or not to cross and remain confined to the ipsilateral side. Extensive work in fruit flies, worms, fish, chicks, and mice has established that the midline is a rich source of chemoattractants and chemorepellents (**Figure A3.1a**) (Dickson and Zou, 2010). Vertebrate Netrin-1 is a robust chemoattractant for spinal commissural axons and is secreted by floor plate cells located at the ventral midline. Despite its strong and long-range attractive capabilities, Netrin-1 collaborates with several additional cues to direct precrossing commissural axons toward the floor plate. Chemorepellents, including BMPs and Draxin, are released by the roof plate and initially "push" commissural axons ventrally into an increasing Netrin-1 gradient. The floor plate also secretes the morphogen Sonic Hedgehog (Shh). Like Netrin-1, Shh is a chemoattractant for precrossing commissural axons. Once at the floor plate, commissural axons lose their interest in Netrin-1 and Shh, and acquire responsiveness to floor plate-derived repellents, including Slits and Semaphorins, allowing them to exit the floor plate and move on to the second leg of their journey (Dickson and Zou, 2010). Remarkably, precrossing spinal

commissural neurons exposed to a Netrin-1-deficient floor plate in the presence of Shh signaling inhibitors show residual attraction, indicating the existence of additional, unidentified floor plate attractant(s) (Charron et al., 2003).

In the developing visual system, retinal ganglion cell (RGC) axons arriving at the chiasm face the same challenge as precrossing axons in the ventral spinal cord: to cross or not to cross the midline. As they approach the optic chiasm, RGCs segregate into ipsilaterally and contralaterally projecting fibers (**Figure A3.1b**). Proper crossing, or decussation, at the chiasm is essential for organisms with prominent binocular vision. The mouse has laterally positioned eyes and limited binocular vision. A large population of RGC axons cross the midline, and a relatively small population does not cross and project ipsilaterally. Seemingly quite different molecular strategies have evolved for proper growth cone navigation at the optic chiasm and spinal cord midline structures. Molecular gatekeepers such as Netrin-1 and Slits are either absent from the optic chiasm or do not directly participate in midline crossing of RGCs. Growth inhibitory cues, on the other hand, are abundant (Erskine and Herrera, 2007). These include the midline repellent EphrinB2, an established guidance cue at the mouse optic chiasm. EphB1 is expressed by ipsilaterally projecting RGCs and EphrinB2 is necessary for the proper formation of these projections. More recent evidence suggests that Shh repels ipsilateral RGC axons at the optic chiasm via its receptor Boc (Fabre et al., 2010). Semaphorin5A and Slits are molecules that define the boundary of the optic pathway but do not directly participate in midline crossing (Erskine and Herrera, 2007). Much less is known about the molecular mechanisms that promote midline crossing at the chiasm. In zebrafish, the secreted semaphorin Sema3D is expressed at the midline and is thought to provide inhibitory signals at the chiasm midline to help channel RGC axons to the contralateral optic tract (Sakai and Halloran, 2006). The cell adhesion

molecule NrCAM is expressed at the mouse chiasm and also in a small subset of late born RGCs, and it promotes their midline crossing *in vivo* (Williams et al., 2006). Cell culture experiments raised the possibility that a growth-promoting factor that mediates RGC axon crossing at the midline is present at the optic chiasm, suggesting that decussation is not a default mechanism but an active process involving unknown chemoattractive cue(s) (Tian et al., 2008).

A pair of exciting new studies (Erskine et al. [2011] and Ruiz de Almodovar et al. [2011]) demonstrate for the first time that vascular endothelial growth factor (VEGF)-A released at the CNS midline functions as a chemoattractant for spinal commissural and RGC axons *in vivo*. Erskine et al. show that in the mammalian visual system, VEGF functions as a growth-promoting factor that promotes extension of contralaterally projecting RGC axons across the midline, while Ruiz de Almodovar et al. find that in the spinal cord, VEGF secreted from the floor plate is an attractant for precrossing spinal commissural axons. VEGF is best known for its proangiogenic function during blood vessel growth *in vivo*, and recent studies have revealed that VEGF also promotes neural progenitor proliferation, survival, migration, and differentiation (Greenberg and Jin, 2005). However, these present studies demonstrate the versatility of VEGF-A, expanding its repertoire to include chemoattractant function essential for proper nervous system wiring.

In their search for guidance cues that function as chemoattractants at the mammalian optic chiasm, Erskine and colleagues initially observe that mice lacking Neuropilin-1 (Npn-1), a transmembrane receptor for class 3 Semaphorins and select isoforms of VEGF-A (Adams and Eichmann, 2010), display increased ipsilateral projections at the optic chiasm at embryonic day (E)14.5 *in vivo*. No defects at the chiasm were observed in mice deficient for the related Neuropilin-2 receptor. Despite the early lethality of Npn-1 germline null mice, the chiasm

appears to develop normally, and no changes in expression of EphrinB2 or Slits were observed. Furthermore, the ventrotemporal domain of the retina that gives rise to most ipsilateral RGC projections is not enlarged in Npn-1 mutants. When coupled with the strong expression of Npn-1 on contralaterally projecting RGC axons, this phenotype suggested a role for Npn-1 in promoting RGC axon midline crossing. Interestingly, expression of class 3 Semaphorin family members (Sema3s) at the chiasm is not observed, or is extremely low, at the time when RGCs cross. To rule out potential influences from more remote Sema3 sources, mice carrying a Npn-1 point mutation that abolishes Sema3, but not VEGF, signaling ($Npn1^{Sema-/-}$) (Gu et al., 2003) were analyzed. Similar to wild-type mice, $Npn1^{Sema-/-}$ mice show no midline crossing defects at the optic chiasm. With a vital role for Sema3s eliminated, Erskine et al. (2011) turned their attention to isoforms of VEGF-A, a second class of Npn-1 ligands. VEGF-A is strongly expressed at the embryonic optic chiasm in the mouse. To explore the possibility that VEGF is the Npn-1 ligand that promotes contralateral RGC axon growth, Erskine et al. (2011) analyzed $Vegfa^{120/120}$ mice, which cannot produce the Npn-1-binding isoforms VEGF164 or VEGF188, but do express VEGF120, which does not bind Npn-1 and supports blood vessel formation. Similar to Npn-1 null mice, $Vegfa^{120/120}$ mice display increased ipsilateral projections and decreased contralateral projections, supporting the idea that VEGF/Npn-1 interactions promote RGC axon crossing at the optic chiasm. $Vegfa^{120/120}$ mice survive to birth, so retrograde DiI labeling was employed to independently assess ipsilaterally projecting RGC axons and determine the origin of misrouted axons within the retina. In wild-type mice, ipsilateral RGCs are primarily restricted to the ventrotemporal region of the retina (**Figure A3.1b**). In $Vegfa^{120/120}$ mice, however, retrogradely labeled RGCs were found throughout the temporal and nasal retina. To directly test whether VEGF functions as a chemoattractant, RGC growth cones were exposed

to a VEGF164 gradient. Consistent with a previous study showing that VEGF promotes regenerative growth of axotomized RGCs in culture (Bocker-Meffert et al., 2002), VEGF164 was found to act as a selective attractant for dorsotemporal RGC growth cones (neurons that give rise to contralateral projections) but not for ventrotemporal RGC growth cones (neurons that give rise to ipsilateral projections). Collectively, these studies show that VEGF164 functions as a chemoattractant to promote midline crossing of Npn-1-expressing RGC axons at the optic chiasm *in vivo*.

VEGF also functions as an attractant for spinal commissural axons, as reported in the study by Ruiz de Almodovar et al. (2011). VEGF is expressed at the floor plate at the time when spinal commissural axons cross the midline (**Figure A3.1a**). Mice lacking function of a single VEGF allele specifically in the floor plate ($Vegf^{FP+/-}$) secrete less VEGF and exhibit concomitant abnormal pathfinding of precrossing commissural axons. While most Robo3-positive commissural axons reach the floor plate in $Vegf^{FP+/-}$ mice, labeled commissural axons in embryonic spinal cord sections are observed to be defasciculated, and they often project to the lateral edge of the ventral spinal cord. Important control experiments show that the defects observed are not secondary to altered expression of Netrin-1 or Shh in the floor plate of $Vegf^{FP+/-}$ mice. *In vitro*, an attractive response by commissural axons to a gradient of VEGF-A was observed in the Dunn chamber assay. Interestingly, VEGF-A attraction was completely abolished in the presence of a function blocking, anti-Flk1 (KDR/VEGFR2) antibody or by pharmacological inhibition of Src family kinases. Anti-Npn1 in this same assay had no effect on VEGF-A attraction. Immunolabeling of precrossing commissural axons revealed coexpression of Flk1 and Robo3, and conditional ablation of Flk1 in commissural neurons ($Flk1^{CN-ko}$) phenocopies defects observed in the $Vegf^{FP+/-}$ mice. The patterns and expression

levels of Netrin-1 and Shh in the floor plate in *Flk1*$^{CN\text{-}ko}$ mice are comparable to wild-type littermates, indicating that Flk1 cell-autonomously controls VEGF-mediated attraction of precrossing commissural axons *in vivo*.

Taken together, these studies are the first to report that VEGF is essential for proper axon guidance at the CNS midline *in vivo*. VEGF-A functions as a midline-derived chemoattractant for RGC axons in the diencephalon and functions similarly for commissural axons in the developing spinal cord. In the visual system, Npn-1 is an obligatory receptor for VEGF attraction, while in the developing spinal cord, Flk1 is required for the VEGF-mediated attractive response. No significant expression of Flk1 or Flt1 is detected in developing RGCs (Erskine et al., 2011), and conversely, Npn-1 is not expressed by precrossing spinal commissural neurons (Ruiz de Almodovar et al., 2011). Although Flk1 mutants have not been examined for RGC midline crossing defects, the current data suggest that RGCs and spinal commissural neurons employ distinct and independent signaling mechanisms for VEGF attraction.

How does VEGF signal attraction in RGCs? Npn-1 is a type-1 transmembrane protein with a short cytoplasmic domain, and one possibility is that Npn-1 signals attraction through its cytoplasmic domain, independent of a coreceptor(s). Alternatively, Npn-1 might form a complex with a coreceptor to form a holoreceptor complex that signals VEGF attraction. NrCAM has been shown to regulate neuropilin signaling in response to Sema3s during commissural axon guidance in the anterior commissure (Falk et al., 2005). When coupled with NrCAM's role in promoting RGC axon midline crossing *in vivo*, it is possible that NrCAM is part of a Npn-1/VEGF receptor complex which promotes midline crossing. Arguing against this possibility, however, are the distinct temporal requirements for NrCAM and Npn-1/VEGF for proper decussation of RGC axons. Defective RGC midline crossing in Npn-1and *Vegfa*$^{120/120}$

mutant mice is observed as early as E14, while defects in NrCAM mutants are observed only late in visual system development, from E17.5 onward (Williams et al., 2006). Recent evidence suggests that Flk1 functions as the signal transducing receptor component for Sema3E, providing additional evidence for shared mechanisms involving Sema3s and VEGF (Bellon et al., 2010). These present studies do not address whether VEGF influences guidance in a Plexin-dependent manner. Npn-1 forms a complex with Plexin receptors, and Plexins are regulators of both attractive and repulsive axon guidance (Kolodkin and Tessier-Lavigne, 2010). Genetic tools are available, and it will be interesting to examine whether Plexin mutants show guidance defects at the CNS midline related to impaired VEGF function.

The identification of VEGF as a novel midline attractant released by the floor plate begs the question as to how VEGF might fit in with previously identified spinal commissural axon guidance mechanisms. For precrossing, Flk1-positive axons, VEGF released by the floor plate presumably collaborates with Netrin-1 and Shh in commissural axon attraction. While most Robo3-positive axons reach the floor plate in $Vegf^{FP+/-}$ mice, some of these axons stall and are misrouted into a more lateral trajectory. The most noticeable phenotype in $Vegf^{FP+/-}$ mice is axon defasciulation. Defects observed in $Vegf^{FP+/-}$ mice are similar to those observed in mice deficient for the Shh receptor Boc and the Shh signaling component Smoothened (Charron et al., 2003; Okada et al., 2006). However, these phenotypes are less pronounced than the Netrin-1 phenotype, since the majority of precrossing commissural axons are able to reach the midline. In Netrin-1 mutants on the other hand, most precrossing commissural axons stall and fail to enter the ventral spinal cord. This suggests that in the absence of Netrin-1, the ventral spinal cord may be nonpermissive for commissural axon growth. Thus, Shh and VEGF may function primarily in commissural axon attraction, while Netrin-1 is important for outgrowth and attraction.

Consistent with this idea, Shh and VEGF attract precrossing commissural axons, but exhibit no growth-promoting effects *in vitro* (Charron et al., 2003; Ruiz de Almodovar et al., 2011).

Next on the agenda will be questions concerning how commissural axons cope with VEGF attraction after they have entered the floor plate. Are there mechanisms in place that modulate or silence VEGF attraction, similar to those reported for Netrin-1 and Shh? Alternatively, is loss of Netrin-1 attraction, in conjugation with acquisition of Slit and Sema3 inhibition, sufficient to prevent postcrossing commissural axons from recrossing the midline as they travel rostrally, despite continuing VEGF attraction? Ultimately, a detailed understanding of growth cone navigation at the midline requires a combination of tools that allow temporal and spatial regulation of guidance cues, their receptors, and downstream effectors. When combined with live imaging of commissural axon subpopulations, this approach will reveal insights into the contributions of individual cues as they promote proper axon navigation at the CNS midline. The identification of VEGF as a midline attractant by Erskine et al. (2011) and Ruiz de Almodovar et al. (2011) represents an important advancement toward this goal.

Acknowledgments

This article has been published (see citation below) and permission was received from the editors to use this work as part of a dissertation:

Dickendesher TL, Giger RJ (2011) VEGF shows its attractive side at the midline. **Neuron** 70:808-812.

This article refers to the work of the following two studies:

Erskine L, Reijntjes S, Pratt T, Denti L, Schwarz Q, Vieira JM, Alakakone B, Shewan D, Ruhrberg C (2011) VEGF signaling through neuropilin 1 guides commissural axon crossing at the optic chiasm. Neuron 70:951-956.

Ruiz de Almodovar C, Fabre PJ, Knevels E, Coulon C, Segura I, Haddick PC, Aerts L, Delattin N, Strasser G, Oh WJ, Lange C, Vinckier S, Haigh J, Fouquet C, Gu C, Alitalo K, Castellani V, Tessier-Lavigne M, Chedotal A, Charron F, Carmeliet P (2011) VEGF mediates commissural axon chemoattraction through its receptor Flk1. Neuron 70:966-978.

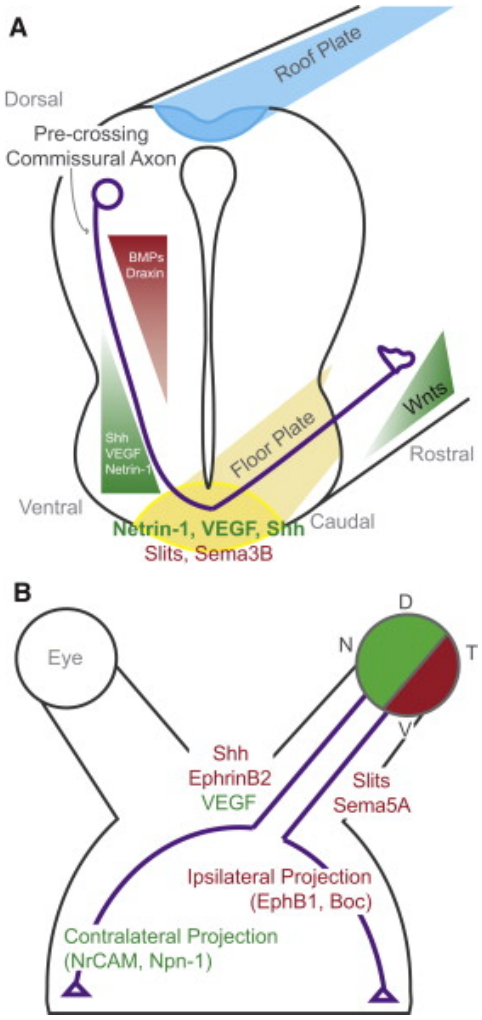

Figure A3.1: Axon guidance mechanisms at the CNS midline. (**a**) Embryonic spinal cord showing trajectory of commissural axons. Precrossing spinal commissural axons are initially pushed ventrally by roof plate-derived inhibitory cues, including BMPs and Draxin (red gradient). Chemoattractants secreted by the floor plate include Netrin-1, Shh, and VEGF (green gradient). After crossing the midline, commissural axons lose attraction to Netrin-1 and Shh. Conversely, factors such as Slits and Sema3B, which have no effect on commissural axons before crossing, become potent repellents after crossing. (**b**) In vertebrates with frontally located eyes, subpopulations of RGC axons are segregated at the optic chiasm to project to targets on both the ipsilateral and contralateral side of the brain. EphrinB2 and Shh at the chiasm midline are repellents for EphB1- and Boc-expressing RGCs destined for the ipsilateral optic tract. NrCAM expressed by RGCs is required in a small subset of late born neurons to form contralateral projections. The VEGF-A isoform VEGF164 is expressed at the midline where it functions as a chemoattractant for Npn-1-positive RGCs to instruct contralateral growth. D, dorsal; V, ventral; N, nasal; T, temporal retina.

Bibliography

Adams RH, Eichmann A (2010) Axon guidance molecules in vascular patterning. Cold Spring Harb Perspect Biol 2:a001875.

Bellon A, Luchino J, Haigh K, Rougon G, Haigh J, Chauvet S, Mann F (2010). VEGFR2 (KDR/Flk1) signaling mediates axon growth in response to semaphorin 3E in the developing brain. Neuron 66:205-219.

Bocker-Meffert S, Rosenstiel P, Rohl C, Warneke N, Held-Feindt J, Sievers J, Lucius R (2002) Erythropoietin and VEGF promote neural outgrowth from retinal explants in postnatal rats. Invest Ophthalmol Vis Sci 43:2021-2026.

Charron F, Stein E, Jeong J, McMahon AP, Tessier-Lavigne M (2003). The morphogen sonic hedgehog is an axonal chemoattractant that collaborates with netrin-1 in midline axon guidance. Cell 113:11-23.

Dickson BJ, Zou Y (2010) Navigating intermediate targets: the nervous system midline. Cold Spring Harb Perspect Biol 2:a002055.

Erskine L, Herrera E (2007) The retinal ganglion cell axon's journey: insights into molecular mechanisms of axon guidance. Dev Biol 308:1-14.

Fabre PJ, Shimogori T, Charron F (2010). Segregation of ipsilateral retinal ganglion cell axons at the optic chiasm requires the Shh receptor Boc. J Neurosci 30:266-275.

Falk J, Bechara A, Fiore R, Nawabi H, Zhou H, Hoyo-Becerra C, Bozon M, Rougon G, Grumet M, Puschel AW, Sanes JR, Castellani V (2005). Dual functional activity of semaphorin 3B is required for positioning the anterior commissure. Neuron 48:63-75.

Greenberg DA, Jin K (2005) From angiogenesis to neuropathology. Nature 438:954-959.

Gu C, Rodriguez ER, Reimert DV, Shu T, Fritzsch B, Richards LJ, Kolodkin AL, Ginty DD (2003). Neuropilin-1 conveys semaphorin and VEGF signaling during neural and cardiovascular development. Dev Cell 5:45-57.

Kolodkin AL, Tessier-Lavigne M (2011) Mechanisms and molecules of neuronal wiring: a primer. Cold Spring Harb Perspect Biol 3:a001727.

Okada A, Charron F, Morin S, Shin DS, Wong K, Fabre PJ, Tessier-Lavigne M, McConnell, SK (2006) Boc is a receptor for sonic hedgehog in the guidance of commissural axons. Nature 444:369-373.

Sakai JA, Halloran MC (2006) Semaphorin 3d guides laterality of retinal ganglion cell projections in zebrafish. Development 133:1035-1044.

Tian NM, Pratt T, Price DJ (2008) Foxg1 regulates retinal axon pathfinding by repressing an ipsilateral program in nasal retina and by causing optic chiasm cells to exert a net axonal growth-promoting activity. Development 135:4081-4089.

Williams SE, Grumet M, Colman DR, Henkemeyer M, Mason CA, Sakurai T (2006). A role for Nr-CAM in the patterning of binocular visual pathways. Neuron 50:535-547.